

# **Pion Photoproduction in Chiral Effective Field Theory with explicit Delta Degrees of Freedom**

Pion-Photoproduktion in chiraler effektiver Feldtheorie mit expliziten Delta-Freiheitsgraden

## **DISSERTATION**

zur  
Erlangung des Grades  
„Doktor der Naturwissenschaften“

an der Fakultät für Physik und Astronomie  
der Ruhr-Universität Bochum

von  
Nora Martina Rijneveen

aus  
Saarbrücken

Bochum (2021)

1. Gutachter: Prof. Dr. Evgeny Epelbaum  
2. Gutachter: Prof. Dr. Maxim Polyakov  
Datum der Disputation: 17.06.2021

---

## **Abstract**

In this work, we study the reaction of pion photoproduction on the nucleon in chiral effective field theory. We consider the heavy baryon as well as the manifestly covariant formulation and analyse the difference in convergence and data description between the two approaches. Furthermore, we take into account explicit delta degrees of freedom in the small-scale-expansion scheme to extend the applicability of the theory into the delta region. Starting from the chiral effective Lagrangian we calculate multipole amplitudes, which contain a set of a priori unknown low-energy constants. These parameters are subsequently fitted to partial-wave analysis data. We estimate theoretical uncertainties of observables and low-energy constants based on a Bayesian model of the truncation of the chiral series. First we consider the framework with only pion and nucleon degrees of freedom, then we upgrade our calculations to explicit delta degrees of freedom, where we first include the leading-order delta tree contributions in both formulations. Afterwards, next-to-leading order delta loop contributions are taken into account in the covariant framework. We analyse the deltaless and deltaful results in detail, furthermore we compare our findings to data of neutral pion production cross sections and polarisation asymmetries. We find that the description of the reaction is clearly improved by the explicit treatment of the delta resonance.

## **Zusammenfassung**

In dieser Arbeit wird der Prozess der Pion-Photoproduktion am Nukleon in chiraler effektiver Feldtheorie untersucht. Sowohl die Schwerbaryonen- als auch die manifest kovariante Formulierung werden verwendet, um Unterschiede zwischen den Ansätzen im Konvergenzverhalten und Beschreibung der Daten zu untersuchen. Weiterhin werden explizite Delta-Freiheitsgrade im „small-scale-expansion“-Zählschema miteinbezogen, um die Anwendbarkeit der Theorie in die Deltaregion zu erweitern. Auf der Grundlage der chiralen effektiven Lagrangedichte werden Multipolamplituden berechnet, welche einen Satz von a priori unbekannten Niederenergiekonstanten enthalten. Diese Parameter werden anschließend an die Daten einer Partialwellenanalyse gefittet. Theoretische Fehler der Observablen und Niederenergiekonstanten werden mithilfe eines Bayesischen Modells der Trunkierung der chiralen Reihe abgeschätzt. Zunächst wird die rein pionische und nukleonische Formulierung betrachtet, anschließend werden die Rechnungen auf explizite Delta-Beiträge erweitert, wobei zunächst die führenden Delta-Baumbeiträge in beiden Formulierungen miteinbezogen werden. Im Folgenden werden die nächstführenden Delta-Schleifenbeiträge in der kovarianten Theorie miteinbezogen. Die deltafreien und deltaguten Ergebnisse werden im Detail analysiert, weiterhin werden die Resultate mit Daten von Wirkungsquerschnitten und Polarisationsasymmetrien im neutralen Pionproduktionskanal verglichen. Es konnte gezeigt werden, dass die Beschreibung der Reaktion durch die explizite Behandlung der Deltaresonanz deutlich verbessert wird.



# Contents

<b>Introduction</b>	<b>1</b>
<b>1 Quantum chromodynamics</b>	<b>5</b>
1.1 Symmetries of QCD . . . . .	5
1.2 Spontaneous symmetry breaking . . . . .	9
<b>2 Chiral Perturbation Theory</b>	<b>11</b>
2.1 Effective field theory . . . . .	11
2.2 ChPT for pions . . . . .	12
2.3 Including the nucleon . . . . .	15
2.3.1 Covariant approach . . . . .	15
2.3.2 Heavy baryon formalism . . . . .	18
2.4 Including the delta . . . . .	20
2.4.1 Covariant approach . . . . .	20
2.4.2 Heavy baryon formalism . . . . .	25
2.5 Effective Lagrangian and low-energy constants . . . . .	26
<b>3 Pion photoproduction</b>	<b>29</b>
3.1 Kinematics . . . . .	29
3.2 Isospin decomposition . . . . .	30
3.3 Spin decomposition and multipole amplitudes . . . . .	31
3.4 The cross section and polarisation asymmetry . . . . .	33
3.5 Renormalisation . . . . .	34
3.5.1 Renormalisation of subprocesses . . . . .	34
3.5.2 Expanding integrals in small parameters and power-counting violating terms . . . . .	38
3.5.3 Renormalisation of LECs . . . . .	41
3.6 Consistency checks . . . . .	43
3.6.1 Independence from off-shell effects . . . . .	43
3.6.2 Cancellation of UV divergences . . . . .	44
3.6.3 Electromagnetic current conservation . . . . .	44
3.6.4 Freedom of power-counting violating terms . . . . .	45
3.6.5 Delta decoupling . . . . .	45
3.7 Comparison of LECs in heavy baryon and covariant approach . . . . .	46
3.8 Resonance saturation of LECs . . . . .	47
3.9 Fitting observables and error estimation . . . . .	48
3.10 Constants and numeric conventions . . . . .	50

<b>4 Technical details on the calculation</b>	<b>51</b>
<b>5 Observables and results</b>	<b>53</b>
5.1 Pion photoproduction in deltaless ChPT . . . . .	53
5.1.1 Fitting procedure . . . . .	53
5.1.2 Order- $q^3$ results, figures and discussion . . . . .	56
5.2 Pion photoproduction with explicit delta degrees of freedom . . . . .	61
5.2.1 The delta mass in the complex mass scheme . . . . .	62
5.2.2 Fitting procedure including delta tree contributions . . . . .	65
5.2.3 Order- $q^3 + \epsilon^2$ results, figures and discussion . . . . .	66
5.2.4 Fitting procedure including delta loop contributions . . . . .	77
5.2.5 Order- $\epsilon^3$ results, figures and discussion . . . . .	78
5.3 Comparison to data of the neutral pion production channel . . . . .	84
<b>6 Summary and outlook</b>	<b>97</b>
<b>A Relating different sets of amplitudes</b>	<b>99</b>
<b>B Feynman diagrams</b>	<b>101</b>
<b>C Renormalisation of the amplitude</b>	<b>107</b>
C.1 Renormalisation of the mesonic sector . . . . .	107
C.2 Heavy baryon renormalisation rules . . . . .	108
C.3 Covariant renormalisation rules . . . . .	109
<b>D Feynman rules</b>	<b>117</b>
D.1 Mesonic sector . . . . .	117
D.2 Heavy baryon Feynman rules . . . . .	118
D.3 Covariant Feynman rules . . . . .	120
<b>Bibliography</b>	<b>125</b>
<b>Curriculum Vitae</b>	<b>139</b>

# Introduction

To this day, there are four different known fundamental forces in nature: gravitation, the electromagnetic force, the weak and the strong interaction. Many observable phenomena have been successfully described using the currently available theories of these forces, which are general relativity for gravitation, electroweak theory for both electromagnetic and weak interaction and quantum chromodynamics (QCD) for the strong force. Moreover, new phenomena have been predicted, such as the Higgs boson more than 50 years ago, which was experimentally confirmed in 2012 [1]. The Higgs boson was considered to be a central puzzle piece in the Standard Model (SM) of particle physics [2–7], which provides a mathematically self-consistent quantum field theory of the strong, electromagnetic and weak interaction. The current formulation of the SM was finalised in the 1970s. An important support for the theory was given by the findings of deep inelastic electron scattering experiments, confirming that baryons are made up of quarks [8]. Although the SM is not a “theory of everything” due to manifold reasons, it has achieved great success in describing or predicting phenomena in the electroweak and strong sector.

The theory of the strong interaction was mainly developed over the second half of the 20th century. In new, powerful experimental facilities more and more unknown particles were detected, so it was increasingly doubted that all of these states could be elementary. The discovery of the  $\Delta^{++}$  [10] was decisive for the introduction of the colour charge, which led to the development of the quark model [11]. A first important step towards a field-theoretical description of the strong interaction was made by Yang and Mills [12], who formulated the first example of a non-Abelian gauge theory. However, the large coupling constant of the strong interaction posed a problem, because the conventional use of perturbation theory was spoiled. The breakthrough was made in the 1970s through the discovery of the asymptotic freedom [13, 14], which finally enabled a perturbative treatment of the strong interaction at high energies, where the coupling constant becomes small. By that time, the quantisation of Yang-Mills theory had already been completed [15] and renormalisability had been shown [16, 17].

However, studying QCD at low energies is still a nontrivial problem. At an energy scale of  $\Lambda \approx 1 \text{ GeV}$ , which corresponds to length scales greater than the size of the nucleon, the coupling constant becomes too large to be used as a small expansion parameter in a perturbation theory. Thus, other methods had to be developed to study the properties of hadrons in the low-energy sector. One approach is the Large- $N_C$  expansion [18, 19], which allows for qualitative conceptions rather than precise numerical results by taking the limit to an infinite number of colour charges. Second, pioneering models such as the Skyrme [20], the MIT bag [21] and the chiral bag model [22] exist. Although reproducing some reasonably accurate low-energy properties of QCD, the approach of these models is not systematic, which makes it a hard

task to provide uncertainties. A third strategy, which has proven to successfully reproduce experimental results in some cases, is Lattice QCD, which studies the strong interaction on a discretised Euclidean spacetime with a finite size and number of grid points. It has a broad range of applicability and is a nonperturbative approach, but it comes at the cost of immense demand for computational power and time, making it a resource-intensive, slow and expensive tool. Since high-performance computing has not yet reached its limit, Lattice QCD is believed to deliver further interesting results in the next years.

In this work we rely on the method of effective field theories. It reaches back to a theorem of Weinberg [23], which states that a fundamental theory can be described by the most general Lagrangian in harmony with all of the symmetries of the fundamental theory. The crucial point is that instead of using the fundamental degrees of freedom, *effective* degrees of freedom can be used which are relevant in the considered energy region. Starting from this idea, Gasser and Leutwyler extended Weinberg's approach to an effective field theory (EFT) up to one-loop level, which only has mesons as degrees of freedom [24, 25]. This EFT of QCD is called chiral perturbation theory (ChPT). It is a perturbative, systematically improvable framework, which is one of its main advantages. By construction, it takes into account the chiral symmetry of QCD and its spontaneous breaking, which leads to the interpretation of the pion triplet as massive Goldstone bosons. ChPT has been extended to the light single-baryon sector [26–29], to the few-baryon sector [30–33] as well as to spin-3/2 particles [34], of which the delta resonance is probably the most prominent example. This resonance has four physical states with different electric charges  $\Delta^{++}$ ,  $\Delta^+$ ,  $\Delta^0$  and  $\Delta^-$ , which predominantly decay into a pion and a nucleon. Its mass  $m_\Delta \approx 1210$  MeV also serves as an estimate for the upper boundary of the energy range in which baryonic ChPT is applicable, because the convergence of the chiral series is limited by the lightest, not included degree of freedom. Because of the small mass difference to the nucleon as well as its strong coupling to the pion-nucleon sector, important contributions of explicitly incorporated deltas are expected even below the delta region. Several calculations of different reactions have confirmed this expectation over the last years, e.g. refs. [35–40].

In this work, we study the process of pion photoproduction on the nucleon, i.e.  $\gamma + N \rightarrow \pi + N$  in the framework of chiral effective field theory with explicit delta degrees of freedom. Studying this reaction is motivated by several reasons. First, it is the photoproduction of the lightest hadron. From the theoretical point of view, it is one of the simplest processes involving three different particles and thus serves as a test field for more complex reactions. From the experimental point of view, this reaction is quite easily accessible close to threshold and there can be no other final hadronic states due to energy conservation. Therefore, there is a lot of experimental data on pion photoproduction available.

As an additional motivation, pion photoproduction contributes as a subprocess to more complicated reactions, e.g. the magnetic form factor of the deuteron [41–43], thus the reaction may serve as an input for studies in the few-nucleon sector [44–46]. Furthermore, in a framework containing explicit delta degrees of freedom, it is possible to access the properties of the delta resonance. The magnetic moment of  $\Delta^+$  and  $\Delta^0$  starts to contribute to the reaction from

the two-loop level, which would require considerably more effort and computational power. However, in the related reaction of radiative pion photoproduction  $\gamma + N \rightarrow \gamma + \pi + N$ , it can be accessed at one-loop order in ChPT, see ref. [47].

Pion photoproduction has been a research topic for many years, with the first model-independent approach made by Kroll and Ruderman in the 1950s [48]. Based on general principles, such as Lorentz and gauge invariance, they derived a low-energy theorem for the matrix element of charged pion photoproduction at threshold, which expressed the production amplitudes in terms of a series in the parameter  $\mu = M_\pi/m_N$ . Later on, these predictions were improved [49, 50] by including the so-called partially conserved axial-vector current hypothesis [51–53] and current algebra [54–56]. Until the 1980s, there was little doubt about the validity of the low-energy predictions. Particularly for the charged production channels, which are dominated by the Kroll-Ruderman terms, the results from the theorem matched the available data well. However, new data of the neutral production channel at threshold [57, 58] showed a nonnegligible disagreement to the theoretical predictions of the  $s$ -wave electric dipole amplitude  $E_{0+}$ . A first important success for ChPT was the study of Bernard, Kaiser, Gasser and Meißner [59, 60] on pion photoproduction, which corrected the low-energy theorems by terms arising from pion loop diagrams. However, these corrections, generated by infrared singularities of the loop integrals, even worsened the agreement with data, which is due to the slow convergence of the chiral series in the neutral pion production channel. Therefore, renewed interest in pion photoproduction was awakened in the following years and multiple experimental groups remeasured pion photo- and electroproduction (e.g. [61–80]), and Bernard et al. worked out all the theoretical details in the different reaction channels within the framework of heavy baryon chiral perturbation theory (HBChPT) [60, 81–89]. The new approaches of the so-called infrared regularisation [90] and the extended-on-mass-shell scheme (EOMS) [91, 92] first enabled the treatment of scattering processes in the pion-nucleon sector in a manifestly covariant framework [90, 93]. Consequently, covariant calculations of  $\gamma + N \rightarrow \pi + N$  were completed up to the leading loop order  $\mathcal{O}(q^3)$  in ref. [94] using the infrared regularisation scheme, followed by an analysis of the full one-loop order  $\mathcal{O}(q^4)$  by Hilt et al. [95, 96] in the EOMS scheme.

After it was worked out how to include the delta resonance as an explicit degree of freedom into ChPT [34, 97], the photoproduction of pions has also been considered in this extended framework. An explicit treatment of the delta is of great interest, because the small gap between the pion production threshold  $\approx 1076$  MeV and the delta mass  $m_\Delta \approx 1210$  MeV gives reason to expect that the effects of the delta become important close above threshold. For example, the  $M_{1+}$  multipole receives dominant effects from the delta resonance for energies close to the delta mass. A first calculation of pion photoproduction with explicit delta degrees of freedom was completed in HBChPT [34], focussing on the neutral production channel close to threshold, which showed only moderate effects of the explicit delta treatment. An subsequent HBChPT study [98] found a more distinct improvement of the description in the HB framework. In the covariant approach, first studies of neutral pion photoproduction were done in refs. [38, 99–101], finding a substantial improvement in the description of the data compared to the HB approach with explicit deltas. However, in these works a different power counting [102] is used, the so-

called  $\delta$  scheme, in which the delta-nucleon mass split  $\Delta$  is considered to be of one order lower than the pion mass  $\Delta \sim \delta, M_\pi \sim \delta^2$ . The motivation for such a counting is given by numerical arguments, whereas the so-called small scale expansion (SSE) treats these parameters as being of the same size  $M_\pi \sim \Delta \sim \epsilon$ . Since there is no clear evidence for a faster convergence or better efficiency of one of the two schemes, it is desirable to consider pion photoproduction in the SSE for comparison purposes. Note, however, that the LECs of the two approaches cannot be compared directly, because their numerical values are scheme-dependent. Comparing the results in two counting schemes can only be done in terms of quality of the data description.

In this thesis, we study pion photoproduction in both HB and covariant formalisms of chiral effective field theory. We also analyse the effects of explicit delta degrees of freedom by taking into account their leading-order contributions in the HB approach and up to next-to-leading order contributions in the covariant formalism of ChPT. To estimate theoretical uncertainties of observables and LECs, we use a Bayesian model [103–105]. First, we study the deltaless case up to order  $q^3$ , which has been considered before [94–96]. Recent studies were mainly focused on the covariant approach, so we provide a detailed comparison of the two formalisms in order to analyse the difference in convergence and data description. In particular we compare the obtained LECs in terms of the effects generated by the infrared regular (IR) parts of the integrals. Next, we upgrade both HB and covariant approaches to leading-order delta tree contributions employing the SSE, which has been used for studies of other reactions such as pion-nucleon scattering and Compton scattering (e.g. refs. [40, 106, 107]). We provide an extended analysis of the combined deltaless leading one-loop order plus tree-level deltaful approach by comparing HB and covariant results in terms of the IR shifts. Furthermore, we discuss the differences to the deltaless case in terms of resonance saturation. We also provide results of  $\gamma + N \rightarrow \pi + N$  up to leading deltaful loop order for the first time. In comparison to the study of ref. [38], we take into account loop diagrams including up to three delta propagators, which give rise to relevant contributions to the amplitude. Furthermore, we give an estimate for the subleading  $\gamma N \Delta$  coupling constant  $h_1$ . A qualitative comparison to the aforementioned studies in the  $\delta$ -scheme is given. Furthermore, we compare our results to recent high-precision data of the neutral pion production channel [78, 108] in order to test the reproduction of the data.

This thesis is structured as follows. In chapter 1, a short introduction into QCD is given. Chapter 2 contains the necessary terms of ChPT, i.e. the full effective Lagrangian needed to calculate pion photoproduction up to the first loop order including explicit deltas. Subsequently, the reaction is addressed in chapter 3, including kinematics, isospin and spin decomposition of the matrix element, followed by the calculation of multipole amplitudes and observables as well as renormalisation. We also discuss the performed consistency checks, the foundation of the IR shifts and resonance saturation. Chapter 4 focuses on the technical details of the calculation and gives an overview how we performed symbolic and numeric calculations. In chapter 5, we present and discuss the results. Chapter 6 concludes with a summary and an outlook.

# 1 Quantum chromodynamics

In this chapter, we introduce the features of quantum chromodynamics (QCD) relevant for our study of pion photoproduction. For the construction of an effective field theory (EFT), the symmetries of the underlying theory are the most important part. Since ChPT is an EFT of QCD, we focus on discussing the symmetries of QCD in this chapter, especially on the spontaneous symmetry breaking. For a profound introduction to the theory of the strong interaction, we refer the reader to the book of T. Muta [109].

## 1.1 Symmetries of QCD

The strong interaction between quarks and gluons is described by a non-Abelian gauge field theory with the symmetry group SU(3), which is called Quantum Chromodynamics (QCD). The QCD Lagrangian reads

$$\mathcal{L}_{\text{QCD}} = -\frac{1}{4}G_a^{\mu\nu}G_{a,\mu\nu} + \bar{q}(iD - M)q, \quad (1.1)$$

where  $\not{a} = a^\mu \gamma_\mu$  is the Feynman slash notation for any vector or operator contracted with the Dirac matrices. In the Lagrangian (1.1), the quark fields are arranged in the vector  $q = (u, d, s, c, b, t)$  and  $M = \text{diag}(m_u, m_d, m_s, m_c, m_b, m_t)$  is the quark mass matrix. The gauge field strength tensor

$$G_{\mu\nu}^a = \partial_\mu G_\nu^a - \partial_\nu G_\mu^a + g f^{abc} G_\mu^b G_\nu^c. \quad (1.2)$$

contains the gauge fields  $G_\mu^a$ , which are associated with the eight gluons, the gauge bosons of QCD. The structure constants  $f^{abc}$  of the gauge group SU(3) are related to the eight group generators  $T_a = \lambda_a/2$  by the Lie algebra

$$[T^a, T^b] = i f^{abc} T^c, \quad (1.3)$$

with  $\lambda_a$  being the eight Gell-Mann matrices. The covariant derivative

$$D^\mu = \partial^\mu - i g T_a G_a^\mu \quad (1.4)$$

introduces the coupling between quarks and gluons.

QCD shares some features with quantum electrodynamics (QED), but there are several crucial differences. First, it can be seen from the last term in eq. (1.2), which generates a three- and a four-gluon interaction, that gluons can couple directly to each other even in the absence

of quarks. This last term also gives rise to a central phenomenon of QCD, the so-called asymptotic freedom. It means that the strength of the interaction decreases at short distances or large energies. This is a major difference to QED, where the gauge bosons (photons) cannot couple to themselves directly and where electrically charged particles interact weaker at larger distances. Because for high energies the coupling constant of QCD is small, a perturbative calculation of observables is possible in this regime.

Second, gluons as well as quarks carry a colour charge, the quantum number associated with the gauge group  $SU(3)$ . In QED, however, photons do not carry electric charge. A major property of QCD is that observable particles must form into colourless objects, this characteristic is known as confinement. So far no individual colour charged particles were detected in experiments, one has found only colourless objects. The two most common examples of colourless particles are mesons and baryons. Mesons consist of a quark and antiquark and baryons consist of three quarks. In these particles, either colour and anti-colour or three colour charges blend to “white”.

Applying perturbation theory in the standard way is not possible in the case of QCD at low energies, because the coupling constant is too large to serve as a small expansion parameter. However, approximate symmetries of the QCD Lagrangian may be used to formulate an EFT, where perturbative calculations are possible. An important step in this direction is based on the observation that the quark masses have a significant gap [110]

$$\begin{pmatrix} m_u & = & 2.16_{-0.26}^{+0.49} \text{ MeV} \\ m_d & = & 4.67_{-0.17}^{+0.48} \text{ MeV} \\ m_s & = & 93_{-5}^{+11} \text{ MeV} \end{pmatrix} \ll 1 \text{ GeV} \lesssim \begin{pmatrix} m_c & = & 1.27_{-0.02}^{+0.02} \text{ GeV} \\ m_b & = & 4.18_{-0.02}^{+0.03} \text{ GeV} \\ m_t & = & 172.76_{-0.30}^{+0.30} \text{ GeV} \end{pmatrix}^1, \quad (1.5)$$

dividing them naturally into the light ( $u, d, s$ ) and heavy ( $c, b, t$ ) quarks. Taking a closer look, we observe that the mass of the strange quark is still at least an order of magnitude higher than the up and down quark, which justifies to also consider the strange quark as heavy. In the low-energy limit, we neglect the effects of heavy quark-antiquark pairs, because the energies necessary to produce them are far beyond our region of interest. Their effects are still taken care of indirectly in the coupling constants.

Next, we observe that even the masses of the lightest mesons (the pions)  $M_\pi \approx 138 \text{ MeV}$  are orders of magnitude larger than the sum of their quark constituents

$$M_{\pi^+} \gg m_u + m_{\bar{d}},$$

which justifies to analyse the theory in the case of vanishing quark masses  $m_u, m_d \rightarrow 0$ . In this

---

<sup>1</sup>Here, the masses of up, down and strange quark are estimates of the so-called current quark masses in the  $\overline{\text{MS}}$  scheme at a renormalisation scale of  $\mu = 2 \text{ GeV}$ . The masses of charm and bottom quarks are the “running” masses in the  $\overline{\text{MS}}$  scheme. The mass of the top quark was obtained from direct measurements [110].

so-called chiral limit, the Lagrangian reduces to the simple form

$$\mathcal{L}_{\text{QCD}}^0 = -\frac{1}{4} \mathcal{G}_a^{\mu\nu} \mathcal{G}_{a,\mu\nu} + \bar{q} i \not{D} q, \quad (1.6)$$

where  $q = (u, d)$ . Now we define the chirality matrix

$$\gamma^5 = \gamma_5 = i \gamma^0 \gamma^1 \gamma^2 \gamma^3, \quad (1.7)$$

which fulfills

$$\{\gamma^\mu, \gamma^5\} = 0 \quad \text{and} \quad \gamma_5^2 = \mathbb{1}, \quad (1.8)$$

and the left- and right-handed quark fields

$$q_{L/R} = P_{L/R} q = \frac{1}{2} (\mathbb{1} \mp \gamma^5) q \quad (1.9)$$

with the projection operators  $P_{L/R}$ , which obey

$$P_{L/R}^2 = P_{L/R} \quad \text{and} \quad P_L + P_R = \mathbb{1}. \quad (1.10)$$

We observe that the quark part of the Lagrangian separates into two independent parts

$$\mathcal{L}_{\text{QCD}}^0 = -\frac{1}{4} \mathcal{G}_a^{\mu\nu} \mathcal{G}_{a,\mu\nu} + \bar{q}_L i \not{D} q_L + \bar{q}_R i \not{D} q_R \quad (1.11)$$

such that it is invariant under separate rotations of the left- and right-handed fields

$$q_L \rightarrow V_L q_L, \quad q_R \rightarrow V_R q_R \quad \text{with} \quad V_L, V_R \in \text{U}(2), \quad (1.12)$$

which is an additional symmetry – the so-called chiral symmetry – compared to our starting point eq. (1.1). It is analogous to

$$\text{U}(2)_L \times \text{U}(2)_R \rightarrow \text{SU}(2)_L \times \text{SU}(2)_R \times \text{U}(1)_V \times \text{U}(1)_A, \quad (1.13)$$

where  $V = L + R$  and  $A = L - R$  are operations from  $V \in \text{U}(1)_V$ ,  $A \in \text{U}(1)_A$ ,  $L \in \text{U}(1)_L$  and  $R \in \text{U}(1)_R$ . The  $\text{U}(1)_V$  symmetry can be interpreted as the baryon number conservation, whereas the  $\text{U}(1)_A$  symmetry is anomalously broken, thus only present in the classical theory and broken by quantum effects [111].

The  $\text{SU}(2)_L \times \text{SU}(2)_R$  (chiral) symmetry is crucial for the construction of chiral perturbation theory (ChPT), the EFT for QCD, which is discussed in the next chapter. From the Noether theorem, it is known that each continuous symmetry is associated with a conserved quantity, the so-called Noether currents, which are in this case

$$J_{L/R}^{\mu,a} = \bar{q}_{L/R} \gamma^\mu \frac{\tau^a}{2} q_{L/R}. \quad (1.14)$$

The associated conserved charges

$$Q_{L/R}^a = \int d^3x J_{L/R}^{0,a} \quad (1.15)$$

satisfy the Lie algebra of  $SU(2)$

$$[Q_{L/R}^a, Q_{L/R}^b] = i\varepsilon^{abc} Q_{L/R}^c, \quad [Q_{L/R}^a, Q_{R/L}^b] = 0 \quad (1.16)$$

and are the group generators of  $SU(2)_L$  and  $SU(2)_R$ . They also can be related to vector and axial vector charges

$$Q_V^a = Q_L^a + Q_R^a, \quad Q_A^a = Q_L^a - Q_R^a, \quad (1.17)$$

which will be used in the next section.

Finally, we want to note that in nature the masses of up- and down-quark are small, but *nonzero*. Thus, the chiral symmetry is explicitly broken by the mass term of the Lagrangian

$$\bar{q}Mq = \bar{q}_L M q_R + \bar{q}_R M q_L, \quad (1.18)$$

but due to the smallness of  $u$ - and  $d$ -quark masses, it remains approximately realised. Thus, the QCD Lagrangian in the case of two quarks consists of a chiral invariant and a chiral symmetry breaking part

$$\mathcal{L}_{QCD} = \mathcal{L}_{QCD}^0 + \mathcal{L}_{SB} \quad \text{with} \quad \mathcal{L}_{SB} = -(m_u \bar{u}u + m_d \bar{d}d). \quad (1.19)$$

In the case of equal quark masses  $m_u = m_d = m_q$ , the mass term exhibits an additional invariance under a rotation  $q \rightarrow V_I q$ ,  $V_I \in SU(2)$

$$\bar{q}Mq = m_q \bar{q}q = m_q(\bar{u}u + \bar{d}d) \quad (1.20)$$

which is called isospin symmetry and is a widely used simplification. It leads to equal pion masses, which is a convenient simplification and still quite accurate. In nature, isospin symmetry is explicitly broken, because the up and down quark have slightly different masses. Rearranging the symmetry breaking term of eq. (1.19) yields

$$\mathcal{L}_{SB} = -(m_u \bar{u}u + m_d \bar{d}d) = -\frac{1}{2}(m_u + m_d)(\bar{u}u + \bar{d}d) - \frac{1}{2}(m_u - m_d)(\bar{u}u - \bar{d}d), \quad (1.21)$$

in which the second term of the RHS explicitly shows the violation of isospin symmetry in the case  $m_u \neq m_d$ . Throughout this work, we apply the isospin symmetric formulation, because isospin-breaking corrections are beyond our aimed accuracy.

## 1.2 Spontaneous symmetry breaking

Through experimental evidence it became clear that the chiral symmetry has to break down spontaneously, that means instead of being realised in the Wigner-Weyl mode, in which the vacuum is invariant under the charges

$$Q_V^a |0\rangle = 0, \quad Q_A^a |0\rangle = 0 \quad (1.22)$$

it is strongly indicated that it is realised in the Nambu-Goldstone mode, in which the chiral symmetry is broken down to its parity conserving subset

$$Q_V^a |0\rangle = 0, \quad Q_A^a |0\rangle \neq 0. \quad (1.23)$$

Support for this assumption is given by the fact that one has not found baryons with negative parity in the low-energy hadron spectrum [110]. A consequence of the realisation in the Nambu-Goldstone mode is that according to the Goldstone theorem [112], we expect for every generator, which does not leave the vacuum invariant, one massless Goldstone boson. These Goldstone bosons share the quantum numbers of the broken generators and can be identified with the three pions ( $\pi^+, \pi^0, \pi^-$ ), which are pseudoscalar mesons. The nonzero, but small masses of the pions

$$M_{\pi^\pm} = 139.57 \text{ MeV}, \quad M_{\pi^0} = 134.98 \text{ MeV} \quad (1.24)$$

are due to the explicit breaking of the chiral symmetry through the nonzero quark masses. However, pions are still very light  $M_\pi \ll 1 \text{ GeV}$  compared to nucleons.

Finally, let us point out an important consequence of the Goldstone theorem. At low energies, the interaction between the mesons (pseudo-Goldstone bosons) becomes weak and tends to zero. This is in contrast to the coupling of the QCD degrees of freedom – quarks and gluons –, which becomes stronger at low energies. This behaviour enables to treat the interaction of the pions in terms of a perturbative series in the small coupling constant at low energies, which is the idea of the EFT. Instead of calculating observables directly from QCD, an effective theory for the interaction of pions and nucleons is constructed, to which perturbation theory can be applied.



## 2 Chiral Perturbation Theory

Effective field theories (EFTs) have emerged as approximations to underlying physical theories. The EFT for the strong interaction in the low-energy region is called chiral perturbation theory (ChPT). In this chapter, we focus on the parts of ChPT which are relevant for pion photoproduction and refer the reader for more detail to other works, e.g. to the book of S. Scherer and M. Schindler [113]. First, we give some general remarks on EFTs, followed by the introduction of ChPT for pions. Subsequently, we show how to consistently include nucleons and deltas employing two commonly used schemes, the covariant and heavy baryon (HB) approach.

### 2.1 Effective field theory

An effective field theory is a model to a fundamental theory, which is obtained by constructing the most general Lagrangian sharing all symmetries of the fundamental theory. This idea was first developed by Weinberg [23], who described the construction of an EFT as follows:

*“If one writes down the most general possible Lagrangian, including all terms consistent with assumed symmetry principles, and then calculates matrix elements with this Lagrangian to any given order of perturbation theory, the result will simply be the most general possible S-matrix consistent with analyticity, perturbative unitarity, cluster decomposition and the assumed symmetry principles.”*

Calculating observables using an EFT sometimes allows one to obtain results in a energy region in which standard perturbative methods are too complicated or not applicable at all. One crucial difference between a fundamental theory and the corresponding EFT is the range of validity. By construction, an EFT is restricted to low energies, where the term “low” indicates that the interaction is considered below an energy scale  $\Lambda_b$ . Only the degrees of freedom below the scale enter the EFT explicitly, whereas those beyond  $\Lambda_b$  are only implicitly taken into account and integrated out of the action. In the case of ChPT, only the hadrons consisting of the lightest quarks are used. The two common conventions are SU(3) ChPT, which incorporates the three lightest quarks ( $u, d, s$ ) as dynamic degrees of freedom, and SU(2) ChPT, which only takes into account the ( $u, d$ ) quark doublet. In this work we restrict ourselves to the SU(2) version.

Another difference between EFT and fundamental theory is that the effective Lagrangian contains in general infinitely many terms. To be able to calculate observables using only a finite number of contributions, one restricts the validity of the EFT further to the region below a second energy scale  $\Lambda_0 < \Lambda_b$  and expands observables in terms of the quotient  $\Lambda_0/\Lambda_b$ . The

smaller  $\Lambda_0$ , the faster the expansion parameter  $(\Lambda_0/\Lambda_b)^n$  decreases and less terms need to be taken into account to obtain results at the desired accuracy. Naturally, the question arises which of the infinitely many terms are more important than others. This issue is addressed by the so-called power counting, which will be discussed in more detail in the next sections.

Finally, every term in the Lagrangian of the EFT is multiplied by a parameter, the low-energy constant (LEC). The numerical values of these constants are unique, but initially unknown, because the symmetries of the fundamental theory only constrain the analytic structure of the Lagrangian terms, but not their prefactors. In principle, the numerical values of LECs can be determined from the underlying theory. If this is impossible in the region of interest, such as in the case of QCD, the LECs can be fitted to experimental data. Once all LECs are determined up to a specific working order, the EFT enables the prediction of new results.

## 2.2 ChPT for pions

The starting point for an EFT describing the interaction of pions is the QCD Lagrangian in the presence of external sources  $s, p, v_\mu, a_\mu$  [25]

$$\mathcal{L}^{\text{QCD}}(G_\mu, q, \bar{q}, s, p, v_\mu, a_\mu) = \mathcal{L}_0^{\text{QCD}} + \bar{q}(\not{p} + \not{d}\gamma_5 - s + i p)q. \quad (2.1)$$

Here,  $s$  is a scalar,  $p$  is a pseudoscalar,  $v_\mu$  is a vector and  $a_\mu$  is an axial-vector source. Then, the generating functional of QCD can be associated with a similar functional of an low-energy effective field theory

$$\begin{aligned} & \mathcal{W}[s, p, v_\mu, a_\mu] \Big|_{\text{low energy}} \\ &= \int [DG_\mu][Dq][D\bar{q}] \exp \left\{ i \int d^4x \mathcal{L}^{\text{QCD}}(G_\mu, q, \bar{q}, s, p, v_\mu, a_\mu) \right\} \Big|_{\text{low energy}} \\ &\equiv \mathcal{N} \int [DU] \exp \left\{ i \int d^4x \mathcal{L}^{\text{eff}}(U, s, p, v_\mu, a_\mu) \right\} \end{aligned} \quad (2.2)$$

and matrix elements can be calculated by functional differentiation with respect to the external sources. According to Weinberg [23], the effective Lagrangian  $\mathcal{L}_{\text{eff}}$  in the low-energy limit can be expressed as an expansion in terms of quark masses and of derivatives of the pion field

$$\mathcal{L}_{\pi\pi}^{\text{eff}} = \sum_n \mathcal{L}_{\pi\pi}^{(n)} = \mathcal{L}_{\pi\pi}^{(0)} + \mathcal{L}_{\pi\pi}^{(2)} + \mathcal{L}_{\pi\pi}^{(4)} + \dots, \quad (2.3)$$

where  $n$  is the so-called chiral order, which must be even due to Lorentz invariance and corresponds to the number of derivatives and/or quark masses in a given term. To construct the leading terms of the effective Lagrangian, we first cluster the pion fields  $\pi_i(x)$  in a unitary

matrix<sup>1</sup>

$$U(x) = \exp\left\{i \frac{\boldsymbol{\tau} \cdot \boldsymbol{\pi}}{F}\right\} = \mathbb{1} + i \frac{\boldsymbol{\tau} \cdot \boldsymbol{\pi}}{F} - \frac{\boldsymbol{\pi}^2}{2F^2} + \dots, \quad (2.4)$$

where  $F$  is the pion decay constant, the Cartesian fields  $\pi_i$  are related to the physical pion fields  $\pi^{\pm,0}$  via

$$\boldsymbol{\tau} \cdot \boldsymbol{\pi} = \begin{pmatrix} \pi_3 & \pi_1 - i\pi_2 \\ \pi_1 + i\pi_2 & -\pi_3 \end{pmatrix} \equiv \begin{pmatrix} \pi^0 & \sqrt{2}\pi^+ \\ \sqrt{2}\pi^- & -\pi^0 \end{pmatrix} \quad (2.5)$$

and  $\tau_i$  are the Pauli matrices in isospin space. The form (2.4) of  $U(x)$  is not the most general form constrained by unitarity, but it can be obtained by fixing unphysical off-shell parameters and thus it is legitimate to stick to the choice above<sup>2</sup>.

To write down the lowest orders of the pionic Lagrangian one constructs all possible terms invariant under the group transformation up to the order of interest. For the lowest order ( $n = 0$ ), there is only one invariant structure  $\text{Tr}(UU^\dagger)$ , but due to unitarity of  $U(x)$ , this is a constant and thus irrelevant for physical observables. The most general Lagrangian of the order  $n = 2$  reads

$$\mathcal{L}_{\pi\pi}^{(2)} = \frac{F^2}{4} \text{Tr} \left( \nabla_\mu U \nabla^\mu U^\dagger \right) + \frac{F^2}{4} \text{Tr} \left( \chi U^\dagger + U \chi^\dagger \right), \quad (2.6)$$

with “Tr” referring to the trace in isospin space. The covariant derivative on the pion field  $\nabla_\mu$  is defined as

$$\nabla_\mu U = \partial_\mu U - i r_\mu U + i U l_\mu \quad (2.7)$$

with

$$l_\mu = v_\mu - a_\mu \quad \text{and} \quad r_\mu = v_\mu + a_\mu \quad (2.8)$$

and

$$\chi = 2B_0(s + ip). \quad (2.9)$$

The constants  $F$  and  $B_0$  are related to the vacuum expectation value of the scalar quark density via

$$\langle 0 | \bar{q} q | 0 \rangle = -F_\pi^2 B_0 (1 + \mathcal{O}(m_q)). \quad (2.10)$$

Note the differentiation of  $F$  and  $F_\pi$ :  $F$  is a bare parameter, whereas the physical quantity  $F_\pi$  is obtained after a renormalisation procedure of  $F$  (see sec. 3.5).

---

<sup>1</sup>Throughout this work, four-vectors are printed normal, three-vectors are printed bold.

<sup>2</sup>For actual calculations, we used a more general parametrisation, given in eq. (3.71). For an even more general form of  $U(x)$ , see e.g. appendix A of ref. [114].

Next, the chiral symmetry breaking terms generated by the nonzero quark masses are included. This can easily be achieved by interpreting them as a scalar external source

$$s = \mathcal{M} = \begin{pmatrix} m_u & 0 \\ 0 & m_d \end{pmatrix}, \quad (2.11)$$

which transforms eq. (2.6) to

$$\mathcal{L}_{\pi\pi}^{(2)} = \frac{F^2}{4} \text{Tr} \left( \nabla_\mu U \nabla^\mu U^\dagger \right) + \frac{F^2 B_0}{2} \text{Tr} \left( \mathcal{M} U^\dagger + U \mathcal{M} \right). \quad (2.12)$$

For a clearer understanding, let us show which types of interactions of the pions and the external fields are generated by the Lagrangian. Therefore, we replace the vector source by  $v_\mu = -eQ A_\mu = -e\frac{1+\tau_3}{2}A_\mu$  to include photons with  $A_\mu$  being the vector field,  $e$  the electric charge and  $Q$  the charge matrix. Using the expansion of the field  $U$  (eq. (2.4)), setting the pseudoscalar and the axial source to zero, eq. (2.6) can be rewritten:

$$\begin{aligned} \mathcal{L}_{\pi\pi}^{(2)} = & \frac{1}{2} [\partial_\mu \boldsymbol{\pi} \cdot \partial^\mu \boldsymbol{\pi} - B_0 \text{Tr}(\mathcal{M}) \boldsymbol{\pi}^2] + e A_\mu (\boldsymbol{\pi}_a \cdot \partial^\mu \boldsymbol{\pi}_b) \varepsilon_{3ab} + \frac{1}{2} e^2 A^2 (\boldsymbol{\pi}^2 - \pi_3^2) \\ & + \mathcal{O}(\boldsymbol{\pi}^4, A^3). \end{aligned} \quad (2.13)$$

Now, it can be seen that the second term  $\sim A_\mu (\boldsymbol{\pi} \cdot \partial^\mu \boldsymbol{\pi})$  generates a Feynman rule with two pions and one photon, whereas the third term corresponds to a two-pion-two-photon interaction. From eq. (2.13), we also read off the leading order pion mass

$$M^2 = B_0 \text{Tr}(\mathcal{M}) = B_0(m_u + m_d). \quad (2.14)$$

Although the light quark masses are slightly different in nature, we work in the isospin symmetric case  $m_q = m_u = m_d$ , so that the pion mass further simplifies to  $M^2 = 2B_0m_q$ . From the two-point function of  $\mathcal{L}_{\pi\pi}^{(2)}$  we deduce the pion propagator

$$\mathcal{G}_\pi(q) = \frac{i}{q^2 - M^2}. \quad (2.15)$$

The next-to-leading pionic Lagrangian was constructed by Gasser and Leutwyler [24]. From ten terms we only give the three which are relevant for pion photoproduction:

$$\begin{aligned} \mathcal{L}_{\pi\pi}^{(4)} = & \frac{l_3}{16} \text{Tr}(\chi_+)^2 \\ & + \frac{l_4}{16} \left( 2 \text{Tr}(\nabla_\mu U (\nabla^\mu U)^\dagger) \text{Tr}(\chi_+) + \text{Tr}(2((\chi U^\dagger)^2 + (U \chi^\dagger)^2) - 4\chi^\dagger \chi - \chi_-^2) \right) \\ & + i \frac{l_6}{2} \text{Tr} \left( F_{R,\mu\nu} \nabla^\mu U (\nabla^\nu U)^\dagger + F_{L,\mu\nu} (\nabla^\mu U)^\dagger \nabla^\nu U \right). \end{aligned} \quad (2.16)$$

The notation is

$$\chi_\pm = u^\dagger \chi u^\dagger \pm u \chi^\dagger u,$$

$$\begin{aligned} F_L^{\mu\nu} &= \partial^\mu l^\nu - \partial^\nu l^\mu - i[l^\mu, l^\nu], \\ F_R^{\mu\nu} &= \partial^\mu r^\nu - \partial^\nu r^\mu - i[r^\mu, r^\nu] \end{aligned} \quad (2.17)$$

and the pion field  $U(x)$  is related to  $u(x) = \sqrt{U(x)}$ .

Since the effective Lagrangian may contain an infinite number of terms, it is vital to systematically assess the importance of individual terms in the Lagrangian and of Feynman diagrams without explicitly calculating them. To accomplish this task, Weinberg [23] introduced the so-called power counting. According to this method, one assigns to every Feynman diagram a so-called chiral dimension

$$D = 2 + 2L + \sum_d (2d - 2)V_{2d}, \quad (2.18)$$

which can be simply read off from the topology of the Feynman graph. In the above expression,  $L$  is the number of loops and  $V_{2d}$  is the number of vertices arising from  $\mathcal{L}_{\pi\pi}^{(2d)}$ , so that  $D \geq 2$  holds and only a finite number of diagrams contributes to a specific chiral order. All topologies with  $D = 2$  are of tree type, and loop diagrams start to contribute from  $D = 4$ . The fact that each loop increases the chiral dimension by 2 can be seen from the naive counting that every loop comes with a factor  $q^2/(4\pi F)^2$ . Numerically,  $4\pi F$  is of the same size as  $\Lambda_b$ , where  $\Lambda_b \approx 1 \text{ GeV}$  is the breaking scale of ChPT. Consequently, observables can be arranged in a series of the small parameter

$$q \in \left\{ \frac{M}{\Lambda}, \frac{k}{\Lambda} \right\} \quad \text{with} \quad \Lambda \in \{\Lambda_b, 4\pi F\}, \quad (2.19)$$

which converges fast if the pion momentum  $k$  is restricted to low energies  $k \ll \Lambda$ . So  $D$  is the power of  $q$  in a considered diagram, which means that topologies with a lower chiral dimension provide the largest contributions to the series.

## 2.3 Including the nucleon

Next, we discuss how to include the nucleon into the effective field theory. In the history of ChPT, this was a problem at first, because the nucleon mass is an additional large scale, which does not vanish in the chiral limit. The problem and its standard solutions are explained in the following.

### 2.3.1 Covariant approach

In the  $SU(2)$  formulation of ChPT, the only two baryons of interest are the proton ( $p$ ) and neutron ( $n$ ). These fields can be combined in an isodoublet representation

$$\Psi_N = \begin{pmatrix} p \\ n \end{pmatrix}, \quad (2.20)$$

where  $p$  and  $n$  both are four-component Dirac fields. Constructing the lowest-order Lagrangian is similar to the construction of the pure mesonic case: invariant structures under the group transformation must be formed based on extending the counting rules of eq. (2.19) with

$$\frac{p_0}{\Lambda} \sim \frac{m}{\Lambda} \sim \mathcal{O}(1) \quad \text{and} \quad \frac{|\mathbf{p}|}{\Lambda} \sim \frac{p_0 - m}{\Lambda} \sim \mathcal{O}(q^1), \quad (2.21)$$

where  $p = (p_0, \mathbf{p})$ .

The leading order pion-nucleon Lagrangian reads (see e.g. ref. [115])

$$\mathcal{L}_{\pi N}^{(1)} = \bar{\Psi}_N \left( i \not{D} - m + \frac{g_A}{2} \not{\psi} \gamma_5 \right) \Psi_N, \quad (2.22)$$

with the definitions of the chiral vielbein  $u_\mu$  and the covariant derivative  $D_\mu$  acting on the nucleon field

$$\begin{aligned} u_\mu &= i(u^\dagger(\partial_\mu - i r_\mu)u - u(\partial_\mu - i l_\mu)u^\dagger), \\ D_\mu &= \partial_\mu - \Gamma_\mu, \end{aligned} \quad (2.23)$$

where

$$\Gamma_\mu = \frac{1}{2} \left\{ u^\dagger(\partial_\mu - i r_\mu)u + u(\partial_\mu - i l_\mu)u^\dagger \right\}, \quad (2.24)$$

is the so-called chiral connection. The bare nucleon mass  $m$  and the bare axial pion-nucleon coupling constant  $g_A$  are related via a renormalisation procedure to their corresponding physical constants  $m_N$  and  $g_A$  (see sec. 3.5.1). The Lagrangian of second order reads [115]

$$\begin{aligned} \mathcal{L}_{\pi N}^{(2)} = \bar{\Psi}_N &\left\{ c_1 \text{Tr}(\chi_+) - \frac{c_2}{8m^2} (\text{Tr}(u_\mu u_\nu) D^{\mu\nu} + \text{h.c.}) + \frac{c_3}{2} \text{Tr}(u \cdot u) \right. \\ &\left. + i \frac{c_4}{4} [u_\mu, u_\nu] \sigma^{\mu\nu} + c_5 \tilde{\chi}_+ + \frac{c_6}{8m} F_{\mu\nu}^+ \sigma^{\mu\nu} + \frac{c_7}{8m} \text{Tr}(F_{\mu\nu}^+) \sigma^{\mu\nu} \right\} \Psi_N. \end{aligned} \quad (2.25)$$

Here, the new field combination

$$F_{\mu\nu}^\pm = u^\dagger F_{\mu\nu}^R u \pm u F_{\mu\nu}^L u^\dagger, \quad (2.26)$$

is introduced and  $\sigma^{\mu\nu} = \frac{i}{2} [\gamma^\mu, \gamma^\nu]$  is the antisymmetric tensor of the Dirac matrices. Note that in the case of pion photoproduction, only the terms with  $c_6$  and  $c_7$  are relevant. Strictly speaking, the constant  $c_1$  also contributes to the nucleon mass, but is fully removed after renormalisation.

The Lagrangian of third order has 23 independent terms, of which we only give those which are relevant for pion photoproduction [115]

$$\mathcal{L}_{\pi N}^{(3)} = \bar{\Psi}_N \left\{ \frac{d_6}{2m} (i [D^\mu, \tilde{F}_{\mu\nu}^+] D^\nu + \text{h.c.}) + \frac{d_7}{2m} (i [D^\mu, \text{Tr}(F_{\mu\nu}^+)] D^\nu + \text{h.c.}) \right\}$$

$$\begin{aligned}
& + \frac{d_8}{2m} (\mathrm{i} \varepsilon^{\mu\nu\alpha\beta} \mathrm{Tr}(\tilde{F}_{\mu\nu}^+ u_\alpha) D_\beta + \mathrm{h.c.}) + \frac{d_9}{2m} (\mathrm{i} \varepsilon^{\mu\nu\alpha\beta} \mathrm{Tr}(F_{\mu\nu}^+) u_\alpha D_\beta + \mathrm{h.c.}) \\
& + \frac{d_{16}}{2} \gamma^\mu \gamma_5 \mathrm{Tr}(\chi_+) u_\mu + \mathrm{i} \frac{d_{18}}{2} \gamma^\mu \gamma_5 [D_\mu, \chi_-] \\
& - \frac{d_{20}}{8m^2} (\mathrm{i} \gamma^\mu \gamma_5 [\tilde{F}_{\mu\nu}^+, u_\alpha] D^{\alpha\nu} + \mathrm{h.c.}) + \mathrm{i} \frac{d_{21}}{2} \gamma^\mu \gamma_5 [\tilde{F}_{\mu\nu}^+, u^\nu] \\
& + \frac{d_{22}}{2} \gamma^\mu \gamma_5 [D^\nu, F_{\mu\nu}^-] \Big\} \Psi_N,
\end{aligned} \tag{2.27}$$

with

$$\tilde{F}_{\mu\nu}^\pm = F_{\mu\nu}^\pm - \frac{1}{2} \mathrm{Tr}(F_{\mu\nu}^\pm). \tag{2.28}$$

We use the convention  $\varepsilon^{0123} = -1$ .

The nucleon propagator deduced from the lowest-order Lagrangian is

$$\mathcal{G}_N(p) = \frac{\mathrm{i}}{\not{p} - m} = \frac{\mathrm{i}(\not{p} + m)}{p^2 - m^2}. \tag{2.29}$$

As mentioned above, the introduction of nucleons to ChPT makes power counting more complicated, because the nucleon mass is an additional large scale besides  $\Lambda_b$ . In loop graphs, the nucleon mass gives rise to so-called power-counting violating terms (PCVTs)<sup>3</sup>, which spoil the assignment of an analogous chiral dimension to a diagram as in eq. (2.18). This leads to the problem that one would need an infinite number of loop diagrams to work beyond tree-level.

Nowadays, there are several strategies to systematically include nucleons into ChPT and to maintain a consistent power counting. The first solution, the so-called heavy baryon (HB) scheme, which was developed by Jenkins and Manohar [116] and by Bernard et al. [81], was inspired by heavy quark physics. The idea is to expand the covariant Lagrangian around the extreme nonrelativistic limit, thus assuming the nucleons to be very slow and heavy. The result is that the nucleon mass dependence is shifted to a series of additional contact interactions, organised in powers of  $1/m$ . In this scheme, the nucleon mass never appears in the numerator of any Feynman diagram. Therefore, eq. (2.19) is modified to

$$q \in \left\{ \frac{M}{\Lambda}, \frac{k}{\Lambda} \right\} \quad \text{with} \quad \Lambda \in \{\Lambda_b, 4\pi F, m\}, \tag{2.30}$$

where  $k$  now is an arbitrary three-momentum (of a meson or a baryon), and the chiral dimension for a diagram including nucleons reads

$$D = 2 + 2L + \sum_d (2d - 2)V_{2d}^M + \sum_d (d - 1)V_d^B, \tag{2.31}$$

---

<sup>3</sup>An example of the PCVTs and how to calculate them is presented in section 3.5.2.

where  $V_d^B$  is the number of vertices with baryons from  $\mathcal{L}_{\pi N}^d$  and we added the superscript  $M$  to  $V_{2d}$  to indicate that this vertex involves only mesons.

The first manifestly Lorentz invariant way to solve the power-counting problem was given by Becher and Leutwyler [90, 93], the so-called infrared regularisation. The original formulation of this scheme is in practice cumbersome to apply, because some nontrivial integrals must be solved. In a subsequent work [117], the infrared regularisation scheme was reformulated in a way which is better suited for practical calculations.

A more recently developed method, which we use in this work, is the extended-on-mass-shell scheme (EOMS), first described by Fuchs, Japaridze, Gegelia and Scherer [91, 92]. The idea of this scheme is to subtract the PCVT and shift lower-order LECs in such a way that the correspondence between naive order and explicitly counted order is restored and consequently, the power counting defined by eq. (2.31) can be applied. However, in this case eq. (2.31) is to be understood in such a way that a diagram assigned with the chiral dimension  $D$  includes terms of order  $D$  and higher. This is due to the higher-order  $1/m$ -corrections to the nucleon propagator, which are still included in this renormalisation scheme. In the HB formalism, the assignment of a chiral dimension to a Feynman diagram is exact.

### 2.3.2 Heavy baryon formalism

In the heavy baryon formalism, the nucleon momentum is split according to

$$p_\mu = mv_\mu + P_\mu, \quad (2.32)$$

where the first part is a large piece close to the on-shell kinematics and the second part  $P_\mu$  is a soft residual contribution  $v \cdot P \ll m$ . The vector  $v_\mu$  is the four-velocity of the nucleon with the properties  $v^2 = 1$ ,  $v^0 \geq 1$  and can be conveniently chosen as  $v = (1, 0, 0, 0)$ . This leaves us with the relation for the soft residual contribution for a nucleon on its mass shell ( $p^2 = m_N^2$ )

$$v \cdot P = P^0 = p^0 - m_N = -\frac{P^2}{2m_N} = -\frac{(v \cdot P)^2 - \mathbf{P}^2}{2m_N}, \quad (2.33)$$

generating a  $1/m_N$  expansion for  $v \cdot P$  after iteratively applying the relation. The nucleon field  $\Psi_N$  is split into the so-called light and heavy fields

$$N_v(x) = e^{imv \cdot x} P_v^+ \Psi_N(x) \quad \text{and} \quad h_v(x) = e^{imv \cdot x} P_v^- \Psi_N(x), \quad (2.34)$$

which are eigenstates of  $\psi$ . The projectors are given by

$$P_v^\pm = \frac{1}{2}(\mathbb{1} \pm \psi) \quad (2.35)$$

and satisfy the usual projector properties

$$P_v^+ + P_v^- = \mathbb{1}, \quad (P_v^\pm)^2 = P_v^\pm, \quad P_v^+ P_v^- = P_v^- P_v^+ = 0. \quad (2.36)$$

For the standard choice of  $v$  and the  $\gamma$  matrices in the Dirac basis, the operators take the simple form

$$P_v^+ = \begin{pmatrix} \mathbb{1} & 0 \\ 0 & 0 \end{pmatrix} \quad \text{and} \quad P_v^- = \begin{pmatrix} 0 & 0 \\ 0 & \mathbb{1} \end{pmatrix}, \quad (2.37)$$

which shows together with eq. (2.34) that the fields  $N$  and  $h$  are equivalent to the upper and lower components of a Dirac spinor, respectively (or to positive and negative energy solutions). The heavy field  $h$  can be integrated out of the action [118] such that the effective Lagrangian only contains the light field  $N$ . Before turning to the effective Lagrangian, we also remark that the heavy mass formulation has the advantage that the Dirac algebra becomes very simple. Any bilinear  $\bar{\Psi}\Gamma\Psi$  with  $\Gamma \in \{\mathbb{1}, \gamma_5, \gamma_\mu, \gamma_5\gamma_\mu, \sigma_{\mu\nu}\}$  can be expressed in terms of the velocity  $v^\mu$  and the Pauli-Lubanski spin vector

$$S_\mu = \frac{i}{2} \gamma_5 \sigma_{\mu\nu} v^\nu, \quad (2.38)$$

which obeys

$$S \cdot v = 0, \quad S^2 = \frac{1-d}{4}, \quad \{S_\mu, S_\nu\} = \frac{1}{2}(v_\mu v_\nu - g_{\mu\nu}), \quad [S_\mu, S_\nu] = i \epsilon_{\mu\nu\alpha\beta} v^\alpha S^\beta \quad (2.39)$$

in  $d$  spacetime dimensions. The relevant terms of the Lagrangians up to third order read [115]

$$\begin{aligned} \hat{\mathcal{L}}_{\pi N}^{(1)} &= \bar{N} (i v \cdot D + g S \cdot u) N, \\ \hat{\mathcal{L}}_{\pi N}^{(2)} &= \bar{N} \left( -\frac{i}{4m} [\hat{c}_6 [S^\mu, S^\nu] F_{\mu\nu}^+ + \hat{c}_7 [S^\mu, S^\nu] \text{Tr}(F_{\mu\nu}^+)] \right) N \\ &\quad + \frac{1}{2m} \bar{N} ((v \cdot D)^2 - D^2 - i g_A \{S \cdot D, v \cdot u\}) N, \\ \hat{\mathcal{L}}_{\pi N}^{(3)} &= \bar{N} \left( \hat{d}_6 [D^\mu, \tilde{F}_{\mu\nu}^+] v^\nu + \hat{d}_7 [D^\mu, \text{Tr}(F_{\mu\nu}^+)] v^\nu \right. \\ &\quad + \hat{d}_8 \text{Tr}(\tilde{F}_{\mu\nu}^+ u_\alpha) \epsilon^{\mu\nu\alpha\beta} v_\beta + \hat{d}_9 \text{Tr}(F_{\mu\nu}^+) u_\alpha \epsilon^{\mu\nu\alpha\beta} v_\beta \\ &\quad + \hat{d}_{16} S \cdot u \text{Tr}(\chi_+) + i \hat{d}_{18} [S \cdot D, \chi_-] + i \hat{d}_{20} S^\mu v^\nu [\tilde{F}_{\mu\nu}^+, v \cdot u] \\ &\quad \left. + i \hat{d}_{21} S^\mu [\tilde{F}_{\mu\nu}^+, u^\nu] + \hat{d}_{22} S^\mu [D^\nu, F_{\mu\nu}^-] \right) N. \end{aligned} \quad (2.40)$$

First, note that the second line in  $\hat{\mathcal{L}}_{\pi N}^{(2)}$  contains the  $1/m$  corrections from  $\hat{\mathcal{L}}_{\pi N}^{(1)}$ . The prefactor of  $1/m$  in the  $c_i$  parts in  $\hat{\mathcal{L}}_{\pi N}^{(2)}$  should not be interpreted as a  $1/m$  correction; it originates from the definition of the constants  $\hat{c}_6$  and  $\hat{c}_7$ , which are dimensionless when defined this way. Unlike the usual treatment in the literature, we from now on consider the  $1/m$  corrections as of two orders higher, so associating them with the third instead of second order. This is a common practice in studies of the nuclear forces [32] and is referred to as  $NN$  counting in this work.

Second, the heavy baryon LECs  $\hat{c}_i$  and  $\hat{d}_i$  are in general not the same as the covariant constants  $c_i$  and  $d_i$ , but they are related via  $1/m$ -shifts, which read [118]:

$$\begin{aligned}\hat{c}_6 &= c_6 + 1, \quad \hat{c}_7 = c_7, \\ \hat{d}_6 &= d_6 - \frac{1}{16m^2}(1 + 2c_6), \quad \hat{d}_7 = d_7 - \frac{1}{8m^2}c_7, \quad \hat{d}_8 = d_8 + \frac{1}{64m^2}\hat{g}_A^\circ, \quad \hat{d}_9 = d_9 + \frac{1}{64m^2}\hat{g}_A^\circ, \\ \hat{d}_{16} &= d_{16}, \quad \hat{d}_{18} = d_{18}, \quad \hat{d}_{20} = d_{20} + \frac{1}{8m^2}\hat{g}_A^\circ(1 + c_6), \quad \hat{d}_{21} = d_{21}, \quad \hat{d}_{22} = d_{22}. \end{aligned}\tag{2.41}$$

Because the constants  $c_6$  and  $c_7$  from the covariant Lagrangian also appear with a prefactor of  $1/m$ , the constants  $c_6$  and  $\hat{c}_6$  as well as  $c_7$  and  $\hat{c}_7$  have the same mass dimension. The  $1/m$ -corrections to the  $d$ -constants are only given for the sake of completeness, we do not need them because the corrections are beyond our working order.

Finally, the HB nucleon propagator takes the simple form

$$\hat{\mathcal{G}}_N(P) = \frac{i}{v \cdot P} P_v^+, \tag{2.42}$$

where  $P$  is the residual part of the nucleon momentum as in eq. (2.32). By construction, the HB scheme encounters no PCVT and thus a Feynman diagram including mesonic and baryonic vertices fulfills the chiral dimension of eq. (2.31).

## 2.4 Including the delta

As seen in the last section, introducing nucleons into ChPT was not straightforward. The same holds for the introduction of heavier particles, but fortunately, the solution proceeds in close analogy to the nucleonic case. Initially, it was assumed that the baryon resonances are very heavy compared to the nucleon. While this approach might be helpful for first calculations and reasonable in the case of heavier resonances, e.g. the Roper resonance ( $m_R \approx 1370$  MeV [110]), it is questionable in the case of the delta resonance ( $m_\Delta \approx 1210$  MeV [110]), which only lies approximately 300 MeV above the nucleon mass. Furthermore, the delta couples strongly to the  $\pi N$  sector, thus it can be expected that it gives rise to relevant contributions also close to the pion photoproduction reaction threshold. In this section, we therefore discuss how to include the delta as an explicit degree of freedom into the theory.

### 2.4.1 Covariant approach

The delta is a particle with both spin and isospin 3/2. In the spin space, each of the physical states can be described by a Rarita-Schwinger field  $\Delta_\mu$  [119], which is constructed by coupling a spin-1 to a spin-1/2 field. This product has 16 degrees of freedom, whereas one expects a spin-3/2 field to have eight. The redundant degrees of freedom are removed by the two

subsidiary conditions

$$\gamma_\mu \Delta^\mu = 0 \quad \text{and} \quad \partial_\mu \Delta^\mu = 0. \quad (2.43)$$

Additionally, the free delta field satisfies the Dirac equation

$$(i\cancel{\partial} - \mathring{m}_\Delta) \Delta^\mu = 0, \quad (2.44)$$

where  $\mathring{m}_\Delta$  is the bare mass of the delta.

In the isospin space, it is convenient to describe the four physical states  $(\Delta_\mu^{++}, \Delta_\mu^+, \Delta_\mu^0, \Delta_\mu^-)$  as an isospin doublet with an additional isovector index  $i$ . We define

$$\Psi_{\Delta,\mu}^i = T^i \Delta_\mu, \quad i \in \{1, 2, 3\} \quad (2.45)$$

with the three matrices

$$T^1 = \frac{1}{\sqrt{6}} \begin{pmatrix} \sqrt{3} & 0 & -1 & 0 \\ 0 & 1 & 0 & -\sqrt{3} \end{pmatrix}, \quad T^2 = \frac{i}{\sqrt{6}} \begin{pmatrix} \sqrt{3} & 0 & 1 & 0 \\ 0 & 1 & 0 & \sqrt{3} \end{pmatrix} \quad \text{and} \\ T^3 = -\sqrt{\frac{2}{3}} \begin{pmatrix} 0 & 1 & 0 & 0 \\ 0 & 0 & 1 & 0 \end{pmatrix}. \quad (2.46)$$

This yields for the three isospin doublets

$$\Psi_{\Delta,1}^\mu = \frac{1}{\sqrt{2}} \begin{pmatrix} \Delta^{++} - \frac{1}{\sqrt{3}} \Delta^0 \\ \frac{1}{\sqrt{3}} \Delta^+ - \Delta^- \end{pmatrix}^\mu, \quad \Psi_{\Delta,2}^\mu = \frac{i}{\sqrt{2}} \begin{pmatrix} \Delta^{++} + \frac{1}{\sqrt{3}} \Delta^0 \\ \frac{1}{\sqrt{3}} \Delta^+ + \Delta^- \end{pmatrix}^\mu, \quad \Psi_{\Delta,3}^\mu = -\sqrt{\frac{2}{3}} \begin{pmatrix} \Delta^+ \\ \Delta^0 \end{pmatrix}^\mu. \quad (2.47)$$

By combining an isodoublet with an isovector, one obtains six possible states, whereas an isospin-3/2 particle only has four. The unphysical isospin-1/2 excess states are decoupled through the condition

$$\tau_i \Psi_{\Delta,\mu}^i = 0. \quad (2.48)$$

This property can easily be verified by introducing the isospin projection operators

$$\xi_{ij}^{3/2} = \frac{2}{3} \delta_{ij} - \frac{i}{3} \varepsilon_{ijk} \tau_k \quad \text{and} \quad \xi_{ij}^{1/2} = \frac{1}{3} \delta_{ij} + \frac{i}{3} \varepsilon_{ijk} \tau_k, \quad (2.49)$$

which satisfy the usual projection conditions

$$\xi_{ij}^I \xi_{jk}^J = \xi_{ik}^I \delta^{IJ}, \quad I, J \in \left\{ \frac{3}{2}, \frac{1}{2} \right\}, \quad \text{and} \quad \xi_{ij}^{3/2} + \xi_{ij}^{1/2} = \delta_{ij}. \quad (2.50)$$

It is straightforward to verify eq. (2.48) with the relations

$$\xi_{ij}^{3/2} \Psi_{\Delta,j}^\mu = \Psi_{\Delta,i}^\mu \quad \text{and} \quad \xi_{ij}^{1/2} \Psi_{\Delta,j}^\mu = 0. \quad (2.51)$$

In addition to the constraints on the delta field, the Lagrangian has to be invariant under the point transformation [120]

$$\Psi_{\Delta,\mu} \rightarrow \Psi_{\Delta,\mu} + a\gamma_\mu\gamma_\nu\Psi_\Delta^\nu, \quad A \rightarrow \frac{A - 2a}{1 + 4a}. \quad (2.52)$$

Here,  $A$  is a free and unphysical parameter, which appears in the most general leading-order Lagrangian ( $A \neq -1/2$ ) and  $a$  is an arbitrary admixture of off-shell spin-1/2 components, which are always present in the relativistic spin-3/2 field. The requirement of invariance under the point transformation means that the effects of the spin-1/2 contributions can be compensated by a corresponding change of the parameter  $A$  such that the Lagrangian is left invariant. The original choice of Rarita and Schwinger was  $A = -1/3$ , whereas more recent works prefer choosing  $A = -1$ , because it leads to a convenient form of the Lagrangian and the delta propagator. Of course, observable quantities are independent of  $A$  [121].

The leading covariant  $\pi\Delta$ -Lagrangian reads (we directly employ the choice  $A = -1$ ) [97, 122]:

$$\mathcal{L}_{\pi\Delta}^{(1)} = -\bar{\Psi}_{\Delta,i}^\mu \left\{ (iD^{ij} - \dot{m}_\Delta \delta^{ij}) g_{\mu\nu} - i(\gamma_\mu D_\nu^{ij} + \gamma_\nu D_\mu^{ij}) + i\gamma_\mu D^{ij}\gamma_\nu + \dot{m}_\Delta \gamma_\mu \gamma_\nu \delta^{ij} + \frac{\dot{g}_1}{2} g_{\mu\nu} \not{u}^{ij} \gamma_5 + \frac{\dot{g}_2}{2} (\gamma_\mu u_\nu^{ij} + u_\mu^{ij} \gamma_\nu) \gamma_5 + \frac{\dot{g}_3}{2} \gamma_\mu \not{u}^{ij} \gamma_5 \gamma_\nu \right\} \Psi_{\Delta,j}^\nu, \quad (2.53)$$

where the covariant derivative in the deltaful case is defined as

$$D_\mu^{ij} = \partial_\mu \delta^{ij} + \Gamma_\mu^{ij} \quad (2.54)$$

with the generalised chiral connection

$$\Gamma_\mu^{ij} = \delta^{ij} \Gamma_\mu - i\varepsilon^{ijk} \text{Tr}(\tau_k \Gamma^\mu). \quad (2.55)$$

Furthermore we define

$$u_\mu^{ij} = \xi_{3/2}^{ik} u_\mu \xi_{3/2}^{kj}, \quad (2.56)$$

with the isospin projectors defined in eq. (2.49). For pion photoproduction, only  $\dot{g}_1$  is relevant, whereas the constants  $\dot{g}_2$  and  $\dot{g}_3$  are off-shell parameters, which must cancel in physical amplitudes. The delta propagator [123] derived from the Lagrangian (2.53) reads

$$\mathcal{G}_{\Delta,ij}^{\mu\nu}(p) = -\frac{i(p + \dot{m}_\Delta)}{p^2 - \dot{m}_\Delta^2} \left( g^{\mu\nu} - \frac{1}{d-1} \gamma^\mu \gamma^\nu + \frac{1}{d-1} \frac{p^\mu \gamma^\nu - p^\nu \gamma^\mu}{\dot{m}_\Delta} + \frac{d-2}{d-1} \frac{p^\mu p^\nu}{\dot{m}_\Delta^2} \right) \xi_{ij}^{3/2}. \quad (2.57)$$

The form given above is convenient because of its compactness. However, sometimes it is preferable to employ the different form [123]

$$\mathcal{G}_{\Delta,ij}^{\mu\nu}(p) = -\frac{i(p + \dot{m}_\Delta)}{p^2 - \dot{m}_\Delta^2} \left( P_{33}^{3/2} \right)^{\mu\nu} \xi_{ij}^{3/2} - \frac{i}{\dot{m}_\Delta \sqrt{d-1}} \left[ \left( P_{12}^{1/2} \right)^{\mu\nu} + \left( P_{21}^{1/2} \right)^{\mu\nu} \right] \xi_{ij}^{3/2}$$

$$+ i \frac{d-2}{d-1} \frac{\not{p} - \not{m}_\Delta}{\not{m}_\Delta^2} \left( P_{22}^{1/2} \right)^{\mu\nu} \xi_{ij}^{3/2} \quad (2.58)$$

with the projection operators on the spin-3/2 and -1/2 states

$$\begin{aligned} \left( P_{33}^{3/2} \right)^{\mu\nu} &= g^{\mu\nu} - \frac{1}{d-1} \gamma^\mu \gamma^\nu - \frac{1}{p^2(d-1)} (\not{p} \gamma^\mu p^\nu + p^\mu \gamma^\nu \not{p}) - \frac{d-4}{d-1} \frac{p^\mu p^\nu}{p^2}, \\ \left( P_{11}^{1/2} \right)^{\mu\nu} &= \frac{1}{d-1} \gamma^\mu \gamma^\nu - \frac{3}{d-1} \frac{p^\mu p^\nu}{p^2} + \frac{1}{p^2(d-1)} (\not{p} \gamma^\mu p^\nu + p^\mu \gamma^\nu \not{p}), \\ \left( P_{12}^{1/2} \right)^{\mu\nu} &= \frac{1}{p^2 \sqrt{d-1}} (p^\mu p^\nu - \not{p} p^\nu \gamma^\mu), \\ \left( P_{21}^{1/2} \right)^{\mu\nu} &= \frac{1}{p^2 \sqrt{d-1}} (\not{p} p^\mu \gamma^\nu - p^\mu p^\nu), \\ \left( P_{22}^{1/2} \right)^{\mu\nu} &= \frac{p^\mu p^\nu}{p^2}, \end{aligned} \quad (2.59)$$

which fulfil, similarly to the isospin projectors, the relations

$$\left( P_{33}^{3/2} \right)^{\mu\nu} + \left( P_{22}^{1/2} \right)^{\mu\nu} + \left( P_{11}^{1/2} \right)^{\mu\nu} = g^{\mu\nu} \quad \text{and} \quad \left( P_{ij}^I \right)^{\mu\alpha} \left( P_{kl}^J \right)_\alpha^\nu = \delta^{IJ} \delta_{jk} \left( P_{il}^I \right)^{\mu\nu}. \quad (2.60)$$

Employing the latter form of the delta propagator enables to switch off the not propagating spin-1/2 components by hand.

For pion photoproduction, it is not necessary to consider higher-order Lagrangians generating interactions of pions and the delta, because these are beyond our working order<sup>4</sup>. However, we need to take into account the nucleon-to-delta transition Lagrangian  $\mathcal{L}_{\pi N \Delta}$  up to third order. Again, we only give the relevant terms for pion photoproduction up to our working order ([97, 124]):

$$\begin{aligned} \mathcal{L}_{\pi N \Delta}^{(1)} &= h_A \left( \bar{\Psi}_{\Delta,i}^\mu \Theta_{\mu\nu}(z_0) w_i^\nu \Psi_N + \bar{\Psi}_N w_i^{\nu\dagger} \Theta_{\nu\mu}(z_0) \Psi_{\Delta,i}^\mu \right), \\ \mathcal{L}_{\pi N \Delta}^{(2)} &= i \frac{b_1}{2} \bar{\Psi}_{\Delta,i}^\mu \Theta_{\mu\nu}(z_1) F_i^{+, \nu\alpha} \gamma_\alpha \gamma_5 \Psi_N + i b_3 \bar{\Psi}_{\Delta,i}^\mu \Theta_{\mu\nu}(z_3) w_i^{\nu\alpha} \gamma_\alpha \Psi_N \\ &\quad - \frac{b_6}{m} \bar{\Psi}_{\Delta,i}^\mu \Theta_{\mu\nu}(z_6) w_i^{\nu\alpha} D_\alpha \Psi_N + \dots + \text{h.c.}, \\ \mathcal{L}_{\pi N \Delta}^{(3)} &= \frac{h_1}{m} \bar{\Psi}_{\Delta,i}^\mu \Theta_{\mu\nu}(y_1) F_i^{+, \nu\alpha} \gamma_5 D_\alpha \Psi_N - i \frac{h_{15}}{2} \bar{\Psi}_{\Delta,i}^\mu \Theta_{\mu\nu}(y_{15}) \text{Tr} \left( [D^\alpha, F^{+, \nu\beta}] \tau^i \right) \sigma_{\alpha\beta} \gamma_5 \Psi_N \\ &\quad + i \frac{h_{16}}{2m} \bar{\Psi}_{\Delta,i}^\mu \Theta_{\mu\nu}(y_{16}) \text{Tr} \left( [D^\alpha, F^{+, \nu\beta}] \tau^i \right) \gamma_\beta \gamma_5 D_\alpha \Psi_N + \dots + \text{h.c.}, \end{aligned} \quad (2.61)$$

---

<sup>4</sup>Strictly speaking, we should also include the term from  $\mathcal{L}_{\pi\Delta}^{(2)}$  proportional to the constant  $c_1^\Delta$ . However, similar to the nucleonic case, this constant only enters the delta mass and is fully removed after renormalisation in our case. This is why we do not show this term.

with

$$w_i^\mu = \frac{1}{2} \text{Tr}(\tau_i u^\mu), \quad w_i^{\mu\nu} = \frac{1}{2} \text{Tr}(\tau_i [D^\mu, u^\nu]), \quad F_{i,\mu\nu}^\pm = \frac{1}{2} \text{Tr}(\tau_i F_{\mu\nu}^\pm) \quad (2.62)$$

and

$$\Theta_{\mu\nu}(z) = g_{\mu\nu} + z\gamma_\mu\gamma_\nu \quad (2.63)$$

is an off-shell function with the off-shell parameter  $z$ . It was shown in ref. [125] that the dependence on the off-shell parameters can be eliminated by a redefinition of the LECs and that they are of higher order in a strict heavy baryon expansion. Thus, we set them to zero in our calculations.

Another subtlety of including spin-3/2 particles is that the correct decoupling of the unphysical spin-1/2 components of the field must be ensured in the theory. In the free case, these components are projected out in the resulting equations of motion, but in the case of interacting spin-3/2 fields, the task is more problematic. Pascalutsa showed that this can be obtained by the requirement that all interactions have the same type of gauge invariance as the kinetic term of the spin-3/2 field [126]. However, this demand for gauge invariance is in contrast to the commonly adapted nonlinear realisation of the chiral symmetry of Coleman, Callan, Wess and Zumino [127, 128]. In ref. [129] it was observed that every gauge noninvariant linear coupling of the delta field can be transformed into a gauge-invariant form by choosing a suitable field redefinition. Krebs, Epelbaum and Meißner [130] provided a similar statement for bilinear couplings of the spin-3/2 field. Because of the proven equivalence of the two approaches by use of a nonlinear field redefinition, it all amounts to the fact that S-matrix elements can be calculated from the standard effective Lagrangian using the standard, naive, Feynman rules.

Incorporating the delta in the theory as an explicit degree of freedom requires additional modification of the power counting scheme (eq. (2.30)). To account for a new parameter related to the delta, one introduces the delta-nucleon-mass split

$$\Delta_0 = \dot{m}_\Delta - m, \quad (2.64)$$

which we count as an additional small parameter  $\mathcal{O}(M_\pi)$ , but which does not vanish in the chiral limit. This results in the new counting rules

$$\epsilon \in \left\{ \frac{M}{\Lambda}, \frac{q}{\Lambda}, \frac{\Delta_0}{\Lambda} \right\} \quad \text{with} \quad \Lambda \in \{\Lambda_b, 4\pi F, m\}, \quad (2.65)$$

with  $\epsilon$  as the new expansion parameter in the deltaful case in contrast to  $q$  in the deltaless theory. This expansion in external momenta, pion mass and the delta-nucleon-mass split is referred to as small scale expansion (SSE) [97].

### 2.4.2 Heavy baryon formalism

The treatment of the delta resonance in the HB formalism is similar to that of the nucleon, however, it is more complex. This is due to the fact that the leading-order Lagrangians in eqs. (2.53) and (2.61) contain on- and off-shell parameters, spin-3/2 and two spin-1/2 components, large and small components of the Dirac spinor and leading and subleading parts in  $1/m_N$ . In the case of the delta, a light spin-3/2 and isospin-3/2 field is defined similarly to the nucleonic case

$$T_i^\mu(x) = P_v^+ \xi_{ij}^{3/2} \left( \hat{P}_{33}^{3/2} \right)^{\mu\nu} \Psi_{\Delta,\nu}^j(x) e^{i mv \cdot x}, \quad (2.66)$$

where  $P_v^+$  was given in eq. (2.37) and  $\xi_{ij}^{3/2}$  in eq. (2.49). The projection operator

$$\left( \hat{P}_{33}^{3/2} \right)^{\mu\nu} = g^{\mu\nu} - v^\mu v^\nu - \frac{4}{d-1} S^\mu S^\nu \quad (2.67)$$

is modified appropriately compared to eq. (2.59). All other projections are counted as heavy and integrated out of the action.

The relevant interaction Lagrangians up to our working order read [97]:

$$\begin{aligned} \hat{\mathcal{L}}_{\pi N \Delta}^{(1)} &= \overset{\circ}{h_A} (\bar{T}_i^\mu w_\mu^i N + \bar{N} w_\mu^i T_i^\mu), \\ \hat{\mathcal{L}}_{\pi N \Delta}^{(2)} &= \bar{T}_i^\mu (i b_1 F_{\mu\nu}^{+i} S^\nu + (b_3 + b_6) i w_{\mu\nu}^i v^\nu) N + \text{h.c.} \\ &\quad - \frac{1}{2m} \bar{T}_i^i \left( \frac{2}{d-1} \overset{\circ}{h_A} g_1 z_0 w_{ij}^\mu \xi_{3/2}^{jk} S \cdot w^k + 2i \overset{\circ}{h_A} D_{ij}^\mu \xi_{3/2}^{jk} v \cdot w^k \right) + \text{h.c..} \end{aligned} \quad (2.68)$$

Note that similar to the nucleon sector, the  $1/m$  correction in the second line of  $\hat{\mathcal{L}}_{\pi N \Delta}^{(2)}$  will be treated as of third order, thus it is irrelevant for the calculation and only given for the sake of completeness.

When including the delta resonance as an explicit degree of freedom, there appears an additional  $1/m$  correction to the pion-nucleon Lagrangian at next-to-leading order:

$$\begin{aligned} \hat{\mathcal{L}}_{\pi N}^{(2),1/m} &= -\frac{\overset{\circ}{h_A}^2}{2m} \bar{N} \left( \frac{4}{d-4} (2z_0 + (d-1)z_0^2) w^{i\dagger} \cdot S \xi_{3/2}^{ij} S \cdot w^j \right. \\ &\quad \left. + \frac{1}{d-1} (4(d-2) + 2(d-3)z_0 - z_0^2) w^{i\dagger} \cdot v \xi_{3/2}^{ij} v \cdot w^j \right) N \end{aligned} \quad (2.69)$$

Also, this  $1/m$  correction will be treated as of third order. In contrast to ref. [97], where these corrections were derived first, here the  $d$  dependence is made explicit. This form of the Lagrangian was taken from ref. [131]. Also, the Lagrangian of Hemmert [97] was constructed with a different definition of the delta field as compared to this work. Hemmerts choice corresponds to a gauge parameter of  $A = 0$ , while in the covariant approach in this work  $A = -1$  is

employed. Matching the Lagrangians can be done by the following redefinitions [131]

$$\tilde{z}_0 = -\frac{1}{2}(1 + z_0), \quad \tilde{g}_2 = -g_1, \quad \tilde{g}_3 = -g_1, \quad (2.70)$$

where  $\tilde{z}_0, \tilde{g}_2$  and  $\tilde{g}_3$  are to be understood as the parameters from ref. [97].

## 2.5 Effective Lagrangian and low-energy constants

Finally, we present the full effective Lagrangian necessary to describe pion photoproduction at one-loop level. In the deltaless case, it is given by

$$\mathcal{L}_{\text{eff}} = \mathcal{L}_{\pi\pi}^{(2)} + \mathcal{L}_{\pi\pi}^{(4)} + \mathcal{L}_{\pi N}^{(1)} + \mathcal{L}_{\pi N}^{(2)} + \mathcal{L}_{\pi N}^{(3)} \quad (2.71)$$

in both covariant and HB approaches. Here, we suppress the hat for the HB Lagrangian and remind the reader that we implicitly include the  $1/m_N$  corrections of the leading order in  $\hat{\mathcal{L}}_{\pi N}^{(3)}$  instead of explicitly printing an additional term  $\hat{\mathcal{L}}_{\pi N}^{(1),1/m}$ , just as stated below eq. (2.40).

In the deltaful case, the full effective Lagrangian in the covariant case is given by

$$\mathcal{L}_{\text{eff}} = \mathcal{L}_{\pi\pi}^{(2)} + \mathcal{L}_{\pi\pi}^{(4)} + \mathcal{L}_{\pi N}^{(1)} + \mathcal{L}_{\pi N}^{(2)} + \mathcal{L}_{\pi N}^{(3)} + \mathcal{L}_{\pi N\Delta}^{(1)} + \mathcal{L}_{\pi N\Delta}^{(2)} + \mathcal{L}_{\pi N\Delta}^{(3)} + \mathcal{L}_{\pi\Delta}^{(1)}. \quad (2.72)$$

In the HB framework, the last two terms are beyond our working order, because we only include tree diagrams with explicit delta degrees of freedom.

To complete the introduction of ChPT, we collect all LECs which appear during our study of pion photoproduction in the table below. Therein, we specify the part of the effective Lagrangian containing the constant and mark all constants with a star, which do not contribute to the full renormalised amplitude up to our working order. Thus, these either appear in subprocesses and are removed by renormalisation, or it turns out that these contributions are effectively beyond our working order. This is explained in detail in sec. 3.5.1. Furthermore, we print constants, whose numerical values were taken from different works bold and additionally provide the corresponding references. More details and numerical values are given in sec. 3.10.

**Table 2.1:** LECs occurring in vertices relevant for pion photoproduction up to our working order. LECs marked with a star do not contribute to the renormalised amplitude of pion photoproduction, constants whose numerical values were taken from other sources are printed bold.

Constant	Lagrangian	Related processes or parameters	Source
<b><math>F_\pi</math></b>	$\mathcal{L}_{\pi\pi}^{(2)}$	pion decay	[110]
$l_3^*, l_4^*, l_6^*$	$\mathcal{L}_{\pi\pi}^{(4)}$	pion field, mass and electromagnetic form factor	
<b><math>g_A</math></b>	$\mathcal{L}_{\pi N}^{(1)}$	axial $\pi N$ coupling	[132]
<b><math>c_6, c_7</math></b>	$\mathcal{L}_{\pi N}^{(2)}$	magnetic moment of proton and neutron	[110]
$d_6^*, d_7^*$	$\mathcal{L}_{\pi N}^{(3)}$	radius of the nucleon	
$d_{16}^*, d_{18}^*$	$\mathcal{L}_{\pi N}^{(3)}$	axial $\pi N$ coupling constant $g_A$	
$d_8, d_9, d_{20}, d_{21}, d_{22}$	$\mathcal{L}_{\pi N}^{(3)}$	$\gamma N \rightarrow \pi N$	
<b><math>h_A</math></b>	$\mathcal{L}_{\pi N \Delta}^{(1)}$	axial $\pi N \Delta$ coupling	[133]
$b_3^*, b_6^*$	$\mathcal{L}_{\pi N \Delta}^{(2)}$	axial $\pi N \Delta$ coupling constant $h_A$	
$b_1$	$\mathcal{L}_{\pi N \Delta}^{(2)}$	electromagnetic $N \Delta$ transition form factor	
$h_1, h_{15}^*, h_{16}^*$	$\mathcal{L}_{\pi N \Delta}^{(3)}$	electromagnetic $N \Delta$ transition form factor	
<b><math>g_1</math></b>	$\mathcal{L}_{\pi \Delta}^{(1)}$	$\pi \Delta$ coupling	[37]



# 3 Pion photoproduction

In this chapter, we consider specifics of pion photoproduction on the nucleon. In the following, we provide the necessary definitions for kinematics, isospin and spin decomposition of the matrix element. We also show how to calculate multipole amplitudes and observables. Furthermore, we discuss renormalisation, performed consistency checks and the fitting procedure including numerics.

## 3.1 Kinematics

In fig. 3.1, we show the definition of the momenta in the reaction

$$\gamma(k, \epsilon) + N(p) \rightarrow \pi^c(q) + N(p'). \quad (3.1)$$

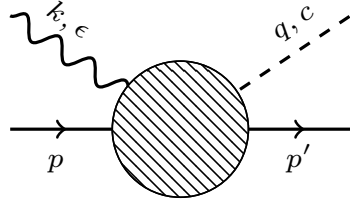


**Figure 3.1:** Kinematics of  $\gamma + N \rightarrow \pi + N$ , where  $p$  ( $k$ ) is the incoming momentum of the nucleon (photon) and  $p'$  ( $q$ ) is the outgoing momentum of the nucleon (pion).  $\epsilon$  is the polarisation vector of the photon and  $c$  is the Cartesian isospin index of the pion.

The three Lorentz-invariant Mandelstam variables are defined as

$$s = (p+k)^2 = (p'+q)^2, \quad t = (p-p')^2 = (k-q)^2, \quad u = (p-q)^2 = (k-p')^2. \quad (3.2)$$

When all particles are on the mass shell, they fulfil the relation

$$s + t + u = 2m_N^2 + M_\pi^2, \quad (3.3)$$

where we have assumed a real photon  $k^2 = 0$ . Using these definitions, all occurring scalar products of four-momenta can be expressed in terms of  $s$  and  $t$  and the masses

$$\begin{aligned} p \cdot k &= \frac{1}{2}(s - m_N^2), & p \cdot q &= \frac{1}{2}(s + t - m_N^2), & p \cdot p' &= \frac{1}{2}(2m_N^2 - t), \\ k \cdot q &= \frac{1}{2}(M_\pi^2 - t), & k \cdot p' &= \frac{1}{2}(s + t - m_N^2 - M_\pi^2), & q \cdot p' &= \frac{1}{2}(s - m_N^2 - M_\pi^2). \end{aligned} \quad (3.4)$$

The energies of the photon  $\omega$  and the pion  $E_\pi$  in the centre-of-mass frame (CM) expressed in terms of the Mandelstam variables read

$$\omega = \frac{s - m_N^2}{2\sqrt{s}}, \quad E_\pi = \frac{s + M_\pi^2 - m_N^2}{2\sqrt{s}}. \quad (3.5)$$

In the laboratory frame, which is defined as the system in which the nucleon is at rest before the scattering, the photon energy can be calculated from the total CM energy using

$$\omega_{\text{lab}} = \frac{s - m_N^2}{2m_N}. \quad (3.6)$$

Furthermore, we define the scattering angle  $\theta$  via  $|\mathbf{k}| |\mathbf{q}| \cos(\theta) = \mathbf{k} \cdot \mathbf{q}$ , such that

$$t = M_\pi^2 - 2(\omega E_\pi - |\mathbf{k}| |\mathbf{q}| \cos(\theta)). \quad (3.7)$$

The pion production threshold lies at the CM energy of  $\sqrt{s} = m_N + M_\pi$ . In the HB formalism, an explicit  $1/m_N$  expansion of the amplitude is performed. Expanding eq. (3.5) in terms of  $1/m_N$ , we can derive an approximate relation between photon and pion CM energy

$$\omega = E_\pi - \frac{M_\pi}{2m_N} + \mathcal{O}\left(\frac{1}{m_N^2}\right). \quad (3.8)$$

Thus, in the HB formalism, we express all kinematic quantities in terms of the pion energy  $E_\pi$ .

## 3.2 Isospin decomposition

In the isospin space, the matrix element of pion photoproduction can be parametrised in terms of three independent structures

$$T_{\gamma N \rightarrow \pi N}^c = \delta_{c3} T_{\gamma N}^{(+)} + \tau_c T_{\gamma N}^{(0)} + i \varepsilon_{c3a} \tau_a T_{\gamma N}^{(-)}, \quad (3.9)$$

where  $c$  is the isospin index of the outgoing pion and  $\tau^i$  are the Pauli matrices in isospin space (in contrast to  $\sigma^i$  in spin space). To be more general, all single pion production processes can be decomposed in the above way. The matrix elements for the four physical pion photoproduction reaction channels

$$\gamma p \rightarrow \pi^0 p, \quad \gamma p \rightarrow \pi^+ n, \quad \gamma n \rightarrow \pi^0 n, \quad \gamma n \rightarrow \pi^- p \quad (3.10)$$

can be obtained from the three isospin structures by using the following relations

$$\begin{aligned} T_{\gamma p \rightarrow \pi^0 p} &= T_{\gamma N}^{(+)} + T_{\gamma N}^{(0)}, & T_{\gamma p \rightarrow \pi^+ n} &= \sqrt{2}(T_{\gamma N}^{(0)} + T_{\gamma N}^{(-)}), \\ T_{\gamma n \rightarrow \pi^0 n} &= T_{\gamma N}^{(+)} - T_{\gamma N}^{(0)}, & T_{\gamma n \rightarrow \pi^- p} &= \sqrt{2}(T_{\gamma N}^{(0)} - T_{\gamma N}^{(-)}). \end{aligned} \quad (3.11)$$

Another commonly used decomposition of the pion photoproduction amplitude is the so-called isospin parametrisation in terms of the three amplitudes  $T_{\gamma N}^{(\frac{3}{2})}, T_{\gamma p}^{(\frac{1}{2})}, T_{\gamma n}^{(\frac{1}{2})}$  where the production amplitudes  $T_{\gamma N}^{(I)}$  are related to the  $T_{\gamma N}^{(0,\pm)}$  via

$$\begin{aligned} T_{\gamma N}^{(\frac{3}{2})} &= T_{\gamma p}^{(\frac{3}{2})} = T_{\gamma n}^{(\frac{3}{2})} = T_{\gamma N}^{(+)} - T_{\gamma N}^{(-)}, \\ T_{\gamma p}^{(\frac{1}{2})} &= T_{\gamma N}^{(0)} + \frac{1}{3}T_{\gamma N}^{(+)} + \frac{2}{3}T_{\gamma N}^{(-)}, \quad T_{\gamma n}^{(\frac{1}{2})} = T_{\gamma N}^{(0)} - \frac{1}{3}T_{\gamma N}^{(+)} - \frac{2}{3}T_{\gamma N}^{(-)}. \end{aligned} \quad (3.12)$$

The isospin parametrisation is a natural choice when working in the isospin symmetric case of ChPT, thus we perform the fits of this work in this basis. For comparison with experimental results, the decomposition (3.11) in terms of the physical reaction channels is required.

### 3.3 Spin decomposition and multipole amplitudes

The matrix element of pion photoproduction is given by

$$\mathcal{M} = \epsilon^\mu \mathcal{M}_\mu = -i e \epsilon^\mu \langle N(p') \pi^c(q) | J_\mu(k^2) | N(p) \rangle, \quad (3.13)$$

with  $J_\mu(k^2)$  the electromagnetic current operator,  $\epsilon^\mu$  the polarisation vector of the photon and  $Q^2 = -k^2$  the virtuality of the photon. Different parametrisations of the matrix element are advantageous for different purposes. The first parametrisation is given in terms of the so-called Ball amplitudes [134]<sup>1</sup>

$$\mathcal{M}^\mu = \sum_{i=1}^8 \bar{u}(p') B_i V_i^\mu u(p). \quad (3.14)$$

We denote by  $u(p)$  ( $\bar{u}(p')$ ) the Dirac spinor of the incoming (outgoing) nucleon and suppress the spin index for the sake of brevity. The basis structures  $V_i^\mu$  are all independent Lorentz-invariant matrices that can be formed using gamma matrices and the polarisation vector, and the coefficients  $B_i$  are scalar functions of the Mandelstam variables. Explicitly, the basis structures read

$$\begin{aligned} V_1^\mu &= \gamma^\mu \gamma_5, & V_2^\mu &= \gamma_5 P^\mu, & V_3^\mu &= \gamma_5 q^\mu, & V_4^\mu &= \gamma_5 k^\mu, \\ V_5^\mu &= \gamma^\mu \not{k} \gamma_5, & V_6^\mu &= \not{k} \gamma_5 P^\mu, & V_7^\mu &= \not{k} \gamma_5 q^\mu, & V_8^\mu &= \not{k} \gamma_5 k^\mu, \end{aligned} \quad (3.15)$$

where  $P = \frac{1}{2}(p+p')$  and  $\not{a} = a_\mu \gamma^\mu$  is the Feynman slash notation for any four-vector contracted with the Dirac matrices. Note that the set of amplitudes (3.14)-(3.15) is not minimal, but convenient in practical calculations due to the simplicity of the basis structures. Imposing transversality of the amplitude  $k_\mu \mathcal{M}^\mu = 0$  leads to the following conditions

$$B_1 + B_6 k \cdot P + B_7 k \cdot q + B_8 k^2 = 0, \quad B_2 k \cdot P + B_3 k \cdot q + B_4 k^2 + B_5 k^2 = 0. \quad (3.16)$$

---

<sup>1</sup>We work with Hilt's convention, given in ref. [95], which is slightly different from Ball's original.

Thus, current conservation reduces the number of basis structures to six. In real pion photoproduction, due to the additional constraint  $\epsilon \cdot k = 0$  and  $k^2 = 0$ , only four structures remain.

The second relevant parametrisation of the matrix element was worked out by Chew, Goldberger, Low and Nambu (CGLN) and constructed in such a way that the basis structures themselves fulfil transversality [134–136]:

$$\begin{aligned} M_1^\mu &= -\frac{i}{2}\gamma_5(\gamma^\mu k - k^\mu), \\ M_2^\mu &= 2i\gamma_5(P^\mu k \cdot (q - \frac{1}{2}k) - (q^\mu - \frac{1}{2}k^\mu)k \cdot P), \\ M_3^\mu &= -i\gamma_5(\gamma^\mu k \cdot q - k^\mu q^\mu), \\ M_4^\mu &= -2i\gamma_5(\gamma^\mu k \cdot P - k^\mu P^\mu) - 2m_N M_1^\mu. \end{aligned} \quad (3.17)$$

with

$$\mathcal{M}^\mu = \sum_{i=1}^4 \bar{u}(p') A_i M_i^\mu u(p). \quad (3.18)$$

Here, the number of basis structures is minimal. Furthermore, this decomposition is only possible for real photons  $k^2 = 0$ .

The third parametrisation for pion photoproduction is given by [135]

$$\epsilon_\mu \bar{u}(p') \left( \sum_{i=1}^4 A_i M_i^\mu \right) u(p) = \frac{4\pi\sqrt{s}}{m_N} \chi_f^\dagger \mathcal{F} \chi_i. \quad (3.19)$$

Here,  $\chi_i$  ( $\chi_f^\dagger$ ) is the initial (final) Pauli spinor.  $\mathcal{F}$  can be expressed in the so-called CGLN amplitudes:

$$\mathcal{F} = i\boldsymbol{\sigma} \cdot \boldsymbol{\epsilon} \mathcal{F}_1 + \frac{\boldsymbol{\sigma} \cdot \mathbf{q} \boldsymbol{\sigma} \cdot (\mathbf{k} \times \boldsymbol{\epsilon})}{|\mathbf{q}| |\mathbf{k}|} \mathcal{F}_2 + i \frac{\boldsymbol{\sigma} \cdot \mathbf{k} \mathbf{q} \cdot \boldsymbol{\epsilon}}{|\mathbf{q}| |\mathbf{k}|} \mathcal{F}_3 + i \frac{\boldsymbol{\sigma} \cdot \mathbf{q} \mathbf{q} \cdot \boldsymbol{\epsilon}}{|\mathbf{q}|^2} \mathcal{F}_4. \quad (3.20)$$

Note that this parametrisation is only possible in the CM frame, in the case of real photons  $k^2 = 0$  and when choosing a polarisation vector with a vanishing time-component  $\epsilon^0 = 0$ , which is possible in a gauge-invariant process. The  $\mathcal{F}_i$ 's can be expanded in a multipole series [134, 135]:

$$\begin{aligned} \mathcal{F}_1 &= \sum_{l=0}^{\infty} \{[l M_{l+} + E_{l+}] P'_{l+1}(x) + [(l+1) M_{l-} + E_{l-}] P'_{l-1}(x)\}, \\ \mathcal{F}_2 &= \sum_{l=1}^{\infty} [(l+1) M_{l+} + l M_{l-}] P'_l(x), \\ \mathcal{F}_3 &= \sum_{l=1}^{\infty} \{[E_{l+} - M_{l+}] P''_{l+1}(x) + [E_{l-} + M_{l-}] P''_{l-1}(x)\}, \end{aligned}$$

$$\mathcal{F}_4 = \sum_{l=2}^{\infty} [M_{l+} - E_{l+} - M_{l-} - E_{l-}] P_l''(x), \quad (3.21)$$

where  $x = \cos(\theta)$ ,  $P_l(x)$  is a Legendre polynomial of degree  $l$ ,  $P_l'(x) = \frac{dP_l}{dx}$  is its first derivative and  $P_l''(x)$  is the second derivative with respect to  $x$ .  $l$  is the orbital angular momentum of the outgoing pion-nucleon system. The subscript  $\pm$  denotes the total angular momentum  $j = l \pm 1/2$ . To calculate multipole amplitudes, eq. (3.21) must be inverted. The angular dependence is integrated out, such that the multipoles

$$\begin{aligned} E_{l+} &= \int_{-1}^1 \frac{dx}{2(l+1)} \left[ P_l \mathcal{F}_1 - P_{l+1} \mathcal{F}_2 + \frac{l}{2l+1} (P_{l-1} - P_{l+1}) \mathcal{F}_3 + \frac{l+1}{2l+3} (P_l - P_{l+2}) \mathcal{F}_4 \right], \\ E_{l-} &= \int_{-1}^1 \frac{dx}{2l} \left[ P_l \mathcal{F}_1 - P_{l-1} \mathcal{F}_2 - \frac{l+1}{2l+1} (P_{l-1} - P_{l+1}) \mathcal{F}_3 + \frac{l}{2l-1} (P_l - P_{l-2}) \mathcal{F}_4 \right], \\ M_{l+} &= \int_{-1}^1 \frac{dx}{2(l+1)} \left[ P_l \mathcal{F}_1 - P_{l+1} \mathcal{F}_2 - \frac{1}{2l+1} (P_{l-1} - P_{l+1}) \mathcal{F}_3 \right], \\ M_{l-} &= \int_{-1}^1 \frac{dx}{2l} \left[ -P_l \mathcal{F}_1 + P_{l-1} \mathcal{F}_2 + \frac{1}{2l+1} (P_{l-1} - P_{l+1}) \mathcal{F}_3 \right] \end{aligned} \quad (3.22)$$

do not depend on the angle anymore. Here, we suppress the  $x$ -dependence of the Legendre polynomials  $P_l$  for the sake of brevity. The multipoles  $E_{l\pm}$  and  $M_{l\pm}$  depend on the total energy in the CM frame  $\sqrt{s}$  and behave like  $|\mathbf{q}|^l$  in the threshold region.

To calculate multipole amplitudes, we proceed as follows: First, we express the pion photo-production amplitude in terms of the Ball amplitudes (eq. (3.14)). Then we rewrite the  $B_i$ 's in terms of  $A_i$ 's to obtain the representation of the amplitude in the minimal basis (eq. (3.18)). Finally, we use the coefficients  $A_i$  to calculate  $\mathcal{F}_1 - \mathcal{F}_4$ . The relation between these representations are given in the appendix A.

### 3.4 The cross section and polarisation asymmetry

In this subsection, we show how to calculate the unpolarised differential cross section and linear polarisation asymmetry of pion photoproduction. The general expression for the differential cross section of a scattering process with two incoming and  $n$  outgoing particles is given by

$$d\sigma = \frac{(2\pi)^4}{2\sqrt{\lambda(s, m_1^2, m_2^2)}} \delta^{(4)} \left( \sum_{i=1}^n p'_i - p_1 - p_2 \right) |\mathcal{M}|^2 \prod_{i=1}^n \frac{d^3 p'_i}{(2\pi)^3 2E_i}. \quad (3.23)$$

In the above expression,  $p_i$  and  $m_i$  are momentum and mass of the incoming particle  $i$ ,  $p'_i$  is the momentum of the outgoing particle  $i$  and  $\lambda(x, y, z) = x^2 + y^2 + z^2 - 2xy - 2xz - 2yz$  is the Källén function. The unpolarised squared matrix element  $|\overline{\mathcal{M}}|^2$  of pion photoproduction can be obtained from

$$|\overline{\mathcal{M}}|^2 = \frac{1}{4} \sum_{\lambda=-1}^1 \sum_{s,s'=-1}^1 |\epsilon_\mu(k, \lambda) \mathcal{M}^\mu(k, p, s, p', s', q)|^2, \quad (3.24)$$

where  $\lambda$  is the helicity of the photon,  $s$  ( $s'$ ) is the spin of the incoming (outgoing) nucleon and the factor of 1/4 arises from averaging over helicity and spin of the incoming particles. Using the simplifications of the CM frame and carrying out the integration, the unpolarised differential cross section reads

$$\frac{d\sigma}{d\Omega} = \frac{1}{64\pi^2 s} \frac{|\mathbf{q}|}{|\mathbf{k}|} |\overline{\mathcal{M}}|^2. \quad (3.25)$$

Furthermore, we calculate the linear polarised photon asymmetry  $\Sigma$ , which is given by

$$\Sigma = \frac{d\sigma_\perp - d\sigma_\parallel}{d\sigma_\perp + d\sigma_\parallel}. \quad (3.26)$$

In eq. (3.26),  $d\sigma_\perp$  and  $d\sigma_\parallel$  refer to angular cross section for photon polarisations perpendicular and parallel to the reaction plane, respectively. The difference to the unpolarised cross sections is that the squared matrix element is not averaged over both incoming polarisations, but calculated individually according to

$$|\mathcal{M}_{\perp/\parallel}|^2 = \frac{1}{2} \sum_{s,s'=-1}^1 \left| \frac{1}{\sqrt{2}} (\epsilon_\mu(1) \pm \epsilon_\mu(-1)) \mathcal{M}^\mu \right|^2 \quad (3.27)$$

with

$$\epsilon^\mu(1) = \frac{1}{\sqrt{2}}(0, -1, -i, 0) \quad \text{and} \quad \epsilon^\mu(-1) = \frac{1}{\sqrt{2}}(0, 1, -i, 0). \quad (3.28)$$

## 3.5 Renormalisation

In this section, we discuss the subtleties of renormalisation, i.e. all steps necessary to remove unphysical infinities from the theory. Furthermore, we address the problem of the power-counting violating terms (PCVT) introduced in the section 2.3.1 and its effects for this work.

### 3.5.1 Renormalisation of subprocesses

To relate the bare constants of the effective Lagrangian to their physical counterparts, we must consider various subprocesses of pion photoproduction. We take care of the appearing integrals and their ultraviolet (UV) divergences by dimensional regularisation. Also, we choose

to renormalise the masses, wave functions and coupling constants by on-shell renormalisation. In the following, we give the renormalisation conditions for all relevant LECs. Because the expressions for the counterterms can be rather lengthy, we provide them in appendix C.

- **Pion mass, field and decay constant**

The pionic constants  $M_\pi$ ,  $Z_\pi$  and  $F_\pi$  are fixed by the conditions

$$\Sigma_\pi(M_\pi^2) = 0, \quad \Sigma'_\pi(M_\pi^2) = 0 \quad \text{and} \quad \langle 0 | A_i^\mu(0) | \pi_j(q) \rangle = i q^\mu \delta_{ij} F_\pi, \quad (3.29)$$

where  $\Sigma_\pi(q^2)$  is the self-energy of the pion and  $A_i^\mu$  is the axial current. The dependence of the amplitude on the LECs  $l_3$  and  $l_4$  is removed by these renormalisation conditions, whereas the dependence on  $l_6$  disappears only for real photons.

- **Nucleon mass and field**

The nucleon mass  $m_N$  and field  $Z_N$  are fixed by similar conditions

$$\Sigma_N(m_N) = 0 \quad \text{and} \quad \Sigma'_N(m_N) = 0 \quad (3.30)$$

with the nucleon self-energy  $\Sigma_N(p)$ . The dependence on the constant  $c_1$  disappears after the nucleon mass and field renormalisation.

- **Delta mass and field**

Up to our working order, loop graphs do not contribute to the renormalisation of the delta. However, similar to the nucleonic case, the constant  $c_1^\Delta$  contributes to the second order, but its dependence is removed such that the second order corrections to the delta mass are set to zero. We chose to implement the complex mass scheme [137–139]. Details and the numerical treatment of the delta mass are discussed in sec. 5.2.1.

- **Axial pion-nucleon coupling**

Instead of using the coupling constant  $g_A^{ph}$  of an axial current to the nucleon, we choose to work with an axial pion-nucleon coupling constant  $g_A$ , which is defined by the direct coupling of a pion to a nucleon

$$\langle N(p') | \pi_i(q) N(p) \rangle = i \frac{m_N}{F_\pi} g_A \tau_i \bar{u}(p') \gamma_5 u(p). \quad (3.31)$$

The two constants are related via the Goldberger-Treiman discrepancy

$$g_A = g_A^{ph} - 2M_\pi^2 d_{18} + \mathcal{O}(q^5) \quad (3.32)$$

and the value for the axial  $\pi N$  coupling constant  $g_A$  is fixed via the Goldberger-Treiman relation [140]

$$g_A = g_{\pi NN} \frac{F_\pi}{m_N}, \quad (3.33)$$

which yields the numerical value of  $g_A = 1.289(1)$ , using the value of the charged pion-nucleon coupling constant  $g_{\pi NN}$  from ref. [132]  $g_{\pi NN}^2 / 4\pi = 13.7(2)$ . Note that using the

axial  $\pi N$  coupling  $g_A$  removes the constants  $d_{16}$  and  $d_{18}$  from the pion photoproduction amplitude, which are redundant for the considered process and chiral order.

- **Electromagnetic form factor of the nucleon**

The  $\gamma NN$  vertex can be parametrised in terms of the so-called Dirac and Pauli form factors  $F_1$  and  $F_2$ , respectively (see e.g. ref. [141]):

$$\langle N(p') | J^\mu(Q^2) | N(p) \rangle = \bar{u}(p') \left\{ \gamma^\mu F_1^N(Q^2) + i \frac{\sigma^{\mu\nu} k_\nu}{2m_N} F_2^N(Q^2) \right\}, \quad N = p, n. \quad (3.34)$$

Here,  $J^\mu$  is the electromagnetic current and  $Q^2 = -k^2$  is the virtuality of the photon. Note that the Pauli form factor comes with a factor of  $1/m_N$  and thus starts to contribute from one order higher than the Dirac form factor. The form factors are fixed by the conditions

$$F_1^p(0) = 1, \quad F_1^n(0) = 0, \quad F_2^p(0) = \kappa_p \quad \text{and} \quad F_2^n(0) = \kappa_n, \quad (3.35)$$

where  $\kappa_N = \{\kappa_p, \kappa_n\}$  is the anomalous magnetic moment of the nucleon. The LECs  $c_6$  and  $c_7$  are related to  $\kappa_N$  via the relations

$$c_6 = \kappa_p - \kappa_n, \quad c_7 = \kappa_n, \quad (3.36)$$

which gives, using  $\kappa_p = 1.793$  and  $\kappa_n = -1.913$  [110]

$$c_6 = 3.706 \quad \text{and} \quad c_7 = -1.913. \quad (3.37)$$

The third-order constants  $d_6$  and  $d_7$  only contribute in the case of virtual photons, thus they are irrelevant for real pion photoproduction.

- **Axial pion-nucleon-delta coupling**

We define the axial pion-nucleon-delta coupling constant  $h_A$  in the same way as  $g_A$  in the deltaless case, namely

$$\langle \Delta_j(p') | \pi_i(q) N(p) \rangle = -\frac{h_A}{F_\pi} \delta_{ij} q^\mu \bar{u}_\mu^\Delta(p') u(p), \quad (3.38)$$

where the spinor of the delta is obtained by coupling a Dirac spinor  $u(p, s)$  to a helicity vector

$$u_\mu^\Delta(p, s_\Delta) = \sum_{\lambda, s} (1, \lambda, \frac{1}{2}, s; \frac{3}{2}, s_\Delta) \epsilon_\mu(p, \lambda) u(p, s) \quad (3.39)$$

and we denote by  $(\cdot, \cdot, \cdot, \cdot; \cdot, \cdot)$  the Clebsch-Gordan coefficients (for details of the Rarita-Schwinger formalism, see ref. [97]). All loop corrections to the axial pion-nucleon-delta coupling are beyond our working order, but second-order tree-level contributions must be taken into account. Eq. (3.38) relates the renormalised constant  $h_A$  with the unrenormalised parameters  $h_A$ ,  $b_3$  and  $b_6$  and enables to remove  $b_3$  and  $b_6$  by a redefinition of  $h_A$ .

There remain residual contributions from  $b_3$  and  $b_6$  from the non-pole part of the order- $\epsilon^3$  tree diagrams, which are however of the same analytic structure as the  $d_i$ 's modulo terms of higher order. Therefore,  $b_3$  and  $b_6$  can be absorbed at order  $\epsilon^3$  by a shift of the  $d_i$ 's given in sec. 3.5.3. Consequently, in our case one can simply set them to zero.

- **Electromagnetic transition form factor**

The general electromagnetic nucleon-to-delta transition form factor can be expressed in terms of three Lorentz scalar form factors, e.g. ref. [35]

$$\langle \Delta(p') | J^\mu(Q^2) | N(p) \rangle = -\sqrt{\frac{2}{3}} \bar{u}_\nu^\Delta(p') \left\{ \begin{aligned} & \frac{\gamma^\mu k^\nu - \not{k} g^{\mu\nu}}{2} G_1(Q^2) \\ & + \frac{k \cdot p' g^{\mu\nu} - k^\nu p'^\mu}{m_N} G_2(Q^2) \\ & + \frac{k^\mu k^\nu - k^2 g^{\mu\nu}}{m_N} G_3(Q^2) \end{aligned} \right\} u(p), \quad (3.40)$$

where  $Q^2 = -k^2 = -(p' - p)^2$  is the virtuality of the photon. We impose the following renormalisation conditions

$$\bar{b}_1 = \text{Re}\{G_1(0)\} \quad \text{and} \quad \bar{h}_1 = \text{Re}\{G_2(0)\} \quad (3.41)$$

with the momentum of the delta satisfying  $p'^2 = m_\Delta^2$ . The first nonzero contributions to the third form factor  $G_3$  appear only at higher orders and are beyond the scope of this work.

The conditions (3.41) relate the renormalised parameters  $\bar{b}_1$  and  $\bar{h}_1$  with the bare constants  $b_1$ ,  $h_1$ ,  $h_{15}$  and  $h_{16}$  and allow to get rid of the redundant LECs  $h_{15}$  and  $h_{16}$ . Similar to  $b_3$  and  $b_6$ , there remain residual contributions from  $h_{15}$  and  $h_{16}$  from the non-pole part of the deltaful tree diagrams of order  $\epsilon^3$ , which are of the same analytic structure as the  $d_i$ 's modulo terms of higher order. With the shifts given in sec. 3.5.3,  $h_{15}$  and  $h_{16}$  can be removed at order  $\epsilon^3$  in our case. Therefore, we set  $h_{15} = 0$  and  $h_{16} = 0$ .

In the literature, one often finds another parametrisation of the electromagnetic transition form factor done in terms of the couplings  $g_E$ ,  $g_M$  and  $g_C$ :

$$\langle \Delta(p') | J^\mu(Q^2) | N(p) \rangle = \sqrt{\frac{3}{2}} C(Q^2) \bar{u}_\nu^\Delta(p') \left\{ \begin{aligned} & \varepsilon^{\nu\mu\kappa\lambda} p'_\kappa k_\lambda g_M(Q^2) \\ & + (k^\nu p'^\mu - k \cdot p' g^{\nu\mu}) i \gamma_5 g_E(Q^2) \\ & + (k^\nu k^\mu - k^2 g^{\mu\nu}) i \gamma_5 g_C(Q^2) \end{aligned} \right\} u(p) \quad (3.42)$$

with

$$C(Q^2) = \frac{m_\Delta + m_N}{m_N[(m_\Delta + m_N)^2 + Q^2]}. \quad (3.43)$$

The relation between  $G_1$ ,  $G_2$ ,  $G_3$  and  $g_M$ ,  $g_E$ ,  $g_C$  is given by the following eqs.

$$\begin{aligned} g_M(Q^2) &= \frac{2}{3} \frac{1}{C(Q^2)} \frac{G_1(Q^2)}{2m_\Delta}, \\ g_E(Q^2) &= \frac{2}{3} \frac{1}{C(Q^2)} \left( \frac{G_2(Q^2)}{m_N} - \frac{G_1(Q^2)}{2m_\Delta} \right), \\ g_C(Q^2) &= -\frac{2}{3} \frac{1}{C(Q^2)} \frac{G_3(Q^2)}{m_N}. \end{aligned} \quad (3.44)$$

This enables to relate the LECs  $\bar{b}_1$  and  $\bar{h}_1$  to  $g_M(0)$  and  $g_E(0)$  via

$$\bar{b}_1 = 3 \operatorname{Re} \left\{ \frac{m_\Delta}{m_N(m_N + m_\Delta)} g_M(0) \right\} \quad \text{and} \quad \bar{h}_1 = \frac{3}{2} \operatorname{Re} \left\{ \frac{1}{m_N + m_\Delta} (g_E(0) + g_M(0)) \right\}. \quad (3.45)$$

- **Pion-delta coupling**

Renormalisation corrections to the  $\pi\Delta\Delta$  coupling constant  $\hat{g}_1$  are beyond the scope of this work. Therefore, in this work the physical coupling  $g_1$  is equal to the bare constant  $\hat{g}_1$ .

### 3.5.2 Expanding integrals in small parameters and power-counting violating terms

As stated before, the naive power counting eq. (2.31) breaks down when including nucleons into ChPT, because the nucleon mass introduces an additional large scale which does not tend to zero in the chiral limit. In the EOMS scheme [91, 92], the power counting is restored by subtracting the PCVT by hand. In this subsection we discuss how to determine the parts of an integral which must be subtracted.

Any  $n$ -point integral  $I$  can be uniquely decomposed into a so-called *infrared singular* (IS) and *infrared regular* (IR) part:

$$I = \mathcal{I} + \mathcal{R}, \quad (3.46)$$

where the infrared singular part contains all fractional powers of any small parameter  $Q$  for a non-integer spacetime dimension  $d$

$$\mathcal{I} = \mathcal{O}(Q^{d-3}) + \mathcal{O}(Q^{d-2}) + \mathcal{O}(Q^{d-1}) + \dots \quad (3.47)$$

and the infrared regular part only contains integer powers of  $Q$ , even for non-integer spacetime dimensions

$$\mathcal{R} = \mathcal{O}(Q^0) + \mathcal{O}(Q^1) + \mathcal{O}(Q^2) + \dots \quad (3.48)$$

Schindler, Gegelia and Scherer noted that “... the infrared regular part of the [...] integral can be obtained by expanding the integrand in small parameters and interchanging summation and integration over loop momenta” [117]. Therefore, to calculate the IR part of a given integral  $I = \int \frac{d^d l}{(2\pi)^d} f(l)$ , we consider the series

$$\begin{aligned} & \sum_{i,j=0}^{\infty} \frac{(p^2 - m^2)^i (M^2)^j}{i! j!} \left[ \left( \frac{1}{2p^2} p_\mu \frac{\partial}{\partial p_\mu} \right)^i \left( \frac{\partial}{\partial M^2} \right)^j f(l) \right]_{p^2=m^2, M^2=0} \\ &= f(l) \Big|_{p^2=m^2, M^2=0} + (p^2 - m^2) \left[ \frac{1}{2p^2} p_\mu \frac{\partial}{\partial p_\mu} f(l) \right]_{p^2=m^2, M^2=0} \\ &+ M^2 \left[ \frac{\partial}{\partial M^2} f(l) \right]_{p^2=m^2, M^2=0} + \dots \end{aligned} \quad (3.49)$$

applied to the integrand  $f(l)$ . Here, the assignment  $[\dots]_{p^2=m^2, M^2=0}$  denotes that the coefficients of  $(p^2 - m^2)^i (M^2)^j$  are only considered for four-momenta  $p$  satisfying the on-mass-shell constraint.

Let us illustrate the counting on a simple example first, such as the integral contributing to the self-energy of the nucleon

$$I_{\pi N} = \int \frac{d^d l}{(2\pi)^d} \frac{1}{(l^2 - M^2)((l+p)^2 - m^2)}, \quad (3.50)$$

where we omit the  $+i\epsilon$  prescription. Using a naive counting, the chiral order of an integral receives  $\mathcal{O}(Q^d)$  from each integration over  $d$  spacetime dimensions,  $\mathcal{O}(Q^{-2})$  from every pion propagator and  $\mathcal{O}(Q^{-1})$  from every nucleon propagator. Thus, we expect eq. (3.50) to be of order  $\mathcal{O}(Q^1)$ , but naive counting fails here. Carrying out the series (3.49) to the integrand of eq. (3.50), we obtain

$$\begin{aligned} & \sum_{i,j=0}^{\infty} \frac{(p^2 - m^2)^i (M^2)^j}{i! j!} \left[ \left( \frac{1}{2p^2} p_\mu \frac{\partial}{\partial p_\mu} \right)^i \left( \frac{\partial}{\partial M^2} \right)^j \frac{1}{(l^2 - M^2)((l-p)^2 - m^2)} \right]_{p^2=m^2, M^2=0} \\ &= a_{00} + a_{01} M^2 + a_{10} (p^2 - m^2) + a_{11} (p^2 - m^2) M^2 + \dots \end{aligned} \quad (3.51)$$

with the coefficients

$$\begin{aligned} a_{00} &= \frac{1}{l^2(l^2 - 2l \cdot p)}, \\ a_{01} &= \frac{1}{l^4(l^2 - 2l \cdot p)}, \\ a_{10} &= \frac{1}{2m^2(l^2 - 2l \cdot p)^2} - \frac{1}{l^2(l^2 - 2l \cdot p)^2} - \frac{1}{2m^2 l^2(l^2 - 2l \cdot p)}, \\ a_{11} &= 0, \end{aligned} \quad (3.52)$$

where we have eliminated the term  $l \cdot p$  in the numerator of  $a_{10}$  through cancellation with a

propagator. Note that when carrying out the derivatives, higher order tensor integrals may occur, which cannot be taken care of as easily as in this case. Such tensor integrals can be reduced to scalar integrals in higher dimensions using the procedure of Passarino and Veltman [142], afterwards the dimensional shift can be eliminated using Davydychev's approach [143]. Finally, the remaining integration is carried out. The solution is commonly known (see e.g. ref. [144])

$$i \int \frac{d^d l}{(2\pi)^d} \frac{1}{(l^2)^\alpha (l^2 - 2l \cdot p)^\beta} \Bigg|_{p^2=m^2} = \frac{i^{2-2(\alpha+\beta)}}{(4\pi)^{d/2}} m^{d-2(\alpha+\beta)} \frac{\Gamma(d-2\alpha-\beta)\Gamma(-\frac{d}{2}+\alpha+\beta)}{\Gamma(\beta)\Gamma(d-\alpha-\beta)}. \quad (3.53)$$

We obtain

$$i I_{\pi N} = A_{00} + A_{01} M^2 + A_{10} (p^2 - m^2) + \mathcal{O}(Q^4) + \mathcal{I}, \quad (3.54)$$

with the coefficients

$$A_{00} = -\frac{m^{d-4}\Gamma(2-\frac{d}{2})}{(4\pi)^{d/2}(d-3)}, \quad A_{01} = \frac{m^{d-6}\Gamma(2-\frac{d}{2})}{2(4\pi)^{d/2}(5-d)}, \quad A_{10} = \frac{m^{d-6}\Gamma(2-\frac{d}{2})}{2(4\pi)^{d/2}(d-3)} \quad (3.55)$$

(cf. ref. [117]). Expanding the IR part of the full integral  $\mu^{4-d} I_{\pi N}$  around the physical point  $d=4$ , we get

$$\mathcal{R}(I_{\pi N}) \approx -\frac{i}{8\pi^2(d-4)} - i \frac{-2 + \gamma_E - \ln(4\pi)}{16\pi^2} + \mathcal{O}(d-4). \quad (3.56)$$

In the common renormalisation procedure according to the  $\widetilde{MS}$  scheme [24, 92], the UV divergent part of the integral plus a constant

$$\bar{\lambda} = \frac{\mu^{d-4}}{16\pi^2} \left( \frac{1}{d-4} + \frac{1}{2}(-1 + \gamma_E - \ln(4\pi)) \right) \quad (3.57)$$

is subtracted. However, in the case of  $I_{\pi N}$

$$\mathcal{R}(I_{\pi N}) \approx -2i\bar{\lambda} + \frac{i}{16\pi^2} + \mathcal{O}(d-4) \quad (3.58)$$

we see that even after the subtraction of  $-2i\bar{\lambda}$ , the term  $\frac{i}{16\pi^2}$  violates the naive power counting. In the extended-on-mass-shell scheme (EOMS) [92], this term is subtracted separately. Consequently, the naive power counting as given in eq. (2.30) is restored. As we have seen from eq. (3.48), power-counting violating terms can only occur in the IR part. Thus it is sufficient to calculate this part to be able to subtract all PCVT.

Note that there is a difference between the EOMS approach and the earlier developed infrared regularisation of Becher and Leutwyler [90], where the whole IR term  $\mathcal{R}$  is subtracted and only the IS term  $\mathcal{I}$ , after having subtracted the singularities in  $d-4$ , is kept. The argument of Becher

and Leutwyler why  $\mathcal{R}$  may be dropped is that it is effectively taken into account through the counterterms in the effective Lagrangian.

For the determination of the PCVT in practical (automatised) calculations, instead of applying eq. (3.49) to an integrand, we proceeded as follows: first all propagators are rewritten with the Schwinger parametrisation

$$\frac{1}{(k^2 - m^2 + i\epsilon)^\alpha} = \frac{(-i)^\alpha}{\Gamma(\alpha)} \int_0^\infty d\lambda \lambda^{\alpha-1} \exp\{i\lambda(k^2 - m^2 + i\epsilon)\}; \quad (3.59)$$

next, the  $d$ -dimensional integration is carried out using the generalised Gaussian formula. Then, the derivatives with respect to Lorentz-invariant dimensionless parameters

$$\begin{aligned} \mathcal{O}(Q) : & \quad \frac{p^2 - m^2}{m^2}, \quad \frac{k \cdot p}{m^2}, \quad \frac{p \cdot q}{m^2}, \\ \mathcal{O}(Q^2) : & \quad \frac{M^2}{m^2}, \quad \frac{k^2}{m^2}, \quad \frac{q^2}{m^2}, \quad \frac{k \cdot q}{m^2} \end{aligned} \quad (3.60)$$

are taken, where it is assumed that the momenta from the nucleon lines are close to the mass shell

$$\frac{(p+k)^2 - m^2}{m^2} \sim \mathcal{O}(Q) \Rightarrow \frac{k \cdot p}{m^2} = \frac{1}{2m^2}((p+k)^2 - p^2 - k^2) \sim \mathcal{O}(Q),$$

and similarly for  $\frac{p \cdot q}{m^2}$ . Finally, the integration over the Schwinger parameters is completed, where the substitution

$$\begin{aligned} \{\lambda_1, \dots, \lambda_n\} &\rightarrow \{\lambda z_1, \lambda z_2(1-z_1), \lambda z_3(1-z_1)(1-z_2), \dots, \lambda z_n(1-z_1) \times \dots \times (1-z_{n-1})\}, \\ \lambda_i &\in [0, \infty], \quad \lambda \in [0, \infty] \quad \text{and} \quad z_j \in [0, 1] \end{aligned} \quad (3.61)$$

comes in handy, because in a lot of cases, the remaining integrals take one of the following forms

$$\int_0^\infty \lambda^a \exp\{b\lambda\} d\lambda = (-b)^{-a-1} \Gamma(a+1) \quad (3.62)$$

and/or

$$\int_0^1 z^{a-1} (1-z)^{b-1} dz = B(a, b) = \frac{\Gamma(a) \Gamma(b)}{\Gamma(a+b)}. \quad (3.63)$$

### 3.5.3 Renormalisation of LECs

Additionally to the UV divergences removed by on-shell renormalisation of the subprocesses, off-shell effects or radius terms can give rise to more UV divergent pieces, which must be

removed separately. This is achieved through an additional shift of all LECs appearing in the contact term. The shift is defined as

$$d_i = \bar{d}_i - \beta_{d_i} \frac{A_0(M_\pi^2)}{2M_\pi^2 F_\pi^2} \quad (3.64)$$

in the covariant approach [24] and as

$$\hat{d}_i = \hat{d}_i^r + \beta_{\hat{d}_i} \frac{\bar{\lambda}}{F_\pi^2} \quad (3.65)$$

in the HB approach [145], where the renormalised LECs are denoted by the superscript “*r*” in the HB approach and by the bar in the covariant case. Note that the subtraction of the pion tadpole function

$$A_0(M_\pi^2) = -2M_\pi^2 \left( \bar{\lambda} + \frac{1}{32\pi^2} \ln \left( \frac{M_\pi^2}{\mu^2} \right) \right) \quad (3.66)$$

is just a convention; it does not change the values of the beta functions, but of course affects the numerical value of the LECs through the additional constant. The quantity  $\bar{\lambda}$  was defined in eq. (3.57).

In the deltaless HB sector, the beta functions were given by Gasser and Ivanov [145]:

$$\beta_{\hat{d}_8} = 0, \quad \beta_{\hat{d}_9} = 0, \quad \beta_{\hat{d}_{20}} = g_A + g_A^3, \quad \beta_{\hat{d}_{21}} = -g_A^3, \quad \beta_{\hat{d}_{22}} = 0. \quad (3.67)$$

In the covariant approach, they can easily be derived by expanding the UV divergent piece of the whole scattering amplitude in the small scales up to the working order. In the deltaless approach, they vanish

$$\beta_{d_8} = \beta_{d_9} = \beta_{d_{20}} = \beta_{d_{21}} = \beta_{d_{22}} = 0, \quad (3.68)$$

but for the full  $\epsilon^3$  amplitude, they read

$$\begin{aligned} \beta_{d_8} &= \frac{19}{54} g_A h_A^2 - \frac{55}{729} g_1 h_A^2, & \beta_{d_9} &= -\frac{97}{324} g_A h_A^2 + \frac{55}{1458} g_1 h_A^2, & \beta_{d_{20}} &= \frac{47}{162} g_A h_A^2 - \frac{2555}{1458} g_1 h_A^2, \\ \beta_{d_{21}} &= -\frac{823}{162} g_A h_A^2 + \frac{10}{27} g_1 h_A^2, & \beta_{d_{22}} &= \frac{40}{27} g_A h_A^2 - \frac{425}{243} g_1 h_A^2. \end{aligned} \quad (3.69)$$

In the EOMS scheme, the power-counting violating terms must be subtracted separately by shifting the LECs. Up to the order we are working in pion photoproduction, it can easily be argued that PCVT cannot occur. Only loop diagrams from the third order can give rise to such terms, which should be absorbed by the constants appearing at one order lower. But because there is no contact interaction at second order, hypothetical PCVT could not be absorbed and thus must cancel. If we were to work up to  $q^4$  or  $\epsilon^4$ , we would not be able to exclude PCVT by this argument, because the contact term of third order is not vanishing. In sec. 3.6.4, we

describe that we explicitly checked the absence of PCVT relevant for our study. We conclude that for our study the EOMS scheme is effectively equivalent to the  $\widetilde{MS}$  scheme [24, 92].

As explained in sec. 3.5.1, the additional shifts to absorb the redundant constants  $b_3, b_6, h_{15}$  and  $h_{16}$  in the covariant order- $\epsilon^3$  amplitude through a redefinition of  $h_A$ ,  $b_1$  and  $h_1$  are given by

$$\delta_{d_8} = \delta_{d_{20}} = -\delta_{d_{21}} = \frac{-b_1(b_3 + b_6) + 2h_A(h_{15} + h_{16})}{9}, \quad \delta_{d_9} = \delta_{d_{22}} = 0. \quad (3.70)$$

## 3.6 Consistency checks

Deriving the scattering amplitude requires multiple steps. Given the full effective Lagrangian described in sec. 2.5, Feynman rules should be derived for both covariant and HB approach. We give all relevant nonzero expressions in the appendix D, which are used next to construct all Feynman diagrams up to our working order. The diagrams are shown explicitly in the appendix B. Summing all contributions up, we obtain the pion photoproduction amplitude, or to be more precise, several amplitudes depending on the chosen framework and the working order. These are in general long and cumbersome analytic expressions, which must fulfil certain constraints imposed by symmetries, Lorentz invariance or basic construction principles. It is highly desirable to explicitly check if the obtained amplitudes fulfil these requirements to minimise the chance of errors, such as missing symmetry factors or Feynman diagrams. In the following, we shortly describe the performed consistency checks.

### 3.6.1 Independence from off-shell effects

As mentioned in section 2.2, eq. (2.4) is not the only possibility to parametrise the pion field. The most general form of such a parametrisation up to  $\pi^4$  (see ref. [114]) is

$$U(x) = \mathbb{1} + i \frac{\boldsymbol{\tau} \cdot \boldsymbol{\pi}}{F} - \frac{\pi^2}{2F^2} - i \alpha \frac{\pi^2 \boldsymbol{\tau} \cdot \boldsymbol{\pi}}{F^3} + (\alpha - \frac{1}{8}) \frac{\pi^4}{F^4} + \mathcal{O}(\pi^5), \quad (3.71)$$

which is constrained by unitarity. The exponential parametrisation  $U(x) = \exp \left\{ i \frac{\boldsymbol{\tau} \cdot \boldsymbol{\pi}}{F} \right\}$  corresponds to the choice  $\alpha = 1/6$ . Another commonly used parametrisation, the so-called sigma gauge

$$U(x) = \sqrt{1 - \frac{\pi^2}{F^2}} + i \frac{\boldsymbol{\tau} \cdot \boldsymbol{\pi}}{F} \quad (3.72)$$

corresponds to  $\alpha = 0$ . Because any choice for  $\alpha$  is possible, observables must not depend on it. Throughout this work, the pion field has been implemented in the general parametrisation and we have explicitly verified that results are independent of  $\alpha$ . This check is, however, only relevant for diagrams with vertices involving three or more pions, because all vertices with a lower number of pions are  $\alpha$ -independent.

### 3.6.2 Cancellation of UV divergences

The full renormalised amplitude must be free of divergent  $(d - 4)^{-1}$  terms. Although the absence of such terms is proven for the subprocesses when performing on-shell renormalisation, we have additionally checked the cancellation in the full photoproduction by replacing the integrals by their UV divergent part and expanding the amplitude up to the working order in small parameters. It is important to note that the amplitude may still have divergent parts in higher orders. These parts originate from the construction of the covariant Lagrangian, which is only unique modulo higher-order terms. The divergent parts only cancel exactly at the working order. However, in practical calculations, one has to choose a specific value for the divergent quantity  $\bar{\lambda}$  (eq. (3.57)). Due to the included subsequent orders, the choice of  $\bar{\lambda}$  has a small numerical effect on the results. We choose to implement  $\bar{\lambda} = 0$ .

### 3.6.3 Electromagnetic current conservation

The invariant amplitude  $\mathcal{M} = \epsilon^\mu \mathcal{M}_\mu$  of pion photoproduction must fulfil electromagnetic current conservation

$$k^\mu \mathcal{M}_\mu = 0. \quad (3.73)$$

This constraint, however, is not required for individual Feynman diagrams and thus can serve as a nontrivial check to see if the full amplitude does not contain mistakes. We proceed the way Bernard et al. described in ref. [60], i.e. to check current conservation in diagrammatic subgroups, which are constructed by first drawing a diagram without a photon line and afterwards attaching the photon in every possible way allowed by the vertices of the leading order Lagrangian. The obtained set of diagrams (in fig. 3.2 an example is depicted) must obey transversality (3.73). If the group contains a diagram with loop corrections to one of the

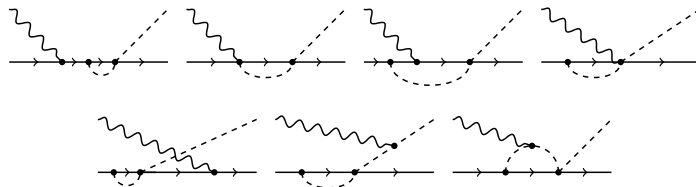


**Figure 3.2:** Example of a gauge invariant subset of deltaless Feynman diagrams: all vertices are of lowest order, i.e. of first order if involving nucleons, of second order if purely bosonic. Wiggly lines correspond to photons, dashed lines to pions and solid lines correspond to nucleons.

external legs, we proceed as follows: we construct the corresponding set of tree diagrams by replacing the loop in the photonless diagram with the third-order counterterm and add the two groups. Because the diagram with the external loop correction is exactly cancelled by its counterterm, we remove these diagrams from the combined set. An example for this case is shown in fig. 3.3. In the heavy baryon approach, this statement holds order by order in the

$1/m_N$  expansion.

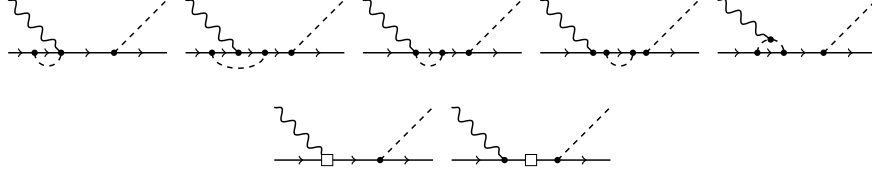


**Figure 3.3:** Example of a gauge invariant subset obtained from combining tree and loop diagrams: empty squares are of third order.

We obtain nine nonvanishing gauge groups in both the deltaless and deltaful case. To see that the diagrams cancel each other, the integrals must be reduced to the minimal set of master integrals [142, 143]. The reduction generates large analytic expressions, which must cancel exactly. Showing transversality for the amplitude provides a nontrivial check that the expressions are correct.<sup>2</sup>

### 3.6.4 Freedom of power-counting violating terms

As was argued in sec. 3.5.3, we expect no PCVT up to the working order we consider. This means that the sum of all diagrams of a given order should respect power counting. However, individual Feynman diagrams can break the power counting, but PCVT should vanish when all diagrams are added. In the deltaless case, we made sure that the power-counting violating contributions of the loops cancel each other. This was done by replacing all occurring integrals by their IR part (see sec. 3.5.2) and performing an explicit expansion in the small scales. We verified that all PCVT cancel out, which provides another valuable check that the amplitude is correct, because nontrivial cancellations are analytically fulfilled. In the deltaful approach at order  $\epsilon^3$ , we refrained from repeating this exercise, since the same argument as in the deltaless case holds and performing the comparable test would require considerably more effort.

### 3.6.5 Delta decoupling

In a deltaful theory, the amplitude  $\mathcal{M}$  receives contributions from the deltaless and deltaful Lagrangian and can be written as

$$\mathcal{M} = \mathcal{M}_\Delta + \mathcal{M}_{\Delta}, \quad (3.74)$$

with the subscript  $\Delta(\Delta)$  indicating the deltaless (deltaful) part. The decoupling theorem [146–148] states that at low energies, the effects of the delta resonance can be implicitly taken care

---

<sup>2</sup>Verification of gauge invariance in the deltaful case was technically more difficult, because the size of the intermediate symbolic expressions greatly exceeded the RAM on our computer. Therefore, to reduce the size of the symbolic expressions, we inserted random integers for all constants and performed the reduction to the minimal set of master integrals. We repeated the procedure for several random integer choices to increase the probability that the exact zero is not generated accidentally.

of through the deltaless effective Lagrangian; modifying the numerical values of the LECs. If one considers the contribution  $\mathcal{M}_\Delta$  in the limit  $m_\Delta - m_N = \Delta \rightarrow \infty$ , the result contains in general both positive and negative powers of the mass split  $\Delta$ . Negative powers of  $\Delta$  contribute to the resonance saturation of the LECs (see sec. 3.8) and vanish in the hypothetical limit of a very heavy delta particle, which corresponds to decoupling this degree of freedom. The positive powers of the mass split spoil the constraint that all explicit effects from the  $\Delta$  must vanish in the heavy mass limit, thus they should be eliminated by a redefinition of the LECs (similar to the absorption of the PCVT in the EOMS scheme).

We checked the explicit decoupling of the delta degree of freedom numerically. For this purpose, we considered the nine deltaful gauge groups, of which two represent a trivial case, because there are no delta propagators inside the loops and two groups containing the  $\pi N \Delta$  vertex were combined for symmetry reasons. Consequently, for six groups of diagrams, we checked the limit  $\Delta \rightarrow \infty$  numerically by increasing the mass split up to  $\Delta = 100$  GeV and checked that the contributions to the multipoles decrease for increasing mass split. Thus, pion photoproduction does not encounter decoupling violation up to our working order.

### 3.7 Comparison of LECs in heavy baryon and covariant approach

The numerical values of LECs in the covariant and in the heavy baryon approach are in general not directly comparable. First, the values are related by  $1/m_N$  corrections, which originate from the construction of the HB Lagrangian, where a strict expansion in terms of the inverse nucleon mass is done, such that the dependence on  $m_N$  is shifted to a series of additional contact interactions suppressed by powers in  $1/m_N$ . Because Lagrangians of subleading order must be constructed in such a way that all possible interaction types are contained,  $1/m_N$  corrections from lower order Lagrangians have the same analytic structure as the subleading terms and therefore effectively modify the LECs (see sec. 2.3.2 for an example). Note that the corrections are only relevant if the working order is beyond the order at which the LECs appear first. For example, the values of  $b_1$  in both frameworks can be compared directly if only the leading delta tree contributions (order  $\epsilon^2$ ) are included, because the difference starts to arise from  $1/m_N$ , which, however, is beyond the working order.

For LECs appearing at loop level, an extra shift generated by the IR part of the loop integrals should be considered. In the covariant framework, the IR part gives rise to additional numerical contributions, which affect the fitted values of the LECs. Because these parts are absent in the HB approach, the covariant LECs cannot be compared with the HB values, even if inverse nucleon mass corrections are irrelevant. However, the contributions of the IR part to the covariant LECs can be calculated analytically and switched off, so comparability can be restored. We determined these IR shifts by replacing the integrals of the covariant amplitude by their corresponding IR term (see sec. 3.5.2) and adjusting the constants in such a way that the obtained expression vanishes. The shifts we found for the relevant  $d_i$ 's at the renormalisation

scale  $\mu = m_N$  are given by

$$\begin{aligned}\Delta d_8^{\text{IR}} &= d_8 - \hat{d}_8 = \frac{g_A}{128F_\pi^2\pi^2}(3 + g_A^2), \\ \Delta d_9^{\text{IR}} &= d_9 - \hat{d}_9 = \frac{g_A}{128F_\pi^2\pi^2}(-1 + g_A^2), \\ \Delta d_{20}^{\text{IR}} &= d_{20} - \hat{d}_{20} = \frac{g_A}{96F_\pi^2\pi^2}(9 - 3\gamma_E(1 + g_A^2) + 3(1 + g_A^2)\ln(4\pi) + 14g_A^2), \\ \Delta d_{21;22}^{\text{IR}} &= d_{21;22} - \hat{d}_{21;22} = \frac{g_A}{96F_\pi^2\pi^2}(-3 + g_A^2(-11 + 3\gamma_E - 3\ln(4\pi))),\end{aligned}\quad (3.75)$$

where we recall that the constants with the hat refer to HB parameters. Furthermore, we remark that the constant  $d_{21;22} = d_{21} - \frac{1}{2}d_{22}$  is a linear combination of the two constants  $d_{21}$  and  $d_{22}$ . In real pion photoproduction, the two constants enter the scattering amplitude only in this particular combination, and since we have performed the calculation only for real photons, we can only extract the shift of the combination of the two LECs. We comment on the fulfilment of these differences in chapter 5.

An additional check for the correctness of the calculated IR parts and the scattering amplitude is to repeat the same exercise with the  $d$ -divergent part of the amplitude and check if the difference between HB and covariant beta functions cancels the remaining divergent terms. Using the expressions given in sec. 3.5.3, we found that this requirement is fulfilled.

## 3.8 Resonance saturation of LECs

The decoupling theorem [146] states that the explicit treatment of the delta resonance affects the numerical values of the LECs. Therefore one cannot compare the constants of a deltaful and deltaless approach directly. However, it is possible to understand their differences analytically by calculating the dominating leading-order contributions of the delta to specific LECs. Because the mass of the delta lies close to the nucleon mass, it is expected that the difference of the LECs in the two approaches is of the same size as the leading order term of the heavy delta mass limit. In our case, this is accomplished by expanding the order- $\epsilon^2$  deltaful tree diagrams (see fig. B.9) in the limit  $m_\Delta - m_N = \Delta \rightarrow \infty$  and matching the obtained expressions with the contact term structures of the deltaless theory. This procedure yields

$$\delta d_8(\Delta) = -\delta d_{21;22}(\Delta) = -\frac{h_A b_1}{9\Delta}, \quad \delta d_9(\Delta) = \delta d_{20}(\Delta) = 0, \quad (3.76)$$

with  $\delta d_i(\Delta) = \bar{d}_i^\Delta - \bar{d}_i^\Delta$  denoting the difference between the constant  $\bar{d}_i$  in the deltaless (superscript  $\Delta$ ) and deltaful (superscript  $\Delta$ ) approach. The review of this estimate is given in sec. 5.2.

### 3.9 Fitting observables and error estimation

To determine the unknown LECs, we fit our results of multipole amplitudes to the MAID2007 partial-wave analysis [149]. We use the method of least squares, which means that the quantity

$$\chi^2 = \sum_{i=1}^N \left( \frac{O_i^{\text{exp}} - O_i^{(n)}}{\delta O_i} \right)^2 \quad (3.77)$$

is minimised with respect to the LECs. Here,  $N$  is the total number of used data points,  $O_i^{\text{exp}}$  is the given value for the data point  $i$ ,  $O_i^{(n)}$  is the calculated result from ChPT to order  $(n)$  and  $\delta O_i$  is the corresponding uncertainty

$$\delta O_i = \sqrt{\left( \delta O_i^{\text{exp}} \right)^2 + \left( \delta O_i^{(n)} \right)^2}, \quad (3.78)$$

combined out of experimental, given uncertainty  $\delta O_i^{\text{exp}}$  and estimated truncation error  $\delta O_i^{(n)}$ , whose determination is described in the following.

The truncation errors are calculated using a Bayesian approach [103–105] adapted for our purposes. Therefore, we explicitly write down the chiral expansion of the observable

$$O = O^{(1)} + \Delta O^{(2)} + \Delta O^{(3)} + \dots =: O_{\text{ref}} (c_0 + c_1 Q + c_2 Q^2 + \dots) \quad (3.79)$$

with  $\Delta O^{(i)} = O^{(i)} - O^{(i-1)}$  defined as the  $i$ th correction to the leading contribution. The RHS of eq. (3.79) defines the dimensionless constants  $c_i$  – the coefficients in the expansion of  $O$  in terms of the small quantity  $Q$ . The overall factor  $O_{\text{ref}}$  serves as a reference scale, which we discuss below. The small quantity

$$Q = \max \left( \frac{E_\pi}{\Lambda_b}, \frac{M_\pi^{\text{eff}}}{\Lambda_b} \right) \quad (3.80)$$

is defined as the quotient of the pion energy and the chiral breakdown scale, and we adopt the constraint from ref. [105] to set a lower boundary of  $M_\pi^{\text{eff}} = 200$  MeV on it.

If a quantity is known up to  $n$ th order, we want to assess the size of the remaining contributions  $\sum_{i>n} \Delta O^{(n)}$ , which are neglected. The idea is that the uncertainty of the observable is smaller if the approximating series converges fast and vice versa. Put another way, we want to calculate the posterior probability distribution function (pdf) for  $\delta O^{(n)}$  under the premise that the observable calculated up to the  $n$ th chiral order  $\{O^{(1)}, O^{(2)}, \dots, O^{(n)}\}$  is known.

In ref. [104], the reference scale  $O_{\text{ref}}$  is set to the leading order contribution

$$O_{\text{ref}} = O^{(1)}, \quad (3.81)$$

which fixes  $c_0 = 1$ . However, Epelbaum et al. have argued [105] that this choice might be too

restrictive under certain circumstances, such as e.g. in the neutral channel of pion photoproduction, where the Kroll-Ruderman term is absent and the NLO is of the same size as the LO. Thus, we alter the choice by defining [105]

$$O_{\text{ref}} = \max \left\{ |O^{(1)}|, \frac{|\Delta O^{(2)}|}{Q}, \frac{|\Delta O^{(3)}|}{Q^2} \right\} \quad (3.82)$$

to take into account the cases where the leading and subleading orders are of the same size. Now let us consider  $c_m = 1$  with  $m \in 1, 2, 3$  to be the coefficient defining the reference scale. The remaining  $c_i$  are assumed to be distributed according to some common pdf  $\text{pr}(c_i|\bar{c})$  with a so-called hyperparameter  $\bar{c}$ . Furthermore, we assume that the truncation error is dominated by  $h$  chiral orders  $n+1, \dots, n+h$ , such that the dimensionless residual can be approximated by

$$\Delta_n = \sum_{j=n+1}^{\infty} c_j Q^j \approx \sum_{j=n+1}^{n+h} c_j Q^j. \quad (3.83)$$

The probability distribution for  $\Delta_n$  to take a certain value  $\Delta_k = \Delta$  is given by [104]<sup>3</sup>

$$\text{pr}_h(\Delta|\{c_{i \leq n}\}) = \frac{\int_0^\infty d\bar{c} \text{pr}_h(\Delta|\bar{c}) \text{pr}(\bar{c}) \prod_{i \in A} \text{pr}(c_i|\bar{c})}{\int_0^\infty d\bar{c} \text{pr}(\bar{c}) \prod_{i \in A} \text{pr}(c_i|\bar{c})} \quad (3.84)$$

with  $A = \{j \in \mathbb{N}_0 | j \leq n \wedge j \neq 1 \wedge j \neq m\}$  and

$$\text{pr}_h(\Delta|\bar{c}) = \left( \prod_{i=n+1}^{n+h} \int_{-\infty}^{\infty} dc_i \text{pr}(c_i|\bar{c}) \right) \delta \left( \Delta - \sum_{j=n+1}^{n+h} c_j Q^j \right). \quad (3.85)$$

We use the Gaussian prior from ref. [104]

$$\text{pr}(c_i|\bar{c}) = \frac{1}{\sqrt{2\pi\bar{c}}} \exp \left\{ -\frac{c_i^2}{4\bar{c}^2} \right\}, \quad (3.86)$$

and assume a log-uniform probability distribution [150]

$$\text{pr}(\bar{c}) = \frac{1}{\ln(\bar{c}_>/\bar{c}_<)} \frac{1}{\bar{c}} \Theta(\bar{c} - \bar{c}_<) \Theta(\bar{c}_> - \bar{c}). \quad (3.87)$$

---

<sup>3</sup>The quantity  $\Delta$  used in this section is not to be confused with the delta-nucleon mass split  $\Delta = m_\Delta - m_N$ .

Fortunately, with these choices, the solution of eq. (3.84) can be given analytically [104]

$$\begin{aligned} \text{pr}_h^C(\Delta | \{c_{i \leq n}\}) &= \frac{1}{\sqrt{\pi \bar{q}^2 c_n^2}} \left( \frac{c_n^2}{c_n^2 + \Delta^2 / \bar{q}^2} \right)^{n/2} \times \\ &\times \frac{\Gamma\left(\frac{n}{2}, \frac{1}{2\bar{c}_>} \left(c_n^2 + \frac{\Delta^2}{\bar{q}^2}\right)\right) - \Gamma\left(\frac{n}{2}, \frac{1}{2\bar{c}_<} \left(c_n^2 + \frac{\Delta^2}{\bar{q}^2}\right)\right)}{\Gamma\left(\frac{n-1}{2}, \frac{c_n^2}{2\bar{c}_>^2}\right) - \Gamma\left(\frac{n-1}{2}, \frac{c_n^2}{2\bar{c}_<^2}\right)}, \end{aligned} \quad (3.88)$$

where  $\bar{q}^2 = \sum_{i=n+1}^{n+h} Q^{2i}$  and  $\Gamma(s, x) = \int_x^\infty t^{s-1} \exp\{-t\}$  is the incomplete Gamma function. Now, the truncation error

$$\delta O^{(k)} = O_{\text{ref}} \Delta_k \quad (3.89)$$

can be obtained after determining the corresponding value of the residual  $\Delta_k$  from numerically integrating the probability distribution  $\text{pr}_h(\Delta | \{c_{i \leq k}\})$  in eq. (3.88) and demanding the result to be equal to a certain degree of belief: we choose to employ 68 %. This, however, can only be obtained by fixing the two remaining parameters  $\bar{c}_<$  and  $\bar{c}_>$ , which impose assumptions on the likeliness of  $\bar{c}$ . We stick to the choice of ref. [105]  $c_< = 0.5$  and  $c_> = 10$ .

### 3.10 Constants and numeric conventions

In this section, the numerical values of constants and conventions related to divergent integrals are given. In table 3.1, we summarise the values for the fundamental constants and masses which we used in this work. Since we fitted the delta mass ourselves, its value is given in sec. 5.2.1. Also, as stated in sec. 3.6.2, we checked the cancellation of the UV-divergent pieces

**Table 3.1:** Numerical values of masses and constants used in this work:  $M_\pi$ ,  $m_N$ ,  $e$  and  $F_\pi$  were taken from ref. [110],  $g_A$  was taken from ref. [132],  $h_A$  was taken from ref. [133] and  $g_1$  was taken from ref. [37].

$M_\pi$ [MeV]	$m_N$ [MeV]	$e$	$F_\pi$ [MeV]	$g_A$	$h_A$	$g_1$
138.03	938.27	0.303	92.4	1.29	1.43	-1.21

of the loop functions at order  $q^3$  and  $\epsilon^3$ . In higher orders, however, UV-divergent pieces remain, therefore one must pick specific values of the finite parts of LECs, which affects the numeric results slightly. The same holds for the renormalisation scale  $\mu$ : at leading order, the dependence on it must cancel, but its choice numerically affects the higher orders. We choose to work in the  $\overline{MS}$  scheme [24, 92], which is equivalent to setting the quantities  $\bar{\lambda} = 0$  and  $\mu = m_N$ . As a consequence, the nucleon tadpole integral vanishes  $A_0(m_N^2) = 0$ .

## 4 Technical details on the calculation

Calculating observables using the effective Lagrangian given in sec. 2.5 requires a lot of intermediate steps and processing of large expressions. Performing such computations by hand is too complicated, that is why we make extensive use of a computer algebra system (CAS) and employ several packages.

In large parts, the calculations in this work were done in the CAS *Mathematica* [151]. The processing of spin and isospin algebra is outsourced to FORM [152], a symbolic manipulation system, which is efficient in calculating traces of gamma matrices. For the numerical evaluation of loop integrals in the covariant case, we rely on the *LoopTools* package for Mathematica<sup>1</sup> [153] and on the *X* package [154]. We use *LoopTools* to obtain the numerical results of tensor loop functions; a procedure which is considerably faster than evaluating the full Passarino-Veltman reduced amplitude [142, 155]. However, *LoopTools* cannot give results for all integrals at unphysical kinematical points arising in the on-mass-shell renormalisation scheme. We evaluate the latter using the *X* package or perform the numerical integration explicitly after rewriting the expressions with the Schwinger parametrisation. In the HB formalism, the solution of all arising integrals can be given analytically, because in the case of real photons, the most complicated integrals are two-point functions.

We briefly describe how we obtained observables in the following:

1. The effective Lagrangian is typed into *Mathematica* as symbolic expressions, all necessary Feynman rules are derived and saved in FORM format. The *Mathematica* code which derives Feynman rules was initially developed by Krebs [156]. We have adjusted this code for our applications.
2. The leading-order tree-level topologies as well as loop topologies for the relevant Feynman graphs are entered as *Mathematica* expressions. Subsequently, Feynman rules are automatically substituted in FORM using the predefined vertices and propagators. Higher-order tree and deltaful topologies are automatically generated.
3. The diagrams are processed in FORM; i.e. spin and isospin algebra reduction in  $d$  dimensions is performed, loop integrals are identified. Afterwards, the expressions are reimported to *Mathematica*.
4. Renormalisation in  $d$  dimensions is performed by inserting the relevant counterterms and shifting the LECs.

---

<sup>1</sup>The quantity  $\Delta$  used in this section is not to be confused with the delta-nucleon mass split  $\Delta = m_\Delta - m_N$ .

5. Further checks, such as verification of gauge invariance and identification of power-counting violating terms are performed (see sec. 3.6).
6. In the HB approach, tensor loop integrals are reduced using the Passarino-Veltman algorithm [142]. The remaining master integrals are replaced by their analytic solutions, which are known. In the covariant approach, we stick to the unreduced tensor loop integrals, which are subsequently evaluated by *LoopTools* (or the *X* package). In the case of deltaful loop diagrams, some high rank integrals with two propagators appear, which *LoopTools* cannot handle directly. We reduced these integrals iteratively until *LoopTools* could evaluate the resulting expressions, such that the reduction was not performed to the minimal set of integrals.
7. The amplitude is evaluated in  $d = 4$  dimensions. To take the limit correctly, we first set  $d$  to 4 as well as  $\bar{\lambda} = 0$  and add the series coefficient of  $(d-4)^0$  of the amplitude where all integrals are replaced by their UV divergent part. This is required to ensure that terms like

$$\frac{d}{d-4} = \frac{4}{d-4} + 1 \quad (4.1)$$

are not forgotten.

8. The observables of interest are calculated from the amplitude, which are numerically evaluated as functions of the unknown LECs. Afterwards, the observables are fitted to the data. The fits are described in more detail in the next chapter.

# 5 Observables and results

In this chapter, we present the results we obtained for pion photoproduction. First, we present our results for the deltaless case. Next, we turn to the deltaful theory and start by discussing how we treat the delta mass and why we fit it instead of relying on the literature values. Afterwards we analyse a special case, where only deltaful tree-level diagrams are included. Subsequently we show our results of the full covariant  $\epsilon^3$  calculation and conclude the section with our results for cross sections and polarisation asymmetries in the neutral pion production channel.

Note that the deltaless case has already been extensively studied in the literature in both covariant and HB formalisms, but we perform our own calculation in order to provide a fully consistent comparison with the deltaful case.

## 5.1 Pion photoproduction in deltaless ChPT

In this subsection, we discuss the case of pion photoproduction in the deltaless case at full one-loop order within HBChPT and covariant ChPT formulation. First, we give some remarks on the fitting procedure. Afterwards, we present our obtained values for the deltaless LECs and our results for observables. We also analyse the numerical difference between HB and covariant LECs in terms of the IR shifts as explained in sec. 3.7.

### 5.1.1 Fitting procedure

In the deltaless case, we are interested in the determination of four parameters  $d_8, d_9, d_{20}$  and  $d_{21;22}$ . These constants stem from the  $q^3 \gamma N \rightarrow \pi N$  contact term. Note that

$$d_{21;22} = d_{21} - \frac{1}{2}d_{22} \quad (5.1)$$

is a linear combination, which is the only way the two constants enter the real pion photoproduction amplitude, thus they cannot be fitted independently. The numerical values of LECs are in general different in the HB and covariant approaches, but the fitting procedure is similar. Thus, when we discuss points applicable to both formalisms, we simply print  $d_i$  for referring to both renormalised parameters  $\bar{d}_i$  and  $\hat{d}_i^r$ .

Ideally, one would fit the LECs to the whole set of available pion photoproduction data in the relevant energy range. However, analysing all the data requires a lot of effort and is an art of its own, since there is a lot of data available on the photoproduction process. This is why we

choose to fit to the multipoles of the partial-wave analysis (PWA) from Mainz, the MAID2007 model [149], which is a more pragmatic approach. Furthermore, we only fit to the real part of the multipoles, because the imaginary part follows from unitarity as stated in Watson's theorem [157] and does not provide new information. Similarly to ref. [158], we fit to the multipoles in the isospin channels. This is a natural choice, because isospin-breaking effects will not be considered in this work. For our particular purposes, the corrections generated by isospin-breaking terms are too small to be of further interest. The four physical reaction channels are just linear combinations of the isospin channels. In the following, we remark on several points relevant for the fits.

**Uncertainties and fitting procedure** The main disadvantage of using the MAID PWA is that uncertainties are not provided. We thus assign a relative 5% error to every multipole, which is a common approach, see e.g. ref. [159] for a similar procedure in the analysis of pion-nucleon elastic scattering, such that the uncertainty of the observables as given in eq. (3.78) reads for our case

$$\delta O_i = \sqrt{\left(0.05 O_i^{\text{exp}}\right)^2 + \left(\delta O_i^{(n)}\right)^2}. \quad (5.2)$$

We have checked that the choice of the relative error has negligible effects on the fit result by varying its size between 2% and 15%. Of course, our choice affects the fit quality, but we found that these effects are relatively small, because the uncertainties are dominated by the Bayesian truncation errors. To obtain the central values of the fit parameters, we minimise the  $\chi^2$  function

$$\chi^2 = \sum_i \left( \frac{O_i^{\text{exp}} - O_i^{(n)}}{\delta O_i} \right)^2, \quad (5.3)$$

where the sum runs over all energy points from every multipole we incorporate in the configuration. Because of the rather complex expressions for the truncation errors, the  $\chi^2$  is a nontrivial function of the LECs and its minimum is in general not easy to find. Therefore, we proceed in two steps.

First, we minimise  $\chi^2$  iteratively. By initially choosing the combined error to be the mere relative 5% error of the PWA multipole amplitudes, the resulting  $\chi^2$  is just a polynomial function of the LECs, whose minimum is easily found. The obtained values for the LECs are subsequently used to calculate the truncation errors, and combined uncertainties can be obtained as given by eq. (5.2). These values are resubstituted in the  $\chi^2$  function, which is minimised again to obtain new LEC fit results. This procedure is repeated several times until the result converges, typically five iterations at the maximum depending on the stability of the fit. In the second step, these values are used as a starting point to find the minimum of the exact  $\chi^2$  function, including the complicated analytical expression for the truncation uncertainties. In this step, we rely on the function `NMinimize` of *Mathematica* [151] to numerically find a minimum. We assume this second minimum to be in close vicinity of the first, itera-

tively found minimum. In all configurations we considered, we found this assumption to be true.

After having obtained the central values of the fit parameters, the corresponding uncertainties are determined from the covariance matrix, which is approximated by the inverse of the Hessian

$$\delta y_i = \sqrt{\text{Cov}(y_i, y_i)}, \quad \text{Cov}(y_i, y_j) = H_{ij}^{-1}, \quad H_{ij} = \frac{1}{2} \frac{\partial^2 \chi^2}{\partial y_i \partial y_j} \Big|_{\mathbf{y}=\bar{\mathbf{y}}}. \quad (5.4)$$

Here, the vector  $\mathbf{y}$  refers to the set of all fitting parameters, and  $\bar{\mathbf{y}}$  is the vector of best fit values.

**Energy range** As stated before, the energy range in which ChPT is applicable is limited by the lowest lying not included resonance, which is in the deltaless formulation the delta particle. Thus, the delta energy region should be excluded completely in the deltaless fit, so that we choose to restrict the upper energy boundary to  $\sqrt{s} = 1200$  MeV. By construction, we expect the range of convergence of HBChPT to be smaller than in the covariant case. Also, in previous studies, it was shown that the HB approach yields good agreement with the neutral pion production data only up to 20 MeV above threshold [160]. Furthermore, we exclude the region very close to the pion production threshold. Since we work in the isospin-symmetric limit, which leads to equal pion masses, our calculation cannot account for effects generated by the mass difference of the pions. The reaction threshold lies at  $\sqrt{s} = 1076.3$  MeV, so we restrict the lower energy boundary of our fits to  $\sqrt{s} = 1090$  MeV. We choose energy steps of 2 MeV, so we have 56 data points per observable in the deltaless case. Briefly stated, we use the energy range  $1090 \text{ MeV} \leq \sqrt{s} \leq 1200 \text{ MeV}$  in the deltaless fit.

**Data configuration** We restrict ourselves to the analysis of  $s$ - and  $p$ -wave multipoles, because they contain by far the largest contributions to the photoproduction cross sections. In figs. 5.1 - 5.3, the results of the MAID analysis are depicted [149]. Furthermore, the results of the energy-dependent [161, 162] and energy-independent [163] GWU-SAID multipole amplitudes are shown in order to illustrate differences between different partial-wave analyses. The agreement between the three sets of data is excellent for the  $M_{1+}^{3/2}$  multipole, which corresponds to the magnetic excitation of the delta resonance in the  $s$ -channel, and reasonably good for the  $E_{0+}$  and  $M_{1-}$  multipoles.

To choose a fit configuration sensitive to the values of the LECs  $d_8, d_9, d_{20}$  and  $d_{21;22}$ , it is instructive to analyse the contributions of the parameters to the various amplitudes. The three multipoles  $E_{0+}$ ,  $M_{1+}$  and  $M_{1-}$  all receive leading-order contributions of one or several LECs in terms of the  $1/m_N$  expansion. Only  $E_{1+}$  gets next-to-leading-order  $1/m_N$  contributions from all four parameters, therefore we exclude  $E_{1+}$  completely from the deltaless fit. We choose to fit the  $I = 3/2$  channel first, which is motivated by the agreement of the data sets, the order of magnitude of the multipoles and bearing in mind that we are interested in analysing the differences to the deltaful theory, which is expected to bring dominant contributions to the

$I = 3/2$  channel. Altogether, we first fit to the three multipole amplitudes  $E_{0+}^{3/2}$ ,  $M_{1+}^{3/2}$  and  $M_{1-}^{3/2}$ , which determines the parameters  $d_8$ ,  $d_{20}$  and  $d_{21;22}$ .

The constant  $d_9$  does not contribute to the  $I = 3/2$  channel and is fitted to the  $I = 1/2$  channels subsequently. We suppose that the constants  $d_8$ ,  $d_{20}$  and  $d_{21;22}$  are sufficiently constrained from the  $I = 3/2$  fit to serve as an input for the  $I = 1/2$  fit. At leading order in  $1/m_N$ ,  $d_9$  contributes to both proton and neutron channels of  $M_{1+}^{1/2}$  and  $M_{1-}^{1/2}$ . However, while performing the fit, we found that there is no value of  $d_9$  which results in an acceptable description of  $M_{1-}^{1/2}$ . We expect that this problem is resolved if higher-order contributions are taken into account. Thus, we decided to exclude  $M_{1-}^{1/2}$  from the second fit and determine  $d_9$  only from  $M_{1+}^{1/2}$ . When removing  $M_{1-}$ , the central value of  $d_9$  only changes very slightly, which supports our strategy, but of course the fit quality is affected. The uncertainty of  $d_9$  is determined analogously to eq. (5.4) by

$$\delta d_9 = \left( \frac{1}{2} \frac{\partial^2 \chi^2_{I=1/2}}{\partial d_9^2} \right)^{1/2}. \quad (5.5)$$

This procedure neglects that  $\delta d_9$  also receives contributions from the uncertainties of the previously determined LECs, but we have checked that these effects only have a small impact, so it seems legitimate to ignore these effects. This insight also supports our idea that  $d_8$ ,  $d_{20}$ ,  $d_{21;22}$  are sufficiently well constrained by the first fit.

### 5.1.2 Order- $q^3$ results, figures and discussion

In table 5.1, we show our fit results for the HB LECs including uncertainties. For the  $I = 3/2$  ( $I = 1/2$ ) fit, we used 168 (112) data points, so that the reduced  $\chi^2/n$  is equal to 1.1 (3.5), where  $n$  stands for the number of data points minus the number of fitted LECs. Table 5.2 collects the corresponding results of the covariant approach, where we emphasise again that the fits are fully comparable in terms of data configuration and energy range. In the covariant formalism, we obtain for the reduced  $\chi^2/n$  0.3 (0.2) for the  $I = 3/2$  ( $I = 1/2$ ) fit.

**Table 5.1:** Low-energy constants obtained from a deltaless order- $q^3$  fit in the HB approach to the real parts of  $s$ - and  $p$ -wave photoproduction multipoles of the MAID model from ref. [149]. All LECs are given in units of  $\text{GeV}^{-2}$ .

	$\hat{d}_8^r$	$\hat{d}_9^r$	$\hat{d}_{20}^r$	$\hat{d}_{21;22}^r$
order $q^3$ HB fit values	-8.1(3)	0.01(2)	-16.5(5)	18.4(5)

The fit results are shown in figs. 5.1 - 5.3 on pages 58 - 60, where the plotted energy range corresponds to our fitting range. We show every isospin channel in a separate figure, in which each left column shows the HB fit result, and each right column depicts the covariant case. At this point we remind that in the  $I = 3/2$  channel,  $E_{1+}^{3/2}$  has not been used in the fit. In

**Table 5.2:** Low-energy constants obtained from a deltaless order- $q^3$  covariant fit to the real parts of  $s$ - and  $p$ -wave photoproduction multipoles of the MAID model from ref. [149]. All LECs are given in units of  $\text{GeV}^{-2}$ .

	$\bar{d}_8$	$\bar{d}_9$	$\bar{d}_{20}$	$\bar{d}_{21;22}$
order $q^3$ cov. fit result	−4.9(2)	0.01(1)	−8.5(3)	9.4(4)

both  $I = 1/2$  channels, only  $M_{1+}^{1/2}$  was used for the fit, all other multipoles are plots. We also remind that we used the 68 % confidence interval for the determination of the truncation errors, but our figures also show the 95 % band. Also, we adopted a more conservative value of the chiral breakdown scale of  $\Lambda_b = 650 \text{ MeV}$  compared to the commonly used assumption in the single-nucleon sector  $\Lambda_b \approx 1 \text{ GeV}$ . The smaller value of  $\Lambda_b$  is motivated by recent studies in the few-nucleon sector [105, 164].

In the  $I = 3/2$  channel, we find both HB and covariant descriptions satisfactory with the exception of the electric delta multipole  $E_{1+}^{3/2}$ . The insufficient reproduction of the latter is probably due to the missing delta contributions. We expect the description of this amplitude to improve when including the leading-order delta contributions, which will be discussed in section 5.2.3. Note that the shape of the  $M_{1+}^{3/2}$  multipole is not well reproduced for CM energies above  $\sqrt{s} = 1150 \text{ MeV}$ , which is also due to missing delta dynamics. We expect that the inclusion of the leading-order delta contributions will correct this behaviour significantly (see also sec. 5.2.3). The  $M_{1-}^{3/2}$  multipole is better described in the covariant case, which explains the differences in the fit quality. The smaller value of  $\chi^2/n$  in the covariant approach may indicate that the Bayesian truncation uncertainties are overestimated or that the fit range is not broad enough to constrain the LECs sufficiently. At this point we emphasise that  $n$  should not be equated with the number of degrees of freedom, because our choice of the number of data points is in some way arbitrary. Varying the energy steps results in different values of the reduced  $\chi^2/n$ , therefore one cannot associate a perfect fit with a value of  $\chi^2/n = 1$ . The fit quality should only be compared to results obtained with the same preconditions.

In the  $I = 1/2$  channels, the difference between HB and covariant approach is more pronounced. The descriptions of  $E_{0+}^{1/2}$  and  $E_{1+}^{1/2}$  are clearly better in the covariant approach, and also the description of  $M_{1+}^{1/2}$  is much better, which is reflected in the fit quality. Clearly, the value of  $\chi^2/n = 3.5$  in the HB case shows that the data cannot be well described. On the other hand, the small value of  $\chi^2/n = 0.2$  obtained in the covariant approach indicates that more data might be required to constrain  $d_9$  better.

With the obtained fit values in both approaches, we now turn to the subject of the IR shifts, as discussed in sec. 3.7. Substituting the constants in eq. (3.75), the numerical values of the

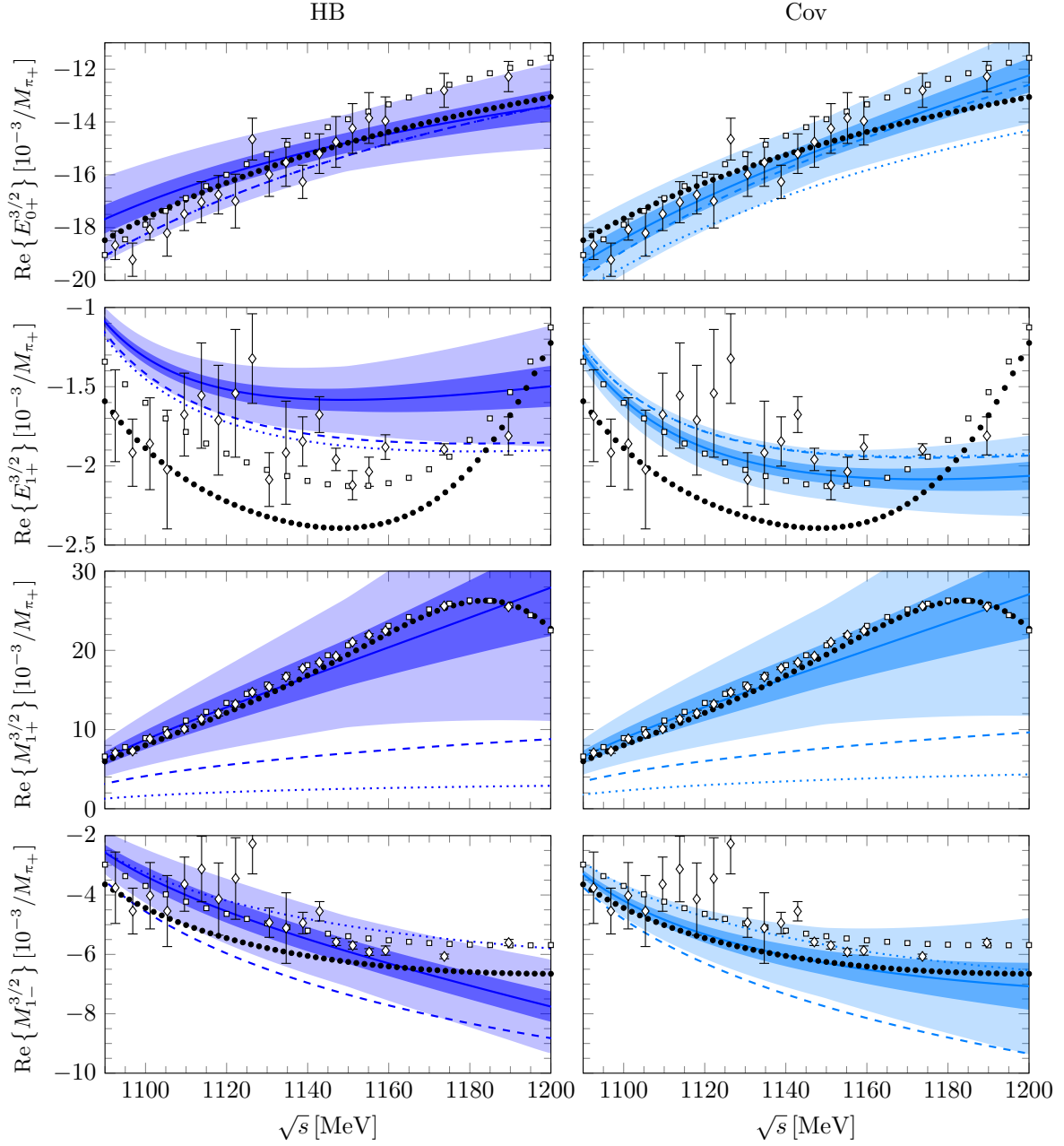


**Figure 5.1:** Order- $q^3$  fits to the real parts of the  $s$ - and  $p$ -wave photoproduction multipoles in the  $I = 3/2$  channel. The solid, dashed and dotted lines denote the  $q^3$ ,  $q^2$  and  $q^1$  results, respectively. The darker (lighter) shaded bands show the estimated truncation errors at order  $q^3$  with 68 % (95 %) confidence. The filled circles show the results of the MAID PWA from ref. [149], the squares (diamonds) are the results of the energy-dependent (independent) SAID analysis from refs. [161, 162] (ref. [163]).

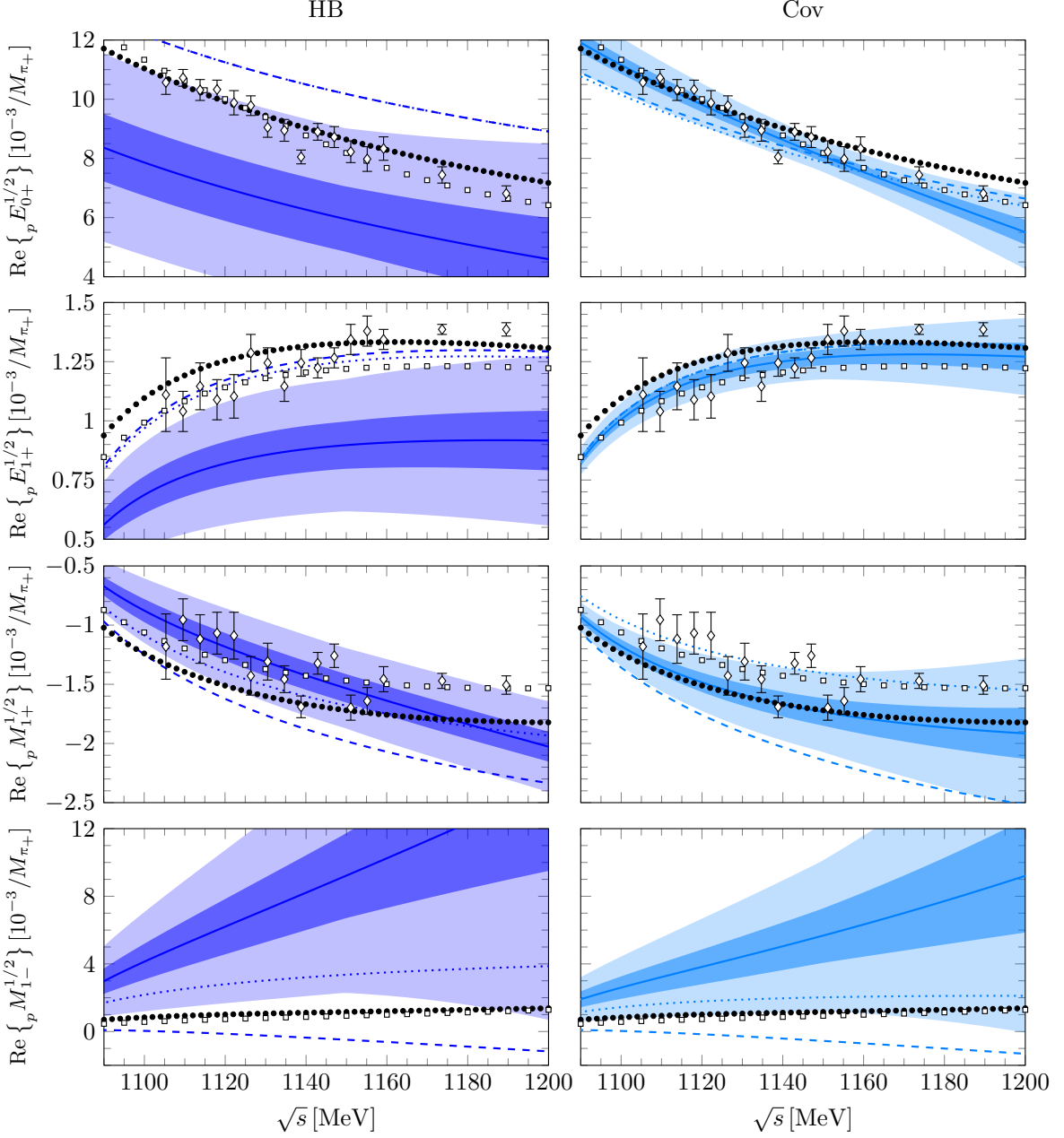


**Figure 5.2:** Order- $q^3$  fits to the real parts of the  $s$ - and  $p$ -wave photoproduction multipoles in the proton  $I = 1/2$  channel. The solid, dashed and dotted lines denote the  $q^3, q^2$  and  $q^1$  results, respectively. The darker (lighter) shaded bands show the estimated truncation errors at order  $q^3$  with 68 % (95 %) confidence. The filled circles show the results of the MAID PWA from ref. [149], the squares (diamonds) are the results of the energy-dependent (independent) SAID analysis from refs. [161, 162] (ref. [163]).

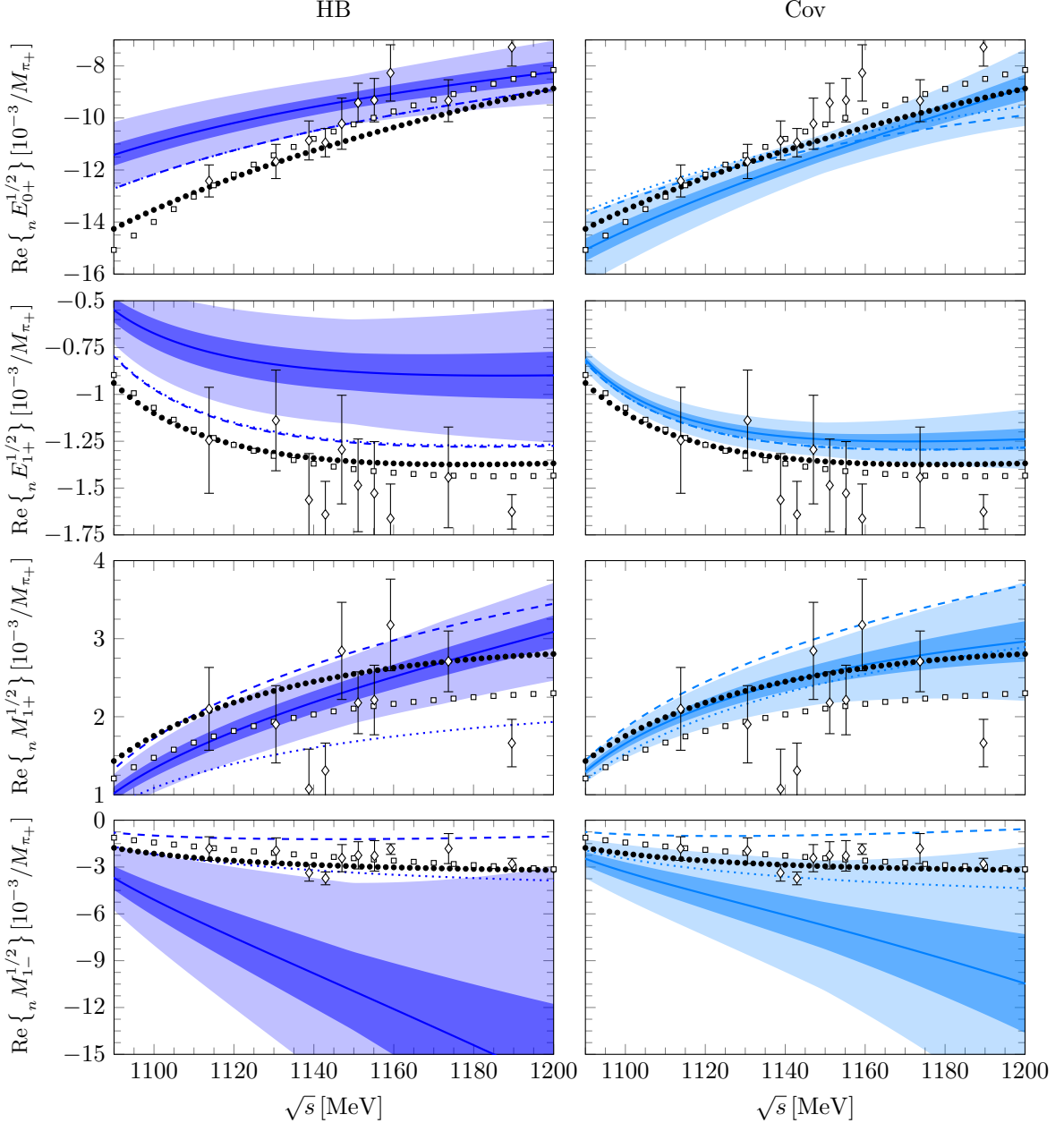


**Figure 5.3:** Order- $q^3$  fits to the real parts of the  $s$ - and  $p$ -wave photoproduction multipoles in the neutron  $I = 1/2$  channel. The solid, dashed and dotted lines denote the  $q^3, q^2$  and  $q^1$  results, respectively. The darker (lighter) shaded bands show the estimated truncation errors at order  $q^3$  with 68 % (95 %) confidence. The filled circles show the results of the MAID PWA from ref. [149], the squares (diamonds) are the results of the energy-dependent (independent) SAID analysis from refs. [161, 162] (ref. [163]).

predicted shifts read

$$\begin{aligned}\Delta d_8^{\text{IR}} &= 0.6 \text{ GeV}^{-2}, & \Delta d_9^{\text{IR}} &= 0.08 \text{ GeV}^{-2}, \\ \Delta d_{20}^{\text{IR}} &= 7.6 \text{ GeV}^{-2}, & \Delta d_{21;22}^{\text{IR}} &= -4.9 \text{ GeV}^{-2},\end{aligned}\quad (5.6)$$

whereas we find for the actual differences from tables 5.1 and 5.2

$$\begin{aligned}\bar{d}_8 - \hat{d}_8^r &= 3.2 \text{ GeV}^{-2}, & \bar{d}_9 - \hat{d}_9^r &= 0.00 \text{ GeV}^{-2}, \\ \bar{d}_{20} - \hat{d}_{20}^r &= 8.0 \text{ GeV}^{-2}, & \bar{d}_{21;22} - \hat{d}_{21;22}^r &= -9.0 \text{ GeV}^{-2}.\end{aligned}\quad (5.7)$$

These results confirm that the IR shifts explain the differences between HB and covariant approach to a large extent. Especially for  $d_9$  and  $d_{20}$ , the agreement is excellent. For  $d_8$  and  $d_{21;22}$ , the difference has the same sign as the IR shift. The remaining gap between the two sets of fit parameters is probably due to the poorer fit quality in the HB approach. We also find that the values of the covariant LECs are more natural as in the HB approach. Here, the term ‘‘natural’’ refers to the naive estimate that the  $d_i$ ’s should roughly be of the size

$$d_i \sim \frac{1}{\Lambda_b} \sim 2.5 \text{ GeV}^{-2} \quad \text{with} \quad \Lambda_b = 650 \text{ MeV}. \quad (5.8)$$

Although being far from this magnitude, the covariant LECs are definitely closer to this estimate.

The results of the deltaless approach can be shortly summarised as follows:

- The manifestly covariant treatment gives an overall better description of the pion photoproduction multipole amplitudes compared to the heavy baryon approach. Both approaches fail to describe  $M_{1-}^{3/2}$ .
- The agreement with the data is limited to CM energies up to approx. 1150 MeV corresponding to approx. 70 MeV above threshold. This can be seen especially from  $M_{1+}^{3/2}$ , which is of particular interest because it dominates the cross sections in the delta region.
- The numerical difference between covariant and HB LEC fit values can be described to a very large extent by the shifts generated by the infrared regular part of the loop integrals.

## 5.2 Pion photoproduction with explicit delta degrees of freedom

In this subsection, we consider pion photoproduction with explicit delta degrees of freedom. First we address the question how to treat the delta mass, subsequently we present our results including leading-order delta contributions and next-to-leading-order terms.

### 5.2.1 The delta mass in the complex mass scheme

The delta is an unstable particle, thus we must take into account its decay width. We choose to implement the complex-mass scheme [137–139], which has the advantage that it preserves gauge-invariance and is straightforward to implement. Furthermore, it has been successfully applied to various problems up to tree-level and one-loop order, e.g. refs. [37, 165–168]. The basic idea is to extend the applicability of the theory into the delta pole region, where the propagator needs to be dressed. The delta mass is parametrised as

$$m_\Delta = m_\Delta^{\text{Re}} - i \frac{\Gamma}{2} \quad (5.9)$$

where  $\Gamma$  is the imaginary part of the delta mass representing its instability.  $\Gamma$  receives the leading-order contributions from the first loop level, thus  $\Gamma \sim \mathcal{O}(\epsilon^3)$ . However, in the complex-mass approach, we already choose a complex value for the delta mass even at tree level and fix the width to a constant value.

From the naive approach of a simple real delta mass, the delta propagator<sup>1</sup> diverges at the real mass

$$\frac{1}{\not{p} - m_\Delta^{\text{Re}}} \xrightarrow{\not{p} \rightarrow m_\Delta^{\text{Re}}} \infty. \quad (5.10)$$

In order to get a correct behaviour in the delta region, we start from the resummed propagator expanded at the renormalisation point  $\not{p} = m_\Delta^{\text{Re}}$

$$\frac{1}{\not{p} - m_\Delta^{\text{Re}} - \Sigma(p)} \simeq \frac{1}{\not{p} - m_\Delta^{\text{Re}} - \Sigma(m_\Delta^{\text{Re}}) - \Sigma'(m_\Delta^{\text{Re}})(\not{p} - m_\Delta^{\text{Re}}) + \mathcal{O}((\not{p} - m_\Delta^{\text{Re}})^2)}, \quad (5.11)$$

where  $(-\text{i})\Sigma(\not{p})$  is the self-energy of the delta isobar. Choosing the conditions

$$\text{Re } \Sigma(m_\Delta^{\text{Re}}) = 0, \quad \text{Im } \Sigma(m_\Delta^{\text{Re}}) = -\frac{\Gamma}{2}, \quad \Sigma'(m_\Delta^{\text{Re}}) = 0 \quad (5.12)$$

transforms the propagator into the form

$$\frac{1}{\not{p} - m_\Delta^{\text{Re}} - \Sigma(p)} \simeq \frac{1}{\not{p} - m_\Delta^{\text{Re}} + i \frac{\Gamma}{2}} + \mathcal{O}((\not{p} - m_\Delta^{\text{Re}})^2). \quad (5.13)$$

This form is finite at the point  $\not{p} = m_\Delta^{\text{Re}}$ , which is the desired behaviour in the delta pole region. Furthermore, in the near-threshold region, the behaviour of eq. (5.10) is recovered by an expansion in  $\Gamma$ , which is in accordance with the strict power-counting  $\not{p} - m_\Delta^{\text{Re}} \sim \mathcal{O}(\epsilon)$  and  $\Gamma \sim \mathcal{O}(\epsilon^3)$ , leading to  $\Gamma \ll \not{p} - m_\Delta^{\text{Re}}$ . But in the delta region it holds  $\not{p} \sim m_\Delta^{\text{Re}}$ , thus  $\Gamma \gtrsim \not{p} - m_\Delta^{\text{Re}}$  and the expansion in  $\Gamma$  is not legit.

---

<sup>1</sup>Here we do not consider the tensor structure in the numerator, because it is not relevant for the main point of this approach.

In practical calculations, it is easier to start from a complex-valued delta mass

$$\frac{1}{\not{p} - m_\Delta - \Sigma(\not{p})} \simeq \frac{1}{\not{p} - m_\Delta} + \mathcal{O}((\not{p} - m_\Delta)^2) \quad (5.14)$$

with the renormalisation conditions

$$\Sigma(m_\Delta) = 0 \quad \text{and} \quad \Sigma'(m_\Delta) = 0. \quad (5.15)$$

At one-loop level, this transforms into

$$\Sigma(m_\Delta^{\text{Re}}) = 0 \quad \text{and} \quad \Sigma'(m_\Delta^{\text{Re}}) = 0. \quad (5.16)$$

Because loop contributions of the delta self-energy are beyond our working order, it all amounts to the fact that in our calculations we can replace the bare delta mass  $\dot{m}_\Delta$  by the complex value  $m_\Delta = \text{Re}(m_\Delta) - i|\text{Im}(m_\Delta)| = m_\Delta^{\text{Re}} - i\frac{\Gamma}{2}$  in all diagrams. However, note that this simple replacement comes at the cost that the near-threshold behaviour is not accounted for, because the width is not approaching zero. This is an artefact of the complex-mass scheme, because as stated, a constant delta width is only a good approximation in the vicinity of the kinematical point  $\not{p} = m_\Delta^{\text{Re}}$ , the delta region.

In the HB approach, the treatment of the delta propagator is analogous. The dressed HB delta propagator is expanded around the delta-nucleon mass split  $v \cdot p = \Delta = m_\Delta - m_N$

$$\frac{1}{v \cdot p - \Delta - \Sigma(v \cdot p)} \simeq \frac{1}{v \cdot p - \Delta - \Sigma(\Delta) - \Sigma'(\Delta)(v \cdot p - \Delta) + \mathcal{O}((v \cdot p - \Delta)^2)}, \quad (5.17)$$

which is equivalent to using

$$\Delta = \Delta^{\text{Re}} - i\frac{\Gamma}{2}. \quad (5.18)$$

The same statements as given above hold for the renormalisation of the delta mass, thus we can also replace the delta-nucleon mass split by its complex value.

In the literature, one finds two standard values for the mass and decay width of the delta. The first is the pole value

$$m_\Delta^{\text{pole}} \approx (1210 - 50i)\text{MeV} \quad (5.19)$$

and the second one is the Breit-Wigner value

$$m_\Delta^{\text{BW}} \approx (1232 - 59i)\text{MeV}, \quad (5.20)$$

both taken from the PDG [110]. The distinction between the two values is briefly explained in e.g. ref. [169].

The deltaful pion photoproduction tree amplitude is quite sensitive to the numerical choice of the delta mass. In particular, the contribution of the  $s$ -channel delta pole tree diagram of order  $\epsilon^2$  to the real part of the magnetic multipole  $M_{1+}$  in the isospin-3/2 channel vanishes at the point  $\sqrt{s} = m_\Delta$ , and this position cannot be shifted by adjustment of other parameters. Consequently, an inappropriate choice of the delta mass would lead to discrepancies with the data even at order  $\epsilon^2$ , which would probably have a large impact on the estimate of the theoretical truncation uncertainties leading to less stable fit results. We are, however, interested in choosing an efficient scheme concerning the convergence of the chiral series. To illustrate the problem, we show in fig. 5.4 the two fits of the  $\epsilon^2$  amplitude using the two literature values (5.19) and (5.20) of the delta mass. In this case,  $b_1$  is the only free parameter and we fit it to the real part of  $M_{1+}^{3/2}$ . Clearly, the zero of  $M_{1+}^{3/2}$  is not well reproduced for either of the delta mass values.

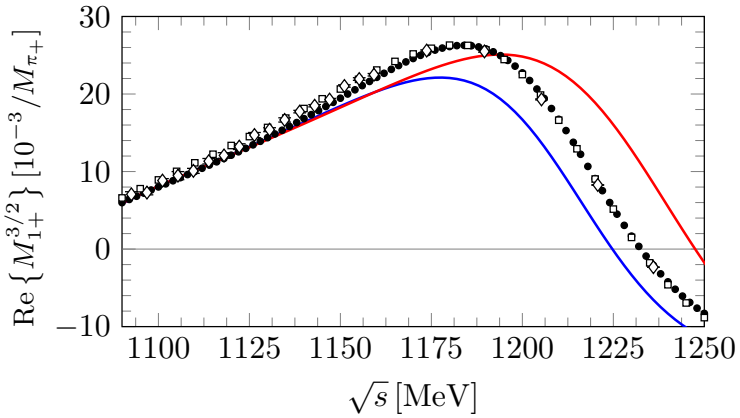


**Figure 5.4:** Order- $\epsilon^2$  fit to the real part of  $M_{1+}^{3/2}$  using the delta pole mass (blue curve) and the Breit-Wigner mass (red curve). The filled circles show the results of the MAID PWA from ref. [149], the squares (diamonds) are the results of the energy-dependent (independent) SAID analysis from refs. [161, 162] (ref. [163]).

Therefore, to get the best description of  $M_{1+}^{3/2}$ , we decided to fit the delta mass together with the LEC  $b_1$  to the real part of the  $M_{1+}^{3/2}$  multipole at deltaful tree order, because it is most sensitive to these parameters. We extend our fitting range up to  $1090 \text{ MeV} \leq \sqrt{s} \leq 1250 \text{ MeV}$  partially into the delta region. Due to the strong nonperturbative dynamics of the pion-nucleon final state, we expect that one can hardly apply ChPT beyond this region. At order  $\epsilon^2$ , the Bayesian truncation uncertainties are not expected to yield reasonable results, because there are only two orders of the chiral series available. This is why we have not included any uncertainties in the  $\chi^2$  and only minimise the squared difference between MAID result and the multipole.

In the HB approach, a strict  $1/m_N$  expansion is performed and only the leading term is kept. This removes higher orders of the  $1/m_N$  effects and changes the numerical contributions of the  $s$ -channel delta pole diagram to the multipoles. This is why we perform two separate fits in the HB and covariant approaches. The tables 5.3 and 5.4 show the results which we obtain for

the delta mass and  $b_1$  in the HB and covariant approach, respectively. The obtained mass in the covariant scheme lies close to the pole mass value of the PDG [110]. We will also use our fit value in the  $\epsilon^3$  calculation 5.2.5. We have checked that the lower value obtained from the HB fit matches the expectation from expanding the delta propagator beyond the leading-order term in  $1/m_N$ .

**Table 5.3:** Delta mass and leading  $\gamma N \Delta$  coupling constant  $b_1$  obtained from a HB order- $\epsilon^2$  fit to the real part of  $M_{1+}^{3/2}$  of the MAID model from ref. [149].

	$m_\Delta^{\text{HB}}[\text{MeV}]$	$b_1[m_N^{-1}]$
order $\epsilon^2$ HB fit result	$1196.1 - 45.2i$	5.4

**Table 5.4:** Delta mass and leading  $\gamma N \Delta$  coupling constant  $b_1$  obtained from a covariant order- $\epsilon^2$  fit to the real part of  $M_{1+}^{3/2}$  of the MAID model from ref. [149].

	$m_\Delta^{\text{cov}}[\text{MeV}]$	$b_1[m_N^{-1}]$
order $\epsilon^2$ cov. fit result	$1219.3 - 53.7i$	5.7

### 5.2.2 Fitting procedure including delta tree contributions

Including the leading-order explicit delta contributions introduces the additional constant  $b_1$  into the theory, which corresponds to the leading-order  $\gamma N \Delta$  coupling. In the  $s$ -channel,  $b_1$  contributes at leading order in  $1/m_N$  only to  $M_{1+}$ , which is already part of our fitting configuration. When including the delta tree diagrams, we do not change the fitting procedure and the way we treat uncertainties (see sec. 5.1.1 for details). As  $b_1$  contributes to the  $I = 3/2$  channel, we obtain its central value as well as  $d_8$ ,  $d_{20}$  and  $d_{21;22}$  from the  $I = 3/2$  fit. Subsequently, we determine  $d_9$  from the  $I = 1/2$  channel as before. At this point we remind that the given statements hold for both HB and covariant LECs, and when simply printing  $d_i$ , we refer to  $\bar{d}_i$  as well as  $\hat{d}_i^r$ . Furthermore, here it is not necessary to mind differentiations between covariant or HB  $b_1$ , because  $1/m_N$  corrections and renormalisation counterterms are beyond the working order.

Note that for the sake of brevity, we will refer to the combined approach of deltaless loop order plus deltaful tree order as order “ $q^3 + \epsilon^2$ ”, which should be understood as the sum of the leading two orders in  $\epsilon$  according to the counting given in eq. (2.65), plus the third order in  $q$  according to the deltaless counting rules given in eq. (2.30). In particular, the deltaless tree diagrams are not included twice, as might be understood from this notation.

Concerning the energy range, we extend the upper boundary up to  $\sqrt{s} = 1250$  MeV, just as in the pure  $\epsilon^2$  case, to partially take into account the delta region. This increases the number

of data points to 81 per multipole. By construction of the complex-mass approach, unitarity is violated due to the constant delta decay width in the delta pole diagrams. However, unitarity will be restored perturbatively when including higher orders. Because at first we only include the delta tree diagrams, we expect the description of the data to be worse near threshold compared to the deltaless approach. However, these effects should be dominant in the imaginary parts of the multipoles. But because we do not fit the imaginary parts, we choose to still include the threshold region in our fitting range and comment on the description of the threshold region in the next section. Stated briefly, we fit between  $1090 \text{ MeV} \leq \sqrt{s} \leq 1250 \text{ MeV}$ .

Special attention should be paid to the choice of  $b_1$  when determining the truncation errors. Strictly speaking, the value of  $b_1$  obtained from the relevant  $\epsilon^2$  fit should be inserted for the first correction to the leading order. However, since we were mainly interested in determining a suitable delta mass from the tree-order fit and refrained from giving an uncertainty of  $b_1$  based on the Bayesian approach, we fit the constant  $b_1$  afresh. Its value alters only slightly when including the other multipole amplitudes, thus we always refit  $b_1$  in the upcoming approaches and review the stability of the constant afterwards.

A comment on the treatment of the delta tree-level contributions in the HB approach is in order. A strict HB expansion corresponds to the nonrelativistic limit of the amplitude. However, this is in contrast to the desire to describe observables in the delta region, which is significantly above threshold. Thus, the question must be addressed whether this strict  $1/m_N$ -expansion is sufficient to describe the multipole amplitudes in the delta region. We decide to clarify this question first by considering two cases which we call “strict HB” and “mixed HB” approach. In the following, we consider the exact, “strict”  $1/m_N$  expansion, where we use the delta mass from table 5.3. Second, we investigate in a “mixed” approach by combining the covariant deltaful tree terms of order  $\epsilon^2$  with the HB  $q^3$  amplitude in order to keep the relativistic behaviour in the delta region. A similar study of Compton scattering was done in ref. [170].

### 5.2.3 Order- $q^3 + \epsilon^2$ results, figures and discussion

We start with the comparison of the strict and mixed HB approaches. In table 5.5, we show our fit results for the LECs obtained from both HB fits. We give a short reminder that the two approaches use different values for the delta mass, as explained in sec. 5.2.1. In both versions, we used 243 (162) data points in the  $I = 3/2$  ( $I = 1/2$ ) fit. The reduced  $\chi^2/n$  is equal to 2.1 (8.1) in the strict HB approach, and equal to 1.5 (3.9) in the mixed approach.

A graphical comparison between these schemes is shown in figs. 5.5 - 5.7, where the depicted energy range corresponds to our fitting range. We remind the reader that the multipoles  $E_{1+}^{3/2}, E_{0+}^{1/2}, E_{1+}^{1/2}$  and  $M_{1-}^{1/2}$  are plotted and have not been used in the fit. For the truncation errors, we kept our choice of  $\Lambda_b = 650 \text{ MeV}$ .

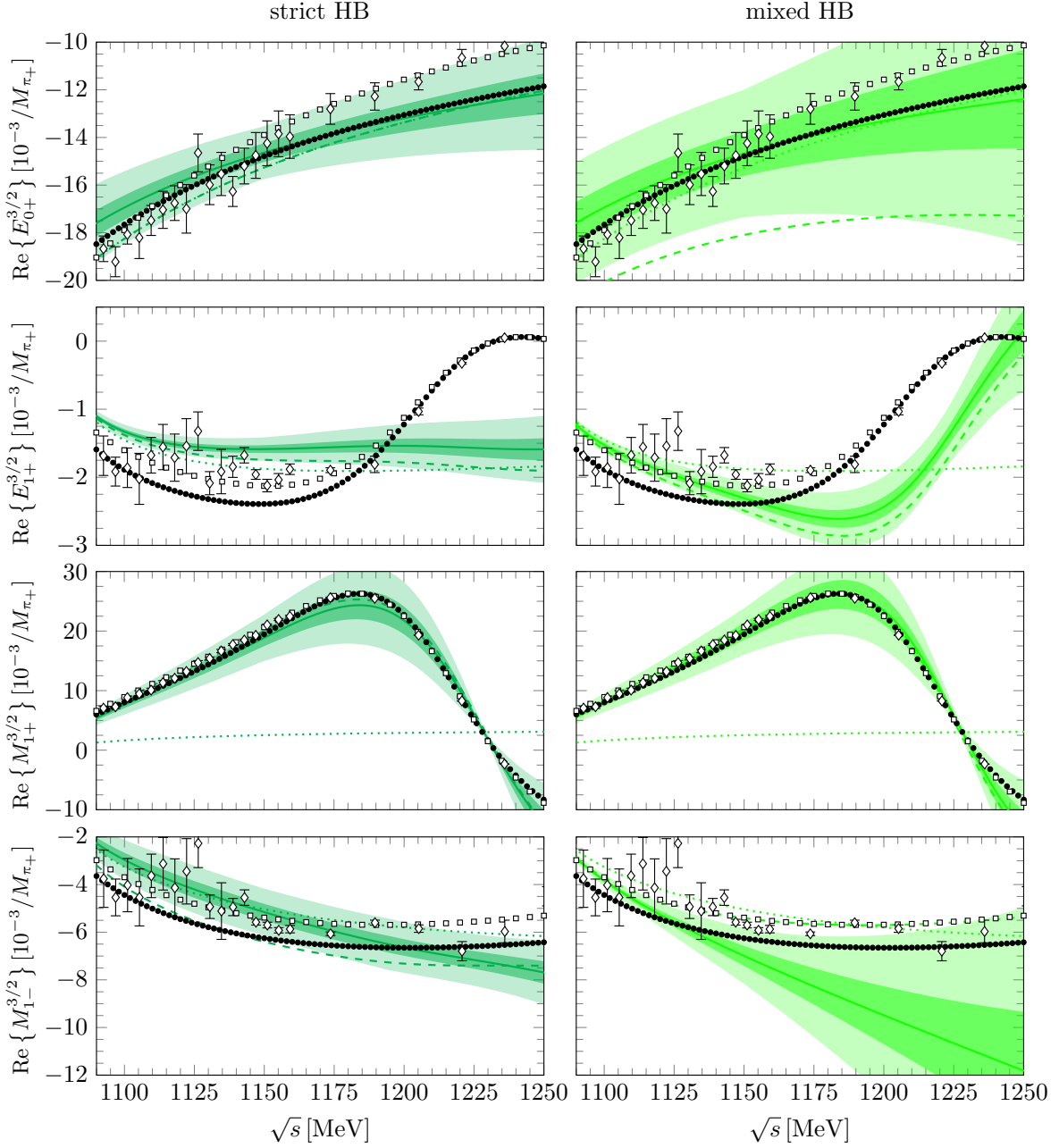


**Figure 5.5:** Order- $q^3 + \epsilon^2$  fits to the real parts of the  $s$ - and  $p$ -wave photoproduction multipoles in the  $I = 3/2$  channel. The solid, dashed and dotted lines denote the  $q^3 + \epsilon^2$ ,  $\epsilon^2$  and  $\epsilon^1$  results, respectively. The darker (lighter) shaded bands show the estimated truncation errors at order  $q^3 + \epsilon^2$  with 68 % (95 %) confidence. The filled circles show the results of the MAID PWA from ref. [149], the squares (diamonds) are the results of the energy-dependent (independent) SAID analysis from refs. [161, 162] (ref. [163]).

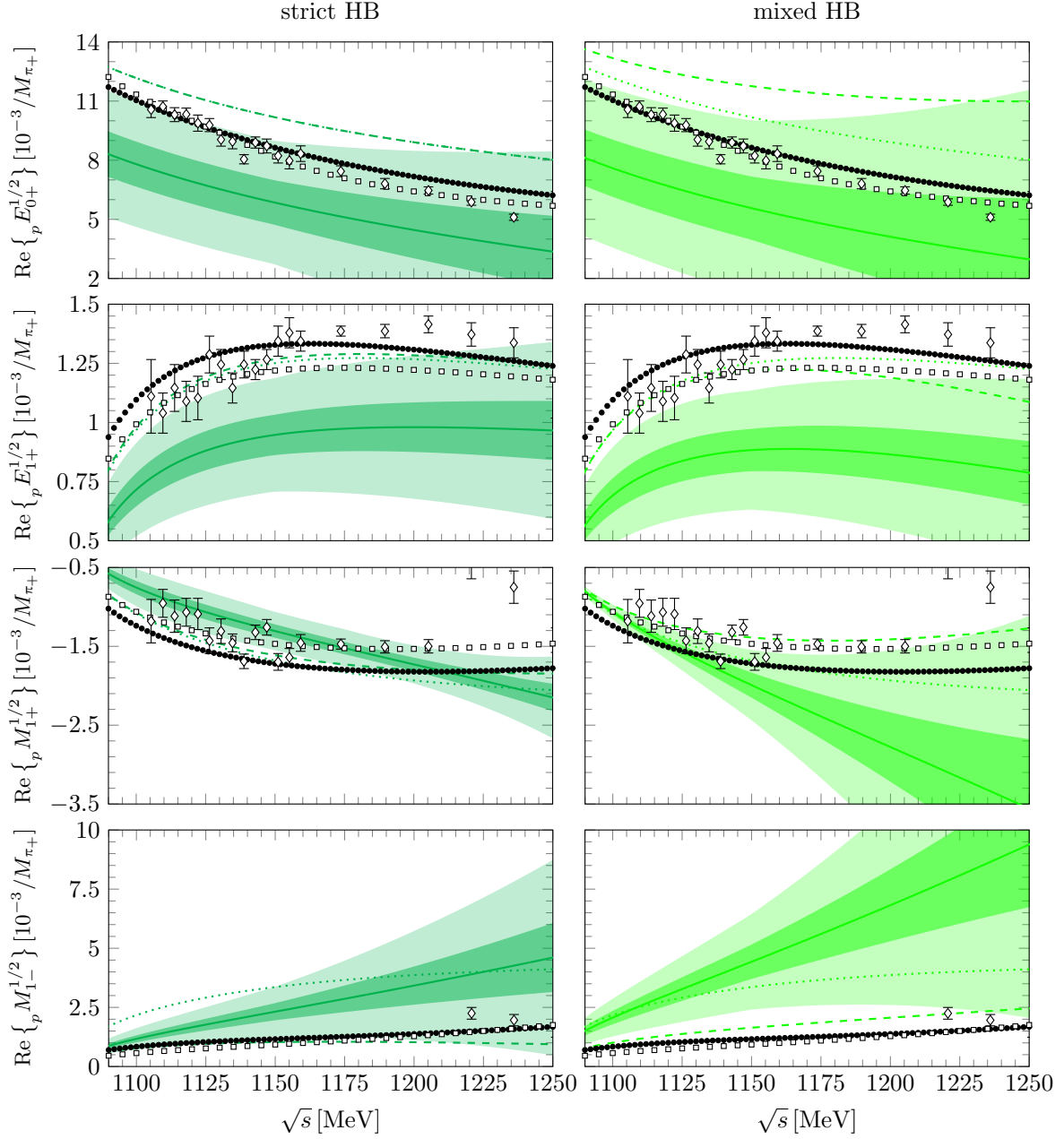


**Figure 5.6:** Order- $q^3 + \epsilon^2$  fits to the real parts of the  $s$ - and  $p$ -wave photoproduction multipoles in the proton  $I = 1/2$  channel. The solid, dashed and dotted lines denote the  $q^3 + \epsilon^2$ ,  $\epsilon^2$  and  $\epsilon^1$  results, respectively. The darker (lighter) shaded bands show the estimated truncation errors at order  $q^3 + \epsilon^2$  with 68 % (95 %) confidence. The filled circles show the results of the MAID PWA from ref. [149], the squares (diamonds) are the results of the energy-dependent (independent) SAID analysis from refs. [161, 162] (ref. [163]).

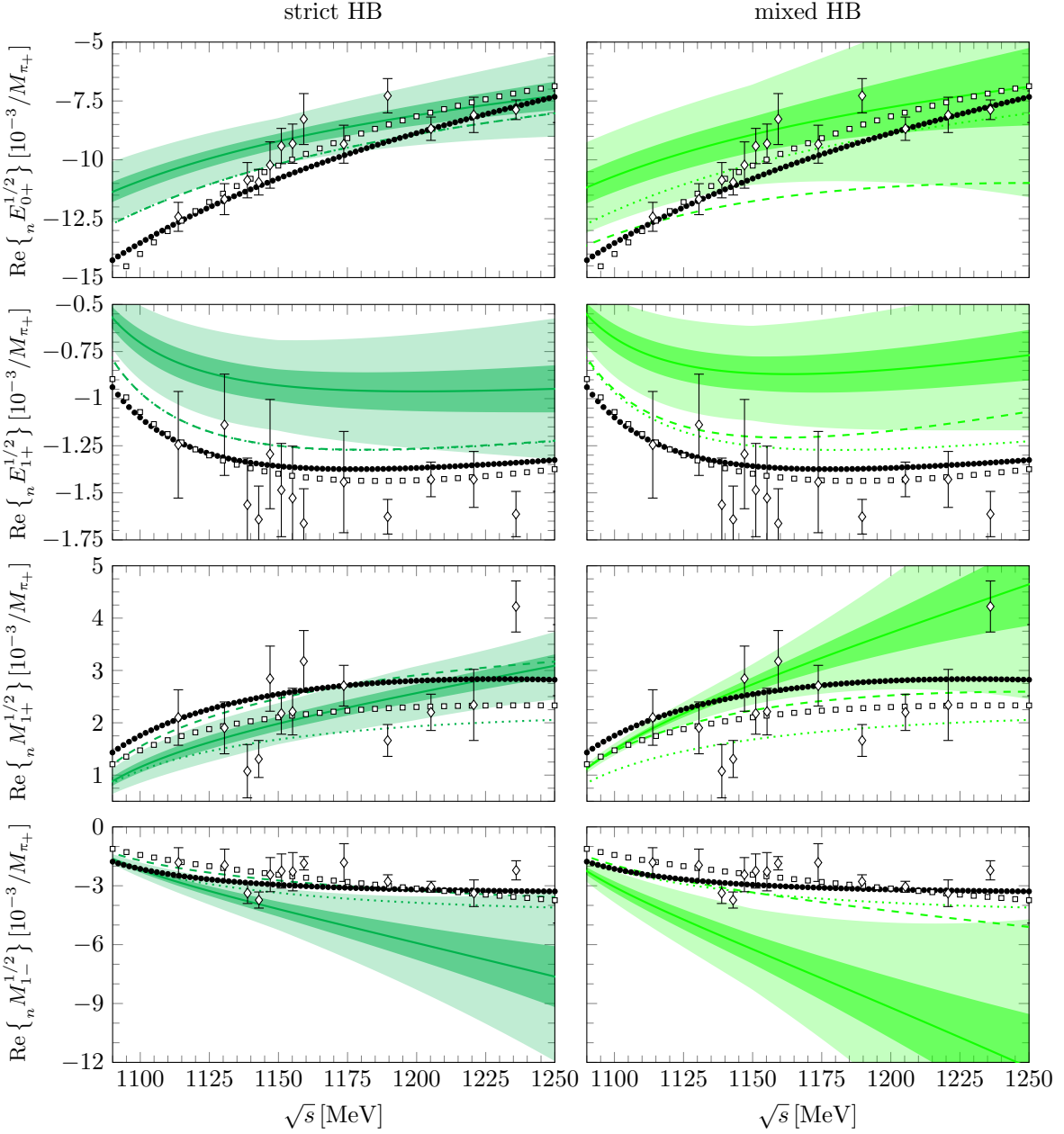


**Figure 5.7:** Order- $q^3 + \epsilon^2$  fits to the real parts of the  $s$ - and  $p$ -wave photoproduction multipoles in the neutron  $I = 1/2$  channel. The solid, dashed and dotted lines denote the  $q^3 + \epsilon^2$ ,  $\epsilon^2$  and  $\epsilon^1$  results, respectively. The darker (lighter) shaded bands show the estimated truncation errors at order  $q^3 + \epsilon^2$  with 68 % (95 %) confidence. The filled circles show the results of the MAID PWA from ref. [149], the squares (diamonds) are the results of the energy-dependent (independent) SAID analysis from refs. [161, 162] (ref. [163]).

**Table 5.5:** Low-energy constants obtained from strict and mixed order- $q^3 + \epsilon^2$  fits in the HB approach to the real parts of  $s$ - and  $p$ -wave photoproduction multipoles of the MAID model from ref. [149]. LECs  $d_i$  are given in units of  $\text{GeV}^{-2}$ ,  $b_1$  is given in  $m_N^{-1}$ .

	$\hat{d}_8^r$	$\hat{d}_9^r$	$\hat{d}_{20}^r$	$\hat{d}_{21;22}^r$	$b_1$
order $q^3 + \epsilon^2$ strict HB fit values	-0.44(4)	0.08(2)	-2.0(1)	3.8(1)	5.6(1)
order $q^3 + \epsilon^2$ mixed HB fit values	-0.06(7)	0.05(2)	-8.6(2)	8.0(2)	6.4(1)

The most outstanding difference to the deltaless case is the significantly improved description of the  $M_{1+}^{3/2}$  multipole in both HB approaches. In comparison to the deltaless approach, the region beyond  $\sqrt{s} = 1150 \text{ MeV}$  is now reproduced excellently in both magnitude and shape. The leading-order term in  $1/m_N$  from the explicit inclusion of the delta suffices to correct the  $q^3$  description of  $M_{1+}^{3/2}$ , subleading terms are less important for this multipole. However, the description of  $E_{1+}^{3/2}$  is unsatisfactory. Clearly, the strict HB approach is not sufficient to describe the energy behaviour. In the mixed HB approach, the shape is improved, but the description still fails.

Moreover, we remark that the strict HB approach does not contain subleading  $1/m_N$  order- $\epsilon^2$  corrections to  $E_{0+}$ ,  $E_{1+}$  and  $M_{1+}$  in the  $I = 1/2$  channel, which diminishes the Bayesian truncation errors. This explains the differences in the fit quality of  $d_9$ , which is not satisfactory in both approaches. Also,  $M_{1-}^{1/2}$  is still overshot, so that the description is not improved compared to the deltaless theory. All in all, we find that the mixed HB results are more preferable, in particular because of the better description of  $E_{1+}^{3/2}$  in terms of shape. Also, as McGovern et al. have argued in ref. [170], it is justifiable to keep the full relativistic  $\epsilon^2$  contribution in an energy region where a nonrelativistic treatment becomes unreliable. This is why we compare the mixed HB approach to the covariant results in the following.

In table 5.6, we show our fit results for the LECs in the covariant approach. The reduced  $\chi^2/n$  is equal to 0.5 (1.0) in the  $I = 3/2$  ( $I = 1/2$ ) channel.

**Table 5.6:** Low-energy constants obtained from an order- $q^3 + \epsilon^2$  covariant fit to the real parts of  $s$ - and  $p$ -wave photoproduction multipoles of the MAID model from ref. [149]. LECs  $d_i$  are given in units of  $\text{GeV}^{-2}$ ,  $b_1$  is given in  $m_N^{-1}$ .

	$\bar{d}_8$	$\bar{d}_9$	$\bar{d}_{20}$	$\bar{d}_{21;22}$	$b_1$
order $q^3 + \epsilon^2$ cov. fit result	0.72(3)	0.02(1)	-2.1(1)	-0.1(1)	5.6(1)

Figs. 5.8 - 5.10 show the corresponding results in direct comparison to the mixed HB approach. In the isospin-3/2 channel, the most remarkable difference can be seen in the description of  $M_{1-}$ , which is clearly improved, but still similar to the one obtained in the deltaless covariant  $q^3$  fit (see fig. 5.1). This explains the difference between the fit quality of the mixed HB and the

covariant approach, because the description of  $E_{0+}^{3/2}$  and  $M_{1+}^{3/2}$  is only slightly changed, where we note that the truncation uncertainties in  $E_{0+}^{3/2}$  are reduced in the relativistic approach. The description of  $E_{1+}^{3/2}$  remains unsatisfying and seems even worse compared to the HB result. However, we presume that including the deltaful loops will improve the description, because the next-to-leading-order  $\gamma N \Delta$  coupling constant  $h_1$  contributes at its leading order in  $1/m_N$  to  $E_{1+}^{3/2}$ . In the  $I = 1/2$  channels, for all  $s$ - and  $p$ -waves, the data description is remarkably improved compared to the HB case. Although only  $M_{1+}^{1/2}$  was fitted for comparability with the deltaless approach, all other multipoles are reproduced to a good extent. Here,  $M_{1+}^{1/2}$  must be accentuated, which could not be described at all by neither deltaless theory nor  $q^3 + \epsilon^2$  HB approach. Furthermore, the general description of  $E_{0+}^{1/2}$  is quite good and we therefore expect that the cross sections will be described well, too.

In all three approaches we considered, we also checked the impact of the threshold region on the obtained values for the LECs due to the complex mass scheme. For this test, we shifted the lower energy boundary up to  $\sqrt{s} = 1150$  MeV in order to remove the region potentially affected by unitarity-violating terms. We found that our results did not change significantly, in particular  $b_1$  remained stable under this variation in both HB and covariant approaches. Furthermore, the LECs did not change significantly when performing a combined fit of  $I = 3/2$  and  $I = 1/2$  channels. The values we obtained from the simple  $\epsilon^2$ -fits in sec. 5.2.1,  $b_1 = 5.4m_N^{-1}$  and  $b_1 = 5.7m_N^{-1}$ , are very close to the  $q^3 + \epsilon^2$  results. This also signalises the stability of the scheme.

In order to check that our determined value of the delta mass in the covariant scheme is consistent with the delta contribution to the  $\pi N$  elastic channel, we plot the imaginary part of  $E_{1+}^{3/2}$  and  $M_{1+}^{3/2}$  in fig. 5.11. Because the phase of the pion photoproduction amplitude is determined by the elastic  $\pi N$  phase shifts, a satisfying reproduction of the imaginary parts is important. We find the agreement reasonable, with the deviation in  $\text{Im}\{M_{1+}^{3/2}\}$  close to threshold probably originating from the usage of the constant delta decay width in the delta pole diagrams. We expect this behaviour to improve when including next-to-leading order delta contributions, because unitarity must be perturbatively restored at higher orders. In sec. 5.2.5, we repeat this exercise in the  $\epsilon^3$  approach and comment on the differences.

Again, we consider the shifts of the LECs from the absorption of the IR part. We remind that the predicted shifts read

$$\begin{aligned} \Delta d_8^{\text{IR}} &= 0.6 \text{ GeV}^{-2}, & \Delta d_9^{\text{IR}} &= 0.08 \text{ GeV}^{-2}, \\ \Delta d_{20}^{\text{IR}} &= 7.6 \text{ GeV}^{-2}, & \Delta d_{21;22}^{\text{IR}} &= -4.9 \text{ GeV}^{-2}, \end{aligned} \quad (5.21)$$

whereas we find for the actual differences between the mixed HB and covariant result

$$\begin{aligned} \bar{d}_8 - \hat{d}_8^r &= 0.8 \text{ GeV}^{-2}, & \bar{d}_9 - \hat{d}_9^r &= -0.03 \text{ GeV}^{-2}, \\ \bar{d}_{20} - \hat{d}_{20}^r &= 6.5 \text{ GeV}^{-2}, & \bar{d}_{21;22} - \hat{d}_{21;22}^r &= -8.1 \text{ GeV}^{-2}. \end{aligned} \quad (5.22)$$

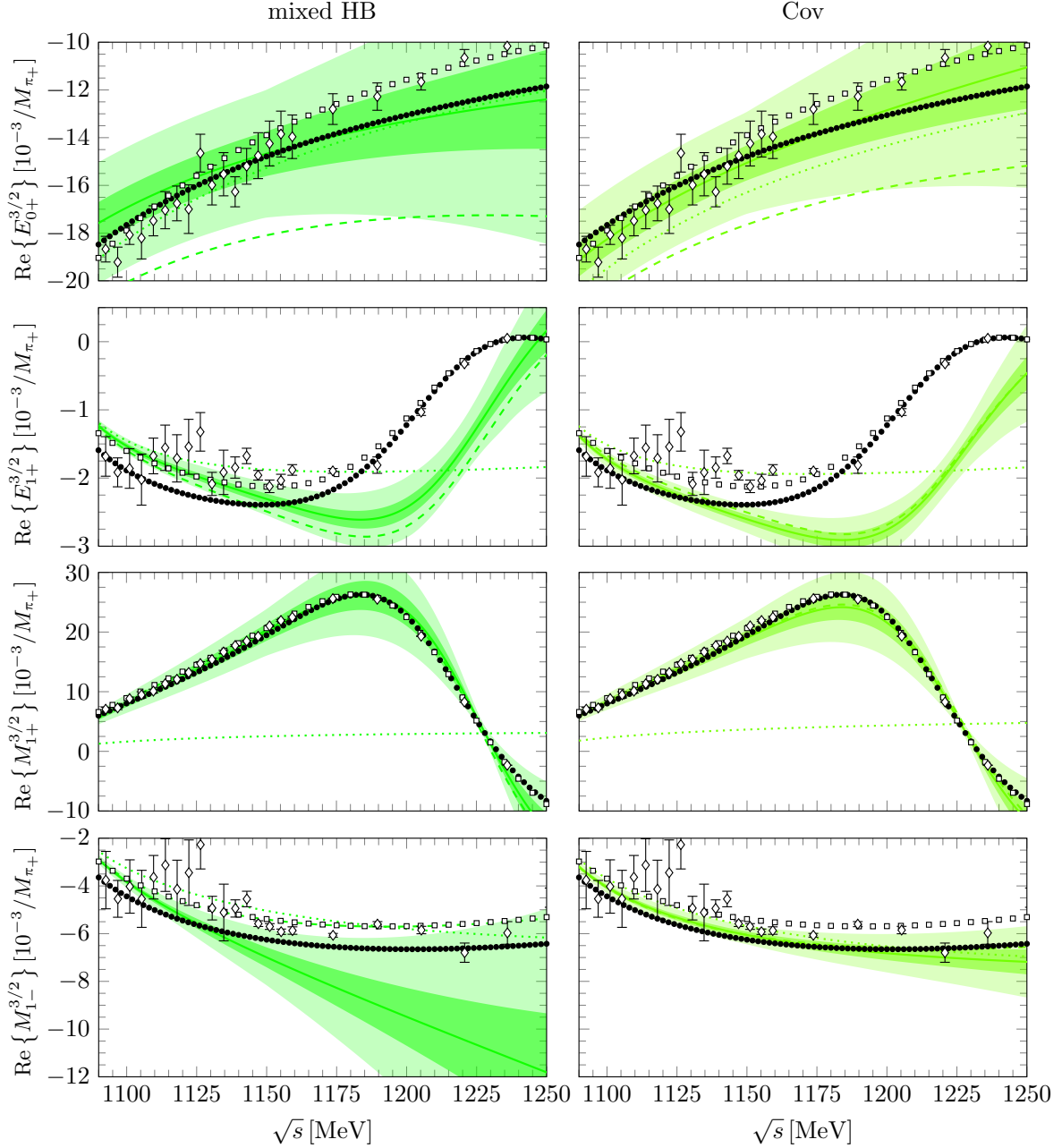


**Figure 5.8:** Order- $q^3 + \epsilon^2$  fits to the real parts of the  $s$ - and  $p$ -wave photoproduction multipoles in the  $I = 3/2$  channel. The solid, dashed and dotted lines denote the  $q^3 + \epsilon^2$ ,  $\epsilon^2$  and  $\epsilon^1$  results, respectively. The darker (lighter) shaded bands show the estimated truncation errors at order  $q^3 + \epsilon^2$  with 68 % (95 %) confidence. The filled circles show the results of the MAID PWA from ref. [149], the squares (diamonds) are the results of the energy-dependent (independent) SAID analysis from refs. [161, 162] (ref. [163]).

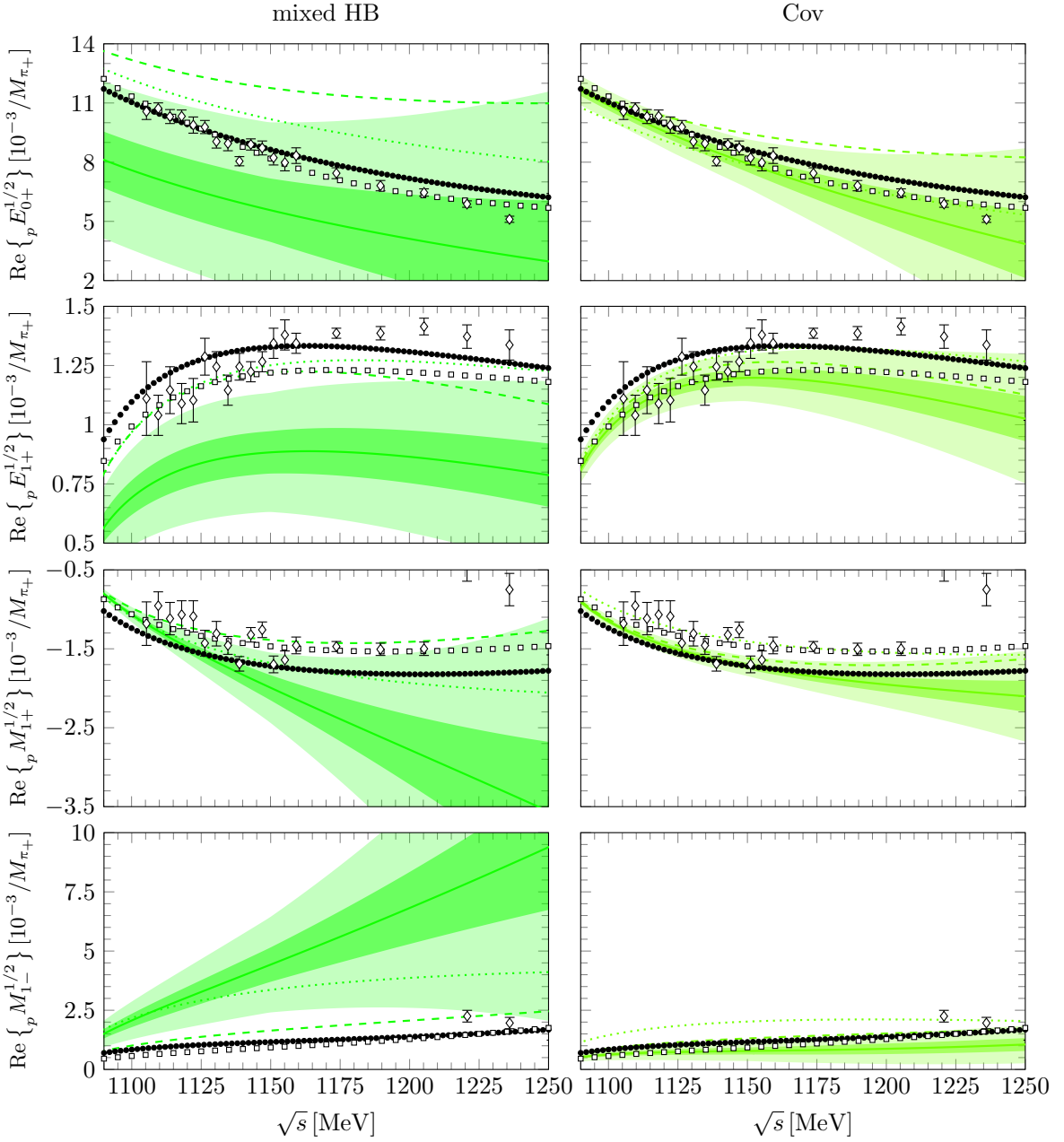


**Figure 5.9:** Order- $q^3 + \epsilon^2$  fits to the real parts of the  $s$ - and  $p$ -wave photoproduction multipoles in the proton  $I = 1/2$  channel. The solid, dashed and dotted lines denote the  $q^3 + \epsilon^2$ ,  $\epsilon^2$  and  $\epsilon^1$  results, respectively. The darker (lighter) shaded bands show the estimated truncation errors at order  $q^3 + \epsilon^2$  with 68 % (95 %) confidence. The filled circles show the results of the MAID PWA from ref. [149], the squares (diamonds) are the results of the energy-dependent (independent) SAID analysis from refs. [161, 162] (ref. [163]).

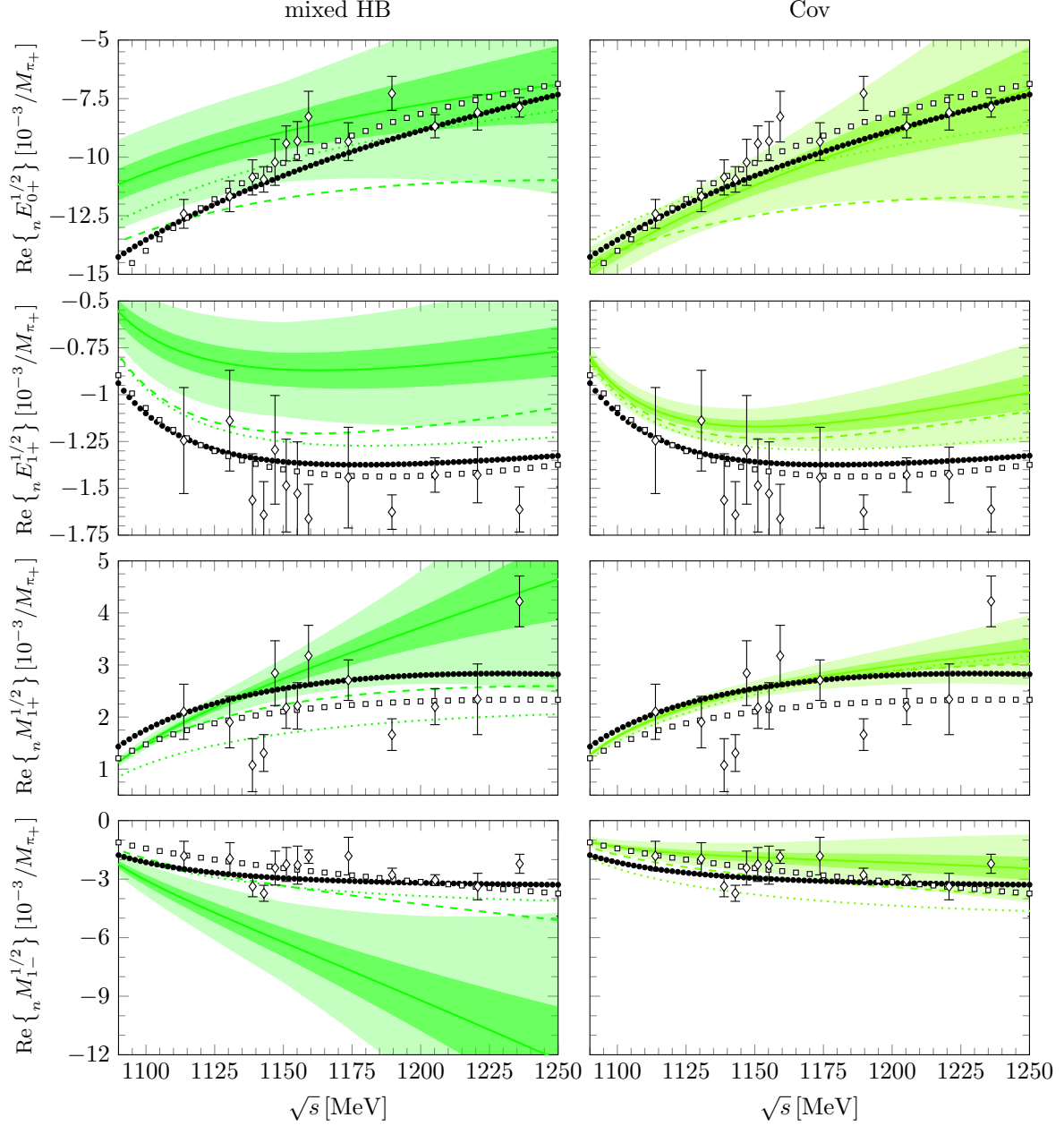


**Figure 5.10:** Order- $q^3 + \epsilon^2$  fits to the real parts of the  $s$ - and  $p$ -wave photoproduction multipoles in the neutron  $I = 1/2$  channel. The solid, dashed and dotted lines denote the  $q^3 + \epsilon^2$ ,  $\epsilon^2$  and  $\epsilon^1$  results, respectively. The darker (lighter) shaded bands show the estimated truncation errors at order  $q^3 + \epsilon^2$  with 68 % (95 %) confidence. The filled circles show the results of the MAID PWA from ref. [149], the squares (diamonds) are the results of the energy-dependent (independent) SAID analysis from refs. [161, 162] (ref. [163]).

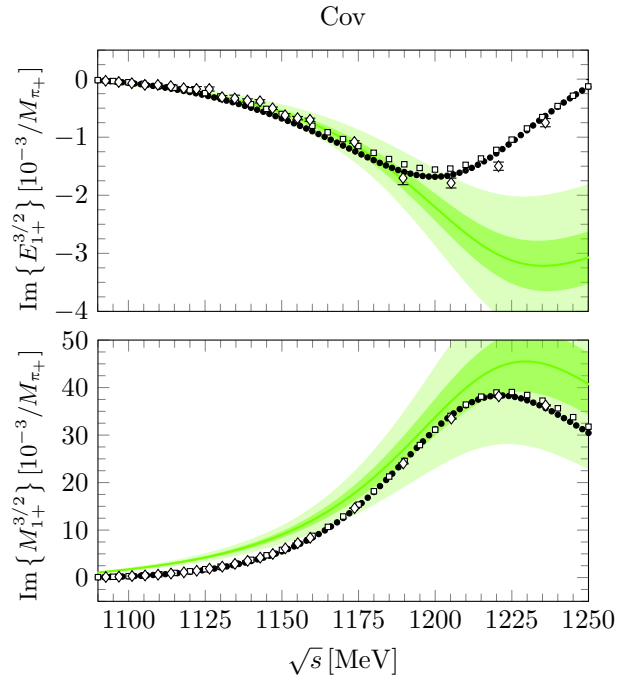


**Figure 5.11:** Imaginary parts of  $E_{1+}^{3/2}$  and  $M_{1+}^{3/2}$  using the order- $q^3 + \epsilon^2$  covariant fit results. The solid lines denote the  $q^3 + \epsilon^2$  results. The darker (lighter) shaded bands show the estimated truncation errors at order  $q^3 + \epsilon^2$  with 68 % (95 %) confidence. The filled circles show the results of the MAID PWA from ref. [149], the squares (diamonds) are the results of the energy-dependent (independent) SAID analysis from refs. [161, 162] (ref. [163]).

The agreement between predicted shifts and actual differences is again very good. Compared to the same exercise in the deltaless theory, the situation for  $d_8$  is clearly improved, and also improved slightly for  $d_{21;22}$ . Also, all LECs are smaller in absolute value and more natural when including the leading-order explicit delta contributions. We also remark again that  $b_1$  remains quite stable between the considered approaches.

Next, we take a look at the differences between the deltaless and -ful fit values of the LECs from the point of delta resonance saturation, as explained in sec. 3.8. Numerically, the expected differences read, using the HB fit value of  $b_1$

$$\delta d_8(\Delta) = -\delta d_{21;22}(\Delta) = -3.9 \text{ GeV}^{-2}, \quad \delta d_9(\Delta) = \delta d_{20}(\Delta) = 0 \text{ GeV}^{-2} \quad (5.23)$$

and for the actual differences in the HB formalism, we find

$$\begin{aligned} \hat{d}_8^{r,\Delta} - \hat{d}_8^{r,\Delta} &= -8.0 \text{ GeV}^{-2}, & \hat{d}_9^{r,\Delta} - \hat{d}_9^{r,\Delta} &= -0.04 \text{ GeV}^{-2}, \\ \hat{d}_{20}^{r,\Delta} - \hat{d}_{20}^{r,\Delta} &= -7.9 \text{ GeV}^{-2}, & \hat{d}_{21;22}^{r,\Delta} - \hat{d}_{21;22}^{r,\Delta} &= 10.4 \text{ GeV}^{-2}. \end{aligned} \quad (5.24)$$

In the covariant case, we find due to the different value of  $b_1$

$$\delta d_8(\Delta) = -\delta d_{21;22}(\Delta) = -3.4 \text{ GeV}^{-2}, \quad (5.25)$$

and for the actual differences

$$\begin{aligned} \bar{d}_8^{\Delta} - \bar{d}_8^{\Delta} &= -5.6 \text{ GeV}^{-2}, & \bar{d}_9^{\Delta} - \bar{d}_9^{\Delta} &= -0.01 \text{ GeV}^{-2}, \\ \bar{d}_{20}^{\Delta} - \bar{d}_{20}^{\Delta} &= -6.4 \text{ GeV}^{-2}, & \bar{d}_{21;22}^{\Delta} - \bar{d}_{21;22}^{\Delta} &= 9.5 \text{ GeV}^{-2}. \end{aligned} \quad (5.26)$$

In both cases, the differences between deltaless and deltaful parameters are mostly explained by the resonance saturation, although in the covariant approach the predicted shifts match the actual differences somewhat better.

The findings of the leading-order deltaful theory can be summarised in the following way:

- The description of the magnetic delta multipole  $M_{1+}^{3/2}$  is improved dramatically by the inclusion of the leading delta corrections, especially in the delta region. In the HB framework, we found that a strict treatment of the delta pole diagrams in the  $1/m_N$ -expansion suffices to reproduce  $M_{1+}^{3/2}$ , but keeping the covariant expressions is preferable.
- The covariant  $q^3 + \epsilon^2$  results give an overall excellent reproduction of the  $s$ - and  $p$ -wave multipole amplitudes. We found the leading-order  $\gamma N \Delta$  constant  $b_1$  to be very stable under variation of the energy fitting range, inclusion of the deltaless loop order and combination of  $I = 3/2$  and  $I = 1/2$  fit.
- Differences of the numerical LEC values between deltaless and deltaful approach can be explained satisfactorily by resonance saturation and between HB and covariant LECs by the infrared regular shifts of the loop integrals.

### 5.2.4 Fitting procedure including delta loop contributions

In the following, we extend our study to the next-to-leading delta order contributions. From this order, deltaful loop diagrams must be taken into account<sup>2</sup>. As we have seen from our comparison of HB and covariant  $q^3 + \epsilon^2$  approach, the description of the multipole amplitudes in the delta region is distinctly worse in the HB formalism. Because we are mainly interested in reproducing the multipole behaviour in the delta region and giving a reliable estimate of the deltaful coupling constants, we do not study pion photoproduction at order  $\epsilon^3$  in the HB scheme and concentrate on the covariant order- $\epsilon^3$  formalism in the following.

At leading deltaful loop order, the next-to-leading  $\gamma N\Delta$  coupling constant  $\bar{h}_1$  starts to contribute. In terms of the  $1/m_N$  expansion, in the dominant delta-pole graphs  $\bar{h}_1$  contributes at leading order to  $E_{0+}$ ,  $E_{1+}$  and  $M_{1+}$  in the isospin-3/2 channel. The  $I = 1/2$  channels do not receive  $\bar{h}_1$  corrections in the  $s$ -channel. Therefore, we slightly modify our fitting procedure and include  $E_{1+}$  in the  $I = 3/2$  fit, which determines in the following the LECs  $\bar{d}_8, \bar{d}_{20}, \bar{d}_{21;22}, \bar{b}_1$  and  $\bar{h}_1$ . Subsequently, we fit  $\bar{d}_9$  to the  $I = 1/2$  channel as before. At this working order, we find it especially important to consider  $I = 3/2$  separately, in order to access  $\bar{h}_1$ . Because  $\bar{h}_1$  starts to contribute from one order higher in the  $1/m_N$  series, we assume that our fits are rather insensitive to this constant. The relation between the bare LEC  $h_1$  and the renormalised LEC  $\bar{h}_1$  was given in sec. 3.5 (the same holds for  $b_1$  and  $\bar{b}_1$ ).

Furthermore, at leading deltaful loop order the  $\gamma\Delta\Delta$  coupling constant  $g_1$  from  $\mathcal{L}_{\pi\Delta}^{(1)}$  first appears in the amplitude. In ref. [37], Yao et al. have determined  $g_1$  from pion-nucleon scattering, which we use as an input for our study. We remark that in principle it is possible to fit  $g_1$  to pion photoproduction at order  $\epsilon^3$  and that we attempted to do it. However, we found that  $g_1$  is not very well constrained by the data in the sense that the uncertainty of such fit does not even allow to determine the sign of this constant. Therefore, we use the value determined from  $\pi N$  scattering [37].

Some remarks should be added concerning the fitting procedure in the  $\epsilon^3$  configuration. The energy range we employ in our fits is already extending in the delta region, this is why we keep the upper energy boundary at  $\sqrt{s} = 1250$  MeV. In contrast to the order- $q^3 + \epsilon^2$  study, we found that the threshold region has a relevant effect on  $\bar{h}_1$ , and insignificant effects on the other LECs. Therefore, as in ref. [47], we fit in the energy range  $1150 \text{ MeV} \leq \sqrt{s} \leq 1250 \text{ MeV}$  in order to remove any possible threshold effects from our utilisation of the complex-mass scheme. Also, similar to the case explained in sec. 5.2.2, we refit  $b_1$  and do not use the value from previous fits for the estimation of the truncation errors. Because we found  $\bar{b}_1$  to be fairly stable in all configurations we considered, effects from refitting  $\bar{b}_1$  are small.

---

<sup>2</sup>See appendix B for the relevant Feynman diagrams.

### 5.2.5 Order- $\epsilon^3$ results, figures and discussion

In table 5.7 we give our results for the LECs determined from the covariant fit at order  $\epsilon^3$ . In the  $I = 3/2$  fit, the number of used data points is 204 due to the inclusion of the  $E_{1+}$  multipole and 102 in the  $I = 1/2$  channel. The reduced  $\chi^2/n$  is equal to 0.2(2.2) in the  $I = 3/2(I = 1/2)$  channel. The corresponding results for the multipoles are depicted in figs. 5.12 - 5.14.

**Table 5.7:** Low-energy constants obtained from an order- $\epsilon^3$  covariant fit to the real parts of  $s$ - and  $p$ -wave photoproduction multipoles of the MAID model from ref. [149]. LECs  $\bar{d}_i$  are given in units of  $\text{GeV}^{-2}$ ,  $\bar{b}_1$  and  $\bar{h}_1$  are given in  $m_N^{-1}$ .

	$\bar{d}_8$	$\bar{d}_9$	$\bar{d}_{20}$	$\bar{d}_{21;22}$	$\bar{b}_1$	$\bar{h}_1$
order $\epsilon^3$ cov. fit result	1.34(4)	-1.99(2)	9.5(1)	-33.2(1)	5.3(1)	0.9(1)

As we can see from fig. 5.12, the reproduction of the  $I = 3/2$  channel has improved compared to the covariant  $q^3 + \epsilon^2$  fit. Especially  $E_{1+}$  is now matched significantly better due to the inclusion of the subleading  $\gamma N\Delta$  coupling constant  $\bar{h}_1$ . In the  $I = 1/2$  channels however, the description is distinctly worse compared to the  $q^3 + \epsilon^2$ -case. Especially the reproduction of the  $E_{0+}^{1/2}$  multipoles fails, which has a substantial effect on the reproduction of cross sections, for example. Also, the fit quality in the  $I = 1/2$  channels of  $\chi^2/n = 2.2$  is significantly worse compared to the  $q^3 + \epsilon^2$  fit, where we found  $\chi^2/n = 1.0$ . We also remark that  $M_{1-}^{1/2}$  is overshot again, but not as bad as in the deltaless case (see figs. 5.2-5.3).

Some comments on the obtained values of the LECs are required. As can be seen from table 5.7, the value of  $d_{21;22}$  stands out. From a naive estimate, the numeric values of  $d_i$ 's should be of the order

$$d_i \sim \frac{1}{\Lambda_b} \sim 2.5 \text{ GeV}^{-2} \quad \text{with} \quad \Lambda_b = 650 \text{ MeV}. \quad (5.27)$$

Clearly,  $d_{21;22}$  is far from this value, and also  $d_{20}$  is also not close to this estimate. However, a more detailed evaluation is necessary. First, we remind that  $d_{21;22}$  is a linear combination of two LECs, and we cannot access the size of the individual constants. Therefore, the combination  $d_{21;22}$  might be accordingly larger as estimated by eq. (5.27), but even this estimate clearly fails.

Second, as a closer look reveals, the large value of  $d_{21;22}$  might in parts be traced back to our fitting procedure.  $\bar{d}_{21;22}$  is constrained by a fit to the  $I = 3/2$  channel, in which  $E_{0+}$  and  $M_{1+}$  have the largest magnitudes, therefore these two multipoles give more weight to the fit. However, the contribution of  $\bar{d}_{21;22}$  to  $M_{1+}^{3/2}$  at leading order in  $1/m_N$  is four times smaller than the contribution of  $\bar{d}_8$ . Consequently,  $\bar{d}_{21;22}$  has to be four times as large to compensate a corresponding numerical shift in  $\bar{d}_8$ . Furthermore,  $E_{0+}^{3/2}$  only receives the linear combination  $\bar{d}_{20} + \bar{d}_{21;22}$  at leading order in  $1/m_N$ , and because our obtained values for  $\bar{d}_{20}$  and  $\bar{d}_{21;22}$  have

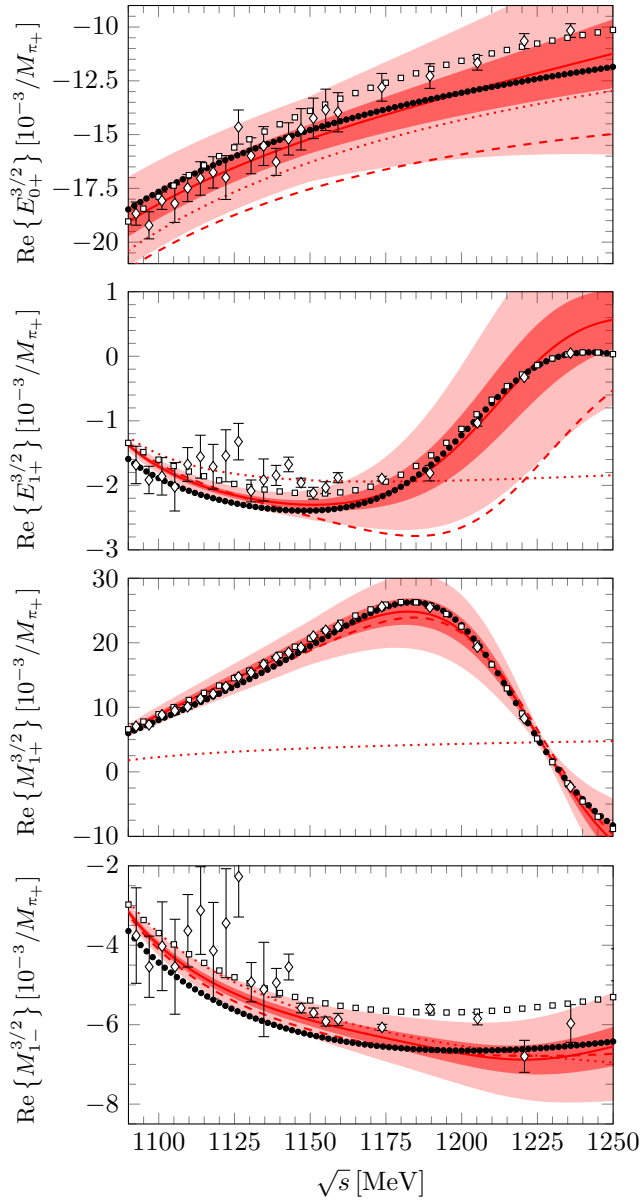


**Figure 5.12:** Order- $\epsilon^3$  fits to the real parts of the  $s$ - and  $p$ -wave photoproduction multipoles in the  $I = 3/2$  channel. The solid, dashed and dotted lines denote the  $\epsilon^3$ ,  $\epsilon^2$  and  $\epsilon^1$  results, respectively. The darker (lighter) bands show the estimated truncation errors at order  $\epsilon^3$  with 68 % (95 %) confidence. The filled circles show the results of the MAID PWA from ref. [149], the squares (diamonds) are the results of the energy-dependent (independent) SAID analysis from refs. [161, 162] (ref. [163]).

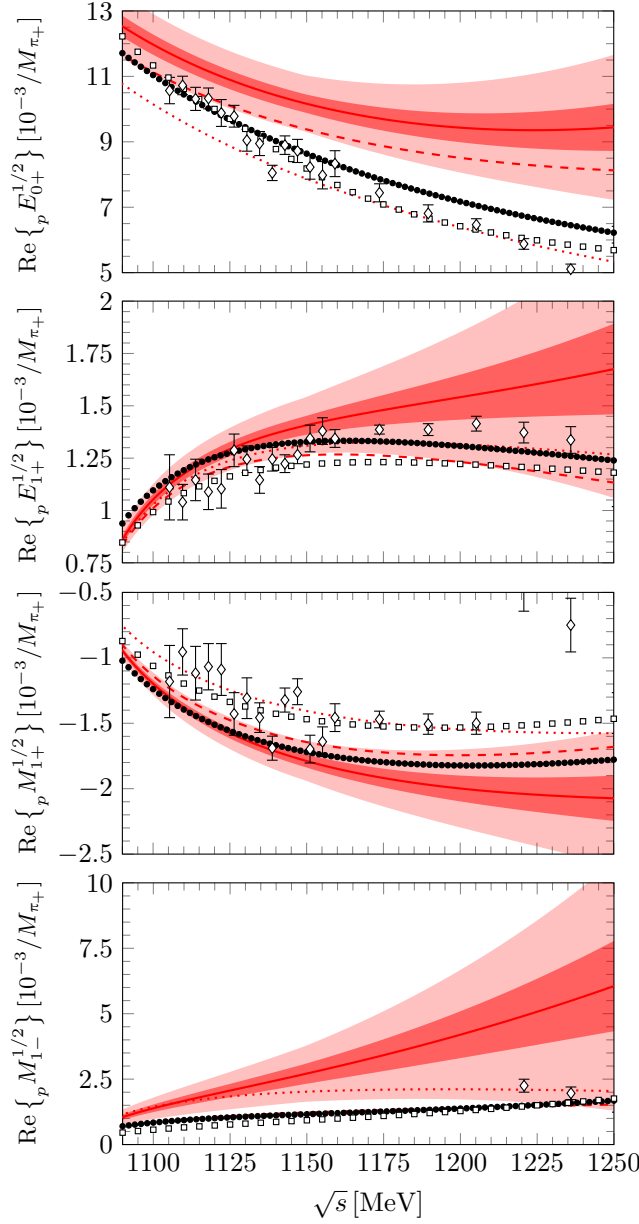


**Figure 5.13:** Order- $\epsilon^3$  fits to the real parts of the  $s$ - and  $p$ -wave photoproduction multipoles in the proton  $I = 1/2$  channel. The solid, dashed and dotted lines denote the  $\epsilon^3$ ,  $\epsilon^2$  and  $\epsilon^1$  results, respectively. The darker (lighter) bands show the estimated truncation errors at order  $\epsilon^3$  with 68 % (95 %) confidence. The filled circles show the results of the MAID PWA from ref. [149], the squares (diamonds) are the results of the energy-dependent (independent) SAID analysis from refs. [161, 162] (ref. [163]).

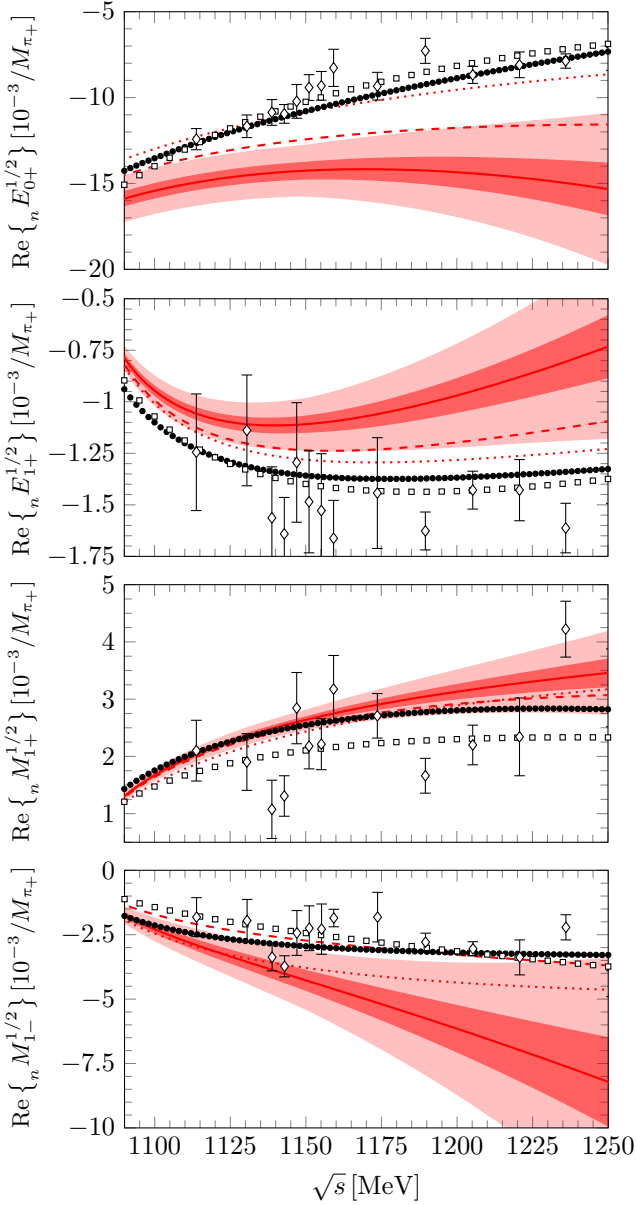


**Figure 5.14:** Order- $\epsilon^3$  fits to the real parts of the  $s$ - and  $p$ -wave photoproduction multipoles in the neutron  $I = 1/2$  channel. The solid, dashed and dotted lines denote the  $\epsilon^3$ ,  $\epsilon^2$  and  $\epsilon^1$  results, respectively. The darker (lighter) bands show the estimated truncation errors at order  $\epsilon^3$  with 68 % (95 %) confidence. The filled circles show the results of the MAID PWA from ref. [149], the squares (diamonds) are the results of the energy-dependent (independent) SAID analysis from refs. [161, 162] (ref. [163]).

opposite signs, their contributions to  $E_{0+}^{3/2}$  cancel to a large extent. Other  $\bar{d}_i$ -contributions to the multipoles  $E_{0+}^{3/2}$  and  $M_{1+}^{3/2}$  are either absent or subleading in  $1/m_N$ . Also, the contribution of  $\bar{d}_{21;22}$  to  $M_{1-}^{3/2}$ , which is smaller in magnitude, is still by a factor of 2 reduced in comparison to  $d_8$ .

As an additional check, we have performed another fit with an extra naturalness constraint. Therefore, we added a weight term  $\sim \exp\{d_i^2/R^2\}$  with the parameter  $R$  to the  $\chi^2$  function, such that large values of  $\bar{d}_{21;22}$  are suppressed. Imposing a naturalness constraint helps to access other distinct minima (if present) in the  $\chi^2$ . We varied the size of the parameter  $R$  to check more or less rigorous constraints, but we did not find another minimum with more natural values of  $\bar{d}_{21;22}$ . Its value was only slightly reduced at the expense of smaller values of  $\bar{b}_1$ , which affects the reproduction of the  $M_{1+}^{3/2}$  multipole. This is in contrast to the aim of our  $\epsilon^3$ -study, to give reliable values of  $\bar{b}_1$  and  $\bar{h}_1$ .

Speaking in terms of Feynman diagrams, we found that the gauge-invariant subset constructed from the topologies shown in fig. 5.15, which contain one or two delta propagators inside the loop, give rise to large contributions to the amplitude, which is reflected in the magnitude of the constant  $\bar{d}_{21;22}$ . In ref. [47], where these diagrams were not taken into account, we found the LEC to be natural. Furthermore, we removed the set of diagrams and also found  $\bar{d}_{21;22}$  to be reduced dramatically in magnitude. Note that this served as a simple test, because such a configuration is not justifiable in terms of our power counting.

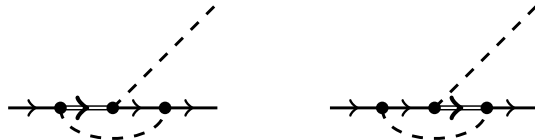


**Figure 5.15:** Delta loop topologies giving rise to large contributions to the amplitude. To construct the gauge invariant set of pion photoproduction diagrams, a photon must be attached wherever possible, yielding 18 diagrams in total.

We again evaluate the imaginary parts of the multipoles and show them in fig. 5.16. In contrast to the  $q^3 + \epsilon^2$  case, the situation is clearly improved (see fig. 5.11). Especially  $\text{Im}\{E_{1+}^{3/2}\}$  is reproduced better in the delta region. Also, the deviation close to threshold originating from the complex-mass scheme is reduced due to the inclusion of higher orders, which restore unitarity perturbatively. Furthermore, the  $E2/M1$  ratio

$$R_{EM} = \left. \frac{\text{Im}\{E_{1+}^{3/2}\}}{\text{Im}\{M_{1+}^{3/2}\}} \right|_{\sqrt{s}=1232 \text{ MeV}} \approx -0.033 \pm 0.014 \quad (5.28)$$

seems consistent with the PDG value  $-0.030 \lesssim R_{EM} \lesssim -0.020$  [110], whereas at order  $q^3 + \epsilon^2$  we found  $R_{EM} \approx -0.071 \pm 0.014$ . This also indicates that our extracted values of  $\bar{b}_1$  and  $\bar{h}_1$

are reliable.

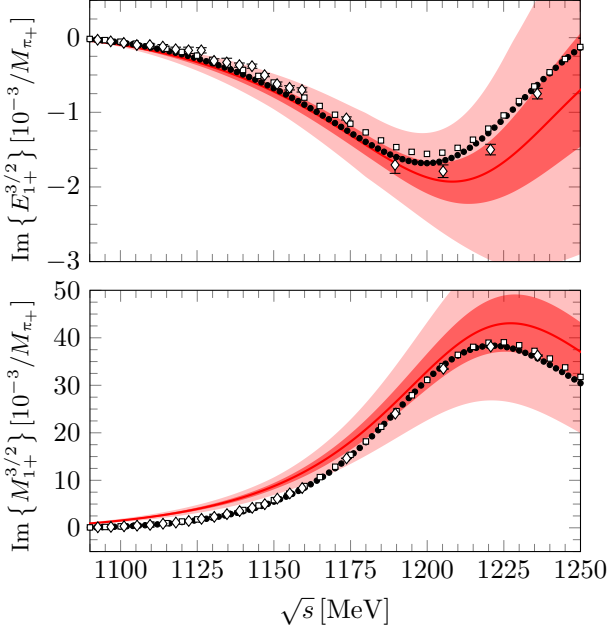


**Figure 5.16:** Imaginary parts of  $E_{1+}^{3/2}$  and  $M_{1+}^{3/2}$  using the covariant order- $\epsilon^3$  fit results. The solid lines denote the  $\epsilon^3$  results. The darker (lighter) shaded bands show the estimated truncation errors at order  $\epsilon^3$  with 68 % (95 %) confidence. The filled circles show the results of the MAID PWA from ref. [149], the squares (diamonds) are the results of the energy-dependent (independent) SAID analysis from ref. [161, 162] (ref. [163]).

For the sake of completeness, we also give the differences to the deltaless LECs in order to check the resonance saturation assumption. The differences between deltaful and deltaless (see tab. 5.2) are

$$\begin{aligned} \bar{d}_8^\Delta - \bar{d}_8^\Delta &= -6.2 \text{ GeV}^{-2}, & \bar{d}_9^\Delta - \bar{d}_9^\Delta &= 2.0 \text{ GeV}^{-2}, \\ \bar{d}_{20}^\Delta - \bar{d}_{20}^\Delta &= -18.0 \text{ GeV}^{-2}, & \bar{d}_{21;22}^\Delta - \bar{d}_{21;22}^\Delta &= 42.6 \text{ GeV}^{-2}. \end{aligned} \quad (5.29)$$

and the calculated differences from the resonance saturation read

$$\delta d_8(\Delta) = -\delta d_{21;22}(\Delta) = -3.1 \text{ GeV}^{-2}, \quad \delta d_9(\Delta) = \delta d_{20}(\Delta) = 0 \text{ GeV}^{-2}. \quad (5.30)$$

Here, the resonance saturation only explains the shift of  $\bar{d}_8$  satisfactorily. It clearly fails in the cases of  $\bar{d}_{20}$  and  $\bar{d}_{21;22}$ .

Finally, we remark that the inclusion of the deltaless order- $q^4$  terms might have a substantial effect on the naturalness of the  $d_i$ s. In ref. [95], pion photoproduction was calculated in deltaless ChPT up to order  $q^4$ . It was found that including the NLO loop diagrams does not

have a great effect on the description of observables in the delta region. However, at this order, 11 additional LECs enter the photoproduction amplitude. Therefore, it is plausible to assume that adding order  $q^4$  improves the naturalness of the  $\bar{d}_i$ 's.

We summarise the findings of the order- $\epsilon^3$  approach as follows:

- The description of the  $s$ - and  $p$ -wave multipole amplitudes in the  $I = 3/2$  channel is improved when including the first deltaful loop order. We found that our extraction of the  $\gamma N \Delta$  coupling constants  $\bar{b}_1$  and  $\bar{h}_1$  can be taken as reliable. In particular,  $\bar{b}_1$  is stable under variation of the energy range and combining the  $I = 3/2$  and  $I = 1/2$  fit. The LEC  $\bar{h}_1$  is more sensitive to the variation of the energy range, but still of the same sign and roughly of the same size when including the threshold energy region. Furthermore,  $\bar{b}_1$  only changes slightly in comparison to our  $q^3 + \epsilon^2$ -study, and the value of  $\bar{h}_1$  is close to the value of our related study [47], where we found  $\bar{h}_1 = 1.0(1)m_N^{-1}$ .
- The reproduction of the isospin-1/2 channels is overall poor. This may be a consequence of our fitting procedure, which focuses on the delta multipoles. We found that the values of the LECs  $\bar{d}_{20}$  and  $\bar{d}_{21;22}$  at order  $\epsilon^3$  are noticeably larger than expected from the naturalness assumption.
- The inclusion of the leading order deltaful loop diagrams gives rise to surprisingly large corrections to the amplitude. Extending the analysis to the next order is desirable in order to see if the overall description of the process can be improved again.

### 5.3 Comparison to data of the neutral pion production channel

In this subsection, we compare our results with data of the neutral pion production channel  $\gamma p \rightarrow \pi^0 p$ . Of the four physical reaction channels given in eq. (3.10), this channel is the most interesting for our purposes. The two charged pion production channels  $\gamma p \rightarrow \pi^+ n$  and  $\gamma n \rightarrow \pi^- p$  are of minor interest for a study in ChPT, because the Kroll-Ruderman terms of leading order comprise by far the dominant contributions to the amplitude, such that subleading terms give only very small corrections. The remaining neutral channel  $\gamma n \rightarrow \pi^0 n$  is difficult to measure in experiments, because a neutron target would be required and therefore, there are no data available on this channel.

The recent experiment at the Mainz Microtron provided high-precision data for the differential cross section  $\frac{d\sigma}{d\Omega}$  and the linear polarised photon asymmetry  $\Sigma$  [78, 108]. We compare our findings with these data and emphasise that our results for both observables were calculated as discussed in sec. 3.4, in particular we do not use the  $s$ - and  $p$ -wave approximation. In all figures shown in this subsection, the depicted error bars show the combined statistic and systematic error

$$\delta O_i = \sqrt{(\delta O_i^{\text{stat}})^2 + (\delta O_i^{\text{sys}})^2}, \quad (5.31)$$

where the systematic uncertainties are 4 % for  $\frac{d\sigma}{d\Omega}$  and 5 % for  $\Sigma$ .

Figs. 5.17 and 5.18 show our results obtained from the HB order- $q^3$  calculation for the differential cross section and polarisation asymmetry, respectively, and figs. 5.19 and 5.20 are the corresponding covariant order- $q^3$  plots. We only give our results up to  $\sqrt{s} = 1180$  MeV, because the deviations get very large for higher energies. Because there were no data taken for asymmetries between  $\sqrt{s} = 1125$  MeV and  $\sqrt{s} = 1160$  MeV, we do not show results in this energy range.

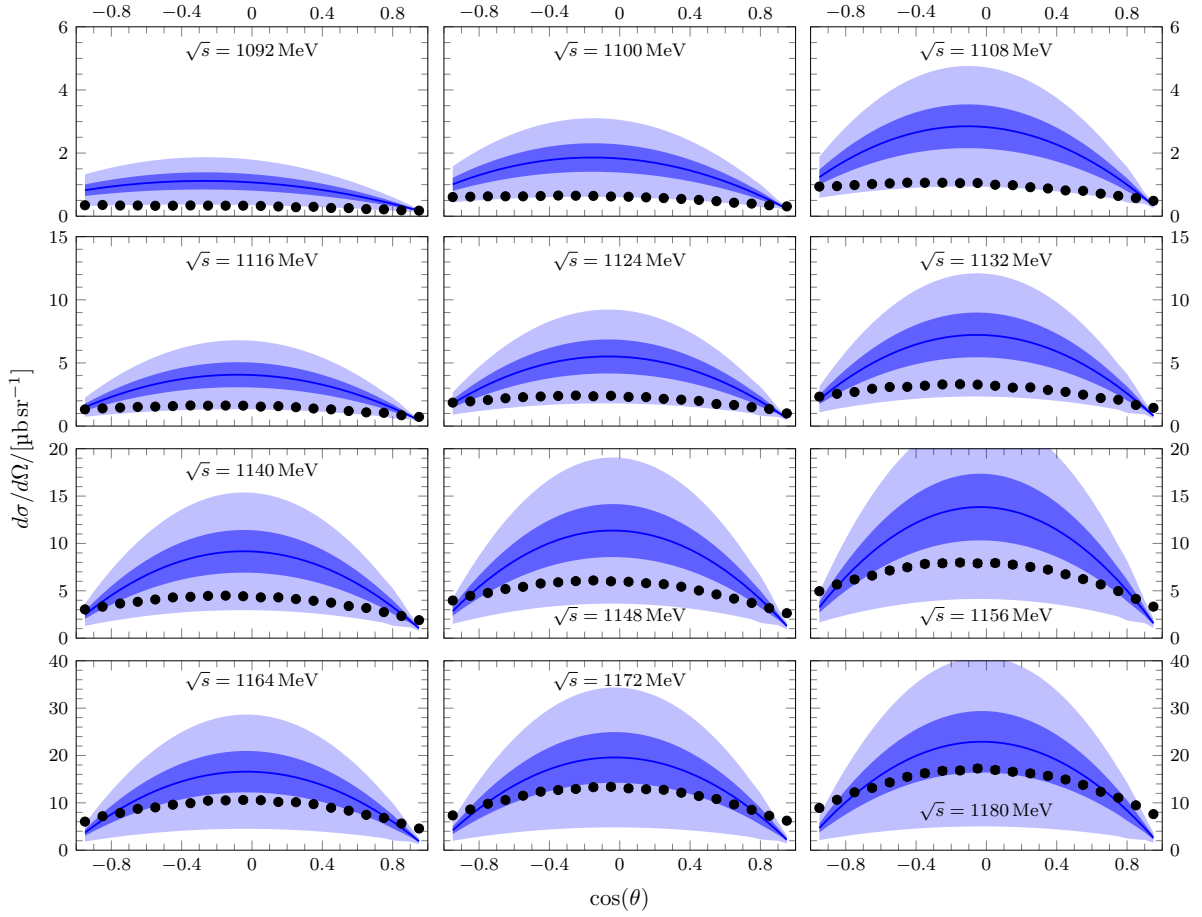


**Figure 5.17:** HB order- $q^3$  result of the unpolarised differential cross section in the channel  $\gamma + p \rightarrow \pi^0 + p$ . The solid lines denote the  $q^3$  results, the darker (lighter) shaded bands show the estimated truncation errors at order  $q^3$  with 68 % (95 %) confidence. The data are from refs. [78, 108], error bars correspond to the combined statistical and systematical error.

In figs. 5.21 and 5.22 we depict our results obtained from the strict HB order- $q^3 + \epsilon^2$  calculation for the differential cross section and polarisation asymmetry, respectively. Figs. 5.23 and 5.24 show the results from the mixed HB order- $q^3 + \epsilon^2$  approach. The subtleties of our considerations in the HB formalisms were explained in sec. 5.2.2. The covariant order- $q^3 + \epsilon^2$

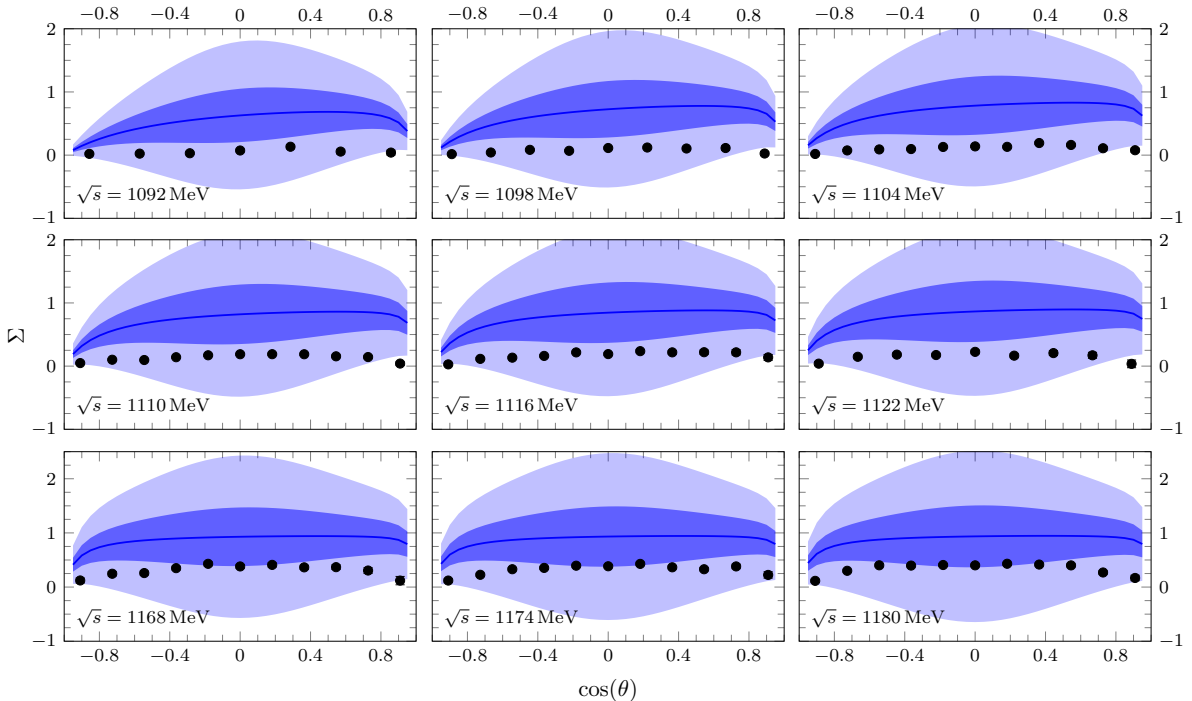


**Figure 5.18:** HB order- $q^3$  result of the linear polarised photon asymmetry in the channel  $\gamma + p \rightarrow \pi^0 + p$ . The solid lines denote the  $q^3$  results, the darker (lighter) shaded bands show the estimated truncation errors at order  $q^3$  with 68 % (95 %) confidence. The data are from refs. [78, 108], error bars correspond to the combined statistical and systematical error.

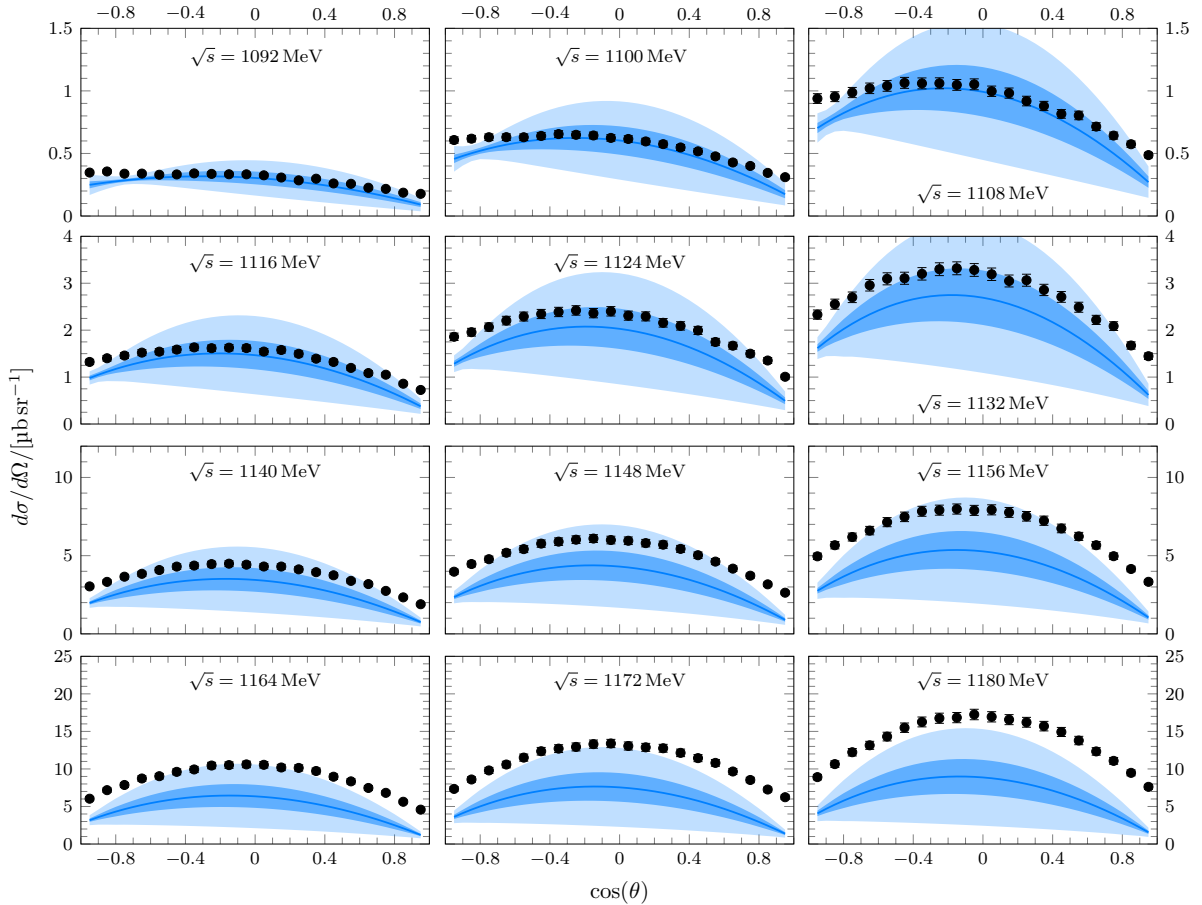


**Figure 5.19:** Covariant order- $q^3$  result of the unpolarised differential cross section in the channel  $\gamma + p \rightarrow \pi^0 + p$ . The solid lines denote the  $q^3$  results, the darker (lighter) shaded bands show the estimated truncation errors at order  $q^3$  with 68 % (95 %) confidence. The data are from refs. [78, 108], error bars correspond to the combined statistical and systematical error.

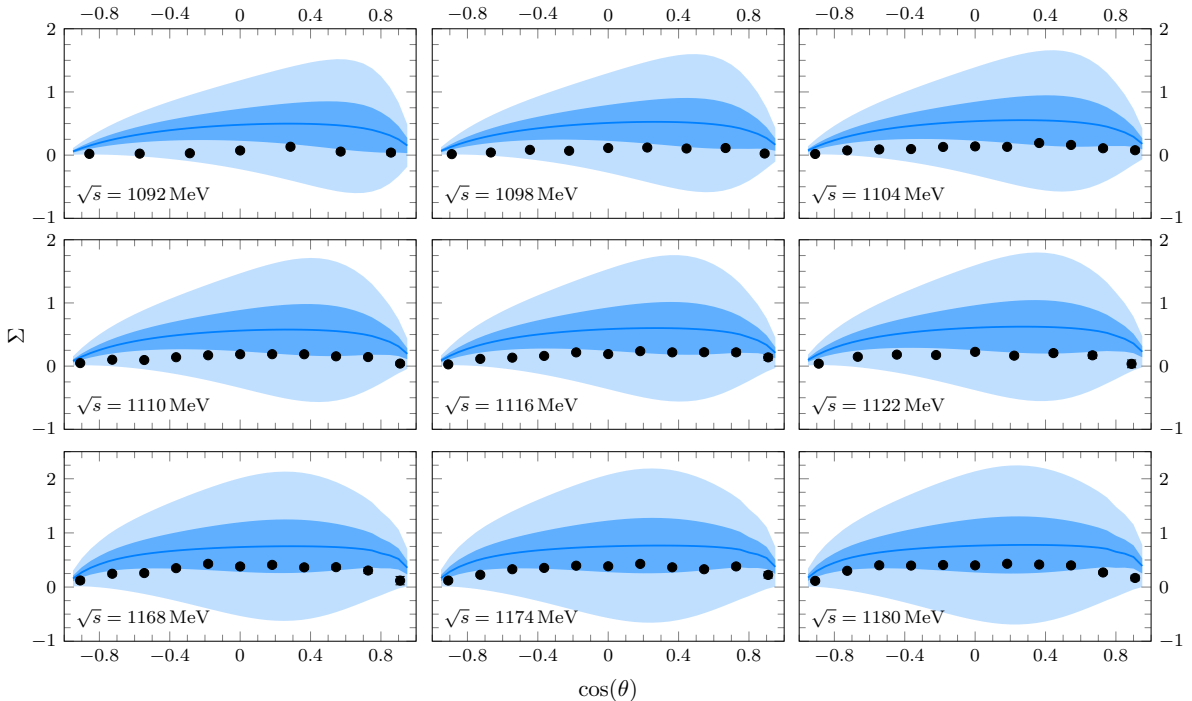


**Figure 5.20:** Covariant order- $q^3$  result of the linear polarised photon asymmetry in the channel  $\gamma + p \rightarrow \pi^0 + p$ . The solid lines denote the  $q^3$  results, the darker (lighter) shaded bands show the estimated truncation errors at order  $q^3$  with 68 % (95 %) confidence. The data are from refs. [78, 108], error bars correspond to the combined statistical and systematical error.

results are shown in figs. 5.25 and 5.26. Because asymmetries were only taken up to an energy of  $\sqrt{s} = 1214$  MeV, we do not show our results for higher energies.

Our findings from the analysis of multipole amplitudes are in general confirmed. In the deltaless approach, the covariant results reproduce the neutral pion production channel better in comparison to the HB approach, especially close to threshold. The HB results overestimate both cross sections and asymmetries. The inclusion of the delta tree contributions improves the situation clearly, especially the overestimation of the observables is reduced significantly. Also, the results of the mixed HB approach match the data better than the strict HB results, and the covariant order- $q^3 + \epsilon^2$  results give by far the best agreement with the data. Especially the polarisation asymmetries are reproduced accurately up to the delta region. We refrain from showing the order- $\epsilon^3$  results for cross sections and asymmetries, because the poor reproduction of the  $I = 1/2$  channels leads to a significant overshooting of the data.

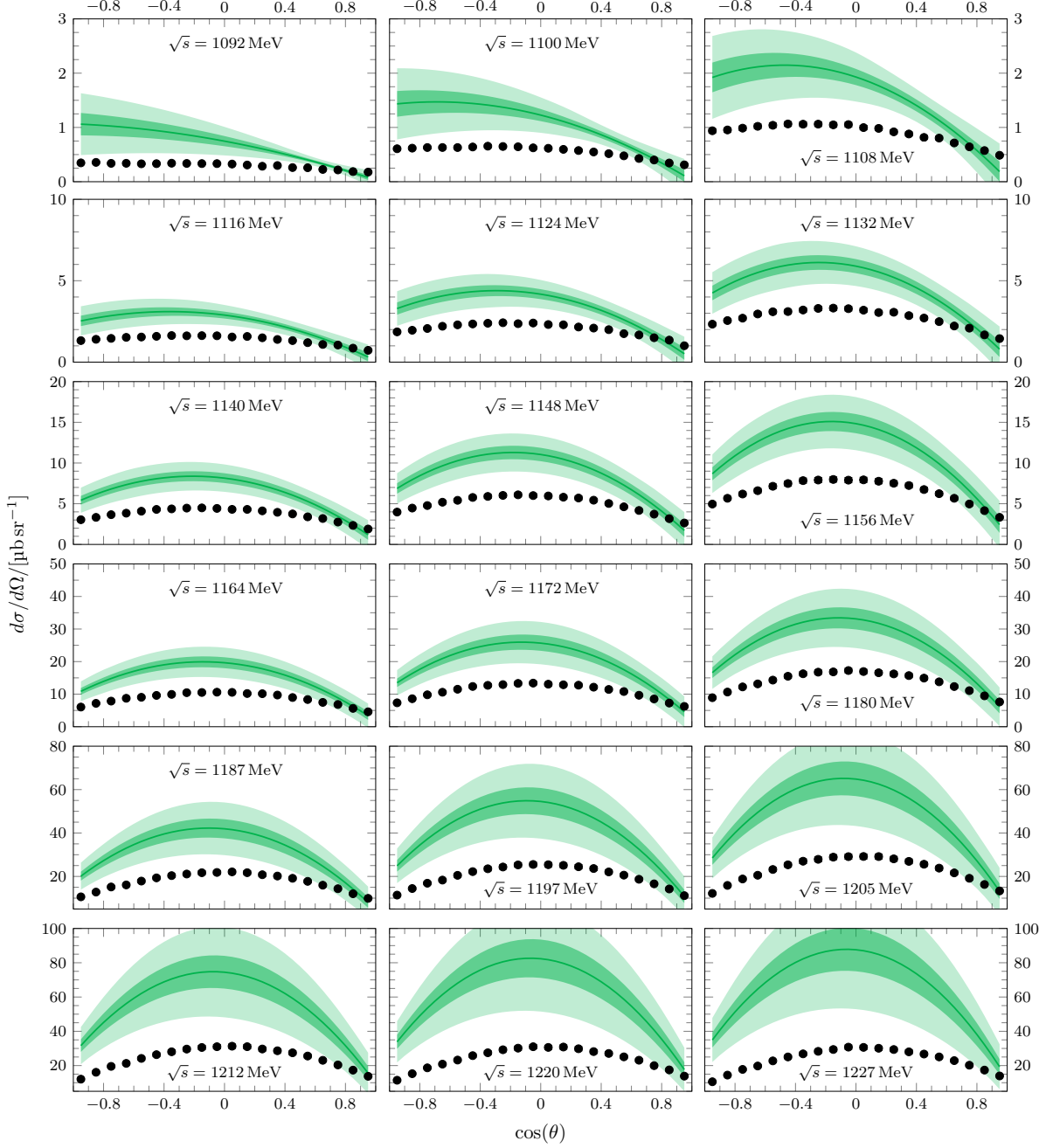


**Figure 5.21:** Strict HB order- $q^3 + \epsilon^2$  result of the unpolarised differential cross section in the channel  $\gamma + p \rightarrow \pi^0 + p$ . The solid lines denote the  $q^3 + \epsilon^2$  results, the darker (lighter) shaded bands show the estimated truncation errors at order  $q^3 + \epsilon^2$  with 68 % (95 %) confidence. The data are from refs. [78, 108], error bars correspond to the combined statistical and systematical error.

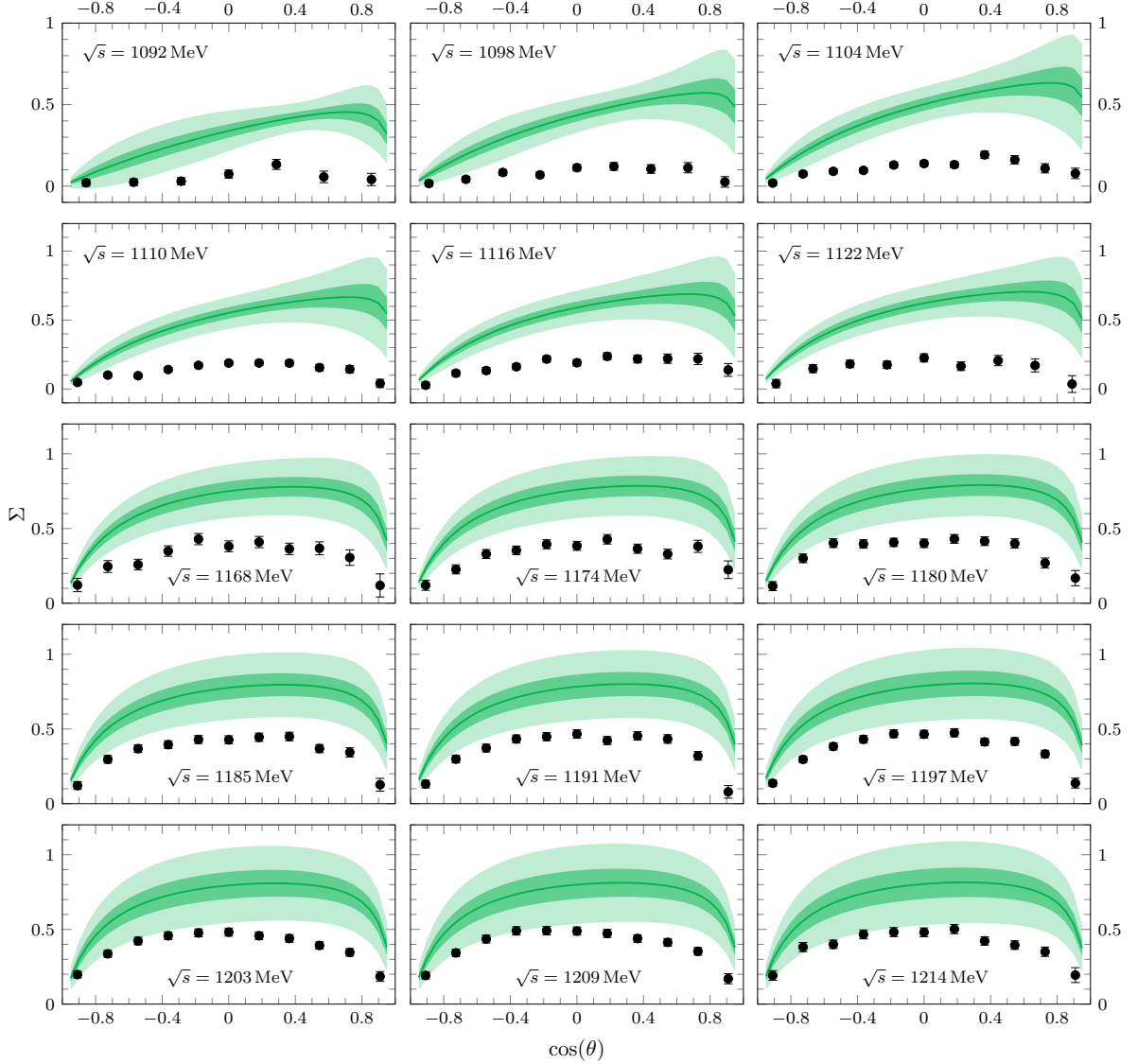


**Figure 5.22:** Strict HB order- $q^3 + \epsilon^2$  result of the linear polarised photon asymmetry in the channel  $\gamma + p \rightarrow \pi^0 + p$ . The solid lines denote the  $q^3 + \epsilon^2$  results, the darker (lighter) shaded bands show the estimated truncation errors at order  $q^3 + \epsilon^2$  with 68 % (95 %) confidence. The data are from refs. [78, 108], error bars correspond to the combined statistical and systematical error.

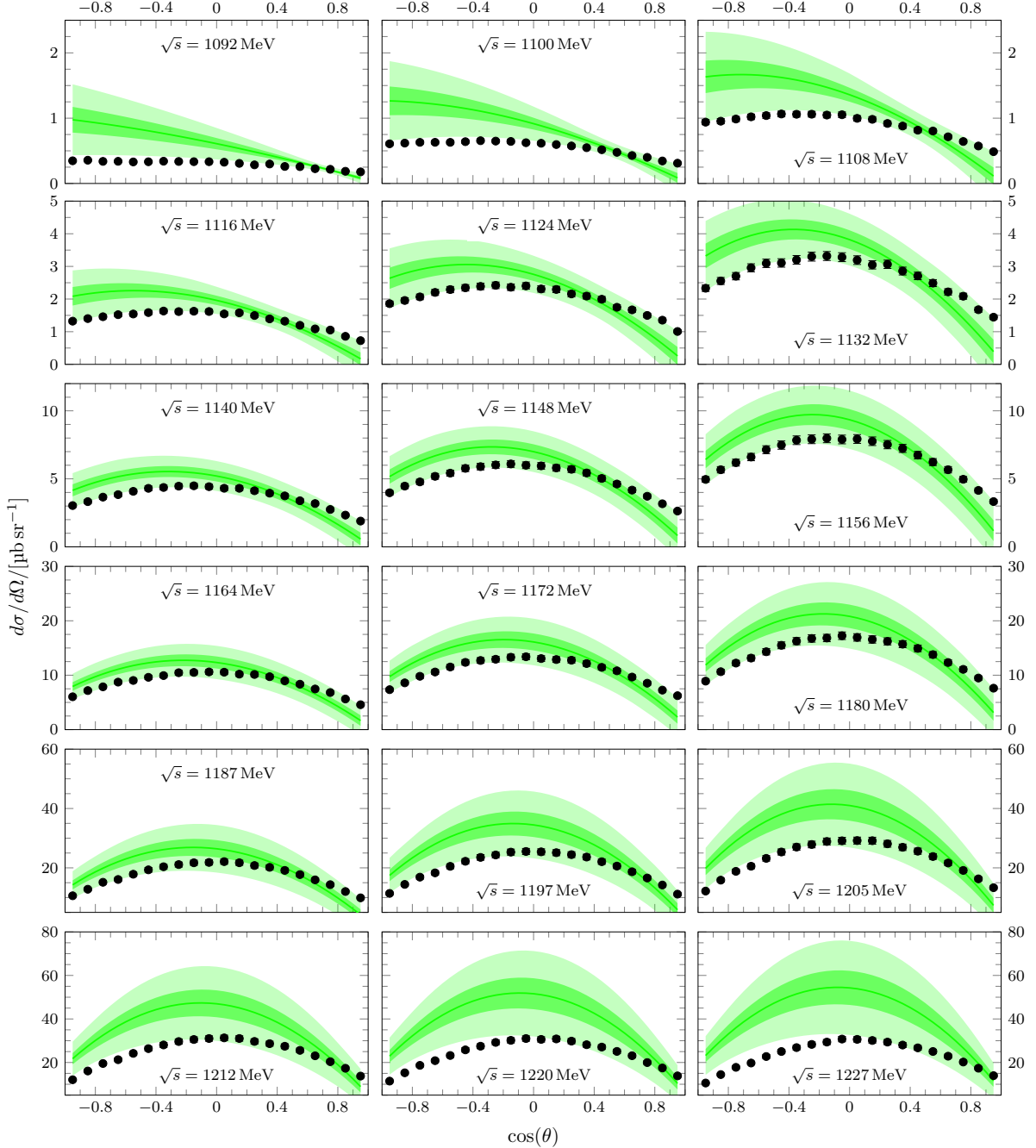


**Figure 5.23:** Mixed HB order- $q^3 + \epsilon^2$  result of the unpolarised differential cross section in the channel  $\gamma + p \rightarrow \pi^0 + p$ . The solid lines denote the  $q^3 + \epsilon^2$  results, the darker (lighter) shaded bands show the estimated truncation errors at order  $q^3 + \epsilon^2$  with 68 % (95 %) confidence. The data are from refs. [78, 108], error bars correspond to the combined statistical and systematical error.

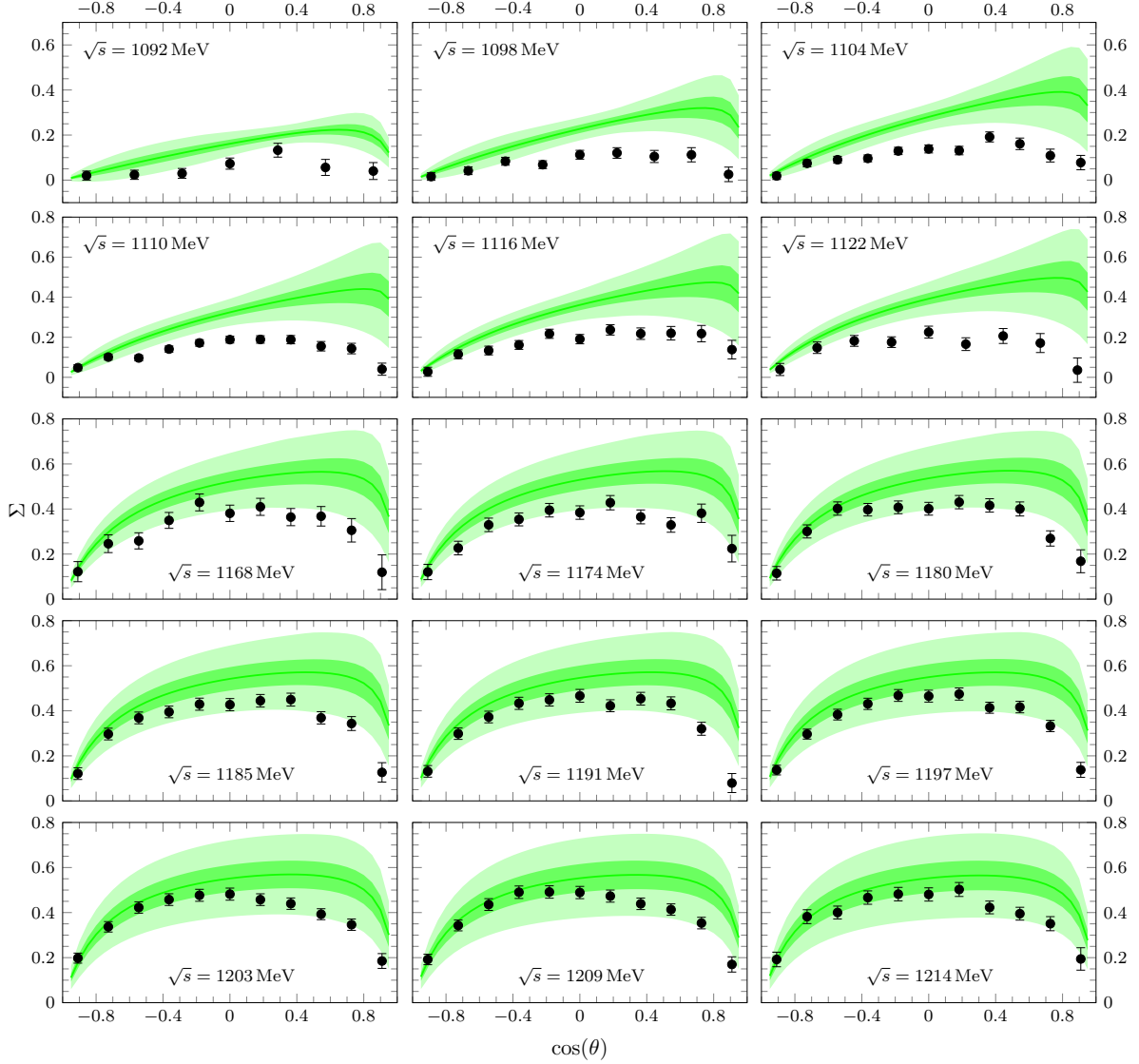


**Figure 5.24:** Mixed HB order- $q^3 + \epsilon^2$  result of the linear polarised photon asymmetry in the channel  $\gamma + p \rightarrow \pi^0 + p$ . The solid lines denote the  $q^3 + \epsilon^2$  results, the darker (lighter) shaded bands show the estimated truncation errors at order  $q^3 + \epsilon^2$  with 68 % (95 %) confidence. The data are from refs. [78, 108], error bars correspond to the combined statistical and systematical error.

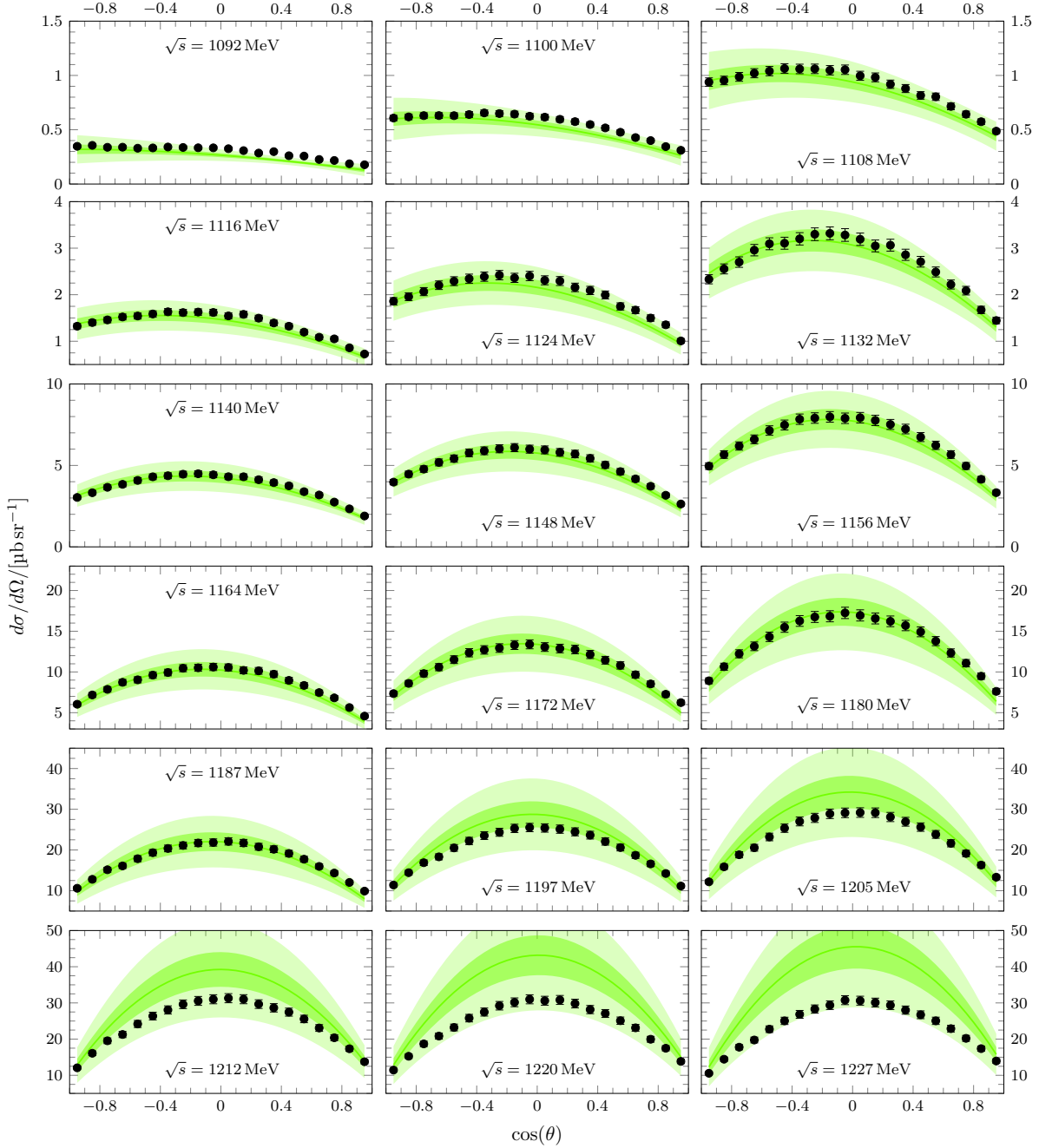


**Figure 5.25:** Covariant order- $q^3 + \epsilon^2$  result of the unpolarised differential cross section in the channel  $\gamma + p \rightarrow \pi^0 + p$ . The solid lines denote the  $q^3 + \epsilon^2$  results, the darker (lighter) shaded bands show the estimated truncation errors at order  $q^3 + \epsilon^2$  with 68 % (95 %) confidence. The data are from refs. [78, 108], error bars correspond to the combined statistical and systematical error.

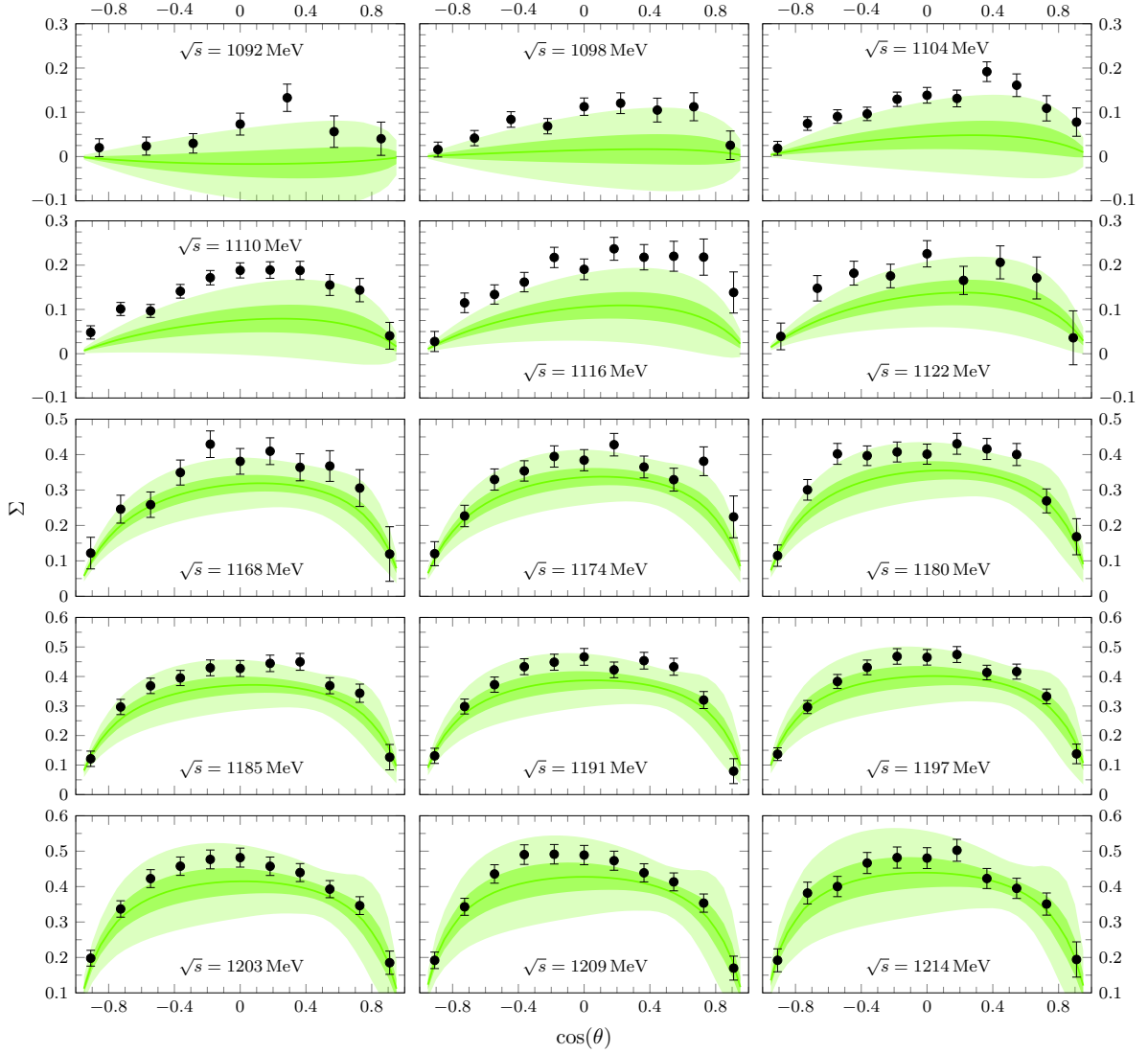


**Figure 5.26:** Covariant order- $q^3 + e^2$  result of the linear polarised photon asymmetry in the channel  $\gamma + p \rightarrow \pi^0 + p$ . The solid lines denote the  $q^3 + e^2$  results, the darker (lighter) shaded bands show the estimated truncation errors at order  $q^3 + e^2$  with 68 % (95 %) confidence. The data are from refs. [78, 108], error bars correspond to the combined statistical and systematical error.



## 6 Summary and outlook

In this work, we studied pion photoproduction in chiral effective field theory with explicit delta degrees of freedom. Starting from the deltaless approach, we considered the reaction up to the leading loop order in the heavy baryon and in the manifestly covariant scheme. In particular, we analysed the difference between the obtained HB and covariant results of low-energy constants in terms of the infrared regular shifts. Next, we extended our calculations to the leading delta contributions employing the complex-mass approach using a fitted delta mass and analysed the importance of subsequent  $1/m_N$  terms from the  $\epsilon^2$  diagrams in the heavy baryon scheme. Furthermore, we studied the effects of resonance saturation to the LECs. Moreover, we gave results of pion photoproduction up to the order  $\epsilon^3$  in the small-scale-expansion scheme, where the leading deltaful loop order is taken into account. The results for the LECs  $\bar{d}_8, \bar{d}_9, \bar{d}_{20}, \bar{d}_{21;22}, \bar{b}_1$  and  $\bar{h}_1$  were obtained by fits to the MAID partial-wave analysis using a Bayesian approach to theoretical uncertainties. Furthermore, we compared our results to cross sections and polarisation asymmetries of the neutral pion production channel.

The main conclusions of our analysis of pion photoproduction can be summarised as follows:

- In the deltaless approach, the description of pion photoproduction is satisfying only in a very limited energy range above threshold and fails approaching the delta region. Especially for the magnetic multipole  $M_{1+}^{3/2}$ , the description agrees with the data only up to approximately  $\sqrt{s} = 1150$  MeV. Studying the reaction in the covariant framework yields a better agreement with the data than the heavy baryon approach. The difference between the numerical values of the LECs obtained in the covariant and heavy baryon formulation of ChPT can be explained to a large extent by the infrared regular shifts.
- Incorporating the leading delta tree contributions significantly extends the energy range in which a good agreement with the  $s$ - and  $p$ -wave multipoles can be achieved. We found that the leading  $\gamma N \Delta$  coupling constant  $b_1$  is stable with respect to variation of the energy range, assigned relative error to the data and combination of  $I = 3/2$  and  $I = 1/2$  fit. The difference between the numerical values of the LECs obtained in a deltaless and deltaful approach can be explained in terms of resonance saturation to a large extent. In particular, the results from the covariant order- $q^3 + \epsilon^2$  calculation reproduce the high-precision data of cross sections and polarisation asymmetries from refs. [78, 108] remarkably well.
- The next-to-leading order delta correction give rise to surprisingly large corrections to the scattering amplitude. However, these corrections are important to achieve a reasonable description of  $E_{1+}^{3/2}$ . At the same time, the description of the  $I = 1/2$  channel worsened

significantly. The overall reproduction of the  $s$ - and  $p$ -wave multipoles is worse than in the  $q^3 + \epsilon^2$  approach, moreover we found that the LECs  $\bar{d}_{20}$  and  $\bar{d}_{21;22}$  do not fulfil the naturalness assumption in this scheme. However, the given estimate of the leading and subleading  $\gamma N\Delta$  coupling constants  $b_1$  and  $h_1$  can be taken as reliable, because the isospin-3/2 channel is very well described. Also, the values agree with our findings from ref. [47].

Based on the conclusions of our analysis of pion photoproduction, we find that it would be very interesting to extend the analysis in the following points:

- In this study, we have focused on calculating the  $s$ - and  $p$ -wave multipoles, because they give by far the largest contributions to cross sections. However, in refs. [171, 172], the importance of  $d$ -waves to observables was pointed out. Therefore, it would be worthwhile to extend the analysis to higher partial waves or to the analysis of observables directly.
- Further insight could be gained from a combined covariant  $q^4 + \epsilon^3$  analysis. A deltaless  $q^4$  calculation was already provided by Hilt et al. [95], but the improvement in the description was only moderate, especially in the delta region. Because our analysis revealed significant improvement in the description of  $I = 3/2$  multipole amplitudes in the delta region, but a insufficient reproduction of the  $I = 1/2$  channels and in parts unnatural LECs, the effects of the  $q^4$  terms in combination with the order- $\epsilon^3$  terms would be most interesting to study. In particular, additional 11 LECs must be determined in such a framework.
- Moreover, extending the calculations to include the Roper resonance [173] would certainly be of interest to see how the applicability of the theory could be extended further into the delta region.

# A Relating different sets of amplitudes

The relation between the coefficients  $A_i$  and  $B_i$  of eq. (3.14) and eq. (3.18) can be found by equating the two representations:

$$\sum_{i=1}^8 B_i V_i^\mu = \sum_{i=1}^4 A_i M_i^\mu. \quad (\text{A.1})$$

Remembering that  $V_4$  and  $V_8$  are not needed for real photons ( $\epsilon \cdot k = 0, k^2 = 0$ ) and using the two relations obtained by current conservation of the matrix element (3.16), the coefficients  $A_i$  can be obtained from  $B_i$  as follows:

$$A_1 = i(B_5 + m_N B_6), \quad A_2 = i \frac{B_3}{k \cdot p + k \cdot p'}, \quad A_3 = i B_7, \quad A_4 = \frac{i}{2} B_6. \quad (\text{A.2})$$

To obtain the relations between the minimal basis (3.18) and the CGLN amplitudes (3.20), we proceed in a similar way. As a first step, we need to rewrite the Dirac spinors  $u(p)$  in terms of Pauli spinors  $\chi$  and Pauli matrices  $\sigma_i$

$$u(p) = \mathcal{N} \begin{pmatrix} \chi \\ \frac{\boldsymbol{\sigma} \cdot \mathbf{p}}{E_p + m_N} \chi \end{pmatrix}, \quad \mathcal{N} = \sqrt{E_p + m_N}. \quad (\text{A.3})$$

and choose the corresponding Dirac representation of the Gamma matrices

$$\gamma^0 = \begin{pmatrix} \mathbb{1}_{2 \times 2} & \mathbb{0}_{2 \times 2} \\ \mathbb{0}_{2 \times 2} & -\mathbb{1}_{2 \times 2} \end{pmatrix}, \quad \gamma^i = \begin{pmatrix} \mathbb{0}_{2 \times 2} & \sigma^i \\ -\sigma^i & \mathbb{0}_{2 \times 2} \end{pmatrix}, \quad \gamma^5 = \begin{pmatrix} \mathbb{0}_{2 \times 2} & \mathbb{1}_{2 \times 2} \\ \mathbb{1}_{2 \times 2} & \mathbb{0}_{2 \times 2} \end{pmatrix}. \quad (\text{A.4})$$

Here,  $E_p = p^0 = \sqrt{m_N^2 + \mathbf{p}^2}$  is the energy of the incoming nucleon (and similarly  $E_{p'}$  is the energy of the outgoing nucleon).

Note that the spinors  $u(p)$  are not normalised to 1 in our convention:  $\bar{u}(p)u(p) = 2m_N$ . With this, we can relate the basis structures  $M_i^\mu$  to the ones of eq. (3.20) and finally obtain the relation between the invariant amplitudes  $A_i$  and the CGLN amplitudes  $\mathcal{F}_i$ :

$$\begin{aligned} \mathcal{F}_1 &= -\frac{W - m_N}{8\pi W} \sqrt{(E_p + m_N)(E_{p'} + m_N)} \left[ A_1 + (W - m_N)A_4 - \frac{2\nu}{W - m_N}(A_3 - A_4) \right], \\ \mathcal{F}_2 &= -\frac{W + m_N}{8\pi W} |\mathbf{q}| \sqrt{\frac{E_p - m_N}{E_{p'} + m_N}} \left[ -A_1 + (W + m_N)A_4 - \frac{2\nu}{W + m_N}(A_3 - A_4) \right], \end{aligned}$$

$$\begin{aligned}\mathcal{F}_3 &= -\frac{W + m_N}{8\pi W} |\mathbf{q}| \sqrt{(E_p - m_N)(E_{p'} + m_N)} \left[ \frac{W^2 - m_N^2}{W + m_N} A_2 + A_3 - A_4 \right], \\ \mathcal{F}_4 &= -\frac{W - m_N}{8\pi W} |\mathbf{q}|^2 \sqrt{\frac{E_p + m_N}{E_{p'} + m_N}} \left[ -\frac{W^2 - m_N^2}{W - m_N} A_2 + A_3 - A_4 \right],\end{aligned}\tag{A.5}$$

where we have used  $\nu = -\frac{1}{2}k \cdot q$  and  $W = \sqrt{s}$  is the CM energy.

## B Feynman diagrams

In this section, we give all Feynman diagrams which are necessary to describe pion photoproduction up to order  $\epsilon^3$  at the maximum. In the following, leading order (LO) contributions are referred to as the first order in the chiral series, which contain nonzero Feynman diagrams. In explicit, the leading order is order  $q^1$  in the deltaless case and order  $\epsilon^2$  in the deltaful case, where  $q$  and  $\epsilon$  are the expansion parameters in deltaless and deltaful formalism, respectively. Consequently, next-to-leading (NLO) contributions refer to the subsequent nonvanishing order in the chiral series, which are  $q^2$  in the deltaless and  $\epsilon^3$  in the deltaful case. The analogous statement holds for next-to-next-to-leading ( $N^2LO$ ) order, which is  $q^3$  in the deltaless theory. In fig. B.1 the four LO tree diagrams are shown, where all vertices are of lowest order, thus

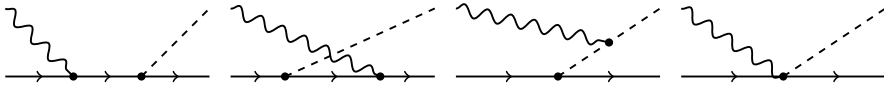


**Figure B.1:** Leading-order tree diagrams: all vertices are of lowest order, i.e. of first order if involving nucleons, of second order if purely bosonic. Wiggly lines correspond to photons, dashed lines to pions and solid lines correspond to nucleons.

either from  $\mathcal{L}_{\pi N}^{(1)}$  or from  $\mathcal{L}_{\pi\pi}^{(2)}$ . Note that we refrain from printing the hat for the HB case in the following discussion. The same diagrams contribute in the HB as in the covariant case, however, a lot of diagrams will be zero and start to arise from higher orders due to the explicit  $1/m_N$  expansion.

NLO tree diagrams can be obtained by replacing a single vertex in the LO diagrams by the corresponding expression of the next order. Here, all vertices except the  $\gamma NN$  vertex of second order are zero, so two diagrams remain, which are depicted in fig. B.2.

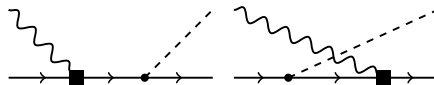


**Figure B.2:** Next-to-leading order tree diagrams: filled squares are of second order.

At  $N^2LO$ , there are 10 nonvanishing diagrams (fig. B.3). They are obtained by replacing a vertex from all possible second order diagrams (also those who vanish at second order) by the corresponding vertex of third order. Diagrams having two vertices of second order are also possible at third order, but they vanish, because the  $\pi NN$  vertex from  $\mathcal{L}_{\pi N}^{(2)}$  is zero.

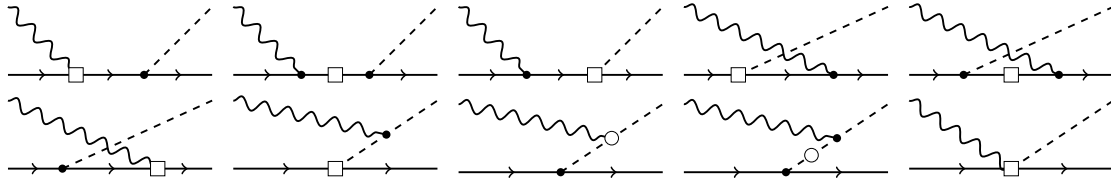


**Figure B.3:**  $N^2LO$  tree diagrams: empty squares are of third order, empty circles are purely bosonic and of fourth order.

Starting from the third order, loop diagrams contribute to the amplitude. We construct them by adding pion loops to the topologies in the following way: specifically in fig. B.4, we show all possible loop diagrams which can be constructed from the first diagram in fig. B.1 by adding a pion loop to the nucleon line, wherever possible. This gives 13 nonzero contributions. In the same way, fig. B.5 shows all loop diagrams which are constructed by adding a pion loop

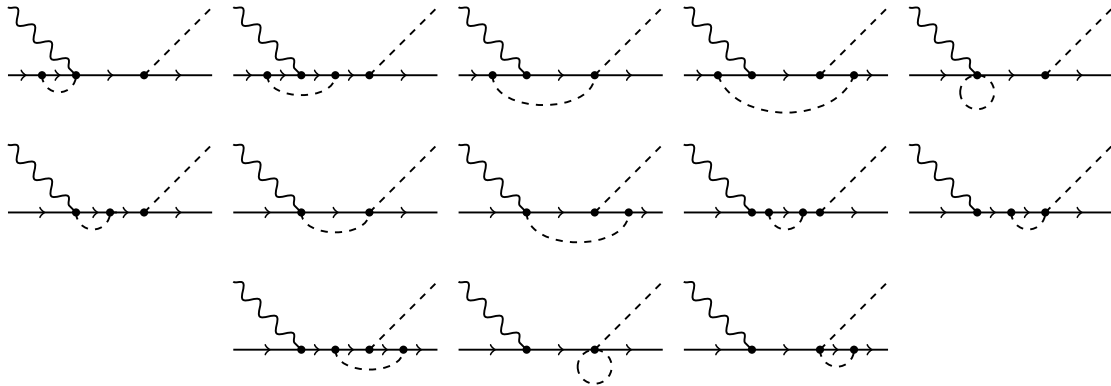


**Figure B.4:** First set of loop diagrams.

to the nucleon line in the second tree diagram in fig. B.1. From symmetry it is clear that this gives 13 diagrams as well. The third set of loop topologies is shown in fig. B.6, constructed from the third diagram in figure B.1 by adding a loop to the nucleon line. We choose to also include the two contributions obtained from adding a pion loop to the outgoing pion line. This yields additional six diagrams. Finally, we obtain another four diagrams (fig. B.7) from the fourth diagram in fig. B.1. The diagrams in fig. B.8 cannot be constructed in a simple way from a LO tree diagram. They share the feature that the photon is absorbed in a pion loop, which is either attached to the nucleon line or to the outgoing pion line. In total, there are 45 loop diagrams at third order in the deltaless case.

When including the delta as an explicit degree of freedom, we have to take into account more topologies. The LO tree delta diagrams are of second order (fig. B.9), which all contain a second-order  $\gamma N \Delta$  vertex. All deltaful tree diagrams of first order vanish.

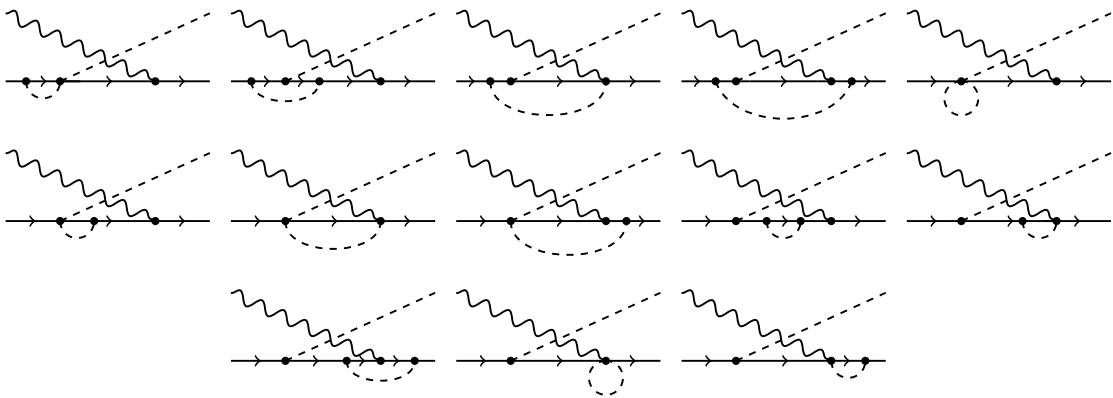


**Figure B.5:** Second set of loop diagrams.

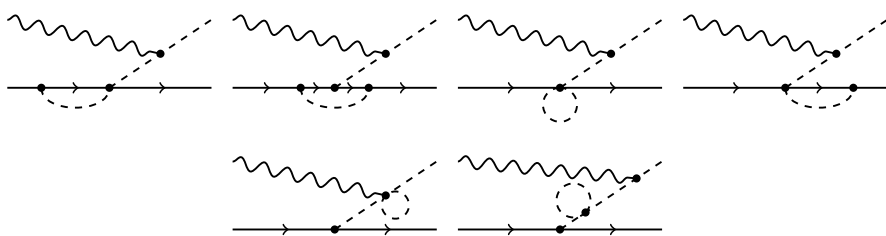


**Figure B.6:** Third set of loop diagrams.

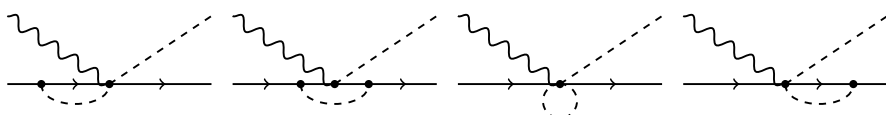


**Figure B.7:** Fourth set of loop diagrams.

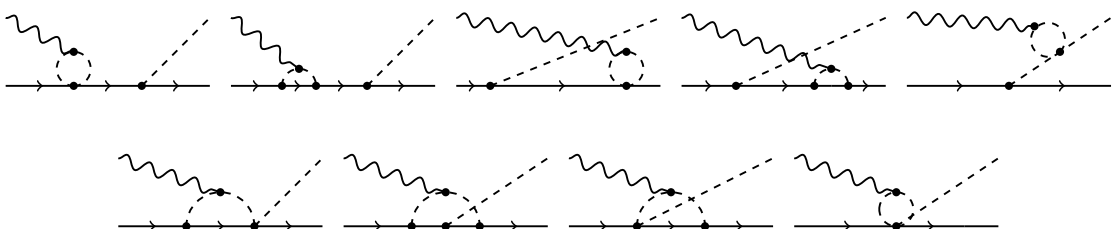


**Figure B.8:** Fifth set of loop diagrams.

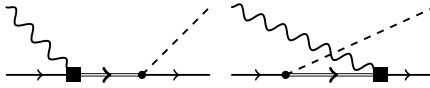


**Figure B.9:** Leading order deltaful tree diagrams: filled squares are of second order.

At NLO, there are another two diagrams (fig. B.10), which both contain a third-order  $\gamma N\Delta$  vertex. We do not show the diagrams which have two vertices from  $\mathcal{L}_{\pi N\Delta}^{(2)}$ , because they are effectively of higher order since they contain the two LECs  $b_3$  and  $b_6$  (as explained in sec. 3.5.1), which we set to zero. From NLO, we have to take deltaful loop diagrams into

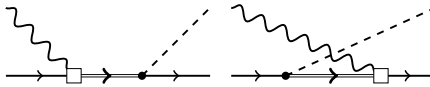


**Figure B.10:** Leading order deltaful tree diagrams: empty squares are of third order.

account. Fig. B.11 shows all nonvanishing topologies which are constructed from the first group of deltaless diagrams (fig. B.4) by replacing an internal nucleon line by a delta line. This yields 19 contributions.

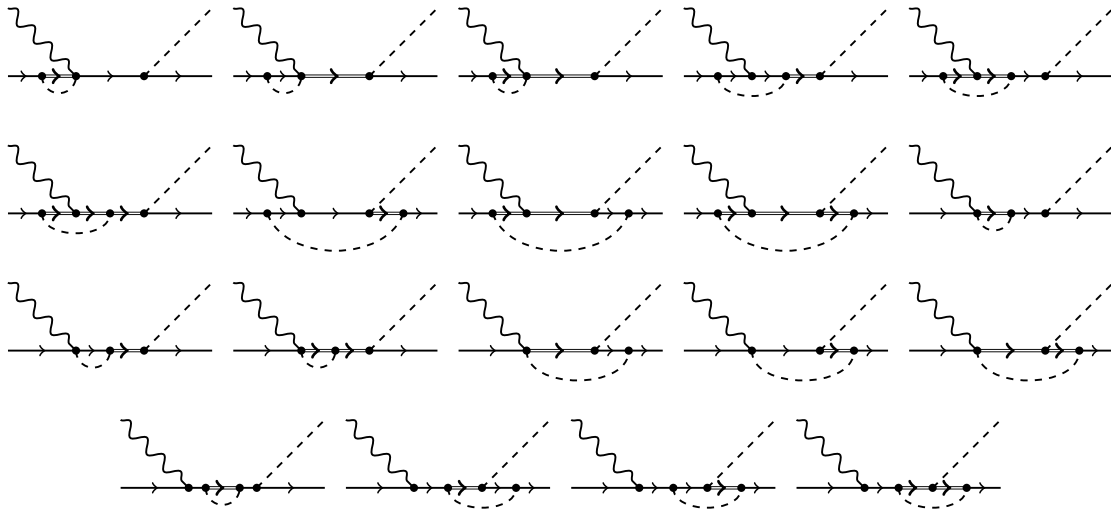


**Figure B.11:** First set of deltaful loop diagrams.

Similarly, fig. B.12 shows the diagrams obtained by replacing an internal nucleon by a delta line in the second group (fig. B.5), again giving 19 diagrams. In fig. B.13, the three deltaful diagrams constructed from the third deltaless group (fig. B.6) are shown. Fig. B.14 depicts the three contributions obtained by modifying group 4 in fig. B.7. Finally, fig. B.15 shows the remaining diagrams obtained from those in fig. B.8. In total, there are 53 deltaful loop diagrams which contribute to pion photoproduction at third order.

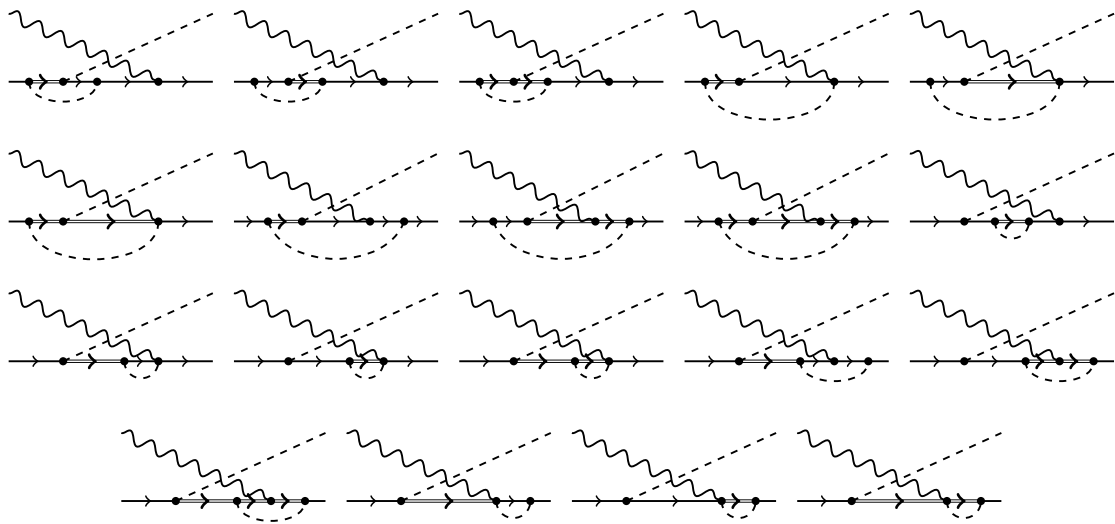


**Figure B.12:** Second set of deltaful loop diagrams.

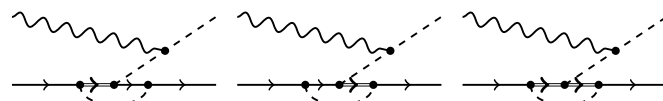


**Figure B.13:** Third set of deltaful loop diagrams.



**Figure B.14:** Fourth set of deltaful loop diagrams.

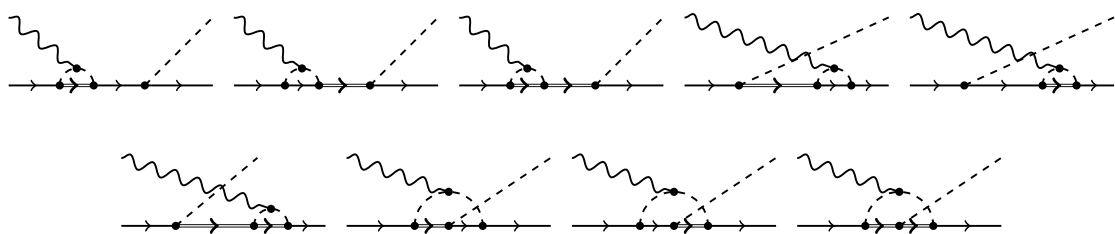


**Figure B.15:** Fifth set of deltaful loop diagrams.



# C Renormalisation of the amplitude

In this chapter, we give all necessary renormalisation rules for the subprocesses of pion photo-production. We denote the loop integrals as

$$\begin{aligned} A_0(m^2) &= \frac{1}{i} \int \frac{d^d l}{(2\pi)^d} \frac{\mu^{4-d}}{l^2 - m^2}, \\ B_0(p^2, m_0^2, m_1^2) &= \frac{1}{i} \int \frac{d^d l}{(2\pi)^d} \frac{\mu^{4-d}}{(l^2 - m_0^2)((l+p)^2 - m_1^2)}, \\ J_0(\omega) &= \frac{1}{i} \int \frac{d^d l}{(2\pi)^d} \frac{\mu^{4-d}}{(l^2 - M_\pi^2)(v \cdot l + \omega)}, \\ C_0(p^2, (p-q)^2, q^2, m_0^2, m_1^2, m_2^2) &= \frac{1}{i} \int \frac{d^d l}{(2\pi)^d} \frac{\mu^{4-d}}{(l^2 - m_0^2)((l+p)^2 - m_1^2)((l+q)^2 - m_2^2)}, \end{aligned} \quad (\text{C.1})$$

where we omit the  $+ i\epsilon$  prescription. Note that we give the renormalisation of the constants in  $d = 4$  dimensions for brevity, although it was calculated for general  $d$ . The transition to  $d = 4$  dimensions has to be taken carefully to ensure that constant terms like

$$\frac{d}{d-4} = \frac{4}{d-4} + 1$$

will not be forgotten. We accomplished this by setting  $d$  to 4 and adding the zeroth order of the expansion in  $d$  where we substituted the integrals by their divergent part. The notation of the counterterms is as follows: the superscript refers to the chiral order of the subprocess, at which the given counterterm was fixed. For example, the first correction to the  $Z$ -factor of the pion field emerges from  $\mathcal{O}(q^4)$  and consequently is denoted as  $\delta Z_\pi^{(4)}$ .

## C.1 Renormalisation of the mesonic sector

The renormalisation rules for the pion mass, field redefinition and decay constant are given below. We remind that the parameter  $\alpha$  is the unphysical constant from the general pion field parametrisation (eq. (3.71)).

$$\begin{aligned} M^2 &= M_\pi^2 + \delta M^{(4)}, \\ \delta M^{(4)} &= \frac{M_\pi^2}{2F_\pi^2} (A_0(M_\pi^2) - 4M_\pi^2 l_3), \\ Z_\pi &= 1 + \delta Z_\pi^{(4)}, \end{aligned}$$

$$\begin{aligned}\delta Z_\pi^{(4)} &= \frac{1}{F_\pi^2} (A_0(M_\pi^2)(1 - 10\alpha) - 2M_\pi^2 l_4), \\ F &= F_\pi + \delta F_\pi^{(4)}, \\ \delta F_\pi^{(4)} &= -\frac{1}{F_\pi} (A_0(M_\pi^2) + M_\pi^2 l_4).\end{aligned}$$

## C.2 Heavy baryon renormalisation rules

### Nucleon mass and field renormalisation

The HB expressions for the redefinition of the nucleon mass and field read

$$\begin{aligned}m &= m_N + \delta m^{(2)} + \delta m^{(3)}, \\ \delta m^{(2)} &= 4c_1 M_\pi^2, \\ \delta m^{(3)} &= -\frac{3g_A^2 M_\pi^2}{4F_\pi^2} J_0(0), \\ Z_N &= 1 + \delta Z_N^{(3)}, \\ \delta Z_N^{(3)} &= -\frac{3g_A^2 M_\pi^2}{32\pi^2 F_\pi^2} + \frac{9g_A^2}{4F_\pi^2} A_0(M_\pi^2).\end{aligned}$$

### Axial pion-nucleon coupling

The renormalisation rules for the axial pion-nucleon coupling constant  $g_A$  in the HB sector are given below. Note that we already employed the Goldberger-Treiman shift to fully remove the for pion photoproduction redundant constant  $d_{18}$  from the rules. Here,  $\mathring{g}_A$  is the bare,  $g_A$  is the physical constant.

$$\begin{aligned}\mathring{g}_A &= g_A + \delta g^{(3)}, \\ \delta g^{(3)} &= \left( -4d_{16} + 2d_{18} + \frac{g_A^3}{16\pi^2 F_\pi^2} \right) M_\pi^2 - \frac{(g_A + 2g_A^3)}{F_\pi^2} A_0(M_\pi^2).\end{aligned}$$

### Electromagnetic form factor of the nucleon

The replacement rules for the counterterms of the constants  $c_6$  and  $c_7$  are given below, where we denote the renormalised quantities by the bar.

$$\begin{aligned}c_6 &= \bar{c}_6 + \delta c_6^{(3)}, \\ \delta c_6^{(3)} &= -\frac{2m_N g_A^2}{F_\pi^2} J_0(0), \\ c_7 &= \bar{c}_7 + \delta c_7^{(3)}, \\ \delta c_7^{(3)} &= \frac{m_N g_A^2}{F_\pi^2} J_0(0).\end{aligned}$$

## C.3 Covariant renormalisation rules

### Nucleon mass and field renormalisation

In the following, we introduce the dimensionless parameters  $\alpha = \frac{M_\pi}{m_N}$  and  $\beta = \frac{m_\Delta}{m_N}$ . The ratio of the masses  $\alpha$  is not to be confused with the unphysical off-shell parameter  $\alpha$ . The renormalisation rules for the nucleon mass and field redefinition are given below. For convenience, we give the contributions arising from the delta resonance separately. This means that all corrections  $\delta x^{(i,\Delta)}$  are set to zero in the deltaless case.

$$\begin{aligned}
 m &= m_N + \delta m_N^{(2)} + \delta m_N^{(3)} + \delta m_N^{(3,\Delta)}, \\
 \delta m_N^{(2)} &= 4M_\pi^2 c_1, \\
 \delta m_N^{(3)} &= -\frac{3g_A^2 m_N}{2F_\pi^2} (A_0(m_N^2) + M_\pi^2 B_0(m_N^2, M_\pi^2, m_N^2)), \\
 \delta m_N^{(3,\Delta)} &= -\frac{h_A^2 m_N^3}{576 \pi^2 F_\pi^2 \beta^2} [\alpha^4(16\beta + 13) - 4\alpha^2(3\beta + 2) + 3\beta^4 - 12\beta^3 - 4\beta^2 + 4\beta + 2] \\
 &\quad + \frac{m_N h_A^2}{6F_\pi^2 \beta^2} \left[ (\alpha^4 - \alpha^2(2\beta^2 - 6\beta - 5) + (\beta - 1)(\beta + 1)^3) A_0(M_\pi^2) \right. \\
 &\quad \left. - (\alpha^4 - 2\alpha^2(\beta^2 + \beta + 1) + \beta^4 + 2\beta^3 - \beta^2 + 2\beta + 1) A_0(m_\Delta^2) \right. \\
 &\quad \left. - (\alpha^2 - (\beta - 1)^2)(\alpha^2 - (\beta + 1)^2)^2 m_N^2 B_0(m_N^2, M_\pi^2, m_\Delta^2) \right], \\
 Z_N &= 1 + \delta Z_N^{(3)} + \delta Z_N^{(3,\Delta)}, \\
 \delta Z_N^{(3)} &= \frac{3g_A^2}{4F_\pi^2(\alpha^2 - 4)} \left[ \frac{M_\pi^2}{4\pi^2} + (5\alpha^2 - 12) A_0(M_\pi^2) - 4\alpha^2 A_0(m_N^2) \right. \\
 &\quad \left. - 4M_\pi^2(\alpha^2 - 3) B_0(m_N^2, M_\pi^2, m_N^2) \right], \\
 \delta Z_N^{(3,\Delta)} &= \frac{h_A^2}{6F_\pi^2 \beta^2} \left[ (3\alpha^4 - \alpha^2(6\beta^2 + 4\beta + 9) + (\beta + 1)^2(3\beta^2 - 2\beta + 5)) A_0(M_\pi^2) \right. \\
 &\quad \left. - (3\alpha^4 + \alpha^2(-6\beta^2 - 4\beta + 2) + 3\beta^4 + 4\beta^3 + \beta^2 - 8\beta - 5) A_0(m_\Delta^2) \right. \\
 &\quad \left. - (3\alpha^6 - \alpha^4(9\beta^2 + 4\beta + 1) - \alpha^2(-9\beta^4 - 8\beta^3 - 2\beta^2 + 4\beta + 7) \right. \\
 &\quad \left. - (\beta + 1)^3(3\beta^3 - 5\beta^2 + 7\beta - 5)) m_N^2 B_0(m_N^2, M_\pi^2, m_\Delta^2) \right].
 \end{aligned}$$

### Axial pion-nucleon coupling

The renormalisation rules for the axial pion-nucleon coupling constant  $g_A$  are given below. Note that we use the auxiliary variables  $a_i, b_i, c_i$  only in this particular context for reasons of clarity and comprehensibility.

$$\mathring{g}_A = g_A + \delta g^{(3)} + \delta g^{(3,\Delta)},$$

$$\begin{aligned}
\delta g^{(3)} = & -2(2d_{16} - d_{18})M_\pi^2 - \frac{3g_A^3 M_\pi^2}{16\pi^2 F_\pi^2(\alpha^2 - 4)} \\
& - \frac{g_A}{F_\pi^2(\alpha^2 - 4)} \left[ (\alpha^2 - 4 + 2g_A^2(2\alpha^2 - 5))A_0(M_\pi^2) \right. \\
& + (8 - (2 + 3g_A^2)\alpha^2)A_0(m_N^2) + g_A^2 m_N^2(\alpha^2 - 4)B_0(M_\pi^2, m_N^2, m_N^2) \\
& + (8 - 2\alpha^2 - 3g_A^2(\alpha^2 - 3))M_\pi^2 B_0(m_N^2, M_\pi^2, m_N^2) \\
& \left. + g_A^2 M_\pi^2 m_N^2(\alpha^2 - 4)C_0(m_N^2, M_\pi^2, m_N^2, M_\pi^2, m_N^2, m_N^2) \right], \\
\delta g^{(3,\Delta)} = & a_0 + a_1 A_0(M_\pi^2) + a_2 A_0(m_N^2) + a_3 A_0(m_\Delta^2) + b_1 B_0(M_\pi^2, m_N^2, m_\Delta^2) \\
& + b_2 B_0(M_\pi^2, m_\Delta^2, m_\Delta^2) + b_3 B_0(m_N^2, M_\pi^2, m_N^2) + b_4 B_0(m_N^2, M_\pi^2, m_\Delta^2) \\
& + c_1 C_0(m_N^2, M_\pi^2, m_N^2, M_\pi^2, m_N^2, m_\Delta^2) + c_2 C_0(m_N^2, M_\pi^2, m_N^2, M_\pi^2, m_\Delta^2, m_\Delta^2), \\
a_0 = & -\frac{g_A h_A^2 m_N^2}{5184 \pi^2 F_\pi^2 \beta^2} \left[ \alpha^4 (24\beta + 325) - 4\alpha^2 (3\beta^4 - 6\beta^3 - 8\beta^2 + 140\beta + 45) \right. \\
& + 12\alpha^6 - 69\beta^4 - 384\beta^3 + 100\beta^2 + 248\beta + 158 \left. \right] \\
& - \frac{5g_1 h_A^2 m_N^2}{31104 \pi^2 F_\pi^2 \beta^4} \left[ 3\alpha^{10} - \alpha^8 (3\beta^2 + 5\beta + 9) - \alpha^6 (3\beta^4 - 10\beta^2 - 30\beta + 60) \right. \\
& + \alpha^4 (3\beta^6 + 5\beta^5 - 3\beta^4 - 20\beta^3 - 114\beta^2 - 248\beta - 34) \\
& - 2\alpha^2 (7\beta^6 + 59\beta^5 - 129\beta^4 - 59\beta^3 - 76\beta^2 - 68\beta - 2) \\
& \left. - 2\beta (17\beta^5 - 82\beta^4 + 18\beta^3 + 28\beta^2 + 42\beta + 20) \right], \\
a_1 = & -\frac{g_A h_A^2}{54 F_\pi^2 \beta^2} \left[ 4\alpha^6 + \alpha^4 (-8\beta^2 - 8\beta + 31) + \alpha^2 (4\beta^4 + 8\beta^3 - 46\beta^2 - 69) \right. \\
& + 23\beta^4 + 4\beta^3 + 12\beta^2 + 56\beta + 25 \left. \right] \\
& + \frac{5g_1 h_A^2}{972 F_\pi^2 \beta^4} \left[ 3\alpha^{10} - \alpha^8 (9\beta^2 + 5\beta + 10) \right. \\
& + \alpha^6 (9\beta^4 + 10\beta^3 + 23\beta^2 + 17\beta + 6) \\
& - \alpha^4 (3\beta^6 + 5\beta^5 + 27\beta^4 + 36\beta^3 + 55\beta^2 + 33\beta - 35) \\
& + 2\alpha^2 (7\beta^6 + 17\beta^5 + 17\beta^4 - 14\beta^3 + 44\beta^2 + 71\beta + 21) \\
& \left. - 2(\beta + 1)^2 (7\beta^4 - 4\beta^3 - 9\beta^2 + 10\beta + 2) \right], \\
a_2 = & \frac{2g_A h_A^2}{27 F_\pi^2 \alpha^2 \beta^2} \left[ 5\alpha^6 + 3\alpha^4 (2\beta + 9) + \alpha^2 (-3\beta^3 - 6\beta^2 + 33\beta + 16) \right. \\
& + 6(\beta - 1)(\beta + 1)^2 \left. \right], \\
a_3 = & \frac{g_A h_A^2}{54 F_\pi^2 \alpha^2 \beta^2} \left[ 4\alpha^8 + \alpha^6 (-8\beta^2 - 8\beta + 15) + \alpha^4 (4\beta^4 + 8\beta^3 - 50\beta^2 - 8\beta + 30) \right. \\
& + \alpha^2 (23\beta^4 + 16\beta^3 + 13\beta^2 - 92\beta - 73) - 24(\beta - 1)(\beta + 1)^2 \left. \right]
\end{aligned}$$

$$\begin{aligned}
 & + \frac{5g_1 h_A^2}{972 F_\pi^2 \beta^4} \left[ 3\alpha^{10} - \alpha^8 (9\beta^2 + 5\beta + 7) + \alpha^6 (9\beta^4 + 10\beta^3 + 17\beta^2 + 12\beta - 1) \right. \\
 & \quad - \alpha^4 (3\beta^6 + 5\beta^5 + 24\beta^4 + 31\beta^3 + 42\beta^2 - 15\beta - 15) \\
 & \quad + 2\alpha^2 (7\beta^6 + 17\beta^5 + 10\beta^4 - 5\beta^3 + 18\beta^2 - 25\beta - 7) \\
 & \quad \left. - 14\beta^6 - 20\beta^5 + 34\beta^4 - 20\beta^3 + 22\beta^2 + 28\beta + 4 \right], \\
 b_1 & = \frac{2g_A h_A^2 m_N^2}{9F_\pi^2 \alpha^2 \beta^2} \left[ \alpha^6 + \alpha^4 \beta (7\beta + 3) + \alpha^2 (-2\beta^4 + \beta^3 + \beta^2 - 5\beta - 3) \right. \\
 & \quad \left. + 2(\beta - 1)^2 (\beta + 1)^3 \right], \\
 b_2 & = - \frac{5g_1 h_A^2 m_N^2}{486 F_\pi^2 \beta^3} \left[ 5\alpha^6 + \alpha^4 (8\beta^2 - 6\beta - 11) \right. \\
 & \quad - 2\alpha^2 (8\beta^4 + 18\beta^3 + 13\beta^2 - 6\beta - 3) \\
 & \quad \left. + 4\beta^2 (3\beta^4 + 6\beta^3 - 2\beta^2 + 6\beta + 3) \right], \\
 b_3 & = \frac{2g_A h_A^2 m_N^2}{27 F_\pi^2 \alpha^2 \beta^2} \left[ 5\alpha^8 + 2\alpha^6 (3\beta + 7) + \alpha^4 (-3\beta^3 - 12\beta^2 + 24\beta + 5) \right. \\
 & \quad \left. + 12\alpha^2 (\beta - 1)(\beta + 1)^2 - 6(\beta^5 - \beta^3 + \beta^2 - 1) \right], \\
 b_4 & = \frac{g_A h_A^2 m_N^2}{54 F_\pi^2 \alpha^2 \beta^2} \left[ 4\alpha^{10} + \alpha^8 (-12\beta^2 - 8\beta + 11) + \alpha^6 (12\beta^4 + 16\beta^3 - 61\beta^2 + 3) \right. \\
 & \quad + \alpha^4 (-4\beta^6 - 8\beta^5 + 73\beta^4 + 48\beta^3 + 2\beta^2 - 96\beta - 79) \\
 & \quad - \alpha^2 (\beta + 1)^2 (23\beta^4 - 30\beta^3 + 26\beta^2 + 66\beta - 85) \\
 & \quad \left. + 24(\beta^5 - \beta^3 + \beta^2 - 1) \right] \\
 & \quad + \frac{5g_1 h_A^2 m_N^2}{972 F_\pi^2 \beta^4} \left[ 3\alpha^{12} - \alpha^{10} (12\beta^2 + 5\beta + 10) \right. \\
 & \quad + \alpha^8 (18\beta^4 + 15\beta^3 + 30\beta^2 + 17\beta + 6) \\
 & \quad - \alpha^6 (12\beta^6 + 15\beta^5 + 44\beta^4 + 48\beta^3 + 54\beta^2 - 7\beta - 16) \\
 & \quad + \alpha^4 (3\beta^8 + 5\beta^7 + 38\beta^6 + 65\beta^5 + 76\beta^4 + 51\beta^3 + 44\beta^2 - 73\beta - 29) \\
 & \quad - 2\alpha^2 (7\beta^8 + 17\beta^7 + 17\beta^6 - 3\beta^5 - 12\beta^4 + 23\beta^3 - 7\beta^2 - 41\beta - 9) \\
 & \quad \left. + 2(\beta + 1)^3 (7\beta^5 + \beta^4 - 17\beta^3 + 19\beta^2 - 8\beta - 2) \right], \\
 c_1 & = \frac{4g_A h_A^2 m_N^4}{9F_\pi^2 \alpha^2 \beta^2} \left[ \alpha^8 + 2\alpha^6 (2\beta^2 + \beta - 1) - 2\alpha^4 \beta (\beta^3 + \beta + 2) \right. \\
 & \quad \left. + 2\alpha^2 (\beta - 1)^2 (\beta + 1)^3 - (\beta - 1)^2 (\beta + 1)^3 (\beta^2 - \beta + 1) \right], \\
 c_2 & = - \frac{5g_1 h_A^2 m_N^4}{81 F_\pi^2 \beta^3} \left[ \alpha^8 + \alpha^6 (2\beta^2 - 2\beta - 3) + \alpha^4 (-6\beta^4 - 6\beta^3 - 7\beta^2 + 4\beta + 3) \right. \\
 & \quad \left. + \alpha^2 (\beta + 1)^2 (5\beta^4 - 4\beta^3 + 8\beta^2 - 1) - 2(\beta - 1)^2 \beta^2 (\beta + 1)^4 \right].
 \end{aligned}$$

## Electromagnetic form factor of the nucleon

The renormalisation rules of the two relevant LECs  $c_6$  and  $c_7$  are given below. We remind the reader that  $\bar{c}_6$  and  $\bar{c}_7$  are the renormalised quantities. Note that we use the auxiliary variables  $a_i, b_i, c_i$  only in this particular context for reasons of clarity and comprehensibility.

$$\begin{aligned} c_6 &= \bar{c}_6 + \delta c_6^{(3)} + \delta c_6^{(3,\Delta)}, \\ \delta c_6^{(3)} &= \frac{g_A^2}{(\alpha^2 - 4)F_\pi^2} \left[ \frac{m_N^2(4 - 3\alpha^2)}{16\pi^2} + (20 - 6\alpha^2)A_0(M_\pi^2) - 2(8 - 3\alpha^2)A_0(m_N^2) \right. \\ &\quad \left. + 2m_N^2(8 - 13\alpha^2 + 3\alpha^4)B_0(m_N^2, M_\pi^2, m_N^2) \right], \\ \delta c_6^{(3,\Delta)} &= a_0 + a_1 A_0(M_\pi^2) + a_2 A_0(m_\Delta^2) + b_1 B_0(m_N^2, M_\pi^2, m_\Delta^2), \\ a_0 &= - \frac{h_A^2 m_N^2}{1296 \pi^2 F_\pi^2 \beta^4} \left[ \alpha^4 (-27\beta^2 + 160\beta + 145) + 20\alpha^2 (6\beta^3 - 7\beta^2 - 9\beta - 4) + 27\beta^6 \right. \\ &\quad \left. + 92\beta^5 - 281\beta^4 - 44\beta^3 + 75\beta^2 + 60\beta + 20 \right], \\ a_1 &= - \frac{2h_A^2}{81F_\pi^2 \beta^4} \left[ \alpha^4 (27\beta^2 + 20\beta + 15) + \alpha^2 (-54\beta^4 - 40\beta^3 - 7\beta^2 + 120\beta + 75) \right. \\ &\quad \left. + 27\beta^6 + 20\beta^5 - 35\beta^4 + 6\beta^3 + 47\beta^2 - 20\beta - 15 \right], \\ a_2 &= \frac{2h_A^2}{81F_\pi^2 \beta^4} \left[ \alpha^4 (27\beta^2 + 20\beta + 15) - 2\alpha^2 (27\beta^4 + 20\beta^3 - 10\beta^2 + 20\beta + 15) + 27\beta^6 \right. \\ &\quad \left. + 20\beta^5 - 62\beta^4 - 86\beta^3 - 62\beta^2 + 20\beta + 15 \right], \\ b_1 &= \frac{2h_A^2 m_N^2}{81F_\pi^2 \beta^4} \left[ \alpha^4 (27\beta^2 + 20\beta + 15) - 2\alpha^2 (27\beta^4 - 7\beta^3 - 30\beta^2 + 5\beta + 15) + 27\beta^6 \right. \\ &\quad \left. - 34\beta^5 - 21\beta^4 + 98\beta^3 - 57\beta^2 - 10\beta + 15 \right] (-1 + \alpha^2 - 2\beta - \beta^2), \\ c_7 &= \bar{c}_7 + \delta c_7^{(3)} + \delta c_7^{(3,\Delta)}, \\ \delta c_7^{(3)} &= \frac{g_A^2}{(\alpha^2 - 4)F_\pi^2} \left[ - \frac{m_N^2}{2\pi^2} - 4A_0(M_\pi^2) + 8A_0(m_N^2) - 4m_N^2(2 - \alpha^2)B_0(m_N^2, M_\pi^2, m_N^2) \right], \\ \delta c_7^{(3,\Delta)} &= a_0 + a_1 A_0(M_\pi^2) + a_2 A_0(m_\Delta^2) + b_1 B_0(m_N^2, M_\pi^2, m_\Delta^2), \\ a_0 &= - \frac{h_A^2 m_N^2}{1296 \pi^2 F_\pi^2 \beta^4} \left[ \alpha^4 (32\beta + 29) + 2\alpha^2 (12\beta^3 - 23\beta^2 - 18\beta - 8) + 4\beta^5 - 67\beta^4 + 2\beta^3 \right. \\ &\quad \left. + 24\beta^2 + 12\beta + 4 \right], \\ a_1 &= \frac{2h_A^2}{81F_\pi^2 \beta^4} \left[ \alpha^4 (4\beta + 3) + \alpha^2 (-8\beta^3 + 4\beta^2 + 24\beta + 15) + 4\beta^5 - 7\beta^4 - 15\beta^3 + 4\beta^2 \right. \\ &\quad \left. - 4\beta - 3 \right], \end{aligned}$$

$$\begin{aligned}
 a_2 &= -\frac{2h_A^2}{81F_\pi^2\beta^4} \left[ \alpha^4(4\beta+3) - 2\alpha^2(4\beta^3 - 2\beta^2 + 4\beta + 3) + 4\beta^5 - 7\beta^4 - \beta^3 - 7\beta^2 \right. \\
 &\quad \left. + 4\beta + 3 \right], \\
 b_1 &= \frac{2h_A^2 m_N^2}{81F_\pi^2\beta^4} \left[ \alpha^4(4\beta+3) - 2\alpha^2(4\beta^3 - 6\beta^2 + \beta + 3) + 4\beta^5 - 15\beta^4 + 25\beta^3 - 6\beta^2 \right. \\
 &\quad \left. - 2\beta + 3 \right] (1 - \alpha^2 + 2\beta + \beta^2).
 \end{aligned}$$

### Axial pion-nucleon-delta coupling

Here, we give the necessary shift of the axial pion-nucleon-delta coupling  $h_A$ :

$$\begin{aligned}
 \bar{h}_A &= h_A + \delta h_A^{(2)}, \\
 \delta h_A^{(2)} &= b_3(m_N - m_\Delta) + b_6 \frac{M_\pi^2 + m_N^2 - m_\Delta^2}{2m_N}.
 \end{aligned}$$

### Electromagnetic transition form factor

Here, we give the shift for the coupling constants  $b_1$  and  $h_1$ . Note that the auxiliary variables  $a_i$ ,  $b_i$  and  $c_i$  are used only in this particular context. Taking the real part of the corrections to  $b_1$  and  $h_1$  ensures that the bare LECs are real, which is necessary for the Lagrangian to be hermitian.

$$\begin{aligned}
 b_1 &= \bar{b}_1 + \delta b_1^{(3)}, \\
 \delta b_1^{(3)} &= \text{Re} \left[ a_0 + a_1 A_0(M_\pi^2) + a_2 A_0(m_N^2) + a_3 A_0(m_\Delta^2) \right. \\
 &\quad + b_1 B_0(m_N^2, M_\pi^2, m_N^2) + b_2 B_0(m_N^2, M_\pi^2, m_\Delta^2) \\
 &\quad + b_3 B_0(m_\Delta^2, M_\pi^2, m_N^2) + b_4 B_0(m_\Delta^2, M_\pi^2, m_\Delta^2) \\
 &\quad + c_1 C_0(0, m_\Delta^2, m_N^2, M_\pi^2, M_\pi^2, m_N^2) + c_2 C_0(0, m_\Delta^2, m_N^2, M_\pi^2, M_\pi^2, m_\Delta^2) \\
 &\quad \left. + c_3 C_0(m_N^2, 0, m_\Delta^2, M_\pi^2, m_N^2, m_N^2) + c_4 C_0(m_N^2, 0, m_\Delta^2, M_\pi^2, m_\Delta^2, m_\Delta^2) \right], \\
 a_0 &= 2m_N(\beta - 1)h_{15} + m_N(\beta^2 - 1)h_{16} - \frac{g_A h_A m_N}{16\pi^2 F_\pi^2(\beta^2 - 1)} \left[ 2\alpha^2 + \beta^2 - 3\beta \right] \\
 &\quad + \frac{5g_A h_A m_N}{10368\pi^2 F_\pi^2 \beta^4 (\beta^2 - 1)} \left[ \alpha^6 (3\beta^3 - 2\beta^2 - 3\beta + 2) \beta \right. \\
 &\quad - \alpha^4 (3\beta^6 + 3\beta^5 + 6\beta^4 + 117\beta^3 + 3\beta^2 + 8\beta + 4) \\
 &\quad - \alpha^2 (3\beta^8 - 2\beta^7 + \beta^6 + 74\beta^5 - 130\beta^4 - 264\beta^3 + 36\beta^2 - 6) \\
 &\quad + 3\beta^{10} + 3\beta^9 - 6\beta^8 - 617\beta^7 - 153\beta^6 + 766\beta^5 \\
 &\quad \left. - 84\beta^4 - 82\beta^3 + 26\beta^2 + 2\beta - 2 \right], \\
 a_1 &= \frac{g_A h_A}{F_\pi^2 m_N(\beta - 1)}
 \end{aligned}$$

$$\begin{aligned}
& + \frac{5g_1 h_A}{324 F_\pi^2 m_N \beta^6 (\beta^2 - 1)} \left[ \alpha^6 \beta^3 (3\beta^3 - 2\beta^2 - 3\beta + 2) \right. \\
& \quad - \alpha^4 (9\beta^8 - \beta^7 + \beta^6 - 7\beta^5 - 2\beta^4 - 2\beta^2 + 2) \\
& \quad + \alpha^2 \beta^2 (9\beta^8 + 4\beta^7 + 5\beta^5 + 43\beta^4 + \beta^3 - 8\beta^2 + 22\beta - 4) \\
& \quad - \beta^3 (3\beta^9 + 3\beta^8 - 4\beta^7 - \beta^6 + 32\beta^5 + 13\beta^4 - 68\beta^3 \\
& \quad \left. + 75\beta^2 + 25\beta - 6) \right], \\
a_2 &= \frac{g_A h_A (1 - 3\beta)}{F_\pi^2 m_N (\beta^2 - 1)}, \\
a_3 &= - \frac{5g_1 h_A}{324 F_\pi^2 m_N \beta^6 (\beta^2 - 1)} \left[ \alpha^6 \beta^3 (3\beta^3 - 2\beta^2 - 3\beta + 2) \right. \\
& \quad - \alpha^4 (9\beta^8 - \beta^7 - 2\beta^6 - 5\beta^5 + \beta^4 - 2\beta^3 - 2\beta^2 + 2) \\
& \quad + \alpha^2 \beta^3 (9\beta^7 + 4\beta^6 - 6\beta^5 + 4\beta^4 + 42\beta^3 - 82\beta^2 + 75\beta + 26) \\
& \quad - \beta^3 (3\beta^9 + 3\beta^8 - 7\beta^7 - 4\beta^6 + 36\beta^5 - 62\beta^4 - 5\beta^3 \\
& \quad \left. + 21\beta^2 + 81\beta + 6) \right], \\
b_1 &= - \frac{g_A h_A m_N}{F_\pi^2 (\beta^2 - 1)^2} \left[ \alpha^2 (\beta^3 - 2\beta^2 - 2\beta - 1) + 2\beta (\beta^2 - \beta + 2) \right], \\
b_2 &= - \frac{5g_1 h_A m_N}{324 F_\pi^2 \beta^3 (\beta^2 - 1)^2} \left[ \alpha^8 (3\beta - 2) (\beta^2 - 1)^2 \right. \\
& \quad - \alpha^6 (12\beta^6 - 3\beta^5 - 14\beta^4 - 2\beta^3 + 13\beta - 6) \beta \\
& \quad + \alpha^4 (18\beta^8 + 3\beta^7 - 20\beta^6 - 3\beta^5 + 46\beta^4 - 47\beta^3 - 104\beta^2 - 41\beta + 4) \beta \\
& \quad + \alpha^2 (-12\beta^{11} - 7\beta^{10} + 22\beta^9 + 4\beta^8 - 84\beta^7 - 10\beta^6 + 152\beta^5 + 72\beta^4 \\
& \quad \left. + 80\beta^3 + 65\beta^2 - 2\beta + 8) \right. \\
& \quad + 3\beta^{13} + 3\beta^{12} - 10\beta^{11} - 7\beta^{10} + 43\beta^9 + 36\beta^8 - 172\beta^7 - 6\beta^6 - 23\beta^5 \\
& \quad \left. + 19\beta^4 - 46\beta^3 + 33\beta^2 - 11\beta - 6 \right], \\
b_3 &= - \frac{g_A h_A m_N \beta}{F_\pi^2 (\beta^2 - 1)^2} \left[ \alpha^2 (3\beta + 1) + \beta^3 - 5\beta^2 + \beta - 1 \right], \\
b_4 &= - \frac{5g_1 h_A m_N}{162 F_\pi^2 \beta^6 (\beta^2 - 1)^2} \left[ \alpha^6 (4\beta^5 - 3\beta^4 - 2\beta^2 + 1) \right. \\
& \quad + 2\alpha^4 \beta^2 (11\beta^5 + 11\beta^4 + 17\beta^3 + 4\beta^2 - 6\beta - 1) \\
& \quad + 2\alpha^2 \beta^4 (23\beta^5 - 23\beta^4 - 62\beta^3 - 21\beta^2 + 6\beta + 5) \\
& \quad \left. + 36 (3\beta^{10} - \beta^9 - \beta^8 + \beta^6) \right], \\
c_1 &= - \frac{2g_A h_A m_N^3 \alpha^2 (\alpha^2 + \beta^2 - 1)}{F_\pi^2 (\beta^2 - 1)}, \\
c_2 &= - \frac{10g_1 h_A m_N^3}{9 F_\pi^2 \beta (\beta^2 - 1)} \left[ \alpha^6 - \alpha^4 (\beta^2 - \beta + 1) + 3\alpha^2 \beta^2 (\beta^2 - 1) \right],
\end{aligned}$$

$$c_3 = -\frac{2g_A h_A m_N^3 \beta}{F_\pi^2 (\beta^2 - 1)} [\alpha^2 - \beta^2 + \beta - 2],$$

$$c_4 = \frac{10g_1 h_A m_N^3}{27 F_\pi^2 (\beta^2 - 1)} [\alpha^4(\beta - 4) - \alpha^2(4\beta^3 - 8\beta^2 - \beta - 4) - 3(3\beta^4 - \beta^3 - \beta^2 + 1)],$$

$$h_1 = \bar{h}_1 + \delta h^{(3)},$$

$$\delta h^{(3)} = \text{Re} \left[ a_0 + a_1 A_0(M_\pi^2) + a_2 A_0(m_N^2) + a_3 A_0(m_\Delta^2) \right.$$

$$+ b_1 B_0(m_N^2, M_\pi^2, m_N^2) + b_2 B_0(m_N^2, M_\pi^2, m_\Delta^2)$$

$$+ b_3 B_0(m_\Delta^2, M_\pi^2, m_N^2) + b_4 B_0(m_\Delta^2, M_\pi^2, m_\Delta^2)$$

$$+ c_1 C_0(0, m_\Delta^2, m_N^2, M_\pi^2, M_\pi^2, m_N^2) + c_2 C_0(0, m_\Delta^2, m_N^2, M_\pi^2, M_\pi^2, m_\Delta^2)$$

$$\left. + c_3 C_0(m_N^2, 0, m_\Delta^2, M_\pi^2, m_N^2, m_N^2) + c_4 C_0(m_N^2, 0, m_\Delta^2, M_\pi^2, m_\Delta^2, m_\Delta^2) \right],$$

$$a_0 = 2m_N h_{15} - \frac{g_A h_A m_N (\alpha^2 - \beta)}{4\pi^2 F_\pi^2 (\beta - 1)^2 (\beta + 1)}$$

$$+ \frac{5g_1 h_A m_N}{10368 \pi^2 F_\pi^2 \beta^4 (\beta - 1)^2 (\beta + 1)} [3\alpha^6(\beta - 1)^2(\beta + 1)\beta$$

$$- \alpha^4(3\beta^6 + 2\beta^5 + 7\beta^4 + 275\beta^3 + 2\beta^2 - 5\beta + 4)$$

$$- \alpha^2(3\beta^8 - 3\beta^7 + \beta^6 - 45\beta^5 - 222\beta^4 - 376\beta^3 + 56\beta^2 + 16\beta - 6)$$

$$+ 3\beta^{10} + 2\beta^9 - 5\beta^8 - 587\beta^7 + 74\beta^6 + 717\beta^5$$

$$- 386\beta^4 - 138\beta^3 + 28\beta^2 + 6\beta - 2],$$

$$a_1 = \frac{2g_A h_A}{F_\pi^2 m_N (\beta - 1)^2}$$

$$+ \frac{5g_1 h_A}{324 F_\pi^2 m_N \beta^6 (\beta - 1)^2 (\beta + 1)} [3\alpha^6(\beta - 1)^2 \beta^3(\beta + 1)$$

$$- \alpha^4(9\beta^8 - 4\beta^7 + 2\beta^6 - 12\beta^5 - 3\beta^4 + 10\beta^3 - 2\beta^2 - 2\beta + 2)$$

$$+ \alpha^2 \beta^2(9\beta^8 + \beta^7 + 2\beta^6 + \beta^5 + 48\beta^4 + 36\beta^3 + 45\beta^2 + 30\beta - 28)$$

$$- \beta^3(3\beta^9 + 2\beta^8 - 3\beta^7 + \beta^6 + 35\beta^5 + 83\beta^4 - 51\beta^3$$

$$+ 37\beta^2 + 40\beta - 3)],$$

$$a_2 = -\frac{4g_A h_A \beta}{F_\pi^2 m_N (\beta - 1)^2 (\beta + 1)},$$

$$a_3 = -\frac{5g_1 h_A}{324 F_\pi^2 m_N \beta^6 (\beta - 1)^2 (\beta + 1)} [3\alpha^6(\beta - 1)^2 \beta^3(\beta + 1)$$

$$- \alpha^4(9\beta^8 - 4\beta^7 - \beta^6 - 9\beta^5 + 7\beta^3 - 2\beta^2 - 2\beta + 2)$$

$$\begin{aligned} & + \alpha^2 \beta^2 (9\beta^8 + \beta^7 - 4\beta^6 + 2\beta^5 + 46\beta^4 - 44\beta^3 + 129\beta^2 + 29\beta - 24) \\ & - \beta^3 (3\beta^9 + 2\beta^8 - 6\beta^7 - \beta^6 + 38\beta^5 + 132\beta^4 + \beta^3 \\ & \quad - 136\beta^2 + 108\beta + 3), \\ b_1 = & - \frac{2g_A h_A m_N}{F_\pi^2 (\beta - 1)^3 (\beta + 1)^2} \left[ \alpha^2 (\beta^3 - 2\beta^2 - 2\beta - 1) + \beta (\beta^2 + 3) \right], \\ b_2 = & - \frac{5g_1 h_A m_N}{324 F_\pi^2 \beta^3 (\beta - 1)^3 (\beta + 1)^2} \left[ 3\alpha^8 (\beta - 1)^3 (\beta + 1)^2 \right. \\ & - \alpha^6 (12\beta^6 - 7\beta^5 - 13\beta^4 - 2\beta^3 - 2\beta^2 + 17\beta - 5) \beta \\ & + \alpha^4 (18\beta^9 - 3\beta^8 - 17\beta^7 - 5\beta^6 + 47\beta^5 - 115\beta^4 - 143\beta^3 \\ & \quad - 79\beta^2 + 3\beta + 6) \\ & - \alpha^2 (12\beta^{10} + 3\beta^9 - 19\beta^8 + 88\beta^6 - 70\beta^5 - 262\beta^4 - 120\beta^3 \\ & \quad - 80\beta^2 - 125\beta - 3) \beta \\ & + 3\beta^{13} + 2\beta^{12} - 9\beta^{11} - 3\beta^{10} + 44\beta^9 + 5\beta^8 - 262\beta^7 - 98\beta^6 \\ & \quad + 15\beta^5 + 84\beta^4 - 65\beta^3 + 13\beta^2 - 14\beta - 3, \\ b_3 = & - \frac{2g_A h_A m_N \beta}{F_\pi^2 (\beta - 1)^3 (\beta + 1)^2} \left[ \alpha^2 (3\beta + 1) - 3\beta^2 - 1 \right], \\ b_4 = & \frac{5g_1 h_A m_N}{162 F_\pi^2 \beta^6 (\beta - 1)^3 (\beta + 1)^2} \left[ \alpha^6 (\beta^5 + 3\beta^4 - 6\beta^3 + 2\beta^2 + \beta - 1) \right. \\ & - 2\alpha^4 \beta^2 (43\beta^5 + 33\beta^4 + 13\beta^3 - 15\beta^2 - 7\beta + 5) \\ & + 2\alpha^2 \beta^4 (23\beta^5 + 69\beta^4 + 43\beta^3 - 4\beta^2 + 12\beta + 1) \\ & \quad \left. - 12\beta^6 (2\beta^5 + 13\beta^4 - 4\beta^2 - 2\beta + 3) \right], \\ c_1 = & - \frac{2g_A h_A m_N^3 \alpha^3 (2\alpha^2 + \beta^2 - 1)}{F_\pi^2 (\beta - 1)^2 (\beta + 1)}, \\ c_2 = & - \frac{10g_1 h_A m_N^3 \alpha^2}{9 F_\pi^2 \beta (\beta - 1)^2 (\beta + 1)} \left[ 2\alpha^4 + \alpha^2 (-\beta^2 + \beta - 2) + \beta (2\beta^3 - \beta^2 - 2\beta + 1) \right], \\ c_3 = & - \frac{2g_A h_A m_N^3}{F_\pi^2 (\beta - 1)^2 (\beta + 1)} \left[ \alpha^2 (\beta + 1) - \beta (\beta^2 + 3) \right], \\ c_4 = & - \frac{10g_1 h_A m_N^3}{27 F_\pi^2 (\beta - 1)^2 (\beta + 1)} \left[ 2\alpha^4 (\beta + 2) - \alpha^2 (4\beta^3 + 11\beta^2 - \beta + 4) \right. \\ & \quad \left. + 2\beta^5 + 13\beta^4 - 4\beta^2 - 2\beta + 3 \right]. \end{aligned}$$

# D Feynman rules

In this chapter, we give all relevant Feynman rules for pion photoproduction up to the maximal working orders in the HB and covariant framework. All relevant vertices equal to zero are not shown. The momenta and their orientation as well as polarisation vectors and the isospin indices are stated in the figures. We use the small black dot for leading order vertices (from  $\mathcal{L}_{\pi N}^{(1)}$ ,  $\hat{\mathcal{L}}_{\pi N}^{(1)}$  or  $\mathcal{L}_{\pi\pi}^{(2)}$ ), an empty big circle for NLO pure bosonic vertices (from  $\mathcal{L}_{\pi\pi}^{(4)}$ ), a filled black square for NLO nucleonic vertices and an empty square for N<sup>2</sup>LO nucleonic vertices.

We remind the reader that we use the convention  $\sigma^{\mu\nu} = \frac{i}{2}[\gamma^\mu, \gamma^\nu]$  and that  $\alpha$  is the unphysical parameter from the parametrisation of  $U(x)$  (see eq. (3.71)).

## D.1 Mesonic sector

### Terms from $\mathcal{L}_{\pi\pi}^{(2)}$

$$\begin{aligned} & \text{Diagram 1: } a_1 \xrightarrow[q \rightarrow]{} a_2 \quad \frac{i \delta_{a_1 a_2}}{q^2 - M_\pi^2 + i\epsilon} \\ & \text{Diagram 2: } a_1 \xrightarrow[q_1 \rightarrow]{} \underset{\downarrow}{\text{---}} \xleftarrow[q_2 \leftarrow]{} a_2 \quad e (q_2^\mu - q_1^\mu) \varepsilon_{3a_1 a_2} \\ & \quad \frac{i}{F_\pi^2} \left( [(q_1 + q_2)^2 - M_\pi^2] \delta_{a_1 a_2} \delta_{a_3 a_4} \right. \\ & \quad \left. + [(q_1 + q_3)^2 - M_\pi^2] \delta_{a_1 a_3} \delta_{a_2 a_4} \right. \\ & \quad \left. + [(q_1 + q_4)^2 - M_\pi^2] \delta_{a_1 a_4} \delta_{a_2 a_3} \right. \\ & \quad \left. + 2\alpha (4M_\pi^2 - q_1^2 - q_2^2 - q_3^2 - q_4^2) \times \right. \\ & \quad \left. (\delta_{a_1 a_2} \delta_{a_3 a_4} + \delta_{a_1 a_3} \delta_{a_2 a_4} + \delta_{a_1 a_4} \delta_{a_2 a_3}) \right) \\ & \text{Diagram 3: } a_2 \xrightarrow[q_2 \rightarrow]{} \underset{\downarrow}{\text{---}} \xleftarrow[q_4 \leftarrow]{} a_4 \quad \frac{4e}{F_\pi^2} \alpha \left( q_1^\mu (\varepsilon_{3a_1 a_2} \delta_{a_3 a_4} + \varepsilon_{3a_1 a_3} \delta_{a_2 a_4} + \varepsilon_{3a_1 a_4} \delta_{a_2 a_3}) \right. \\ & \quad \left. + q_2^\mu (-\varepsilon_{3a_1 a_2} \delta_{a_3 a_4} + \varepsilon_{3a_2 a_3} \delta_{a_1 a_4} + \varepsilon_{3a_2 a_4} \delta_{a_1 a_3}) \right. \\ & \quad \left. - q_3^\mu (\varepsilon_{3a_1 a_3} \delta_{a_2 a_4} + \varepsilon_{3a_2 a_3} \delta_{a_1 a_4} - \varepsilon_{3a_3 a_4} \delta_{a_1 a_2}) \right. \\ & \quad \left. - q_4^\mu (\varepsilon_{3a_1 a_4} \delta_{a_2 a_3} + \varepsilon_{3a_2 a_4} \delta_{a_1 a_3} + \varepsilon_{3a_3 a_4} \delta_{a_1 a_2}) \right) \end{aligned}$$

**Terms from  $\mathcal{L}_{\pi\pi}^{(4)}$** 

$$\begin{array}{ll}
\text{Diagram: } & \text{Expression:} \\
\begin{array}{c} a_1 \xrightarrow[q]{\quad} \text{---} \textcircled{\text{---}} \text{---} \xrightarrow[q]{\quad} a_2 \\ \text{---} \end{array} & -\frac{2i}{F_\pi^2} (l_3 M_\pi^4 + l_4 M_\pi^2 (M_\pi^2 + q^2)) \delta_{a_1 a_2} \\
\\
\begin{array}{c} \mu \\ \nearrow \searrow \\ \text{---} \xrightarrow[q_1]{\quad} \text{---} \textcircled{\text{---}} \text{---} \xleftarrow[q_2]{\quad} a_2 \\ \downarrow \\ \text{---} \end{array} & \frac{2e}{F_\pi^2} \left( q_2^\mu (l_4 M_\pi^2 + l_6 k \cdot q_1) \right. \\
& \left. - q_1^\mu (l_4 M_\pi^2 + l_6 k \cdot q_2) \right) \varepsilon_{3a_1 a_2}
\end{array}$$

## D.2 Heavy baryon Feynman rules

Here, the momentum  $p$  in the HB nucleon propagator refers to the residual part of the momentum.

**Terms from  $\hat{\mathcal{L}}_{\pi N}^{(1)}$** 

$$\begin{array}{ll}
\begin{array}{c} \text{---} \xrightarrow[p]{\quad} \text{---} \\ \text{---} \end{array} & \frac{i}{v \cdot p + i\epsilon} \\
\\
\begin{array}{c} \mu \\ \nearrow \searrow \\ \text{---} \xrightarrow[p_1]{\quad} \bullet \xrightarrow[p_2]{\quad} \text{---} \\ \downarrow \\ \text{---} \end{array} & ie v^\mu \frac{1 + \tau_3}{2} \\
\\
\begin{array}{c} a \\ \downarrow \\ \text{---} \xrightarrow[p_1]{\quad} \bullet \xrightarrow[p_2]{\quad} \text{---} \\ \text{---} \end{array} & \frac{g_A}{2F_\pi} S \cdot q \tau_a \\
\\
\begin{array}{c} a_1 \xrightarrow[q_1]{\quad} \text{---} \textcircled{\text{---}} \text{---} \xrightarrow[q_2]{\quad} a_2 \\ \text{---} \xrightarrow[p_1]{\quad} \bullet \xrightarrow[p_2]{\quad} \text{---} \\ \text{---} \end{array} & \frac{1}{4F_\pi^2} v \cdot (q_1 - q_2) \varepsilon_{a_1 a_2 i} \tau_i \\
\\
\begin{array}{c} a_1 \xrightarrow[q_1]{\quad} \text{---} \textcircled{\text{---}} \text{---} \xrightarrow[q_2]{\quad} a_2 \\ \text{---} \xrightarrow[q_3]{\quad} \bullet \xrightarrow[p_1]{\quad} \text{---} \xrightarrow[p_2]{\quad} \text{---} \\ \text{---} \end{array} & \frac{g_A}{4F_\pi^3} \left( S \cdot (q_1 + q_2) \delta_{a_1 a_2} \tau_{a_3} + S \cdot (q_1 + q_3) \delta_{a_1 a_3} \tau_{a_2} \right. \\
& \left. + S \cdot (q_2 + q_3) \delta_{a_2 a_3} \tau_{a_1} \right) \\
& - \frac{g_A}{F_\pi^3} \alpha \left( S \cdot (q_1 + q_2 + q_3) (\delta_{a_1 a_2} \tau_{a_3} + \delta_{a_1 a_3} \tau_{a_2} + \delta_{a_2 a_3} \tau_{a_1}) \right) \\
\\
\begin{array}{c} \mu \\ \nearrow \searrow \\ \text{---} \xrightarrow[p_1]{\quad} \bullet \xrightarrow[p_2]{\quad} \text{---} \\ \text{---} \end{array} & \frac{ie g_A}{2F_\pi} S^\mu \varepsilon_{3ab} \tau_b
\end{array}$$

$$\frac{i e}{4 F_\pi^2} v^\mu (\delta_{3a_1} \tau_{a_2} + \delta_{3a_2} \tau_{a_1} - 2 \delta_{a_1 a_2} \tau_3)$$

$$-\frac{i e g_A}{F_\pi^3} \alpha S^\mu (\delta_{a_1 a_2} \varepsilon_{3a_3 b} + \delta_{a_1 a_3} \varepsilon_{3a_2 b} + \delta_{a_2 a_3} \varepsilon_{3a_1 b}) \tau_b$$

### Terms from $\hat{\mathcal{L}}_{\pi N}^{(2)}$

$$4 i c_1 M_\pi^2$$

$$-\frac{e}{2m_N} (k \times S)^\mu \left( c_6 \frac{\mathbb{1} + \tau_3}{2} + c_7 \right)$$

### Terms from $\hat{\mathcal{L}}_{\pi N}^{(3)}$

$$i e (k \cdot v k^\mu - k^2 v^\mu) (d_6 \tau_3 + 2 d_7)$$

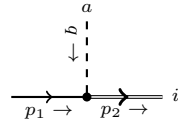
$$+ \frac{i e}{4m_N} (p_1^\mu + p_2^\mu - v^\mu (p_1 \cdot v + p_2 \cdot v)) (\mathbb{1} + \tau_3)$$

$$\frac{M_\pi^2}{F_\pi} S \cdot q (2d_{16} - d_{18}) \tau_a$$

$$- \frac{g_A}{4F_\pi m_N} q \cdot v S \cdot (p_1 + p_2) \tau_a$$

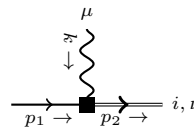
$$\begin{aligned}
 & -\frac{4ie}{F_\pi}(d_8\delta_{3a} + d_9\tau_a)(k \times q)^\mu \\
 & -\frac{ieM_\pi^2}{F_\pi}(2d_{16} - d_{18})S^\mu\varepsilon_{3ab}\tau_b \\
 & +\frac{ie}{F_\pi}d_{20}q \cdot v(k \cdot v S^\mu - S \cdot k v^\mu)\varepsilon_{3ab}\tau_b \\
 & -\frac{ie}{2F_\pi}(2d_{21} - d_{22})(k \cdot q S^\mu - S \cdot k q^\mu)\varepsilon_{3ab}\tau_b \\
 & +\frac{ie}{2F_\pi}d_{22}(k^2 S^\mu - S \cdot k k^\mu)\varepsilon_{3ab}\tau_b \\
 & -\frac{ieg_A}{4F_\pi m_N}v^\mu S \cdot (p_1 + p_2)\varepsilon_{3ab}\tau_b \\
 & -\frac{eg_A}{4F_\pi m_N}S^\mu q \cdot v(\delta_{3a} + \tau_a)
 \end{aligned}$$

**Terms from  $\hat{\mathcal{L}}_{\pi N \Delta}^{(1)}$**



$$-\frac{h_A}{F_\pi}q^\nu\delta_{ai}$$

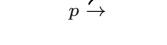
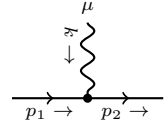
**Terms from  $\hat{\mathcal{L}}_{\pi N \Delta}^{(2)}$**



$$-\frac{ieb_1}{2}(S^\mu k^\nu - g^{\mu\nu}S \cdot k)\delta_{3i}$$

### D.3 Covariant Feynman rules

**Terms from  $\mathcal{L}_{\pi N}^{(1)}$**

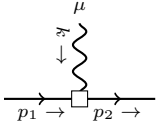
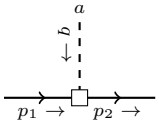
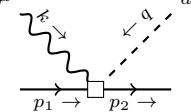
	$\frac{i(\not{p} + m_N)}{p^2 - m_N^2 + i\epsilon}$
	$ie\gamma^\mu\frac{1 + \tau_3}{2}$

	$-\frac{g_A}{2F_\pi} \not{q} \gamma_5 \tau_a$
	$\frac{1}{4F_\pi^2} (\not{q}_1 - \not{q}_2) \varepsilon_{a_1 a_2 i} \tau_i$
	$\begin{aligned} & -\frac{g_A}{4F_\pi^3} \left( (q_1 + q_2) \delta_{a_1 a_2} \tau_{a_3} + (q_1 + q_3) \delta_{a_1 a_3} \tau_{a_2} \right. \\ & \quad \left. + (q_2 + q_3) \delta_{a_2 a_3} \tau_{a_1} \right) \gamma_5 \\ & + \frac{g_A}{F_\pi^3} \alpha \left( (q_1 + q_2 + q_3) (\delta_{a_1 a_2} \tau_{a_3} + \delta_{a_1 a_3} \tau_{a_2} + \delta_{a_2 a_3} \tau_{a_1}) \right) \gamma_5 \end{aligned}$
	$-\frac{i e g_A}{2F_\pi} \gamma^\mu \gamma_5 \varepsilon_{3ab} \tau_b$
	$-\frac{i e}{4F_\pi^2} \gamma^\mu (\delta_{3a_1} \tau_{a_2} + \delta_{3a_2} \tau_{a_1} - 2\delta_{a_1 a_2} \tau_3)$
	$\frac{i e g_A}{F_\pi^3} \alpha \gamma^\mu \gamma_5 (\delta_{a_1 a_2} \varepsilon_{3a_3 b} + \delta_{a_1 a_3} \varepsilon_{3a_2 b} + \delta_{a_2 a_3} \varepsilon_{3a_1 b}) \tau_b$

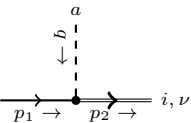
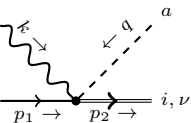
### Terms from $\mathcal{L}_{\pi N}^{(2)}$

	$4 i c_1 M_\pi^2$
	$-\frac{e}{2m_N} \sigma^{\mu\nu} k_\nu \left( c_6 \frac{\mathbb{1} + \tau_3}{2} + c_7 \right)$

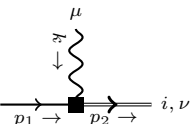
### Terms from $\mathcal{L}_{\pi N}^{(3)}$

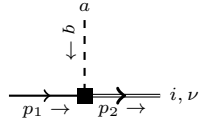
	$-\frac{i e}{2m_N} \left( (p_1^\mu + p_2^\mu) k^2 - k^\mu k \cdot (p_1 + p_2) \right) (d_6 \tau_3 + 2 d_7)$
	$-\frac{M_\pi^2}{F_\pi} \not{q} \gamma_5 \tau_a (2d_{16} - d_{18})$
	$\begin{aligned} & \frac{2 i e}{F_\pi m_N^2} (d_8 \delta_{3a} + d_9 \tau_a) \varepsilon^{\rho \lambda \mu \nu} k_\rho (p_1 + p_2)_\lambda q_\nu \\ & - \frac{2 i e M_\pi^2}{F_\pi} (d_{16} - \frac{1}{2} d_{18}) \gamma^\mu \gamma_5 \varepsilon_{3ab} \tau_b \\ & + \frac{i e}{2F_\pi m_N^2} d_{20} \left( (k \cdot p_1 p_1 \cdot q + k \cdot p_2 p_2 \cdot q) \gamma^\mu \right. \\ & \quad \left. - (p_1 \cdot q p_1^\mu + p_2 \cdot q p_2^\mu) \not{k} \right) \gamma_5 \varepsilon_{3ab} \tau_b \\ & + \frac{i e}{2F_\pi} (2d_{21} - d_{22}) (k \cdot q \gamma^\mu - q^\mu \not{k}) \gamma_5 \varepsilon_{3ab} \tau_b \\ & - \frac{i e}{2F_\pi} d_{22} (k^2 \gamma^\mu - k^\mu \not{k}) \gamma_5 \varepsilon_{3ab} \tau_b \end{aligned}$

### Terms from $\mathcal{L}_{\pi N \Delta}^{(1)}$

	$-\frac{h_A}{F_\pi} q^\nu \delta_{ai}$
	$-\frac{i e h_A}{F_\pi} g^{\mu \nu} \varepsilon_{3ai}$

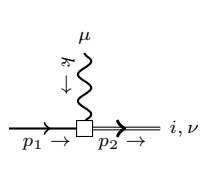
### Terms from $\mathcal{L}_{\pi N \Delta}^{(2)}$

	$-\frac{i e b_1}{2} (\not{k} g^{\mu \nu} - k^\nu \gamma^\mu) \gamma_5 \delta_{3i}$
---	--



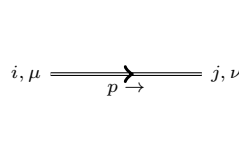
$$\frac{q^\nu}{F_\pi m_N} (b_3 m_N \not{q} + b_6 p_1 \cdot q) \delta_{ai}$$

**Terms from  $\mathcal{L}_{\pi N \Delta}^{(3)}$**

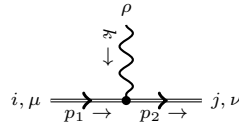


$$\frac{i e}{m_N} \left\{ h_1 (g^{\mu\nu} k \cdot p_1 - p_1^\mu k^\nu) \gamma_5 \right. \\ \left. - i m_N h_{15} \sigma_{\alpha\beta} \gamma_5 k^\alpha (g^{\mu\nu} k^\beta - g^{\mu\beta} k^\nu) \right. \\ \left. + h_{16} k \cdot p_1 (g^{\mu\nu} \not{k} - k^\nu \gamma^\mu) \gamma_5 \right\} \delta_{3i}$$

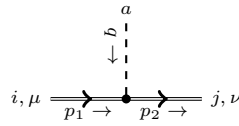
**Terms from  $\mathcal{L}_{\pi \Delta}^{(1)}$**



$$\frac{i(\not{p} + m_\Delta)}{p^2 - m_\Delta^2 + i\epsilon} \left( -g^{\mu\nu} + \frac{1}{d-1} \gamma^\mu \gamma^\nu \right. \\ \left. - \frac{1}{d-1} \frac{p^\mu \gamma^\nu - p^\nu \gamma^\mu}{m_\Delta} + \frac{d-2}{d-1} \frac{p^\mu p^\nu}{m_\Delta^2} \right) \xi_{ij}^{\frac{3}{2}}$$



$$- \frac{i e}{4} \{ [\gamma^\mu, \gamma^\nu], \gamma^\rho \} \frac{1 + 3\tau_3}{2} \delta_{ij}$$



$$\frac{g_1}{2F_\pi} \not{q} \gamma_5 g^{\mu\nu} \delta_{ij} \tau_a$$



# Bibliography

- [1] G. Aad et al. “Observation of a new particle in the search for the Standard Model Higgs boson with the ATLAS detector at the LHC”. In: *Phys. Lett. B* 716 (2012), pp. 1–29. DOI: [10.1016/j.physletb.2012.08.020](https://doi.org/10.1016/j.physletb.2012.08.020). arXiv: [1207.7214 \[hep-ex\]](https://arxiv.org/abs/1207.7214).
- [2] S. Glashow. “Partial Symmetries of Weak Interactions”. In: *Nucl. Phys.* 22 (1961), pp. 579–588. DOI: [10.1016/0029-5582\(61\)90469-2](https://doi.org/10.1016/0029-5582(61)90469-2).
- [3] F. Englert and R. Brout. “Broken Symmetry and the Mass of Gauge Vector Mesons”. In: *Phys. Rev. Lett.* 13 (1964). Ed. by J. Taylor, pp. 321–323. DOI: [10.1103/PhysRevLett.13.321](https://doi.org/10.1103/PhysRevLett.13.321).
- [4] P. W. Higgs. “Broken Symmetries and the Masses of Gauge Bosons”. In: *Phys. Rev. Lett.* 13 (1964). Ed. by J. Taylor, pp. 508–509. DOI: [10.1103/PhysRevLett.13.508](https://doi.org/10.1103/PhysRevLett.13.508).
- [5] G. Guralnik, C. Hagen, and T. Kibble. “Global Conservation Laws and Massless Particles”. In: *Phys. Rev. Lett.* 13 (1964). Ed. by J. Taylor, pp. 585–587. DOI: [10.1103/PhysRevLett.13.585](https://doi.org/10.1103/PhysRevLett.13.585).
- [6] S. Weinberg. “A Model of Leptons”. In: *Phys. Rev. Lett.* 19 (1967), pp. 1264–1266. DOI: [10.1103/PhysRevLett.19.1264](https://doi.org/10.1103/PhysRevLett.19.1264).
- [7] A. Salam. “Weak and Electromagnetic Interactions”. In: *Conf. Proc. C* 680519 (1968), pp. 367–377. DOI: [10.1142/9789812795915\\_0034](https://doi.org/10.1142/9789812795915_0034).
- [8] J. I. Friedman and H. W. Kendall. “Deep inelastic electron scattering”. In: *Ann. Rev. Nucl. Part. Sci.* 22 (1972), pp. 203–254. DOI: [10.1146/annurev.ns.22.120172.001223](https://doi.org/10.1146/annurev.ns.22.120172.001223).
- [9] S. Weinberg. *The Quantum Theory of Fields*. Vol. 2. Cambridge University Press, 1996. ISBN: 0 521 55002 5.
- [10] H. L. Anderson et al. “Total Cross-sections of Positive Pions in Hydrogen”. In: *Phys. Rev.* 85 (1952), p. 936. DOI: [10.1103/PhysRev.85.936](https://doi.org/10.1103/PhysRev.85.936).
- [11] H. Fritzsch, M. Gell-Mann, and H. Leutwyler. “Advantages of the Color Octet Gluon Picture”. In: *Phys. Lett. B* 47 (1973), pp. 365–368. DOI: [10.1016/0370-2693\(73\)90625-4](https://doi.org/10.1016/0370-2693(73)90625-4).
- [12] C.-N. Yang and R. L. Mills. “Conservation of Isotopic Spin and Isotopic Gauge Invariance”. In: *Phys. Rev.* 96 (1954). Ed. by J.-P. Hsu and D. Fine, pp. 191–195. DOI: [10.1103/PhysRev.96.191](https://doi.org/10.1103/PhysRev.96.191).
- [13] D. J. Gross and F. Wilczek. “Ultraviolet Behavior of Nonabelian Gauge Theories”. In: *Phys. Rev. Lett.* 30 (1973). Ed. by J. Taylor, pp. 1343–1346. DOI: [10.1103/PhysRevLett.30.1343](https://doi.org/10.1103/PhysRevLett.30.1343).

- [14] H. Politzer. “Reliable Perturbative Results for Strong Interactions?” In: *Phys. Rev. Lett.* 30 (1973). Ed. by J. Taylor, pp. 1346–1349. DOI: [10.1103/PhysRevLett.30.1346](https://doi.org/10.1103/PhysRevLett.30.1346).
- [15] L. Faddeev and V. Popov. “Feynman Diagrams for the Yang-Mills Field”. In: *Phys. Lett. B* 25 (1967). Ed. by J.-P. Hsu and D. Fine, pp. 29–30. DOI: [10.1016/0370-2693\(67\)90067-6](https://doi.org/10.1016/0370-2693(67)90067-6).
- [16] G. ’t Hooft. “Renormalization of Massless Yang-Mills Fields”. In: *Nucl. Phys. B* 33 (1971), pp. 173–199. DOI: [10.1016/0550-3213\(71\)90395-6](https://doi.org/10.1016/0550-3213(71)90395-6).
- [17] G. ’t Hooft and M. J. G. Veltman. “Regularization and Renormalization of Gauge Fields”. In: *Nucl. Phys. B* 44 (1972), pp. 189–213. DOI: [10.1016/0550-3213\(72\)90279-9](https://doi.org/10.1016/0550-3213(72)90279-9).
- [18] G. ’t Hooft. “A Planar Diagram Theory for Strong Interactions”. In: *Nucl. Phys. B* 72 (1974). Ed. by J. C. Taylor, p. 461. DOI: [10.1016/0550-3213\(74\)90154-0](https://doi.org/10.1016/0550-3213(74)90154-0).
- [19] E. Witten. “Baryons in the 1/n Expansion”. In: *Nucl. Phys. B* 160 (1979), pp. 57–115. DOI: [10.1016/0550-3213\(79\)90232-3](https://doi.org/10.1016/0550-3213(79)90232-3).
- [20] T. Skyrme. “A Unified Field Theory of Mesons and Baryons”. In: *Nucl. Phys.* 31 (1962), pp. 556–569. DOI: [10.1016/0029-5582\(62\)90775-7](https://doi.org/10.1016/0029-5582(62)90775-7).
- [21] A. Chodos et al. “A New Extended Model of Hadrons”. In: *Phys. Rev. D* 9 (1974), pp. 3471–3495. DOI: [10.1103/PhysRevD.9.3471](https://doi.org/10.1103/PhysRevD.9.3471).
- [22] G. Brown and M. Rho. “The Little Bag”. In: *Phys. Lett. B* 82 (1979), pp. 177–180. DOI: [10.1016/0370-2693\(79\)90729-9](https://doi.org/10.1016/0370-2693(79)90729-9).
- [23] S. Weinberg. “Phenomenological Lagrangians”. In: *Phys. A Stat. Mech. its Appl.* 96.1-2 (1979), pp. 327–340. DOI: [10.1016/0378-4371\(79\)90223-1](https://doi.org/10.1016/0378-4371(79)90223-1).
- [24] J. Gasser and H. Leutwyler. “Chiral Perturbation Theory to One Loop”. In: *Annals Phys.* 158.1 (1984), pp. 142–210. DOI: [10.1016/0003-4916\(84\)90242-2](https://doi.org/10.1016/0003-4916(84)90242-2).
- [25] J. Gasser and H. Leutwyler. “Chiral Perturbation Theory: Expansions in the Mass of the Strange Quark”. In: *Nucl. Phys. B* 250 (1985), pp. 465–516. DOI: [10.1016/0550-3213\(85\)90492-4](https://doi.org/10.1016/0550-3213(85)90492-4).
- [26] J. Gasser, M. E. Sainio, and A. Švarc. “Nucleons with chiral loops”. In: *Nucl. Phys. B* 307.4 (1988), pp. 779–853. DOI: [10.1016/0550-3213\(88\)90108-3](https://doi.org/10.1016/0550-3213(88)90108-3).
- [27] V. Bernard, N. Kaiser, and U.-G. Meißner. “Chiral dynamics in nucleons and nuclei”. In: *Int. J. Mod. Phys. E* 4 (1995), pp. 193–346. DOI: [10.1142/S0218301395000092](https://doi.org/10.1142/S0218301395000092). arXiv: [hep-ph/9501384](https://arxiv.org/abs/hep-ph/9501384).
- [28] V. Bernard and U.-G. Meißner. “Chiral perturbation theory”. In: *Ann. Rev. Nucl. Part. Sci.* 57 (2007), pp. 33–60. DOI: [10.1146/annurev.nucl.56.080805.140449](https://doi.org/10.1146/annurev.nucl.56.080805.140449). arXiv: [hep-ph/0611231](https://arxiv.org/abs/hep-ph/0611231).
- [29] V. Bernard. “Chiral Perturbation Theory and Baryon Properties”. In: *Prog. Part. Nucl. Phys.* 60.1 (2008), pp. 82–160. DOI: [10.1016/j.ppnp.2007.07.001](https://doi.org/10.1016/j.ppnp.2007.07.001). arXiv: [arXiv: 0706.0312v1](https://arxiv.org/abs/0706.0312v1).

- 
- [30] S. Weinberg. “Nuclear forces from chiral Lagrangians”. In: *Phys. Lett. B* 251 (1990), pp. 288–292. DOI: [10.1016/0370-2693\(90\)90938-3](https://doi.org/10.1016/0370-2693(90)90938-3).
  - [31] C. Ordóñez, L. Ray, and U. van Kolck. “The Two-Nucleon Potential from Chiral Lagrangians”. In: *Phys. Rev. C* 53 (1996), pp. 2086–2105. DOI: [10.1103/PhysRevC.53.2086](https://doi.org/10.1103/PhysRevC.53.2086). arXiv: [hep-ph/9511380](https://arxiv.org/abs/hep-ph/9511380).
  - [32] E. Epelbaum, H. W. Hammer, and U.-G. Meißner. “Modern theory of nuclear forces”. In: *Rev. Mod. Phys.* 81.4 (2009), pp. 1773–1825. DOI: [10.1103/RevModPhys.81.1773](https://doi.org/10.1103/RevModPhys.81.1773). arXiv: [0811.1338](https://arxiv.org/abs/0811.1338).
  - [33] R. Machleidt and D. R. Entem. “Chiral effective field theory and nuclear forces”. In: *Phys. Rep.* 503.1 (2011), pp. 1–75. DOI: [10.1016/j.physrep.2011.02.001](https://doi.org/10.1016/j.physrep.2011.02.001). arXiv: [1105.2919](https://arxiv.org/abs/1105.2919).
  - [34] T. R. Hemmert, B. R. Holstein, and J. Kambor. “Systematic 1/M expansion for spin 3/2 particles in baryon chiral perturbation theory”. In: *Phys. Lett. B* 395 (1997), pp. 89–95. DOI: [10.1016/S0370-2693\(97\)00049-X](https://doi.org/10.1016/S0370-2693(97)00049-X). arXiv: [hep-ph/9606456](https://arxiv.org/abs/hep-ph/9606456).
  - [35] V. Pascalutsa and M. Vanderhaeghen. “Chiral effective-field theory in the Delta(1232) region: I. Pion electroproduction on the nucleon”. In: *Phys. Rev. D* 73 (2006), p. 034003. DOI: [10.1103/PhysRevD.73.034003](https://doi.org/10.1103/PhysRevD.73.034003). arXiv: [hep-ph/0512244](https://arxiv.org/abs/hep-ph/0512244).
  - [36] V. Pascalutsa and M. Vanderhaeghen. “Chiral effective-field theory in the Delta(1232) region. II. Radiative pion photoproduction”. In: *Phys. Rev. D* 77 (2008), p. 014027. DOI: [10.1103/PhysRevD.77.014027](https://doi.org/10.1103/PhysRevD.77.014027). arXiv: [0709.4583 \[hep-ph\]](https://arxiv.org/abs/0709.4583).
  - [37] D. L. Yao et al. “Pion-nucleon scattering in covariant baryon chiral perturbation theory with explicit Delta resonances”. In: *JHEP* 05.5 (2016), p. 038. DOI: [10.1007/JHEP05\(2016\)038](https://doi.org/10.1007/JHEP05(2016)038). arXiv: [1603.03638v1](https://arxiv.org/abs/1603.03638v1).
  - [38] A. N. Hiller Blin, T. Ledwig, and M. J. Vicente Vacas. “ $\Delta(1232)$  resonance in the  $\gamma p \rightarrow p\pi^0$  reaction at threshold”. In: *Phys. Rev. D* 93.9 (2016), p. 094018. DOI: [10.1103/PhysRevD.93.094018](https://doi.org/10.1103/PhysRevD.93.094018). arXiv: [1602.08967 \[hep-ph\]](https://arxiv.org/abs/1602.08967).
  - [39] D. Siemens et al. “Elastic and inelastic pion-nucleon scattering to fourth order in chiral perturbation theory”. In: *Phys. Rev. C* 96.5 (2017), p. 055205. DOI: [10.1103/PhysRevC.96.055205](https://doi.org/10.1103/PhysRevC.96.055205). arXiv: [1704.08988 \[nucl-th\]](https://arxiv.org/abs/1704.08988).
  - [40] M. Thürmann et al. “Nucleon polarizabilities in covariant baryon chiral perturbation theory with explicit  $\Delta$  degrees of freedom”. In: *Phys. Rev. C* 103 (2021), p. 035201. DOI: [10.1103/PhysRevC.103.035201](https://doi.org/10.1103/PhysRevC.103.035201). arXiv: [2007.08438 \[nucl-th\]](https://arxiv.org/abs/2007.08438).
  - [41] S. Kölling, E. Epelbaum, and D. R. Phillips. “The magnetic form factor of the deuteron in chiral effective field theory”. In: *Phys. Rev. C* 86 (2012), p. 047001. DOI: [10.1103/PhysRevC.86.047001](https://doi.org/10.1103/PhysRevC.86.047001). arXiv: [1209.0837 \[nucl-th\]](https://arxiv.org/abs/1209.0837).
  - [42] M. Piarulli et al. “Electromagnetic structure of  $A = 2$  and  $3$  nuclei in chiral effective field theory”. In: *Phys. Rev. C* 87.1 (2013), p. 014006. DOI: [10.1103/PhysRevC.87.014006](https://doi.org/10.1103/PhysRevC.87.014006). arXiv: [1212.1105 \[nucl-th\]](https://arxiv.org/abs/1212.1105).

- [43] R. Schiavilla et al. “Local chiral interactions and magnetic structure of few-nucleon systems”. In: *Phys. Rev. C* 99.3 (2019), p. 034005. DOI: 10.1103/PhysRevC.99.034005. arXiv: 1809.10180 [nucl-th].
- [44] S. Kölling et al. “Two-nucleon electromagnetic current in chiral effective field theory: One-pion exchange and short-range contributions”. In: *Phys. Rev. C* 84 (2011), p. 054008. DOI: 10.1103/PhysRevC.84.054008. arXiv: 1107.0602 [nucl-th].
- [45] H. Krebs, E. Epelbaum, and U.-G. Meißner. “Nuclear Electromagnetic Currents to Fourth Order in Chiral Effective Field Theory”. In: *Few Body Syst.* 60.2 (2019), p. 31. DOI: 10.1007/s00601-019-1500-5. arXiv: 1902.06839 [nucl-th].
- [46] S. Pastore et al. “Electromagnetic Currents and Magnetic Moments in (chi)EFT”. In: *Phys. Rev. C* 80 (2009), p. 034004. DOI: 10.1103/PhysRevC.80.034004. arXiv: 0906.1800 [nucl-th].
- [47] J. Rijneveen et al. “Radiative pion photoproduction in covariant chiral perturbation theory”. In: *Phys. Rev. C* (2021), to appear. arXiv: 2006.03917.
- [48] N. M. Kroll. “A Theorem on photomeson production near threshold and the suppression of pairs in pseudoscalar meson theory”. In: *Phys. Rev.* 93 (1954), pp. 233–238. DOI: 10.1103/PhysRev.93.233.
- [49] P. De Baenst. “An improvement on the Kroll-Ruderman theorem”. In: *Nucl. Phys. B* 24 (1970), pp. 633–652. DOI: 10.1016/0550-3213(70)90451-7.
- [50] A. Vainshtein and V. Zakharov. “Low-energy theorems for photoproduction and electropion production at threshold”. In: *Nucl. Phys. B* 36 (1972), pp. 589–604. DOI: 10.1016/0550-3213(72)90238-6.
- [51] Y. Nambu. “Axial vector current conservation in weak interactions”. In: *Phys. Rev. Lett.* 4 (1960). Ed. by T. Eguchi, pp. 380–382. DOI: 10.1103/PhysRevLett.4.380.
- [52] J. Bernstein, M. Gell-Mann, and L. Michel. “On the renormalization of the axial vector coupling constant in  $\beta$ -decay”. In: *Nuovo Cim.* 16.3 (1960), pp. 560–568. DOI: 10.1007/BF02731920.
- [53] M. Gell-Mann and M Levy. “The axial vector current in beta decay”. In: *Nuovo Cim.* 16 (1960), p. 705. DOI: 10.1007/BF02859738.
- [54] S. L. Adler and R. F. Dashen. *Current Algebras and Applications to Particle Physics*. Benjamin, New York, 1968.
- [55] S. Treiman, R. Jackiw, and D. J. Gross. *Lectures on Current Algebra and Its Applications*. Princeton University Press, Princeton, NJ, 1972.
- [56] V. de Alfaro et al. *Currents in Hadron Physics*. North-Holland, Amsterdam, 1973.
- [57] E. Mazzucato et al. “A Precise Measurement of Neutral Pion Photoproduction on the Proton Near Threshold”. In: *Phys. Rev. Lett.* 57 (1986), p. 3144. DOI: 10.1103/PhysRevLett.57.3144.
- [58] R. Beck et al. “Measurement of the  $p(\gamma, \pi^0)$  cross-section at threshold”. In: *Phys. Rev. Lett.* 65 (1990), pp. 1841–1844. DOI: 10.1103/PhysRevLett.65.1841.

- [59] V. Bernard et al. “Neutral pion photoproduction at threshold”. In: *Phys. Lett. B* 268.2 (1991), pp. 291–295. DOI: [10.1016/0370-2693\(91\)90818-B](https://doi.org/10.1016/0370-2693(91)90818-B).
- [60] V. Bernard, N. Kaiser, and U.-G. Meißner. “Threshold pion photoproduction in chiral perturbation theory”. In: *Nucl. Phys. B* 383.3 (1992), pp. 442–496. DOI: [10.1016/0550-3213\(92\)90085-P](https://doi.org/10.1016/0550-3213(92)90085-P).
- [61] T. Welch et al. “Electroproduction of  $\pi^0$  on the Proton near Threshold”. In: *Phys. Rev. Lett.* 69.19 (1992), pp. 2761–2764. DOI: [10.1103/PhysRevLett.69.2761](https://doi.org/10.1103/PhysRevLett.69.2761).
- [62] H. B. Van Den Brink et al. “Neutral-pion electroproduction on the proton near threshold”. In: *Phys. Rev. Lett.* 74.18 (1995), pp. 3561–3564. DOI: [10.1103/PhysRevLett.74.3561](https://doi.org/10.1103/PhysRevLett.74.3561).
- [63] K. I. Blomqvist et al. “Precise pion electroproduction in the  $p(e, e'\pi^+)n$  reaction at  $W = 1125$  MeV”. In: *Z. Phys. A* 353 (1996), pp. 415–421. DOI: [10.1007/BF01285153](https://doi.org/10.1007/BF01285153).
- [64] M. Fuchs et al. “Neutral pion photoproduction from the proton near threshold”. In: *Phys. Lett. B* 368 (1996), pp. 20–25. DOI: [10.1016/0370-2693\(95\)01488-8](https://doi.org/10.1016/0370-2693(95)01488-8).
- [65] J. C. Bergstrom et al. “Measurement of the  ${}^1H(\gamma, \pi^0)$  cross section near threshold”. In: *Phys. Rev. C* 53.3 (1996), pp. 1052–1056. DOI: [10.1103/PhysRevC.53.R1052](https://doi.org/10.1103/PhysRevC.53.R1052).
- [66] J. C. Bergstrom, R. Igarashi, and J. M. Vogt. “Measurement of the  ${}^1H(\gamma, \pi^0)$  cross section near threshold. II: Pion angular distributions”. In: *Phys. Rev. C* 55.4 (1997), pp. 2016–2023. DOI: [10.1103/PhysRevC.55.2016](https://doi.org/10.1103/PhysRevC.55.2016).
- [67] A. M. Bernstein et al. “Observation of a unitary cusp in the threshold  $\gamma p \rightarrow \pi^0 p$  reaction”. In: *Phys. Rev. C* 55 (1997), pp. 1509–1516. DOI: [10.1103/PhysRevC.55.1509](https://doi.org/10.1103/PhysRevC.55.1509). arXiv: [nucl-ex/9610005](https://arxiv.org/abs/nucl-ex/9610005).
- [68] M. A. Kovash. “Total cross-sections for  $\pi^- p \rightarrow \gamma n$  at 10 MeV to 20 MeV”. In: *PiN Newslett.* 12N3 (1997), pp. 51–55.
- [69] M. O. Distler et al. “Measurement of Separated Structure Functions in the  $p(e, e'p)\pi^0$  Reaction at Threshold and Chiral Perturbation Theory”. In: *Phys. Rev. Lett.* 80.11 (1998), pp. 2294–2297. DOI: [10.1103/PhysRevLett.80.2294](https://doi.org/10.1103/PhysRevLett.80.2294).
- [70] A. Liesenfeld et al. “A measurement of the axial form-factor of the nucleon by the  $p(e, e'\pi^+)n$  reaction at  $W = 1125$  MeV”. In: *Phys. Lett. B* 468 (1999), pp. 20–27. DOI: [10.1016/s0370-2693\(99\)01204-6](https://doi.org/10.1016/s0370-2693(99)01204-6).
- [71] E. Korkmaz et al. “Measurement of the  $\gamma p \rightarrow \pi^+ n$  reaction near threshold”. In: *Phys. Rev. Lett.* 83 (1999), pp. 3609–3612. DOI: [10.1103/PhysRevLett.83.3609](https://doi.org/10.1103/PhysRevLett.83.3609).
- [72] A. Schmidt et al. “Test of Low-Energy Theorems for  ${}^1H(\gamma, \pi^0){}^1H$  in the Threshold Region”. In: *Phys. Rev. Lett.* 87 (2001). [Erratum: *Phys. Rev. Lett.* 110, 039903 (2013)], p. 232501. DOI: [10.1103/PhysRevLett.87.232501](https://doi.org/10.1103/PhysRevLett.87.232501). arXiv: [nucl-ex/0105010](https://arxiv.org/abs/nucl-ex/0105010).
- [73] H. Merkel et al. “Neutral pion threshold production at  $Q^2 = 0.05\text{GeV}^2/c^2$  and chiral perturbation theory”. In: *Phys. Rev. Lett.* 88 (2002), p. 012301. DOI: [10.1103/PhysRevLett.88.012301](https://doi.org/10.1103/PhysRevLett.88.012301). arXiv: [nucl-ex/0108020](https://arxiv.org/abs/nucl-ex/0108020).

- [74] D. Baumann. “ $\pi^+$ -Elektroproduktion an der Schwelle”. PhD thesis. Johannes Gutenberg-Universität Mainz, 2005.
- [75] M. Weis et al. “Separated cross sections in  $\pi^0$  electroproduction at threshold at  $Q^2 = 0.05\text{GeV}^2/c^2$ ”. In: *Eur. Phys. J. A* 38 (2008), pp. 27–33. DOI: [10.1140/epja/i2007-10644-6](https://doi.org/10.1140/epja/i2007-10644-6). arXiv: [0705.3816](https://arxiv.org/abs/0705.3816).
- [76] H. Merkel. “Experimental results from MAMI”. In: *PoS CD09* (2009), p. 112. DOI: [10.22323/1.086.0112](https://doi.org/10.22323/1.086.0112).
- [77] H. Merkel et al. *Consistent threshold  $\pi^0$  electro-production at  $Q^2 = 0.05, 0.10$  and  $0.15\text{GeV}^2/c^2$* . 2011. arXiv: [1109.5075 \[nucl-ex\]](https://arxiv.org/abs/1109.5075).
- [78] D. Hornidge et al. “Accurate Test of Chiral Dynamics in the  $\gamma \rightarrow \pi^0 p$  Reaction”. In: *Phys. Rev. Lett.* 111.6 (2013), pp. 1–5. DOI: [10.1103/physrevlett.111.062004](https://doi.org/10.1103/physrevlett.111.062004). arXiv: [1211.5495v3](https://arxiv.org/abs/1211.5495v3).
- [79] D. Hornidge. “Asymmetries for neutral pion photoproduction in the threshold region”. In: *Proc. Sci. CD12* (2013), p. 070. arXiv: [1308.2345v1](https://arxiv.org/abs/1308.2345v1).
- [80] R. Lindgren, K. Chirapatimol, and L. C. Smith. “Precision Measurement of Neutral Pion Electroproduction near Threshold: A Test of Chiral QCD Dynamics”. In: *Proc. Sci. CD12* (2013), p. 073. DOI: [10.22323/1.172.0073](https://doi.org/10.22323/1.172.0073).
- [81] V. Bernard et al. “Chiral structure of the nucleon”. In: *Nucl. Phys. B* 388.2 (1992), pp. 315–345. DOI: [10.1016/0550-3213\(92\)90615-I](https://doi.org/10.1016/0550-3213(92)90615-I).
- [82] V. Bernard, N. Kaiser, and U.-G. Meißner. “Determining the Axial Radius of the Nucleon from Data on Pion Electroproduction”. In: *Phys. Rev. Lett.* 69.13 (1992), pp. 1877–1879. DOI: [10.1103/PhysRevLett.69.1877](https://doi.org/10.1103/PhysRevLett.69.1877).
- [83] V. Bernard et al. “Threshold pion electroproduction in chiral perturbation theory”. In: *Phys. Rep.* 246.6 (1994), pp. 315–363. DOI: [10.1016/0370-1573\(94\)90088-4](https://doi.org/10.1016/0370-1573(94)90088-4). arXiv: [9310329 \[hep-ph\]](https://arxiv.org/abs/9310329).
- [84] V. Bernard, N. Kaiser, and U.-G. Meißner. “Novel pion electroproduction low-energy theorems”. In: *Phys. Rev. Lett.* 74 (1995), pp. 3752–3755. DOI: [10.1103/PhysRevLett.74.3752](https://doi.org/10.1103/PhysRevLett.74.3752). arXiv: [hep-ph/9412282](https://arxiv.org/abs/hep-ph/9412282).
- [85] V. Bernard, N. Kaiser, and U.-G. Meißner. “Threshold neutral pion electroproduction in heavy baryon chiral perturbation theory”. In: *Nucl. Phys. A* 607 (1996). [Erratum: Nucl.Phys.A 633, 695–697 (1998)], pp. 379–401. DOI: [10.1016/0375-9474\(96\)00184-4](https://doi.org/10.1016/0375-9474(96)00184-4). arXiv: [hep-ph/9601267](https://arxiv.org/abs/hep-ph/9601267).
- [86] V. Bernard, N. Kaiser, and U.-G. Meißner. “Neutral pion photoproduction off nucleons revisited”. In: *Z. Phys. C* 70 (1996), pp. 483–498. DOI: [10.1007/s002880050126](https://doi.org/10.1007/s002880050126). arXiv: [hep-ph/9411287](https://arxiv.org/abs/hep-ph/9411287).
- [87] V. Bernard, N. Kaiser, and U.-G. Meißner. “Chiral corrections to the Kroll-Ruderman theorem”. In: *Phys. Lett. B* 383 (1996), pp. 116–120. DOI: [10.1016/0370-2693\(96\)00699-5](https://doi.org/10.1016/0370-2693(96)00699-5). arXiv: [hep-ph/9603278](https://arxiv.org/abs/hep-ph/9603278).

- [88] V. Bernard, N. Kaiser, and U.-G. Meißner. “Chiral symmetry and the reaction  $\gamma p \rightarrow \pi^0 p$ ”. In: *Phys. Lett. B* 378 (1996), pp. 337–341. DOI: 10.1016/0370-2693(96)00356-5. arXiv: [hep-ph/9512234](#).
- [89] H. W. Fearing et al. “Radiative pion capture by a nucleon”. In: *Phys. Rev. C* 62 (2000), p. 054006. DOI: 10.1103/PhysRevC.62.054006. arXiv: [hep-ph/0005213](#).
- [90] T. Becher and H. Leutwyler. “Baryon chiral perturbation theory in manifestly Lorentz invariant form”. In: *Eur. Phys. J. C* 9 (1999), pp. 643–671. DOI: 10.1007/PL00021673. arXiv: [hep-ph/9901384](#).
- [91] J. Gegelia and G. Japaridze. “Matching heavy particle approach to relativistic theory”. In: *Phys. Rev. D* 60 (1999), p. 114038. DOI: 10.1103/PhysRevD.60.114038. arXiv: [hep-ph/9908377](#).
- [92] T. Fuchs et al. “Renormalization of relativistic baryon chiral perturbation theory and power counting”. In: *Phys. Rev. D* 68 (2003), p. 056005. DOI: 10.1103/PhysRevD.68.056005. arXiv: [hep-ph/0302117](#).
- [93] P. J. Ellis and H.-B. Tang. “Pion nucleon scattering in a new approach to chiral perturbation theory”. In: *Phys. Rev. C* 57 (1998), pp. 3356–3375. DOI: 10.1103/PhysRevC.57.3356. arXiv: [hep-ph/9709354](#).
- [94] V. Bernard, B. Kubis, and U.-G. Meißner. “The Fubini-Furlan-Rosetti sum rule and related aspects in light of covariant baryon chiral perturbation theory”. In: *Eur. Phys. J. A* 25 (2005), pp. 419–425. DOI: 10.1140/epja/i2005-10144-9. arXiv: [nucl-th/0506023](#).
- [95] M. Hilt et al. “Pion photo- and electroproduction in relativistic baryon chiral perturbation theory and the chiral MAID interface”. In: *Phys. Rev. C* 88 (2013), p. 055207. DOI: 10.1103/PhysRevC.88.055207. arXiv: [1309.3385 \[nucl-th\]](#).
- [96] M. Hilt, S. Scherer, and L. Tiator. “Threshold  $\pi^0$  photoproduction in relativistic chiral perturbation theory”. In: *Phys. Rev. C* 87.4 (2013), pp. 1–21. DOI: 10.1103/PhysRevC.87.045204. arXiv: [arXiv:1301.5576v1](#).
- [97] T. R. Hemmert, B. R. Holstein, and J. Kambor. “Chiral Lagrangians and delta(1232) interactions: Formalism”. In: *J. Phys. G* 24 (1998), pp. 1831–1859. DOI: 10.1088/0954-3899/24/10/003. arXiv: [hep-ph/9712496](#).
- [98] L. W. Cawthorne and J. A. McGovern. “Impact of the Delta (1232) resonance on neutral pion photoproduction in chiral perturbation theory”. In: *PoS* CD15 (2016), p. 072. DOI: 10.22323/1.253.0072. arXiv: [1510.09136 \[nucl-th\]](#).
- [99] A. N. Hiller Blin, T. Ledwig, and M. J. Vicente Vacas. “Chiral dynamics in the  $\gamma p \rightarrow p\pi^0$  reaction”. In: *Phys. Lett. B* 747 (2015), pp. 217–222. DOI: 10.1016/j.physletb.2015.05.067. arXiv: [1412.4083 \[hep-ph\]](#).
- [100] G. H. Guerrero Navarro et al. “Pion photoproduction off nucleons in covariant chiral perturbation theory”. In: *Phys. Rev. D* 100.9 (2019), p. 094021. DOI: 10.1103/PhysRevD.100.094021. arXiv: [1908.00890 \[hep-ph\]](#).

- [101] G. H. Guerrero Navarro and M. J. Vicente Vacas. “Threshold pion electro- and photo-production off nucleons in covariant chiral perturbation theory”. In: *Phys. Rev. D* 102.11 (2020), p. 113016. DOI: [10.1103/PhysRevD.102.113016](https://doi.org/10.1103/PhysRevD.102.113016). arXiv: [2008.04244](https://arxiv.org/abs/2008.04244) [hep-ph].
- [102] V. Pascalutsa and D. R. Phillips. “Effective theory of the delta(1232) in Compton scattering off the nucleon”. In: *Phys. Rev. C* 67 (2003), p. 055202. DOI: [10.1103/PhysRevC.67.055202](https://doi.org/10.1103/PhysRevC.67.055202). arXiv: [nucl-th/0212024](https://arxiv.org/abs/nucl-th/0212024).
- [103] R. J. Furnstahl et al. “Quantifying truncation errors in effective field theory”. In: *Phys. Rev. C* 92.2 (2015), pp. 1–23. DOI: [10.1103/PhysRevC.92.024005](https://doi.org/10.1103/PhysRevC.92.024005). arXiv: [1506.01343](https://arxiv.org/abs/1506.01343).
- [104] J. A. Melendez, S. Wesolowski, and R. J. Furnstahl. “Bayesian truncation errors in chiral effective field theory: Nucleon-nucleon observables”. In: *Phys. Rev. C* 96.2 (2017), pp. 1–24. DOI: [10.1103/PhysRevC.96.024003](https://doi.org/10.1103/PhysRevC.96.024003). arXiv: [1704.03308](https://arxiv.org/abs/1704.03308).
- [105] E. Epelbaum et al. “Towards high-order calculations of three-nucleon scattering in chiral effective field theory”. In: *Eur. Phys. J. A* 56.3 (2020). DOI: [10.1140/epja/s10050-020-00102-2](https://doi.org/10.1140/epja/s10050-020-00102-2). arXiv: [1907.03608](https://arxiv.org/abs/1907.03608).
- [106] D. Siemens et al. “Elastic pion-nucleon scattering in chiral perturbation theory: A fresh look”. In: *Phys. Rev. C* 94.1 (2016). DOI: [10.1103/PhysRevC.94.014620](https://doi.org/10.1103/PhysRevC.94.014620). arXiv: [arXiv: 1602.02640v1](https://arxiv.org/abs/1602.02640v1).
- [107] D. Siemens et al. “Reconciling threshold and subthreshold expansions for pion–nucleon scattering”. In: *Phys. Lett. B* 770 (2017), pp. 27–34. DOI: [10.1016/j.physletb.2017.04.039](https://doi.org/10.1016/j.physletb.2017.04.039). arXiv: [1610.08978](https://arxiv.org/abs/1610.08978) [nucl-th].
- [108] D. Hornidge. *private communication*.
- [109] T. Muta. *Foundations of Quantum Chromodynamics*. 2nd edition. World Scientific Publishing Co. Pte. Ltd., 1998. ISBN: 981-02-2674-8.
- [110] P. A. Zyla et al. “Review of Particle Physics”. In: *PTEP* 2020.8 (2020), p. 083C01. DOI: [10.1093/ptep/ptaa104](https://doi.org/10.1093/ptep/ptaa104).
- [111] G. ’t Hooft. “Symmetry Breaking Through Bell-Jackiw Anomalies”. In: *Phys. Rev. Lett.* 37 (1976), pp. 8–11. DOI: [10.1103/PhysRevLett.37.8](https://doi.org/10.1103/PhysRevLett.37.8).
- [112] J. Goldstone. “Field Theories with Superconductor Solutions”. In: *Nuovo Cim.* 19 (1961), pp. 154–164. DOI: [10.1007/BF02812722](https://doi.org/10.1007/BF02812722).
- [113] S. Scherer and M. R. Schindler. *A Primer for Chiral Perturbation Theory*. Springer, 2012. ISBN: 978-3-642-19253-1.
- [114] C. Hanhart and A. Wirzba. “Remarks on  $NN \rightarrow NN\pi$  beyond leading order”. In: *Phys. Lett. B* 650 (2007), pp. 354–361. DOI: [10.1016/j.physletb.2007.05.038](https://doi.org/10.1016/j.physletb.2007.05.038). arXiv: [nucl-th/0703012](https://arxiv.org/abs/nucl-th/0703012).
- [115] N. Fettes et al. “The Chiral effective pion nucleon Lagrangian of order  $p^4$ ”. In: *Annals Phys.* 283 (2000). [Erratum: Annals Phys. 288, 249–250 (2001)], pp. 273–302. DOI: [10.1006/aphy.2000.6059](https://doi.org/10.1006/aphy.2000.6059). arXiv: [hep-ph/0001308](https://arxiv.org/abs/hep-ph/0001308).

- 
- [116] E. Jenkins and A. V. Manohar. “Baryon chiral perturbation theory using a heavy fermion Lagrangian”. In: *Phys. Lett. B* 255 (1991), pp. 558–562. DOI: [10.1016/0370-2693\(91\)90266-S](https://doi.org/10.1016/0370-2693(91)90266-S).
  - [117] M. R. Schindler, J. Gegelia, and S. Scherer. “Infrared regularization of baryon chiral perturbation theory reformulated”. In: *Phys. Lett. B* 586 (2004), pp. 258–266. DOI: [10.1016/j.physletb.2004.02.056](https://doi.org/10.1016/j.physletb.2004.02.056). arXiv: [hep-ph/0309005](https://arxiv.org/abs/hep-ph/0309005).
  - [118] N. Fettes. “Pion-Nucleon Physics in Chiral Perturbation Theory”. PhD thesis. Rheinische Friedrich-Wilhelms-Universität Bonn, 2000.
  - [119] W. Rarita and J. Schwinger. “On a theory of particles with half integral spin”. In: *Phys. Rev.* 60 (1941), p. 61. DOI: [10.1103/PhysRev.60.61](https://doi.org/10.1103/PhysRev.60.61).
  - [120] L. M. Nath, B. Etemadi, and J. D. Kimel. “Uniqueness of the Interaction Involving Spin-3/2 particles”. In: *Phys. Rev. D* 3 (1971), pp. 2153–2161. DOI: [10.1103/PhysRevD.3.2153](https://doi.org/10.1103/PhysRevD.3.2153).
  - [121] S. Kamefuchi, L. O’Raifeartaigh, and A. Salam. “Change of variables and equivalence theorems in quantum field theories”. In: *Nucl. Phys.* 28 (1961), pp. 529–546. DOI: [10.1016/0029-5582\(61\)90056-6](https://doi.org/10.1016/0029-5582(61)90056-6).
  - [122] T. R. Hemmert. “Heavy Baryon Chiral Perturbation Theory with Light Deltas”. PhD thesis. University of Massachusetts Amherst, 1999.
  - [123] V. Bernard, T. R. Hemmert, and U.-G. Meißner. “Infrared regularization with spin-3/2 fields”. In: *Phys. Lett. B* 565 (2003), pp. 137–145. DOI: [10.1016/S0370-2693\(03\)00538-0](https://doi.org/10.1016/S0370-2693(03)00538-0). arXiv: [hep-ph/0303198](https://arxiv.org/abs/hep-ph/0303198).
  - [124] C. Zöller. “Effective Chiral Nucleon-Delta Lagrangian at Order  $Q^3$ ”. Master thesis. Ruhr-Universität Bochum, 2014.
  - [125] H. Krebs, E. Epelbaum, and U.-G. Meißner. “Redundancy of the off-shell parameters in chiral effective field theory with explicit spin-3/2 degrees of freedom”. In: *Phys. Lett. B* 683 (2010), pp. 222–228. DOI: [10.1016/j.physletb.2009.12.023](https://doi.org/10.1016/j.physletb.2009.12.023). arXiv: [0905.2744 \[hep-th\]](https://arxiv.org/abs/0905.2744).
  - [126] V. Pascalutsa. “Quantization of an interacting spin-3/2 field and the Delta isobar”. In: *Phys. Rev. D* 58 (1998), p. 096002. DOI: [10.1103/PhysRevD.58.096002](https://doi.org/10.1103/PhysRevD.58.096002). arXiv: [hep-ph/9802288](https://arxiv.org/abs/hep-ph/9802288).
  - [127] S. R. Coleman, J. Wess, and B. Zumino. “Structure of phenomenological Lagrangians. 1.” In: *Phys. Rev.* 177 (1969), pp. 2239–2247. DOI: [10.1103/PhysRev.177.2239](https://doi.org/10.1103/PhysRev.177.2239).
  - [128] C. G. Callan et al. “Structure of phenomenological Lagrangians. 2.” In: *Phys. Rev.* 177 (1969), pp. 2247–2250. DOI: [10.1103/PhysRev.177.2247](https://doi.org/10.1103/PhysRev.177.2247).
  - [129] V. Pascalutsa. “Correspondence of consistent and inconsistent spin-3/2 couplings via the equivalence theorem”. In: *Phys. Lett. B* 503 (2001), pp. 85–90. DOI: [10.1016/S0370-2693\(01\)00140-X](https://doi.org/10.1016/S0370-2693(01)00140-X). arXiv: [hep-ph/0008026](https://arxiv.org/abs/hep-ph/0008026).

- [130] H. Krebs, E. Epelbaum, and U.-G. Meißner. “On-shell consistency of the Rarita-Schwinger field formulation”. In: *Phys. Rev. C* 80 (2009), p. 028201. DOI: [10.1103/PhysRevC.80.028201](https://doi.org/10.1103/PhysRevC.80.028201). arXiv: 0812.0132 [hep-th].
- [131] D. Siemens. “Pion-Nucleon Physics in Chiral Perturbation Theory with explicit  $\Delta(1232)$  Degrees of Freedom”. PhD thesis. Ruhr-Universität Bochum, 2016.
- [132] V. Baru et al. “Precision calculation of the  $\pi^-d$  scattering length and its impact on threshold  $\pi N$  scattering”. In: *Phys. Lett. B* 694 (2011), pp. 473–477. DOI: [10.1016/j.physletb.2010.10.028](https://doi.org/10.1016/j.physletb.2010.10.028). arXiv: 1003.4444 [nucl-th].
- [133] V. Bernard et al. “New insights into the spin structure of the nucleon”. In: *Phys. Rev. D* 87.5 (2013), p. 054032. DOI: [10.1103/PhysRevD.87.054032](https://doi.org/10.1103/PhysRevD.87.054032). arXiv: 1209.2523 [hep-ph].
- [134] J. S. Ball. “Application of the Mandelstam Representation to Photoproduction of Pions from Nucleons”. In: *Phys. Rev.* 124.6 (1961), pp. 2014–2028. DOI: [10.1103/PhysRev.124.2014](https://doi.org/10.1103/PhysRev.124.2014).
- [135] G. F. Chew et al. “Relativistic dispersion relation approach to photomeson production”. In: *Phys. Rev.* 106.6 (1957), pp. 1345–1355. DOI: [10.1103/PhysRev.106.1345](https://doi.org/10.1103/PhysRev.106.1345).
- [136] D. Drechsel and L. Tiator. “Threshold pion photoproduction on nucleons”. In: *J. Phys. G* 18 (1992), pp. 449–497. DOI: [10.1088/0954-3899/18/3/004](https://doi.org/10.1088/0954-3899/18/3/004).
- [137] A. Denner et al. “Predictions for all processes  $e^+e^- \rightarrow 4$  fermions + $\gamma$ ”. In: *Nucl. Phys. B* 560 (1999), pp. 33–65. DOI: [10.1016/S0550-3213\(99\)00437-X](https://doi.org/10.1016/S0550-3213(99)00437-X). arXiv: hep-ph/9904472.
- [138] A. Denner et al. “Electroweak corrections to charged-current  $e^+e^- \rightarrow 4$  fermion processes: Technical details and further results”. In: *Nucl. Phys. B* 724 (2005). [Erratum: Nucl.Phys.B 854, 504–507 (2012)], pp. 247–294. DOI: [10.1016/j.nuclphysb.2011.09.001](https://doi.org/10.1016/j.nuclphysb.2011.09.001). arXiv: hep-ph/0505042.
- [139] A. Denner and S. Dittmaier. “The Complex-mass scheme for perturbative calculations with unstable particles”. In: *Nucl. Phys. B Proc. Suppl.* 160 (2006). Ed. by J. Blumlein, S. Moch, and T. Riemann, pp. 22–26. DOI: [10.1016/j.nuclphysbps.2006.09.025](https://doi.org/10.1016/j.nuclphysbps.2006.09.025). arXiv: hep-ph/0605312.
- [140] M. L. Goldberger and S. B. Treiman. “Decay of the pi meson”. In: *Phys. Rev.* 110 (1958), pp. 1178–1184. DOI: [10.1103/PhysRev.110.1178](https://doi.org/10.1103/PhysRev.110.1178).
- [141] B. Kubis and U.-G. Meißner. “Low-energy analysis of the nucleon electromagnetic form-factors”. In: *Nucl. Phys. A* 679 (2001), pp. 698–734. DOI: [10.1016/S0375-9474\(00\)00378-X](https://doi.org/10.1016/S0375-9474(00)00378-X). arXiv: hep-ph/0007056.
- [142] G. Passarino and M. Veltman. “One-loop corrections for  $e^+e^-$  annihilation into  $\mu^+\mu^-$  in the Weinberg model”. In: *Nucl. Phys. B* 160 (1979), pp. 151–207.
- [143] A. I. Davydychev. “A Simple formula for reducing Feynman diagrams to scalar integrals”. In: *Phys. Lett. B* 263 (1991), pp. 107–111. DOI: [10.1016/0370-2693\(91\)91715-8](https://doi.org/10.1016/0370-2693(91)91715-8).
- [144] E. Boos and A. Davydychev. “A Method of evaluating massive Feynman integrals”. In: *Theor. Math. Phys.* 89 (1991), pp. 1052–1063. DOI: [10.1007/BF01016805](https://doi.org/10.1007/BF01016805).

- [145] J. Gasser et al. “Ground state energy of pionic hydrogen to one loop”. In: *Eur. Phys. J. C* 26 (2002), pp. 13–34. DOI: 10.1007/s10052-002-1013-z. arXiv: hep-ph/0206068.
- [146] T. Appelquist and J. Carazzone. “Infrared Singularities and Massive Fields”. In: *Phys. Rev. D* 11 (1975), p. 2856. DOI: 10.1103/PhysRevD.11.2856.
- [147] V. Bernard, N. Kaiser, and U.-G. Meißner. “Aspects of chiral pion-nucleon physics”. In: *Nucl. Phys. A* 615 (1997), pp. 483–500. DOI: 10.1016/S0375-9474(97)00021-3. arXiv: hep-ph/9611253.
- [148] H. Krebs, A. Gasparyan, and E. Epelbaum. “Three-nucleon force in chiral EFT with explicit  $\Delta(1232)$  degrees of freedom: Longest-range contributions at fourth order”. In: *Phys. Rev. C* 98.1 (2018), p. 014003. DOI: 10.1103/PhysRevC.98.014003. arXiv: 1803.09613 [nucl-th].
- [149] D. Drechsel, S. S. Kamalov, and L. Tiator. “Unitary isobar model - MAID2007”. In: *Eur. Phys. J. A* 34.1 (2007), pp. 69–97. DOI: 10.1140/epja/i2007-10490-6. arXiv: 0710.0306.
- [150] M. R. Schindler and D. R. Phillips. “Bayesian Methods for Parameter Estimation in Effective Field Theories”. In: *Annals Phys.* 324 (2009). [Erratum: *Annals Phys.* 324, 2051–2055 (2009)], pp. 682–708. DOI: 10.1016/j.aop.2008.09.003. arXiv: 0808.3643 [hep-ph].
- [151] *Wolfram Mathematica*. URL: <https://www.wolfram.com/mathematica/> (Accessed: 01 Apr. 2021).
- [152] J. Kuipers et al. “FORM version 4.0”. In: *Comput. Phys. Commun.* 184.5 (2013), pp. 1453–1467. DOI: 10.1016/j.cpc.2012.12.028. arXiv: 1203.6543.
- [153] T. Hahn and M. Pérez-Victoria. “Automated one-loop calculations in four and D dimensions”. In: *Comput. Phys. Commun.* 118.2 (1999), pp. 153–165. DOI: 10.1016/S0010-4655(98)00173-8.
- [154] H. H. Patel. “Package-X: A Mathematica package for the analytic calculation of one-loop integrals”. In: *Comput. Phys. Commun.* 197 (2015), pp. 276–290. DOI: 10.1016/j.cpc.2015.08.017. arXiv: 1503.01469.
- [155] A. Denner. “Techniques for the Calculation of Electroweak Radiative Corrections at the One-Loop Level and Results for  $W$ -physics at LEP200”. In: *Fortsch. Phys.* 41.4 (1993), pp. 307–420. DOI: 10.1002/prop.2190410402. arXiv: 0709.1075.
- [156] H. Krebs. *private communication*.
- [157] K. M. Watson. “Some general relations between the photoproduction and scattering of pi mesons”. In: *Phys. Rev.* 95 (1954), pp. 228–236. DOI: 10.1103/PhysRev.95.228.
- [158] A. Gasparyan and M. F. M. Lutz. “Photon- and pion-nucleon interactions in a unitary and causal effective field theory based on the chiral Lagrangian”. In: *Nucl. Phys. A* 848.1-2 (2010), pp. 126–182. DOI: 10.1016/j.nuclphysa.2010.08.006. arXiv: arXiv: 1003.3426v2.

- [159] N. Fettes, U.-G. Meißner, and S. Steininger. “Pion - nucleon scattering in chiral perturbation theory. 1. Isospin symmetric case”. In: *Nucl. Phys. A* 640 (1998), pp. 199–234. DOI: 10.1016/S0375-9474(98)00452-7. arXiv: hep-ph/9803266.
- [160] C. Fernández-Ramírez and A. M. Bernstein. “Upper energy limit of heavy baryon chiral perturbation theory in neutral pion photoproduction”. In: *Phys. Lett. B* 724.4-5 (2013), pp. 253–258. DOI: 10.1016/j.physletb.2013.06.020. arXiv: arXiv:1212.3237v2.
- [161] W. Briscoe et al. “Cross section for  $\gamma n \rightarrow \pi^0 n$  at the Mainz A2 experiment”. In: *Phys. Rev. C* 100.6 (2019), p. 065205. DOI: 10.1103/PhysRevC.100.065205. arXiv: 1908.02730 [nucl-ex].
- [162] I. Strakovsky. *private communication*.
- [163] R. L. Workman et al. “Unified Chew-Mandelstam SAID analysis of pion photoproduction data”. In: *Phys. Rev. C* 86 (2012), p. 015202. DOI: 10.1103/PhysRevC.86.015202. arXiv: 1202.0845 [hep-ph].
- [164] E. Epelbaum, H. Krebs, and U.-G. Meißner. “Improved chiral nucleon-nucleon potential up to next-to-next-to-next-to-leading order”. In: *Eur. Phys. J. A* 51.5 (2015), p. 53. DOI: 10.1140/epja/i2015-15053-8. arXiv: 1412.0142 [nucl-th].
- [165] D. Djukanovic et al. “Complex-mass renormalization in chiral effective field theory”. In: *Phys. Lett. B* 680 (2009), pp. 235–238. DOI: 10.1016/j.physletb.2009.08.068. arXiv: 0902.4347 [hep-ph].
- [166] D. Djukanovic, J. Gegelia, and S. Scherer. “Chiral structure of the Roper resonance using complex-mass scheme”. In: *Phys. Lett. B* 690 (2010), pp. 123–128. DOI: 10.1016/j.physletb.2010.05.022. arXiv: 0903.0736 [hep-ph].
- [167] T. Bauer, J. Gegelia, and S. Scherer. “Magnetic moment of the Roper resonance”. In: *Phys. Lett. B* 715 (2012), pp. 234–240. DOI: 10.1016/j.physletb.2012.07.032. arXiv: 1208.2598 [hep-ph].
- [168] D. Djukanovic et al. “Complex-mass renormalization in hadronic EFT: applicability at two-loop order”. In: *Eur. Phys. J. A* 51 (2015), p. 101. DOI: 10.1140/epja/i2015-15101-5. arXiv: 1507.06771 [hep-ph].
- [169] S. Ceci et al. “Fundamental properties of resonances”. In: *Sci. Rep.* 7 (2017), p. 45246. DOI: 10.1038/srep45246. arXiv: 1608.06485 [hep-ph].
- [170] J. A. McGovern, D. R. Phillips, and H. W. Grießhammer. “Compton scattering from the proton in an effective field theory with explicit Delta degrees of freedom”. In: *Eur. Phys. J. A* 49 (2013), p. 12. DOI: 10.1140/epja/i2013-13012-1. arXiv: 1210.4104 [nucl-th].
- [171] C. Fernández-Ramírez, A. M. Bernstein, and T. W. Donnelly. “Unexpected impact of D waves in low-energy neutral pion photoproduction from the proton and the extraction of multipoles”. In: *Phys. Rev. C* 80.6 (2009), pp. 1–15. DOI: 10.1103/PhysRevC.80.065201.
- [172] C. Fernández-Ramírez, A. M. Bernstein, and T. W. Donnelly. “Low-Energy D-Wave Effects in Neutral Pion Photoproduction”. In: *Phys. Lett. B* 679 (2009), pp. 41–44. DOI: 10.1016/j.physletb.2009.07.011. arXiv: 0902.3412 [nucl-th].

- [173] J. Gegelia, U.-G. Meißner, and D.-L. Yao. “The width of the Roper resonance in baryon chiral perturbation theory”. In: *Phys. Lett. B* 760 (2016), pp. 736–741. DOI: 10.1016/j.physletb.2016.07.068. arXiv: 1606.04873 [hep-ph].



---

# **Curriculum vitae**

Nora Martina Rijneveen

## **Personal information**

Date of birth            16 August 1991

Place of birth            Saarbrücken, Germany

## **Education**

since 02/2016            Institute of Theoretical Physics II, Ruhr-Universität Bochum  
                                  PhD student  
                                  Advisor: Prof. Dr. Evgeny Epelbaum

10/2013 – 09/2015       Graduate student in Physics, Ruhr-Universität Bochum  
                                  Degree: Master of Science (M.Sc.)  
                                  Thesis: Reduction formalism of two-loop integrals

10/2010 – 09/2013       Undergraduate student in Physics, Ruhr-Universität Bochum  
                                  Degree: Bachelor of Science (B.Sc.)  
                                  Thesis: Anomalies in quantum mechanics and possible applications  
                                  in molecular physics

09/2001 – 06/2010       Secondary education, Gymnasium Holthausen, Hattingen (Ruhr)  
                                  Degree: Abitur

Bochum, 1 April 2021